Joint PhD program at Universitá degli studi di Napoli "Federico II" and Universität of Zürich

Doctoral Thesis

Ultimate precision for the Drell-Yan process: mixed QCDxQED(EW) corrections, final state radiation and power suppressed contributions

Author:
Luca Buonocore

Supervisor:
Prof. Dr. Massimiliano Grazzini
Prof. Dr. Francesco Tramontano

Ciclo XXXII, Coordinatore: Salvatore Capozziello
Sezione scientifico disciplinare FIS/02

Dipartimento di Fisica "Ettore Pancini" and Physik-Institut

Scuola Politecnica e delle Scienze di Base and Mathematisch-naturwissenschaftlichen Fakultät

Years 2017/2020

"With diligent effort he has established that there is no statistical basis for Murphys Law. He has also established that he believes in it anyway. "

John Barnes, Mother of Storms (1994)

Abstract

Ultimate precision for the Drell-Yan process: mixed QCDxQED(EW) corrections, final state radiation and power suppressed contributions

The discovery of the Higgs Boson at the Large Hadron Collider in 2012 represented a breakthrough in particle physics, providing a strong confirmation of the mechanism of Electro-Weak-Symmetry-Breaking, which is in turn responsible for the generation of elementary particle masses. The Higgs discovery, however, was not followed by any evidence of physics Beyond the Standard Model, and it is difficult to reconcile our current description of the fundamental particles and their interactions with long-standing problems like neutrino masses, matter-anti matter asymmetry, the existence of dark matter and dark energy and the hierarchy problem.

The lack of new-physics signals has stimulated a new precision collider programme, which was made possible by the advances on both the experimental and theoretical sides. Indeed, the precision target accuracy expected by the end of the planned LHC data taking in 2038 is at the (sub)percent level. For a meaningful comparison with experimental data, we need theoretical predictions which have a similar level of accuracy. This translates into the necessity of computing higher order terms in perturbation theory, known as radiative corrections in the language of Quantum Field Theory. At an hadronic collider as the LHC the effects due to the strong interaction (described by Quantum CromoDynamics (QCD)) dominate. In the last decades a big effort has been profused to compute QCD radiative corrections and nowadays Next-to-Next-to Leading Order (NNLO) computations represent the state of the art for many $2 \to 2$ processes.

The production of a dilepton pair via the Drell-Yan mechanism has a special place in the precision phenomenology program at LHC for its importance in experimental calibrations and for the precise determination of important electro-weak (EW) parameters such as the W mass. From the theoretical side, Drell-Yan is one of the most studied processes. QCD corrections are known up to NNLO and in part at N^{3}LO, while EW corrections are known at NLO. At this level of accuracy, it becomes relevant to assess the relative importance of the mixed QCD-EW corrections.

In this thesis, we set up a subtraction framework to compute the full set of mixed QCD-EW(QED) corrections to the the Drell-Yan process at the differential level. We rely on the transverse momentum resummation formalism to handle the genuine NNLO-type infrared divergences associated to both initial and final state radiation in the small transverse momentum limit, exploiting the corresponding results for heavy-quark pair production. In particular, we have to deal with massive leptons in the final state as the their mass acts as a regulator for final-state collinear divergences. This may challenge the numerical stability since the physical lepton masses are very small. We extensively study the radiation pattern of massive emitters, building a dedicated momentum mapping which smoothly approaches the massless limit. Furthermore, we study, for the first time, the leading power suppressed contributions appearing at small transverse momenta, and we show that they are driven by final-state soft radiation. As a validation of our construction, we show results both for the inclusive and the relevant differential distribution for the mixed QCD-QED corrections to the production of an on-shell Z boson.

Zusammenfassung

Die Entdeckung des Higgs Boson am Large Hadron Collider(LHC) im Jahr 2012 stellte einen Durchbruch in der Teilchenphysik dar und lieferte eine Bestätigung des Mechanismus der Elektro-Schwach-Symmetrie-Brechung, der für die Erzeugung von Elementarteilchenmassen verantwortlich ist. Auf die Higgs-Entdeckung folgte jedoch keine weiteren Hinweise für Physik jenseits des Standardmodells, und es bleibt weiterhin schwierig, die aktuelle Beschreibung der fundamentalen Teilchen und ihre Wechselwirkungen mit lang bestehenden Problemen wie den Neutrinomassen, der Materie-Antimaterie-Asymmetrie, die Existenz von dunkler Materie und dunkler Energie und das Hierarchieproblem in Einklang zu bringen.

Das Fehlen von Signalen neuer Physik hat ein neues Präzisions-Beschleuniger-Programm ins Leben gerufen, das erst durch die Fortschritte auf sowohl experimenteller als auch auf theoretischer Seite ermöglicht wurde. Bis Ende der geplanten LHC-Datenaufnahme im Jahr 2038, wird eine auf dem (sub)prozentualen Präzisions-Zielgenauigkeit erwartet.

Für einen Vergleich mit experimentellen Daten benötigen wir theoretische Vorhersagen, mit vergleichbarem Genauigkeitsgrad. Dies verlangt die Berechnung von Termen höherer Ordnung in der Störungstheorie, auch bekannt als Strahlungskorrekturen in der Sprache der Quantenfeldtheorie. An einem hadronischen Collider, wie dem LHC, dominieren die Effekte der starken Wechselwirkung, beschrieben durch die Quantum Cromo Dynamics (QCD). Im letzten Jahrzehnt gab es groSSe Anstrengungen, um insbesondere QCD Korrekturen zu berechnen, und heutzutage stellen Next-to-Next-to-Leading Order (NNLO)-Berechnungen den Stand der Technik für viele $2 \to 2$-Streuprozesse dar.

Die Erzeugung eines Dileptonpaares über den Drell-Yan-Mechanismus spielt eine besondere Rolle in der Präzisionsphänomenologie am LHC, wegen seiner Bedeutung für die experimentelle Kalibrierungen und für die präzise Bestimmung bedeutsamer elektroschwacher (EW) Parameter wie der W-Masse. Auf der theoretischen Seite ist Drell-Yan einer der am meisten untersuchten Prozesse. QCD-Korrekturen sind bis NNLO und teilweise bis N^{3}LO bekannt, während EW-Korrekturen bislang nur auf NLO bekannt sind. Bei diesem Präzisionsgrad ist es relevant, das relative Gewicht der gemischten QCD-EW-Korrekturen zu bestimmen.

In dieser Dissertation entwickeln wir einen Subtraktions-Framework, um den vollständigen Satz von gemischten QCD-EW(QED)-Korrekturen des Drell-Yan-Prozesses auf der differentieller Ebene zu berechnen. Wir bauen auf den Formalismus der Transversalimpuls-Resummation auf, um die tatsächlichen NNLO Infrarot-Divergenzen, die an Abstrahlungen im Anfangs- und Endzustände in Bereichen kleiner transversal Impulse zugeordnet sind, unter Ausnutzung entsprechender Ergebnisse für die Produktion von Schwere-Quark-Paaren, zu behandeln. Insbesondere betrachten wir Leptonen im Endzustand massiv, da deren Masse als Regulator für kollineare Divergenzen wirkt. Dies kann zu numerischen Instabilitäten führen, da die physikalischen Leptonenmassen sehr klein sind. Wir analysieren ausgiebig das Strahlungsmuster massiver Emitter und erstellen eine dedizierte Impulsabbildung, die sich nahtlos dem masselosen Fall nähert. Des Weiteren untersuchen wir zum ersten Mal die führenden power-suppressed Beiträge, die bei kleinen transversalen Momenten auftreten, und wir zeigen, dass sie durch Softe-Strahlung im Endzustand angetrieben werden. Als Validierung berechnen wir Ergebnisse sowohl für die Inklusiv- als auch relevante differentielle Verteilungen für gemischten QCD-QED-Korrekturen zur Produktion eines on-shell Z-Bosons.

Contents

List of Figures

List of Tables

To Sara (the right one).

Introduction

Our knowledge of fundamental elementary particles and their interactions is enclosed in the Standard Model (SM) of Particle Physics, which has been established and confirmed in a number of experiments during the last fifty years. Its great success is culminated with the discovery of the last missing building block, the Higgs boson, at the Large Hadron Colliders (LHC) of CERN in 2012. Since then, the LHC has been carrying on its program of data taking searching for any signs of new physics around the TeV scale. There is indeed strong evidence that the SM it not the ultimate theory as it fails to explain long-standing problems as, among the others, the matter-anti matter asymmetry in the Universe, the origin of neutrino masses, the astrophysical evidence of dark matter and dark energy. From the theoretical point of view, the presence of an elementary scalar particle, the Higgs boson itself, is unpleasant because, within the SM alone, it requires an extreme *fine tuning* of the parameters to preserve the relative small value of the Higgs mass from large quadratic radiative corrections. Furthermore, it cannot accommodate the gravitational interaction in a unified framework.

The fact that, so far, experiments at the LHC have not yet reported any sign of New Physics, has made even more pressing the necessity to consider complementary exploration strategies to the direct searches at the energy frontier. The unprecedented integrated luminosity of 147 fb^{-1} delivered by the LHC during the Run 2, together with the continuous progress of the experimental methods of reconstruction and processing of the data, allows to test several properties of the SM with increasing precision. This represents just the beginning of a rich experimental program set up to pursue the precise measurement of many fundamental SM parameters with an incredible sub-percent/percent target accuracy. In particular, one of the main goals is to precisely probe the Higgs sector, as there are still parameters, as the Higgs self coupling, which have not yet been measured. The LHC operation with the current configuration is planned to last up to 2023 (Run 3), reaching a total integrated luminosity of over 300 fb^{-1}; its High Luminosity upgrade has been approved and will extend up to at least 2038 with the goal of reaching 3000 fb^{-1}. The design of Future Linear and Circular colliders is proceeding fast and their approval would extend the program for more then 40 years from now.

The experimental effort, which has already brought the LHC in its “precision” phase, has to be supported by the theory with very accurate predictions. Indeed, measurements alone can tell a lot about Nature, but when compared with the theoretical predictions, their discrimination power greatly increase. Any significant deviations from the SM predictions can indeed be interpreted as an indirect sign of New Physics and potentially give hints on how the SM breaks and what has to replace it. Obtaining very accurate predictions for scattering processes within the SM is in general a highly non-trivial task. Indeed, the SM Lagrangian, despite its “simplicity”, underlies a very complicated non-linear dynamics that for realistic physical cases cannot be solved in a closed analytic form. As it has proven successful in other fields of physics, the main approach to overcome this issue is provided by the idea of successive approximations. Rephrasing it in a more rigorous language, the theoretical framework to deal with scattering processes in Quantum Field Theory is provided by Perturbation Theory that can be formulated in the language of Feynman diagrams. Therefore, to get a meaningful comparison between data and theory, the computation of radiative corrections up to a certain order it is usually required depending on the accuracy target.

The production of leptons pairs at high transverse momentum, namely the Drell-Yan process, is one of the central process for the precision physics program at the LHC. The case in which the leptons come from the decay of a Z boson (*neutral current*), represents, for its clean final-state signature, a "standard candle" for luminosity measurement and detector calibration. It is important for the measurement of parton distribution functions at the LHC and for searches of New Physics in the high region of the lepton-pair mass spectrum. Furthermore, it allows a precision determination of some relevant EW parameters as the EW mixing angle and some properties of the Z boson.

The case in which leptons come from the decay of the W (*charged current*) is of primary importance for the precise determination of the W boson mass. The comparison of the measured value of the W mass with the SM prediction, in a global fit of the EW parameters, which includes also, among others, the top and the Higgs boson masses, is a stringent test of the SM and might highlight possible tensions [1]. Recently, the ATLAS collaboration has published a measurement of the $M_W = 80.370 \pm 19$ MeV [2] with an accuracy comparable to the world average and both the ATLAS and the CMS experiments are planning to measure M_W with an accuracy of 15 MeV (or eventually 10 MeV).

This precision program requires that the SM predictions for the Drell-Yan process should have a target accuracy of order $\mathcal{O}(1\%)$ or better, which implies the inclusion of radiative corrections. In hadronic collisions, QCD radiative corrections are the dominant contribution, and for the inclusive DY cross section they have been computed up to next-to-leading order (NLO) [3] and next-to-next-to-leading order (NNLO) [4]. The NNLO QCD calculation has been extended to fully differential level [5–8]. NLO EW corrections are also known [9–12]: their impact is typically at the percent level, and of the same order of the NNLO contributions. NNLO QED corrections have been computed in Ref. [13]. In some phase space regions, and for specific kinematic distributions, QCD and EW corrections are enhanced to the several percent level, thereby calling for the evaluation of perturbative corrections of even higher order [1], and, in particular of *mixed* QCD-EW corrections. First analytic results for mixed QCD-EW corrections have been presented in [15–17]. Mixed QCD-QED corrections for on-shell Z bosons have been obtained in [13] for the inclusive cross section, and in [18] for the differential distributions. Complete QCD-EW corrections to on-shell Z production have been obtained in Ref. [19]. An exact fully differential computation of mixed QCD-EW corrections, including the leptonic decay, would be highly valuable.

The main subject of this thesis is the construction of a consistent framework to treat infrared (soft and collinear) divergences occurring at intermediate steps in the computation of fully differential mixed QCD-EW corrections to Drell-Yan and other relevant hadron collider processes. The structure of the mixed corrections is equivalent to that of NNLO in a single coupling, so that, in other words, what we are looking for is a generalization of a NNLO QCD subtraction scheme to mixed QCD-EW corrections.

To introduce the problem, consider first the situation at NLO for a simple inclusive reaction with no identified hadrons in the initial-state (a more exhaustive presentation is given in Chapter 1). As it is well known, the numerical generation of tree-level and one-loop scattering amplitudes can be considered nowadays a solved problem [2]. At this order, to produce the prediction for the physical cross section, the squared tree-level amplitude associated to the real emission process and the one-loop virtual correction must be combined to achieve the cancellation of soft and collinear singularities. The two contributions are defined in two different phase spaces and cannot be naively added. The cancellation only occurs after the integration over the corresponding phase spaces has been carried out introducing a suitable

[1] Very recently, the N^{3}LO QCD corrections to the photon contribution to DY have been presented [14].

[2] The only caveat is given by the number of external legs as the computational load increases going to higher multiplicities. Some important progresses have been achieved in this direction [20].

infrared (IR) regulator, as the dimensional regulator ϵ. Moreover, while the singularities of the virtual correction are explicitly exposed as poles in ϵ at the integrand level, they emerge in the real term only after integrating out the radiation. The regularization procedure requires that the integration must be performed analytically. This is a severe drawback as the two integrals become soon intractable with analytical methods when kinematic cuts are applied. To overcome this issue, general multi-purpose local subtraction schemes at NLO have been proposed, such as Catani-Seymour dipole subtraction [21] and FKS [22–24], which, together with the progress in the computation of one-loop amplitudes, has lead to the complete automation of fully differential NLO radiative corrections, which goes under the name of *NLO revolution*.

We are still far from reaching the same level of automation at NNLO. The main bottleneck is the computation of two-loop amplitudes. Indeed, at variance with the one-loop case, for which the class of basic integrals (*master integrals*) needed to decompose every amplitude has been established, at two-loop the functional space required to represent the amplitudes is not yet fully determined. Moreover, even the *reduction* of the amplitude to a set of master integrals, a problem that can be formulated [25] in the terms of the resolution of a huge algebraic linear system, becomes cumbersome when there are more than four scales in the problem.[3].

Besides the problem of the computation of the amplitudes, also the treatment of the soft and collinear divergences becomes more complicated moving from NLO to NNLO. Indeed, here one has to consider processes with up to two unresolved emissions leading to three different phase spaces to be consistently combined in order to achieve the cancellation of the singularities. The most difficult part is the double real emission which exhibits a richer structure of singularities corresponding to both the situation of a single parton becoming unresolved and of two partons becoming unresolved. This can lead to the introduction of counterterms that, designed to cancel a specific singularity, for example a double unresolved limit, are themselves divergent in the singular unresolved region. Despite different methods have been proposed so far, in large part inspired by the formulation of the Catani-Seymour dipoles and FKS, none of them has reached a level of generality and maturity comparable with what we have at NLO.

In this work, we rely on the q_T subtraction formalism [28] as the starting point to build the framework for the computation of the mixed corrections to the Drell-Yan process. The q_T subtraction formalism is a well-established framework to handle and cancel the IR divergences appearing in QCD computations at NNLO (and beyond[4]) based on the formulation of the transverse-momentum resummation in QCD (further details are given in Chapter 3). In its original formulation it has been successfully applied to carry out a variety of NNLO QCD computations for the production of colourless final states in hadronic collisions [7, 30–43]. In the last few years, thanks to the formulation of transverse-momentum resummation for heavy-quark production [44–48] the method has been extended and applied to the production of top-quark pairs [49–51]. As we will argue in the following, the latter progress is of great importance for our purposes.

Strictly speaking, the infrared and collinear divergences in the computation of EW corrections are associated to the propagation (as a virtual particle in the loop or as a real final-state) of massless photons, so that the subtraction scheme only "sees" the QED subset. This leads to a great simplification in the construction of the framework for the mixed corrections. The key idea [52] is that the abelian subset of QCD is formally equivalent to QED, so that it is possible to develop a procedure to *derive* the QED result starting from the more complicated

[3]We mention that there have been recent progresses applying finite fields approaches [26, 27]

[4]A first application of q_T subtraction to the computation of the approximate next-to-next-to-next-to-leading order (N^3LO) QCD corrections to Higgs boson production through gluon fusion has been presented recently [29]

QCD one without performing any new computation. For our purposes, this translates in the following strategy: we start from the structure of the pure NNLO QCD q_T subtraction formula and determine the abelian components; then, we effectively trade a gluon with a photon by applying suitable replacement rules of colour with electric charge factors taking into account any differences in symmetry factors and colour averages.

Starting from the q_T subtraction formula for the computation of NNLO corrections to the production of a color-singlet system, this strategy allows us to derive the analog formula for the mixed corrections to the production of a generic color-singlet and color-neutral object. We have explicitly implemented the new formula in the computation of the mixed QCD-QED corrections to on-shell Z boson production which represents a highly non-trivial consistency check for our construction. Indeed, thanks to the abelianisation procedure, all the ingredients needed to bring the computation to completion are available, including the two-loop virtual amplitude. In addition, we have the chance to compare our prediction for the inclusive hadronic cross section with the analytical computation recently reported in the literature [13]. We mention that very recently the same differential computation, based on the abelianised version of the nested soft-collinear subtraction scheme [18], has been performed by another group including, in the narrow-width approximation, the decay of the Z boson to a pair of leptons.

The recent extension of the q_T subtraction formalism to heavy-quark pair production allows us to construct a consistent subtraction framework for the full set of mixed radiative corrections to the production of a pair of leptons via the Drell-Yan mechanism, including the treatment of the genuine mixed initial-final soft singularities and off-shell effects. We have made the first fundamental step in this direction computing the NLO EW corrections to both the neutral- and charge-current Drell-Yan processes as a proof-of-concept of the abelianisation procedure in the case in which initial and final-state radiation is taken into account More importantly, we have studied the numerical stability of the q_T subtraction formalism for heavy charged fermions in the limit of very small masses. In fact, in the way in which it is currently formulated, the q_T subtraction method cannot handle final-state collinear divergences. This requires that the mass of the leptons must be kept finite. On one hand, this represents a stress test for the numerical implementation because mass values as small as the muon mass (and possibly electron) are the target for the physical applications. On the other, this allows us to retain the full-dependence on the lepton mass, which is the true physical cut-off of collinear singularities. In precision QED/EW calculation the leading mass effects are usually retained (see for example Refs. [53, 54]), and in the case the calculation is matched with a parton-shower program to achieve the resummation at leading logarithmic accuracy of multi soft-collinear photon emissions, the finite lepton mass naturally represents the physical cut-off [55] scale where the shower is stopped.

In order to be confident on the numerical stability of the method, there is another fundamental aspect to take into account which in principle can have an interplay with the small mass limit. The q_T subtraction counterterm is constructed by exploiting the universal behavior of the associated transverse-momentum (q_T) distribution and, therefore, the subtraction is intrinsically *non local*. In practice the computation is carried out by introducing a cut, $r_{\rm cut}$, on the transverse momentum of the produced final state system normalised to its invariant mass. When evaluated at finite $r_{\rm cut}$ both the contributions of the real emission and the one of the counterterm exhibit logarithmically divergent terms plus additional power suppressed contributions that vanish as $r_{\rm cut} \to 0$. In the final result, the logarithms cancel leaving a residual power-suppressed dependence on $r_{\rm cut}$. The efficiency of the subtraction procedure crucially depends on the size of such power suppressed contributions. Indeed, from one side, the cut-off should be chosen sufficiently small to keep the power corrections negligible. On the hand, it cannot be taken arbitrarily small because the cancellation will occur between logarithmic contributions which become numerically larger and larger, requiring to increase the target accuracy of the integrator in order to avoid the consequent loss of precision.

In the inclusive production of a colourless final state the power suppressed contributions are known to be *quadratic* in $r_{\rm cut}$ (modulo logarithmic enhancements) [39]. This allows us to obtain precise predictions by either evaluating the cross section at sufficiently small $r_{\rm cut}$, or carrying out the $r_{\rm cut} \to 0$ extrapolation [56] [5]. The power suppressed contributions to the next-to-leading order (NLO) total cross section have been explicitly evaluated in Refs. [58, 59]. In the case of heavy-quark production the $r_{\rm cut}$ dependence is found to be *linear* [50, 51, 60]. We have investigated the $r_{\rm cut}$ dependence in our NLO EW computation finding a similar linear behavior. This confirms, as it could have been expected, that the effect is directly related to soft emission off massive final-state particles regardless it is in QCD or QED. In the simplified case of final-state emission in pure QED, we analytically compute the form of the first power correction at NLO to the q_T subtraction formula for the inclusive cross-section showing that it is pure linear (no logarithmic enhancements), and relating it to corrections to the soft approximation.

The thesis is structured as follows. In Chapter 1, we review in general terms the construction of a local subtraction scheme at NLO and we outline the main features of the FKS scheme. Then, we present a new phase mapping required to deal with the soft singularity associated to a massive emitter in the FKS scheme. The original idea underlying its construction was the study of the radiation emitted off heavy quarks and its application to open heavy-flavour production at NLO+PS accuracy within the POWHEG framework [61]. Furthermore, it has been applied for the NLO EW corrections described in Chapter 4, to deal with the small-lepton mass limit.

In Chapter 2 we briefly report on the extension of local subtraction schemes to NNLO, highlighting the main issues which so far have prevented the construction of a general-purpose subtraction framework. An alternative strategy to this approach is provided by the so-called non-local subtraction/slicing schemes, which are first introduced in general terms and then specialized to the case of the q_T subtraction method both for the production of a color-singlet and for heavy-quark production.

Having reviewed the q_T subtraction formalism, in Chapter 3 we describe in details the abelianisation procedure used to derive the subtraction formula to handle initial-state mixed corrections. We show results for a complete implementation of the mixed QCD-QED correction to on shell Z boson production, focusing on the stability with respect the $r_{\rm cut}$ regulator and including the relevant differential distributions.

Chapter 4 is dedicated to the treatment of final-state radiation at NLO EW and the investigation of mass effects and power corrections. In the first part, we give the main formula to deal with the computation of NLO EW corrections within the q_T subtraction formalism and present numerical results for both neutral- and charged-current Drell-Yan processes. In particular, we focus on the $r_{\rm cut}$ dependence and on the small lepton mass limit. In the second part, we consider a simplified process in pure QED and study with analytical methods the first power correction to the NLO q_T subtraction formula associated both to initial- and final-state radiation. In the last section, we propose a strategy to remove the final-state soft linear power correction at fully differential level.

In Chapter 5 we summarise our work.

The work presented in this thesis appeared or is going to appear in the following publications

[5] The only exception is the production of direct photons ($\gamma\gamma$ [30, 31], $Z\gamma$ [33], $W\gamma$ [35]....), for which a fully inclusive cross section cannot be defined, and an isolation prescription is required. The interplay of the isolation prescription with the subtraction procedure makes the $r_{\rm cut}$ dependence stronger [56, 57].

1. L. Buonocore, P. Nason and F. Tramontano, "Heavy quark radiation in NLO+PS POWHEG generators," Eur. Phys. J. C **78** (2018) no.2, 151.
2. L. Buonocore, M. Grazzini and F. Tramontano, "The q_T subtraction method: electroweak corrections and power suppressed contributions," arXiv:1911.10166 [hep-ph], accepted by EPJC.
3. L. Buonocore, M. Grazzini, S. Kallweit and F. Tramontano, "Mixed QCD-QED corrections to the Drell-Yan process", in preparation.

Chapter 1

Subtraction at NLO and massive FKS mapping

The most fundamental observable in collider physics is the cross section for a given scattering process. The theoretical framework to deal with the computation of cross sections in Quantum Field Theory is Perturbation Theory. We are mainly interested in applications to hadron-hadron collision as occurring at the LHC, where the strong interaction described by the Quantum Cromodynamics (QCD) dominates the scene.

At hadronic colliders, the situation is complicated by the fact that the incoming initial particles are hadrons, while perturbative QCD deals with quarks and gluons (collectively denoted as partons) at high energies. A pertubative approach is still possible for processes characterized by a large momentum transfer and sufficiently inclusive with respect to further radiation, as it will be motivated in the following. Consider for example the inclusive production of a given final state F, namely $h_1 + h_b \to F + X$. According to the factorization theorems, for large momentum transfers, the inclusive cross section can be written as the convolution of collinear hadron parton density functions (pdfs) with the elementary scattering cross section for the process in the given final state F plus additional particles radiation:

$$\sigma(h_1 h_2 \to F + X) = \sum_{a,b} \int_0^1 dx_1 \int_0^1 dx_1 f_{a/h_1}(x_1, \mu_F^2) f_{b/h_2}(x_2, \mu_F^2) \hat{\sigma}(ab \to F + X), \tag{1.1}$$

where $f_{a/h_1}(f_{b/h_2})$ is the customary parton density function of the parton $a(b)$ inside the hadron $h_1(h_2)$, μ_F is the factorization scale and $\hat{\sigma}(ab \to F + X)$ is the short distance partonic cross section.

The elementary cross section is calculable as a power series in the strong coupling constant. The lowest order is denoted as Leading Order (LO) or Born cross section. In the language of the Feynman diagrams, it usually corresponds to tree-level diagrams. Higher order terms are called radiative corrections. It is well known that scattering amplitudes required for the calculation of radiative corrections are plagued by several and various kinds of divergences.

The ultra-violet (UV) divergences are associated to the high energy behavior of the theory. They are well-understood and, for renormalizable Quantum Field Theory, they can be systematically reabsorbed by a redefinition of a finite number of parameters to all orders in perturbation theory (*renormalization procedure*).

There is another type of divergences associated to the low-energy or infrared (IR) limit of a gauge theory with massless particles. Focusing on the QCD case, these divergences are associated to the configurations where a real or a virtual gluon has vanishing energy (**soft**) or becomes **collinear** to another parton.

The cancellation of the infrared and collinear singularities for inclusive observables is the fundamental result of the Kinoshita-Lee-Nauenberger (KLN) [62, 63] theorem. This means that together with virtual loop corrections, one has to add processes with the emission of real partons (up to 1 emission for a NLO computation, up two 2 emissions for a NNLO and son on). In this chapter we present the general local subtraction formalism needed to compute any infrared observables ensuring the cancellation of the infrared divergences in a fully differential manner, suitable for the numerical integration of exclusive cross sections.

Our interest will be mainly in the FKS subtraction scheme, for which we have developed a new phase space mapping to deal with soft radiation emitted off a massive parton. The original motivation was the study of the radiation emitted by a massive quark, as the bottom, at high transverse-momentum much larger than the mass of the quark. In this limit, the approximation of massless quark allows to effectively resum the large logarithmic enhancements of the transverse-momentum over the quark mass in the framework of the fragmentation function [64, 65][1].

Our idea has been that of introducing a new FKS singular region in the POWHEG framework associated to a quasi-collinear emission from a heavy quark line and to match it to a parton shower in order to improve the description of the heavy quark radiation including a subleading (NLL) logarithm contribution. Indeed, the comparison between the available generators and the data on bottom production shows that there are still discrepancies to be understood.

The mapping that we have developed is not limited to the specific topic discussed above. It has a general applicability in case one is interested in a massive emitter. It has revealed itself very useful in the application to the NLO EW corrections discussed in the Chapter 4.

This chapter is structured into two parts. In the first part, we present the local subtraction formalism for NLO computations and we detail the main characteristic of the FKS scheme. Then, we discuss the new phase space mapping for the massive emitter. In the second part, we present the application to the description of radiation off heavy quarks in the context of POWHEG generators describing heavy quark production.

1.1 Subtraction method

In this section, we review the main features of a QCD NLO differential calculation in a generic subtraction formalism. First we focus on processes with no hadrons in the initial state, such as lepton collisions or non-hadron particles decay. Identified hadrons in the initial state introduce some specific issues which make the picture more complicated. We will discuss them after presenting the basic aspects of the subtraction formalism.To be definite, consider there are n partons in the final state, whose on-shell momenta $\{k_i\}_{i=1}^{n}$ are constrained by the energy-momentum conservation

$$q = k_1 + \cdots + k_n, \tag{1.2}$$

being q the total initial momentum. We denote the collection of such momenta with Φ_n and we use the short notation

$$d\Phi_n = (2\pi)^4 \delta^{(4)} \left(q - \sum_{i=1}^{n} k_i \right) \prod_{i=1}^{n} \frac{d^3 k_i}{(2\pi)^3 2k_i^0}, \tag{1.3}$$

for the n-body phase space. At LO, the master formula for the total cross section is given by the integral over phase space of the Born or tree-level squared matrix element denoted by $\mathcal{B}(\Phi_n)$

$$\sigma_{\text{LO}} = \int d\Phi_n \mathcal{B}(\Phi_n). \tag{1.4}$$

[1]The necessity to resum collinear radiation off heavy quark to all-order has been pointed out in a recent work [66].

At NLO, together with the n-body process (*Born configuration*), we have to consider the process of real emission with an extra parton in the final state (*real configuration*); let Φ_{n+1} denote the corresponding set of momenta. At this order, the total cross section gets contribution from

- the tree-level squared amplitudes for the process with $n+1$ partons (real contribution);
- the interference between the virtual one-loop amplitudes and the LO one (virtual contribution).

We assume that the virtual contribution has been renormalized in order to get an ultraviolet finite, but still infrared divergent, quantity that we denote by $\mathcal{V}(\Phi_n)$. Then the total cross section up to NLO is given by the formula

$$\sigma_{\mathrm{NLO}} = \int d\Phi_n[\mathcal{B}(\Phi_n) + \mathcal{V}(\Phi_n)] + \int d\Phi_{n+1}\mathcal{R}(\Phi_{n+1}). \tag{1.5}$$

The above formula should be effectively read as an average value according to the non normalized distribution function given by the differential cross section: each point in phase space can be seen as a weighted event, having care to distinguish between Born event and real event, and the integral is given by the sum of such weights over all the possible events. In this sense it has to be read as our basic formula. More in general, one is interested in computing an observable of phenomenological relevance $\mathcal{O}$, function of the final state momenta. The observable $\mathcal{O}$ can be effectively thought as a bin (or a collection of bins) of an histogram for the distribution of some kinematic variables (invariant mass, transverse momentum, rapidity, etc.), with functional form given by the product of two theta functions. Then, its expectation value is given by the weighted average in phase space

$$\langle\mathcal{O}\rangle = \int d\Phi_n\mathcal{O}_n(\Phi_n)[\mathcal{B}(\Phi_n) + \mathcal{V}(\Phi_n)] + \int d\Phi_{n+1}\mathcal{O}_{n+1}(\Phi_{n+1})\mathcal{R}(\Phi_{n+1}), \tag{1.6}$$

where $\mathcal{O}_n$ and $\mathcal{O}_{n+1}$ are the specific realizations of the observable $\mathcal{O}$ in the Born and in real phase space respectively.

The above integrals are usually too difficult to be performed analytically because of the involved form of the observable $\mathcal{O}$. On the other hand, their evaluation is more naturally accomplished by means of a numerical approach such as the Monte Carlo integration. Within this framework, one can accommodate the computation of the average value in an easy fashion: the **weighted events** that are generated at random and summed in order to obtain the integral can be stored one by one into the bins of the desired histogram.

Life is not so simple: as they stand, the above formulae are not suitable for numerical computations because of the presence of infrared divergences. We recall the well-known result given by the KLN theorem: the total cross section is infrared finite since the full integrated divergent parts arising from virtual and real contribution exactly cancel each others. These divergences arise from soft, collinear and soft-collinear singularities that manifest themselves as single and double poles in the parameter $\epsilon = 2 - D/2$, having adopted the customary conventional dimensional regularization [67, 68]. This statement can be generalized to other observables, which define the class of *infrared safe* observables. We remark that the virtual and real term live in different phase spaces so that the above mentioned cancellation can occur only after their complete integration, but in this way we are completely inclusive.

On the other hand, the essence of the KLN theorem is that in the infrared divergent regions a real configuration is not distinguishable from a Born one so that we can think to "remove" such events from the real contribution and to place them in the Born one. This can be realized introducing, in correspondence of the singular regions, events with negative weights, called real counterterms, in such a way that they balance the divergent contribution of the real events. This constitutes the core of the so called subtraction formalism [69] that can be stated in a more systematic way as a rigorous integration method. In the following, we adopt the notation of ref. [24]. For each particular singular region labeled with the index α, we introduce a counterterm function $\mathcal{C}^{(\alpha)}$ and a mapping $M^{(\alpha)}$

$$M^{(\alpha)}\Phi_{n+1} = \tilde{\Phi}^{(\alpha)}_{n+1} \tag{1.7}$$

that maps a real configuration into a singular one in the α region. It is required that the mappings $M^{(\alpha)}$ is smooth near the singular limit and that there it must reduce to the identity in order to get the disordered cancellation effect. The counterterms $C^{(\alpha)}$ have to be chosen in such a way that, for any infrared-safe observable $\mathcal{O}$, the function

$$\mathcal{R}(\Phi_{n+1})\mathcal{O}_{n+1}(\Phi_{n+1}) - \sum_{\alpha}\mathcal{C}^{(\alpha)}(\Phi_{n+1})\mathcal{O}_{n+1}(M^{(\alpha)}\Phi_{n+1}) \tag{1.8}$$

has at most integrable singularities in the real phase space. Before going on, some observations about the above formula are in order. The property of infrared-safety of the observable $\mathcal{O}_{n+1}$ guarantees that it remains finite in any singular limits and that, furthermore, it reduces with continuity to its form in the Born-like kinematics $\mathcal{O}_n$. This ensures that there is no proliferation of new divergent structures. The singularities arise only from the real emission term $\mathcal{R}$. This implies that the counterterms required to cancel the divergent behavior of the real differential cross section can be defined in a universal way, independently of the specific observable. As it will be shown in the following, this is accomplished by means of the mappings $M^{(\alpha)}$ and for this reason they appear in the argument of the $\mathcal{O}_{n+1}$ in the subtracted contributions in Eq. (1.23).
In the cases under consideration, two kinds of singular configurations are possible:

- the soft configuration in which there is a final-state parton with null four-momentum;
- the collinear configuration in which there are two massless partons with parallel three-momenta.

As stated before, a singular configuration is indistinguishable from a Born one so that it is possible to associate to each $\tilde{\Phi}^{(\alpha)}_{n+1}$ a corresponding *underlying Born configuration* $\overline{\Phi}^{(\alpha)}_n$ according to the following prescriptions:

- for the soft singular configuration, the null-momentum parton is removed;
- for the collinear singular configuration, the two momenta of the collinear partons are replaced by a single momentum given by their sum.

Adding and subtracting the contribution of the counterterms, Eq. (1.6) can be now rewritten in the following form

$$\begin{aligned}\langle\mathcal{O}\rangle = &\int d\Phi_n\mathcal{O}_n(\Phi_n)[\mathcal{B}(\Phi_n)+\mathcal{V}(\Phi_n)] + \sum_{\alpha}\int d\Phi_{n+1}[\mathcal{C}(\Phi_{n+1})\mathcal{O}_n(\overline{\Phi}_n)]_{\alpha} \\ &+\int d\Phi_{n+1}\left\{\mathcal{R}(\Phi_{n+1})\mathcal{O}_{n+1}(\Phi_{n+1}) - \sum_{\alpha}\left[\mathcal{C}(\Phi_{n+1})\mathcal{O}_n(\overline{\Phi}_n)\right]_{\alpha}\right\},\end{aligned} \tag{1.9}$$

In the above formula, we have made use of the replacement

$$\mathcal{O}_{n+1}(\tilde{\Phi}^{(\alpha)}_{n+1}) \to \mathcal{O}_n(\overline{\Phi}^{(\alpha)}_n) \tag{1.10}$$

which crucially relies on the fact that $\mathcal{O}$ is infrared-safe. In the following, we adopt the short notation

$$[\cdots]_\alpha \tag{1.11}$$

with the meaning that all the variables which are affected by the superscript of the singular region appearing inside the square brackets have to be evaluated in the α region. The last term in Eq. (1.9) is now integrable in the whole real phase space in $D = 4$ dimension, as a result of the "subtraction", while the counterterm contribution added back

$$\sum_\alpha \int d\Phi_{n+1}[\mathcal{C}(\Phi_{n+1})\mathcal{O}_n(\overline{\Phi}_n)]_\alpha \tag{1.12}$$

and the virtual term in the Born phase space are still separately divergent. The next step consists in combining them together to achieve the complete cancellation of infrared divergences, as stated by the KLN theorem. To this aim, we observe that we cannot simply add them as they stand, since the counterterms and the virtual term live in different space. We will see in the following how to deal with this issue, proving in this way the success of the subtraction procedure. As a preliminary step, we notice that a generic singular configuration can be parameterized by the variables of its underlying Born configuration plus the variables associated with the state of an extra parton, referred to, with obvious meaning, as the radiation parton,

$$\Phi_{n+1}^{(\alpha)} \Longleftrightarrow \left\{\overline{\Phi}_n^{(\alpha)}, \Phi_{\text{rad}}^{(\alpha)}\right\}, \tag{1.13}$$

in such a way that the phase space element can be written in the factorized form

$$d\Phi_{n+1} = d\overline{\Phi}_n^{(\alpha)} d\Phi_{\text{rad}}^{(\alpha)}. \tag{1.14}$$

In the above formula, we have absorbed in the definition of $d\Phi_{\text{rad}}^{(\alpha)}$ the Jacobian associated to the new parametrization. We then require that the counterterms $C^{(\alpha)}$ and the relative mappings $M^{(\alpha)}$ are chosen in such a way that the integrand in Eq. (1.12), which contains the real divergent configurations, can be analytically integrated over the whole radiation phase space $d\Phi_{\text{rad}}$ in $D = 4 - 2\epsilon$ dimension

$$\left[\int d\Phi_{\text{rad}}\mathcal{C}(\Phi_{n+1}) = \overline{C}(\overline{\Phi})\right]_\alpha. \tag{1.15}$$

The resulting "integrated counterterms" $\overline{C}^{(\alpha)}(\overline{\Phi})$ exhibit single and double poles in ϵ that takes into account the singular contributions of the real emission process. Since they live in the Born space, we can now coherently add them to the virtual part: the quantity

$$V(\Phi_n) = \mathcal{V}(\Phi_n) + \left[\sum_\alpha \overline{C}^{(\alpha)}(\overline{\Phi}_n)\right]_{\overline{\Phi}_n = \Phi_n} \tag{1.16}$$

is free from divergences as the ϵ poles analytically cancel between the two contributions in the r.h.s. of Eq. (1.16).

We observe that the successful completion of this program is based upon the introduction of the mappings $M^{(\alpha)}$, the concept of the underlying Born configurations and the factorization of the real phase space. We are now in the position to write down the master formula for the NLO calculation in the subtraction formalism

$$\langle \mathcal{O} \rangle = \int d\Phi_n \mathcal{O}_n(\Phi_n)[\mathcal{B}(\Phi_n) + V(\Phi_n)] + \int d\Phi_{n+1} R(\Phi_{n+1}), \tag{1.17}$$

having defined

$$R(\Phi_{n+1}) \equiv \mathcal{R}(\Phi_{n+1})\mathcal{O}_{n+1}(\Phi_{n+1}) - \sum_{\alpha} \left[\mathcal{C}(\Phi_{n+1})\mathcal{O}_n(\overline{\Phi}_n)\right]_{\alpha} . \tag{1.18}$$

All the integrals are now finite and can be numerically integrated in $D = 4$ dimensions.

1.1.1 Identified hadrons in the initial-state

We discuss now the generalization of the subtraction method to the case of hadrons in the initial state. To be definite, consider a $2 \to n$ reaction in which the incoming particle 1 is a hadron h carrying momentum P_1 and the incoming particle 2 is a lepton carrying momentum p_2. The case with two hadrons in the initial state follows straightforwardly. According to the parton model [70], the hadronic cross section is given by the incoherent sum of all the possible partonic contributions convoluted with the customary parton density function $f_{a/h}$ of the hadron

$$\sigma_{hl} = \sum_a f_{a/h} \otimes \hat{\sigma}_{al} \equiv \sum_a \int dx f_{a/h}(x)\hat{\sigma}_{al} . \tag{1.19}$$

In the above formula, the index a runs over all the possible partons in h and $\hat{\sigma}_{al}$ denotes the partonic cross section initiated by the parton a. The variable x represents the fraction of the incoming momentum P_1 of h carried by the parton a. Then, the conservation of energy in the partonic process reads

$$xP_1 + p_2 \equiv p_1 + p_2 = \sum_{i=1}^{n} k_i \tag{1.20}$$

where, as before, we label with the collection $\{k_i\}_{i=1}^n$ the on-shell momenta in the final state. For ease of notation, in the following, we suppress the partonic sum and the dependence on the index a. The parton density function (pdf), will be denoted simply by f. The kinematics is fixed by assigning together with $\{k_i\}_{i=1}^n$ the fraction x, so that now $\Phi_n = \{x; k_1, \ldots, k_n\}$ and we include the extra integration in the phase space element $d\Phi_n$

$$d\Phi_n = dx \times (2\pi)^4 \delta^{(4)}\left(q - \sum_{i=1}^{n} k_i\right) \prod_{i=1}^{n} \frac{d^3 k_i}{(2\pi)^3 2k_i^0} . \tag{1.21}$$

The discussion of the subtraction formalism follows closely what has been done in the previous section. Let us start from Eq. (1.6) for the expectation value of a generic infrared-safe observable $\mathcal{O}$ at NLO, that now reads

$$\langle \mathcal{O} \rangle = \int d\Phi_n f(\Phi_n)\mathcal{O}_n(\Phi_n)[\mathcal{B}(\Phi_n) + \mathcal{V}(\Phi_n)] + \int d\Phi_{n+1} f(\Phi_{n+1})\mathcal{O}_{n+1}(\Phi_{n+1})\mathcal{R}(\Phi_{n+1}). \tag{1.22}$$

The presence of a parton in the initial state leads to an additional singular configuration when

- a final-state parton becomes collinear to the incoming parton direction.

We then introduce a set of suitable mappings M^{α}, which maps a real configuration into a singular one in the region α according to Eq.(1.7), and suitable counterterm functions C^{α} such that

$$\mathcal{R}(\Phi_{n+1}) f(\Phi_{n+1})\mathcal{O}_{n+1}(\Phi_{n+1}) - \sum_{\alpha} f(M^{(\alpha)}\Phi_{n+1})\mathcal{C}^{(\alpha)}(\Phi_{n+1})\mathcal{O}_{n+1}(M^{(\alpha)}\Phi_{n+1}) \tag{1.23}$$

is integrable all over the real phase space. Collinear initial-state singular configurations differ from soft and collinear final-state ones in the fact that they modified the momentum fraction x, carried by the incoming parton before entering the hard scattering process. This affects the way the *underlying Born* configuration is defined, i.e. the mapping

$$\tilde{\Phi}_{n+1} = \{\tilde{x};\tilde{k}_1,\ldots,\tilde{k}_{n+1}\} \to \overline{\Phi}_n = \{\overline{x};\overline{k}_1,\ldots,\overline{k}_{n+1}\}\,. \tag{1.24}$$

In the case of soft and collinear final-state configurations, we have that

$$\tilde{x} = \overline{x}, \tag{1.25}$$

while for collinear initial-state configurations

$$\overline{x} < \tilde{x}. \tag{1.26}$$

Then, in the latter case, the *underlying Born* configuration is obtained

- by deleting the radiated collinear parton, and by replacing the momentum fraction of the initial-state radiating parton with its momentum fraction after radiation, Eq. (1.26).

After replacing whenever possible the singular regions with the corresponding underlying Born ones, the integral of the counterterms now reads

$$\sum_\alpha \int d\Phi_{n+1} f(\tilde{\Phi}_{n+1})[\mathcal{C}(\Phi_{n+1})\mathcal{O}_n(\overline{\Phi}_n)]_\alpha \tag{1.27}$$

We stress that we cannot make the replacement in the argument of f because of the presence of the collinear initial-state singular regions. We distinguish to cases: the soft plus final-state singular regions and the collinear initial-state one. In the former case, the condition in Eq. (1.25) allow us to make the identification

$$f(\tilde{\Phi}_{n+1}) = f(\overline{\Phi}_n)\,. \tag{1.28}$$

We then factor out the pdf f, so that we can introduce the integrated counterterms as in Eq. (1.15) and add it to the virtual contribution. In the collinear initial-state case, we cannot factor out the luminosity so easily because of Eq. (1.26). We consider the restriction of the integrals in Eq. (1.27) only to the case of collinear initial-state singular regions (IS) and we write

$$\begin{aligned}
&\left[\int d\Phi_{n+1} f(\tilde{\Phi}_{n+1})\mathcal{C}(\Phi_{n+1})\mathcal{O}_n(\overline{\Phi}_n)\right]_{\alpha\in IS} \\
&\qquad = \left[\int d\overline{\Phi}_n \mathcal{O}_n(\overline{\Phi}_n) \int d\Phi_{\text{rad}} f(\tilde{x})\mathcal{C}(\Phi_{n+1})\right]_{\alpha\in IS} \\
&\qquad = \left[\int d\overline{\Phi}_n \mathcal{O}_n(\overline{\Phi}_n)\frac{dz}{z} f\left(\frac{\overline{x}}{z}\right) \int d\Phi_{\text{rad}} \mathcal{C}(\Phi_{n+1}))z\delta\left(z-\frac{\overline{x}}{\tilde{x}}\right)\right]_{\alpha\in IS} \\
&\qquad \equiv \left[\int d\overline{\Phi}_n \frac{dz}{z} f\left(\frac{\overline{x}}{z}\right) \mathcal{O}_n(\overline{\Phi}_n)\overline{C}(\overline{\Phi},z)\right]_{\alpha\in IS}\,,
\end{aligned} \tag{1.29}$$

where in the last step we have introduced the z dependent integrated counterterms

$$\left[\overline{C}(\overline{\Phi},z) = \int d\Phi_{\text{rad}} \mathcal{C}(\Phi_{n+1}))z\delta\left(z-\frac{\overline{x}}{\tilde{x}}\right)\right]_{\alpha\in IS}\,. \tag{1.30}$$

In order to disentangle the pdf from the integration of the counterterms over the radiation phase space, we have introduced the extra integration in the momentum fraction z. The resulting integral has a different structure and cannot be combined to the virtual contribution, so that it seems that in this case the cancellation of the IR divergences does not occur. This result is not unexpected and it signals the failure of the naive parton model [70]. We recall that the cancellation of the IR divergences requires a sufficient level of inclusiveness in the particle configuration. In the case of collinear initial-state radiation, where the parton momentum xP_1 is further reduced by some factor z, the hard scattering process is effectively initiated by the momentum zxP_1 with a weight depending on z non-trivially. Since in this case, we are not fully inclusive on the z variable, the IR singularities from collinear initial-state radiation remain after summing virtual and real corrections. The cure to this issue is provided by *factorization* which allows to absorb the collinear initial-state singularities in re-definition of the pdf beyond the leading order. This procedure effectively separates the long-distance physics effects caused by the collinear initial-state emissions, considered part of the definition of the hadron, from the short distance physics going on in the hard scattering process. Within the subtraction formalism, this can be formally taken into account by

- interpreting the pdf f as "redifined pdf"
- introducing an additional collinear counterterm which subtracts the collinear initial-state divergence:
$$\int d\overline{\Phi}_n \frac{dz}{z} \mathcal{O}(\overline{\Phi}_n) \mathcal{G}_0(\overline{\Phi}_n, z) \,. \tag{1.31}$$

Then, as a result of the factorization, the combination of this new contribution with the collinear initial-state integrated counterterms has the form

$$\mathcal{G}_0(\overline{\Phi}_n, z) + \sum_{\alpha \in IS} \overline{C}^{\alpha}(\overline{\Phi}_n, z) = \mathcal{G}(\overline{\Phi}_n, z) + \delta(1-z)\mathcal{G}^{\text{div}}(\overline{\Phi}_n) \tag{1.32}$$

where the function $\mathcal{G}(\overline{\Phi}_n, z)$ is finite in $D = 4$ dimensions while $\mathcal{G}^{\text{div}}(\overline{\Phi}_n)$ contains a pole in ϵ of soft origin. The latter term is combined with the virtual contribution and the soft + collinear final-state integrated counterterms (that we denote as S+FS). In the resulting quantity

$$\mathcal{V}(\Phi_n) + \left[\sum_{\alpha \in S+FS} \overline{C}^{(\alpha)}(\overline{\Phi}_n) + \mathcal{G}^{\text{div}}(\overline{\Phi}_n) \right]_{\overline{\Phi}_n = \Phi_n} \equiv V(\Phi_n) \tag{1.33}$$

all the poles in ϵ analytically cancel. Finally, we get the master formula of the subtraction method with an identified hadron in the initial state

$$\begin{aligned} \langle \mathcal{O} \rangle = & \int d\Phi_n \mathcal{O}_n(\Phi_n) [\mathcal{B}(\Phi_n) + V(\Phi_n)] + \int d\overline{\Phi}_n \frac{dz}{z} \mathcal{O}(\overline{\Phi}_n) \mathcal{G}(\overline{\Phi}_n, z) \\ & + \int d\Phi_{n+1} \left\{ \mathcal{O}(\Phi_{n+1}) \mathcal{R}(\Phi_{n+1}) - \sum_{\alpha} [\mathcal{O}(\overline{\Phi}_n) C(\Phi_{n+1})]_{\alpha} \right\} , \end{aligned} \tag{1.34}$$

which is now suited to be integrated numerically, since all the integrals that appear in it are finite and can be evaluated in 4 dimensions.

1.2 FKS Subtraction method

The basic assumption of the Frixione-Kunszt-Signer (FKS) subtraction formalism [22–24] subtraction method is that in each singular region there is at most one collinear and one soft singularity associated with one parton, called the FKS parton. This is accomplished by means of a set of non-negative projection functions $\mathcal{S}_{ij}$

$$\sum_{ij} \mathcal{S}_{ij} = 1. \tag{1.35}$$

They are associated to regions in which a final-state parton, labeled with i, becomes collinear and/or soft to an other final-state parton, labeled with j. They are defined by the following list of properties ([24])

$$\lim_{k_m^0 \to 0} \sum_j \mathcal{S}_{ij} = \delta_{im}, \tag{1.36}$$

$$\lim_{\vec{k}_m \| \vec{k}_l} (\mathcal{S}_{ij} + \mathcal{S}_{ji}) = \delta_{im}\delta_{jl} + \delta_{il}\delta_{jm}, \tag{1.37}$$

$$\tag{1.38}$$

With the help of the unitary relation Eq. (1.35), the real contributions $\mathcal{R}$ can be decomposed as

$$\mathcal{R} = \sum_{ij} \mathcal{R}_{ij}, \quad \mathcal{R}_{ij} = \mathcal{S}_{ij}\mathcal{R}. \tag{1.39}$$

The divergent contribution of the $\mathcal{R}_{ij}$ comes only from the region in which the parton i becomes collinear or soft to the j parton (FSR radiation). We observe that in this way one have to deal with just a well defined divergent structure resulting in a great simplification of the corresponding construction of the counterterms to be subtracted as it will be shown in the next section.

For the sake of completeness, we report also an actual implementation of the projection functions, given in [24]. We start defining a set of functions d_{ij} each one vanishes only in correspondence of a particular singular region. In the c.m. frame they are defined as:

$$d_{ij} = (E_j E_i)^a \, (1 - \cos\vartheta_i j)^b, \tag{1.40}$$

where ϑ_{ij} is the angle between $\vec{k}_i$ and $\vec{k}_j$, and a and b are positive arbitrary real numbers. Then, introducing the quantity

$$\mathcal{D} = \sum_{ij} \frac{1}{d_{ij}}, \tag{1.41}$$

the $\mathcal{S}$-functions are given by

$$\mathcal{S}_{ij} = \frac{1}{\mathcal{D} d_{ij}} h\left(\frac{E_i}{E_i + E_j}\right), \tag{1.42}$$

where the function $h(z)$ satisfies the properties

$$\lim_{z\to 0} h(z) = 1, \quad \lim_{z\to 1} h(z) = 0, \quad h(z) + h(1-z) = 1. \tag{1.43}$$

A possible choice is

$$h(z) = \frac{(1-z)^c}{z^c + (1-z)^c}, \tag{1.44}$$

where c is a positive arbitrary real number.

1.2.1 The real counterterms

The subtraction formalism is implemented in a natural way if one adopt the plus distribution prescription that is at the basis of the FKS subtraction method. In what follows, we will show in details how this works.

Let us start from the phase space element of the emitted parton in the real $(n+1)$-kinematics, that is denoted as the FKS parton; according to the dimensional regularization approach we have adopted, we write it down in D dimensions as:

$$\frac{d^{D-1}k}{2k_0(2\pi)^{D-1}} = \frac{dk_1dk_2d^{D-3}k_\perp}{2k_0(2\pi)^{D-1}} = \frac{dk_1dk_2k_\perp^{d-4}dk_\perp\Omega^{D-3}}{2k_0(2\pi)^{D-1}}, \tag{1.45}$$

where in the last step we have parametrized the $(D-3)$-dimensional space in spherical coordinates, with $k_\perp > 0$ as radius and Ω^{D-3} represents the result of the angular integral in the $D-3$-space. The reason of the above parametrization is easily understood if one consider the physical limiting case $D=4$, where the tri-impulse of the FKS parton is given in terms of its components in the k_1k_2-plane and the magnitude of the component perpendicular to this plane, since its versus does not matter for symmetry reason and we have summed over the two possibilities. We recall the result for the total solid angle in a a-dimensional space:

$$\Omega^a = \frac{2\pi^{a/2}}{\Gamma\left(\frac{a}{2}\right)} = \frac{2^a\pi^{a/2}}{\sqrt{\pi}\Gamma(a)}\Gamma\left(\frac{1+a}{2}\right), \tag{1.46}$$

where in the last step the duplication property of the gamma function has been used

$$\Gamma(z)\Gamma\left(z+\frac{1}{2}\right) = 2^{1-2z}\sqrt{\pi}\Gamma(2z). \tag{1.47}$$

For $D = 4-2\epsilon$ dimension we get

$$d^{D-1}k = dk_1dk_2k_\perp^{-2\epsilon}\frac{2(4\pi)^{-\epsilon}\Gamma(1-\epsilon)}{\Gamma(1-2\epsilon)} \tag{1.48}$$

Since we are interested in the singular limits, i.e. when the FKS parton becomes soft or collinear to the emitter (if the latter is massless too), we change coordinates to spherical coordinates, assuming that the polar angle ϑ is defined with respect to the direction of the emitter parton

$$k_1 = k_0\cos\vartheta, \quad k_2 = k_0\sin\vartheta\cos\phi, \quad k_\perp = k_0\sin\vartheta\sin\phi, \tag{1.49}$$

Note that $0 < \phi < \pi$, according to the constraint $k_\perp > 0$; there is still a freedom in the choice of its reference direction, being it not fixed by any singularities. In this parametrization, $k^0 \to 0$ and $y \equiv \cos\vartheta \to 1$ represent respectively the soft and collinear limits. Taking into account the Jacobian of the transformation

$$\left|\frac{\partial(k_1,k_2,k_\perp)}{\partial(k_0,y,\phi)}\right| = k_0^2 \tag{1.50}$$

the radiation phase space element becomes

$$\frac{d^{D-1}k}{2k_0(2\pi)^{D-1}} = \frac{\pi^\epsilon\Gamma(1-\epsilon)}{\Gamma(1-2\epsilon)}\frac{1}{(2\pi)^3}k_0^{1-2\epsilon}(\sin\vartheta\sin\phi)^{-2\epsilon}dk_0dyd\phi \tag{1.51}$$

We adopt the common practice choice to use the dimensionless energy fraction defined by the relation

$$k_0 = \xi\frac{\sqrt{s}}{2}, \tag{1.52}$$

and we factor out the overall normalization factor $\mathcal{N}$

$$\mathcal{N} = (4\pi)^\epsilon r_\Gamma, \quad r_\Gamma = \frac{\Gamma^2(1-\epsilon)\Gamma(1+\epsilon)}{\Gamma(1-2\epsilon)} = \frac{1}{\Gamma(1-\epsilon)} + O(\epsilon^3), \tag{1.53}$$

as it is usually done in the computation of the virtual one-loop contributions. Since

$$\frac{\Gamma^2(1-\epsilon)}{\Gamma(1-2\epsilon)} = 1 - \frac{\pi^2}{6}\epsilon^2 + O(\epsilon^3), \tag{1.54}$$

we get

$$\frac{d^{D-1}k}{2k_0(2\pi)^{D-1}} = \mathcal{N}\left[1 - \frac{\pi^2}{6}\epsilon^2 + O(\epsilon^3)\right]\frac{1}{(2\pi)^3}s^{-\epsilon}\frac{s}{4}\xi^{1-2\epsilon}(\sin\vartheta\sin\phi)^{-2\epsilon}d\xi dy d\phi. \tag{1.55}$$

According to the FKS construction, each of the $\mathcal{R}^{(\alpha)}$ contains just one singular soft and/or collinear region. We focus on one of these contributions, referred simply as $\mathcal{R}$, omitting the α index. Since the structure of the soft and collinear singularities are universal, the quantity $\xi^2(1-y)\mathcal{R}$ is free from divergences and regular for $\xi \to 0$ and $y \to 1$. We rewrite the contribution in the polar angle to the integral as

$$\int_{-1}^{1} dy(\sin\vartheta)^{-2\epsilon} = \int_{-1}^{1} dy(1-y^2)^{-\epsilon} = \int_{-1}^{1} dy(1-y)^{-\epsilon}(1+y)^{-\epsilon} \tag{1.56}$$

so that the singular part of the integration is proportional to

$$\int_{-1}^{1} dy(1-y)^{-1-\epsilon}\int_0^1 d\xi\xi^{-1-2\epsilon}[\xi^2(1-y)\mathcal{R}]. \tag{1.57}$$

To deal with these singularities, we consider $(1-y)^{-1-\epsilon}$ and $\xi^{-1-2\epsilon}$ as distributions and expand them around $\epsilon = 0$. At this scope, we use the usual trick of subtracting the value of the function to which the distribution is applied at the singular point in order to get an integrable quantity, which means to subtract a delta function; for example we have:

$$\begin{aligned}\int_0^1 d\xi f(\xi)\xi^{-1-2\epsilon} &= \int_0^1 d\xi[f(\xi) - f(0)\Theta(\xi_c - \xi)]\xi^{-1-2\epsilon} + f(0)\int_0^{\xi_c} d\xi\xi^{-1-2\epsilon}\\ &= \int_0^1 d\xi[f(\xi) - f(0)\Theta(\xi_c - \xi)]\left(\frac{1}{\xi} - 2\epsilon\frac{\log\xi}{\xi} + O(\epsilon^2)\right)\\ &\qquad - \frac{\xi_c^{-2\epsilon}}{2\epsilon}\int_0^1 f(\xi)\delta(\xi)\end{aligned} \tag{1.58}$$

from which we get the identity

$$\xi^{-1-2\epsilon} = -\frac{\xi_c^{-2\epsilon}}{2\epsilon}\delta(\xi) + \left(\frac{1}{\xi}\right)_{\xi_c} - 2\epsilon\left(\frac{\log\xi}{\xi}\right)_{\xi_c} + O(\epsilon^2). \tag{1.59}$$

The Heaviside Θ-function limits the range of integration for the subtracted term to the interval $[0, \xi_c]$ resulting in a generalized plus-prescription distribution

$$\int_0^1 d\xi f(\xi) \left(\frac{1}{\xi}\right)_{\xi_c} = \int_0^1 d\xi \frac{f(\xi) - f(0)\Theta(\xi_c - \xi)}{\xi}, \tag{1.60}$$

$$\int_0^1 d\xi f(\xi) \left(\frac{\log \xi}{\xi}\right)_{\xi_c} = \int_0^1 d\xi [f(\xi) - f(0)\Theta(\xi_c - \xi)] \frac{\log(\xi)}{\xi}. \tag{1.61}$$

Analogously, we obtain the other expansion

$$(1-y)^{-1-\epsilon} = -\frac{2^{-\epsilon}}{\epsilon}\delta(1-y) + \left(\frac{1}{1-y}\right)_\delta + O(\epsilon), \tag{1.62}$$

where

$$\int_{-1}^1 dy f(y) \left(\frac{1}{1-y}\right)_\delta = \int_{-1}^1 dy \frac{f(y) - f(1)\Theta(y - 1 + \delta)}{1-y}. \tag{1.63}$$

In this general formulation, there is a freedom in the choice of the parameters, $0 < \xi_c < 1$ and $0 < \delta < 2$, that can be exploit to increase the numerical efficiency.

Inserting the above expansions in Eq. (1.57), and denoting the regular term $[\xi^2(1-y)\mathcal{R}]$ as $f(\xi, y)$, we get the decomposition

$$\begin{aligned} \int_{-1}^1 dy (1-y)^{-1-\epsilon} \int_0^1 d\xi \xi^{-1-2\epsilon} f(\xi, y) &= -\frac{\xi_c^{-2\epsilon}}{2\epsilon} \int_{-1}^1 dy (1-y)^{-1-\epsilon} f(0, y) \\ &- \int_0^1 d\xi \left[\frac{2^{-\epsilon}}{\epsilon}\left(\frac{1}{\xi}\right)_{\xi_c} - 2\left(\frac{\log \xi}{\xi}\right)_{\xi_c}\right] f(\xi, 1) \\ &+ \int_{-1}^1 dy \int_0^1 d\xi \left(\frac{1}{1-y}\right)_\delta \left(\frac{1}{\xi}\right)_{\xi_c} f(\xi, y) + O(\epsilon). \end{aligned} \tag{1.64}$$

The first two terms can be integrated analytically over the full radiation variables giving raise to contributions with the same structure of the virtual term to which they will be combined. In this way, the singular parts cancels each other so that we get a finite contribution, that is we have found a possible choice of the real counterterms. The first term, proportional to $\delta(\xi)$, corresponds to the soft limit; we remark that, in order to calculate $\xi^2(1-y)\mathcal{R}$ in this limit, it is not necessary to evaluate the full real matrix element squared in D-dimension since it can be obtained applying the eikonal approximation for the soft gluon emission. Analogously, the second term corresponds to the collinear limit; also in this case, it is possible to extract the function $f(\xi, 1)$ without calculate the full real contribution in D-dimension. In the last term, the two distributions act over the regular function $f(\xi, y)$ so that it produces a finite result and we can interpret it as the contribution to R (see Eq. (1.18)):

$$\int_{-1}^1 dy \int_0^1 d\xi \left(\frac{1}{1-y}\right)_\delta \left(\frac{1}{\xi}\right)_{\xi_c} [\xi^2(1-y)\mathcal{R}] = \int_{-1}^1 dy \int_0^1 d\xi \xi R \tag{1.65}$$

with

$$R = \frac{1}{\xi}\left[\xi^2(1-y)\mathcal{R}\right] \tag{1.66}$$

and we can restrict ourselves to evaluate the integrand and to perform the integration in 4-dimensions. We emphasize that the integration limits can be in general different from that shown in Eq. (1.65), as they depend upon the particular form of the parametrization of the real phase space given by the radiation variables. We will show in Sec. 1.3 that the radiation phase space has the form

$$-1 \leq y \leq 1, \qquad 0 \leq \xi \leq X(y) \tag{1.67}$$

with an y-dependent upper bound for the ξ variable.

1.3 The FKS mapping for the massive emitter case

Let us assume for definiteness to deal with a scattering process involving n partons in the final state at lowest order in perturbation theory.We adopt a notation similar to that of Sec.1.1: the generic point in the Born phase space (Born configuration) will be denoted with barred momenta

$$\overline{\Phi}_n = \{\overline{k}_1, \ldots, \overline{k}_n\}. \tag{1.68}$$

with the corresponding phase space volume element given by

$$d\overline{\Phi}_n = \prod_{i=1}^{n} \frac{d^3\vec{\overline{k}}_i}{(2\pi)^3 2\overline{k}_i^0} (2\pi)^4 \delta^{(4)} \left(q - \sum_{i=1}^{n} \overline{k}_i \right), \tag{1.69}$$

where q is the total incoming 4-momentum.[2] At Next-to-Leading order (NLO), one must also include processes of emission of one more real massless extra parton, resulting in a $n+1$-body kinematics which we will denote as

$$\Phi_n = \{k_1, \ldots, k_{n+1}\}. \tag{1.70}$$

The singular regions of the real phase space are separated by means of suitable projection operators; in each of them, the radiated parton phase space is parametrized in terms of the FKS variables [22] (the notations $\vec{p}$ and $\underline{p}$ for a generic momentum p denote the tri-impulse and its modulus respectively)

$$\xi = \frac{2\underline{k}_{n+1}}{q^0}, \quad y = \frac{\vec{k}_n \cdot \vec{k}_{n+1}}{\underline{k}_n \underline{k}_{n+1}}, \tag{1.71}$$

as shown in Fig. 1.1, where we have assumed that the emitter and the FKS partons are respectively the n-th and the $n+1$-th parton. The rescaled energy ξ is related to the soft limit ($\xi \to 0$), and the variable y to the collinear one ($y \to \pm 1$). The kinematics is completed by specifying the azimuthal angle whose definition retains some degrees of arbitrariness. We adopt the definition in the `POWHEG` framework, which departs from the standard FKS one. It is taken as the polar angle of the splitting around the axis parallel to the momentum of the recoil system, in the rest frame where $q = (q^0, \vec{0})$.

In what follows, we will construct a one-to-one map from a real configuration with radiation variables (ξ, y, ϕ) into a Born one. This leads to a factorisation of the real phase space in term of Born and radiation variables.

The mapping can be reduced to the case of the map from a 3-body phase space into a 2-body one. Inserting into the $(n+1)$-body phase space volume element the identities

$$1 = \int d^4 k_{\rm rec} \delta^{(4)} \left(k_{\rm rec} - \sum_{i=1}^{n-1} k_i \right) \tag{1.72}$$

[2]The system we are considering can be either the full final state, or the system of decay products of a resonance, according to the origin of the heavy quark.

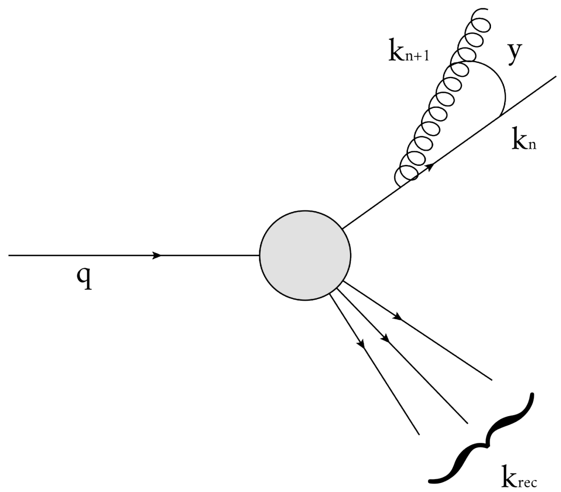

FIGURE 1.1: Kinematics for a real configuration: k_n is the massive emitter, k_{n+1} is the radiated parton. y denotes the cosine of the angle between the two tri-vectors.

and

$$1 = \int \mathrm{d}M_{\mathrm{rec}}^2 \delta(M_{\mathrm{rec}}^2 - k_{rec}^2), \tag{1.73}$$

the phase space is decomposed into a chain of two consecutive processes. With reference to Fig. 1.1, they are: the decay of a particle with momentum q into the 3-body system formed by the emitter k_n, the FKS-parton k_{n+1} and the "recoil" system, with momentum and invariant mass

$$k_{\mathrm{rec}} = \sum_{i=1}^{n-1} k_i = q - k_n - k_{n+1}, \quad M_{\mathrm{rec}}^2 = k_{\mathrm{rec}}^2, \tag{1.74}$$

followed by the decay of the latter into the other $n-1$ particles. In formula, we have

$$\mathrm{d}\Phi_{n+1} = \mathrm{d}\Phi_3 \mathrm{d}\Phi_{\mathrm{rec}}, \tag{1.75}$$

where

$$\mathrm{d}\Phi_3 = \frac{\mathrm{d}M_{\mathrm{rec}}^2}{2\pi} \frac{\mathrm{d}^3\vec{k}_n}{2k_n^0(2\pi)^3} \frac{\mathrm{d}^3\vec{k}_{n+1}}{2k_{n+1}^0(2\pi)^3} \frac{\mathrm{d}^3\vec{k}_{\mathrm{rec}}}{2k_{\mathrm{rec}}^0(2\pi)^3} \times (2\pi)^4 \delta^{(4)}(q - k_n - k_{n+1} - k_{\mathrm{rec}}), \tag{1.76}$$

$$\mathrm{d}\Phi_{\mathrm{rec}} = \prod_{i=1}^{n-1} \frac{\mathrm{d}^3\vec{k}_i}{2k_i^0(2\pi)^3} (2\pi)^4 \delta^{(4)} \left(k_{\mathrm{rec}} - \sum_{i=1}^{n-1} k_i \right). \tag{1.77}$$

We now focus on the 3-body process; under the action of the mapping, the k_n and k_{n+1} partons will be replaced by a single parton with mass m and momentum $\bar{k}_n$. We define

$$k \equiv k_n + k_{n+1}, \tag{1.78}$$

so that

$$k_{\mathrm{rec}} = q - k \implies k_{\mathrm{rec}}^0 = q^0 - k^0, \vec{k}_{\mathrm{rec}} = -\vec{k}. \tag{1.79}$$

We fix the transformation by demanding $\vec{\bar{k}}_n \parallel \vec{k}$. Care must be taken to ensure the conservation of energy-momentum also for the resulting Born configuration. This is accomplished by performing a boost Λ in the direction $\vec{k}$ and defining

$$\bar{k}_n = q - \Lambda k_{\rm rec}, \tag{1.80}$$

We determine the velocity parameter β of the boost transformation from the mass-shell condition

$$\bar{k}_n^2 = (q - \Lambda k_{\rm rec})^2 = m^2. \tag{1.81}$$

We get

$$\beta = \frac{-4\underline{k}_{\rm rec} k^0_{\rm rec} q^2}{(q^2 - m^2 + M^2_{\rm rec})^2 + 4\underline{k}^2_{\rm rec} q^2} + \frac{(q^2 - m^2 + M^2_{\rm rec})\sqrt{(q^2 - m^2 + M^2_{\rm rec})^2 - 4M^2_{\rm rec} q^2}}{(q^2 - m^2 + M^2_{\rm rec})^2 + 4\underline{k}^2_{\rm rec} q^2}. \tag{1.82}$$

We define the other barred variables as

$$\bar{k}_i = \Lambda k_i, \quad i = 1, \ldots, n-1. \tag{1.83}$$

Their mass relations are preserved by the boost transformation and, furthermore, we have

$$\sum_{i=1}^{n} \bar{k}_i = \sum_{i=1}^{n-1} \bar{k}_i + \bar{k}_n = q + \sum_{i=1}^{n-1} \Lambda k_i - \Lambda k_{\rm rec} = q + \Lambda\left(\sum_{i}^{n-1} k_i - k_{\rm rec}\right) = q, \tag{1.84}$$

which is the energy-momentum conservation for the Born configuration.

1.3.1 Inverse map

We now detail the construction of the inverse map, which is what is actually needed in the applications. Suppose that a Born event has been generated, i.e. the barred variables $\bar{k}_i$ $(i = 1, \cdots, n)$ are given. Then, $M^2_{\rm rec}$ is obtained inverting Eq. (1.80):

$$M^2_{\rm rec} = (\Lambda k_{\rm rec})^2 = (q - \bar{k}_n)^2 = q^2 + m^2 - 2q^0 \bar{k}^0_n. \tag{1.85}$$

We want to attach to it a radiation described by the radiation variables ξ, y and ϕ. For future convenience we introduce the largest allowed value for ξ

$$\xi_{\max} \equiv 1 - \frac{(m + M_{\rm rec})^2}{q^2}. \tag{1.86}$$

The energy of the radiated parton is

$$k^0_{n+1} = \underline{k}_{n+1} = \frac{q^0}{2}\xi. \tag{1.87}$$

Energy conservation requires that

$$q^0 = k^0_{n+1} + \sqrt{\underline{k}_n^2 + m^2} + \sqrt{\underline{k}^2_{\rm rec} + M^2_{\rm rec}}, \tag{1.88}$$

where

$$\underline{k}^2_{\rm rec} = \underline{k}_n^2 + \underline{k}^2_{n+1} + 2\underline{k}_n \underline{k}_{n+1} y. \tag{1.89}$$

We can solve equation (1.88) for $\underline{k}_n$ in a standard way, by bringing in turn each single square root on one side of the equation and squaring both sides. By doing this we actually find the solutions of all of the following equations

$$q^0 = k^0_{n+1} \pm \sqrt{\underline{k}_n^2 + m^2} \pm \sqrt{\underline{k}_{\mathrm{rec}}^2 + M_{\mathrm{rec}}^2}, \tag{1.90}$$

for all possible combinations of the signs in front of the square root. The solutions are given by

$$\underline{k}_n^{(\pm)} = \frac{-(2\bar{k}_n^0 - q^0\xi)\xi y}{(2-\xi)^2 - \xi^2 y^2} \pm \frac{(2-\xi)\sqrt{(2\bar{k}_n^0 - q^0\xi)^2 - m^2\xi^2(1-y^2) - 4m^2(1-\xi)}}{(2-\xi)^2 - \xi^2 y^2}. \tag{1.91}$$

In order for them to exist, the argument of the square root must be positive. This leads to the bound

$$(q^2 - m^2 + m^2 y^2)\xi^2 - 4(q^0\bar{k}_n^0 - m^2)\xi + 4\underline{\bar{k}}_n^2 > 0, \tag{1.92}$$

with $\underline{\bar{k}}_n^2 = (\bar{k}_n^0)^2 - m^2$. Eq.(1.92) is satisfied if either $\xi > \xi^{(+)}(y)$ or $\xi < \xi^{(-)}(y)$, with

$$\begin{aligned}\xi^{(\pm)}(y) &= 2\frac{\bar{k}_n^0 q^0 - m^2 \pm m\sqrt{(q^0 - \bar{k}_n^0)^2 - \underline{\bar{k}}_n^2 y^2}}{q^2 - m^2 + m^2 y^2} \\ &= \frac{q^2 - m^2 - M_{\mathrm{rec}}^2 \pm 2m\sqrt{M_{\mathrm{rec}}^2 + \underline{\bar{k}}_n^2(1-y^2)}}{q^2 - m^2 + m^2 y^2} \\ &= \frac{4\underline{\bar{k}}_n^2}{q^2 - m^2 - M_{\mathrm{rec}}^2 \mp 2m\sqrt{M_{\mathrm{rec}}^2 + \underline{\bar{k}}_n^2(1-y^2)}}. \end{aligned} \tag{1.93}$$

The last equality follows from the fact that

$$\xi^{(+)}\xi^{(-)} = \frac{4\underline{\bar{k}}_n^2}{q^2 - m^2 + m^2 y^2}. \tag{1.94}$$

We see that $\xi^{(+)}$ is a decreasing function of y^2. Thus

$$\xi^{(+)}(y) > \xi^{(+)}(1) = 1 - \frac{(m - M_{\mathrm{rec}})^2}{q^2} > \xi_{\max}. \tag{1.95}$$

that is larger than the maximum value allowed by energy conservation. Thus, the corresponding $\underline{k}_n^{(\pm)}$ values should be the solutions of one among equations (1.90) where some minus signs appear. On the other hand, $\xi^{(-)}(y)$ is an increasing function of y^2, so

$$\xi^{(-)}(y) < \xi^{(-)}(1) = 1 - \frac{(m + M_{\mathrm{rec}})^2}{q^2}, \tag{1.96}$$

that is perfectly acceptable. Furthermore, in the $\xi < \xi^{(-)}(y)$ case the value $\xi = 0$ is allowed, that lead to the solutions $\underline{k}_n^{(\pm)} = \pm\underline{\bar{k}}_n^0$ satisfying Eq. (1.88) with the correct signs of the square roots. Since the $\underline{k}_n^{(\pm)}$ must always satisfy one of the equations (1.90), and since they are smooth function of both ξ and y in their allowed range (that includes the $\xi = 0$ point), we infer by continuity that they satisfy equation (1.90).

Up to now we have not imposed the positivity of $\underline{k}_n$. On the other hand, negative $\underline{k}_n$ values still have a physical interpretation, as illustrated in Fig. 1.2. Thus, provided we interpret negative values of $\underline{k}_n$ according to the construction of Fig. 1.2, we have two solutions of

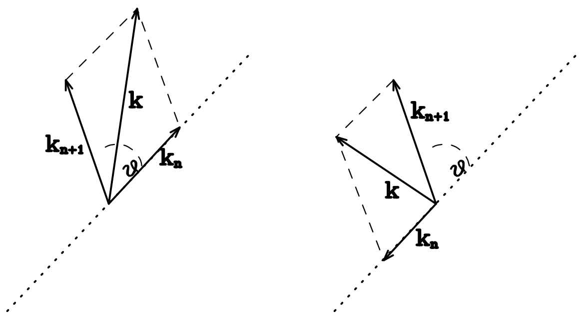

FIGURE 1.2: Kinematic reconstruction of the real emission kinematics with positive (left) and negative $\underline{k}_n$ values. The angle θ is fixed by $y = \cos\theta$.

equation (1.88). They are however related, since

$$\underline{k}_n^{(+)}(\xi, y) = -\underline{k}_n^{(-)}(\xi, -y). \tag{1.97}$$

If we pick just one of them, we have a single-value map from the underlying Born configuration and the radiation variables ξ, y and ϕ to a real emission configuration. We pick the solution $\underline{k}_n^{(+)}(\xi, y)$, since for $m = 0$ it corresponds to the usual solution in the massless case. Unlike in the massless case, however, $\underline{k}_n^{(+)}(\xi, y)$ is not always positive: it is negative in the region

$$y > 0\,, \quad \xi > \xi^{(-)}(0) = 2\frac{\overline{k}_n^0 - m}{q - m} = \frac{(q^0 - m)^2 - M_{rec}^2}{q^0\,(q^0 - m)}. \tag{1.98}$$

For continuity, $\underline{k}_n^{(+)}(\xi, y)$ vanishes on the boundary line $y > 0$, $\xi = \xi^{(-)}(0)$ separating the positive and negative regions. The points lying on this curve are degenerate and correspond to the same real configuration with the emitter at rest in the partonic centre-of-mass frame. Apart from them, that constitute a set of zero measure, the map is well defined and bijective. The inverse map is well defined also on the boundary line $y > 0$, $\xi = \xi^{(-)}(0)$. This means that the corresponding Jacobian vanishes on that curve. Then, the inverse map can be safely used both for the integration of the real differential cross section and for the generation of radiation.
In Fig. 1.3 we display the ξ, y kinematic region. We remark that the negative $\underline{k}_n^{(+)}(\xi, y)$ region includes neither soft nor collinear singularities, since ξ is large, and since the angular separation of the quark and the radiated gluon is larger than $\pi/2$. From now on we will drop the suffix $(-)$ and will use $\xi(y)$ and $\xi(0)$ instead of $\xi^{(-)}(y)$ and $\xi^{(-)}(0)$.

In Fig. 1.4 we show the partition of the kinematic region represented in the more familiar Dalitz plane. Notice that in the massless limit the physical region in the Dalitz plot develops an acute angle in the lower right, corner corresponding to the gluon being anticollinear with the b quark. Thus, the problematic region $\xi > \xi(0)$ is not a singular one.

1.3.2 Full kinematic reconstruction of the real emission

So far, we have got the length of the tri-vectors $\vec{k}_n$ and $\vec{k}_{n+1}$. It is a standard kinematic problem to determine their directions in such a way that their sum $\vec{k}$ is parallel to $\vec{\overline{k}}_n$. We do not enter in further details about it.

The last step is to calculate the β parameter of the boost transformation Λ, Eq. (1.82), and to boost "back" the other barred momenta in the real event

$$k_i = \Lambda^{-1}\overline{k}_i, \quad i = 1, \cdots, n-1. \tag{1.99}$$

The above mapping allows us to write the $(n+1)$-body phase space element in the factorized form

$$d\Phi_{n+1} = d\Phi_{\rm rad} d\overline{\Phi}_n = J(\xi, y, \phi) d\xi dy d\phi d\overline{\Phi}_n, \tag{1.100}$$

where we have expressed the radiation phase space in terms of the FKS variables with the Jacobian function $J(\xi, y, \phi)$ taking into account the change of variables involved in the transformation. In order to extract the Jacobian, we have to manipulate and compare the l.h.s and the r.h.s of Eq. (1.100). Recalling Eq. (1.75), we perform the change of variables

$$\vec{k}_n \to \vec{k} - \vec{k}_{n+1} \tag{1.101}$$

in the three-body phase space, Eq. (1.76),

$$d\Phi_3 = \frac{dM_{\rm rec}^2}{2\pi} \frac{d^3\vec{k}}{2k_n^0(2\pi)^3} \frac{d^3\vec{k}_{n+1}}{2k_{n+1}^0(2\pi)^3} \frac{d^3\vec{k}_{\rm rec}}{2k_{\rm rec}^0(2\pi)^3} \times (2\pi)^4 \delta^{(4)}(q - k - k_{\rm rec})\,. \tag{1.102}$$

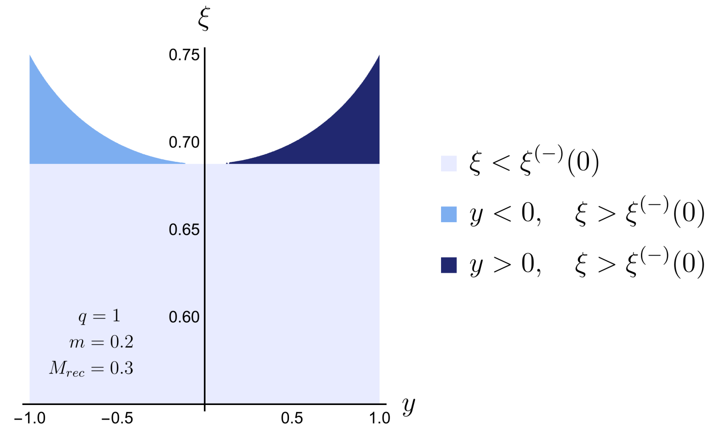

FIGURE 1.3: Plot of the physical region in the ξy plane. The shaded orange region is where $\underline{k}_n^{(+)}(\xi, y)$ is negative. It is physically equivalent to the (positive) $\underline{k}_n^{(-)}(\xi, -y)$ solution in the dark blue region. If we insisted upon considering only positive $\underline{k}_n$ solutions, the blue region would be doubly covered, and the dark blue one would not be there.

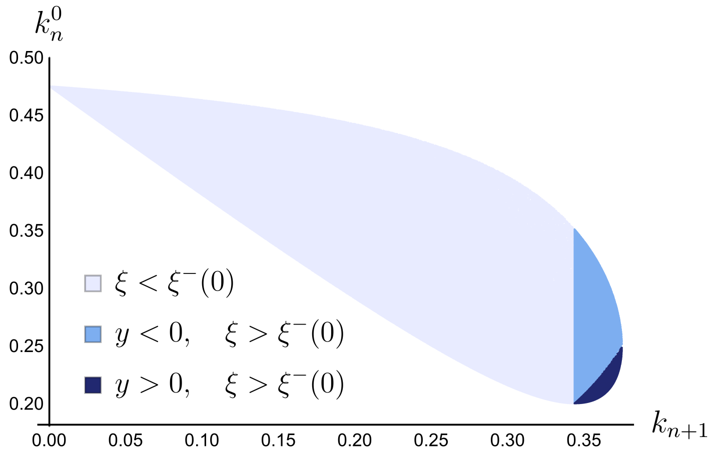

FIGURE 1.4: Dalitz plot for the three-body phase space of the system comprising the heavy flavour, the radiated gluon and the recoiling system.

In polar coordinates, we have

$$\mathrm{d}^3\vec{k} = \underline{k}^2 \mathrm{d}\underline{k}\mathrm{d}\Omega \tag{1.103}$$

and, using as reference direction that of $\vec{k}$,

$$\frac{\mathrm{d}^3\vec{k}_{n+1}}{2k^0_{n+1}(2\pi)^3} = \frac{q^2}{(4\pi)^3}\xi \mathrm{d}\xi \mathrm{d}\cos\alpha \mathrm{d}\phi\,, \tag{1.104}$$

where α is the angle between $\vec{k}_{n+1}$ and $\vec{k}$ and ϕ is the azimuthal angle taking $\vec{k}$ as the reference direction. Hence

$$\mathrm{d}\Phi_{n+1} = \frac{q^2}{(4\pi)^3}\xi \mathrm{d}\xi \mathrm{d}\cos\alpha \mathrm{d}\phi \frac{\underline{k}^2 \mathrm{d}\underline{k}\mathrm{d}\Omega}{2k^0_n(2\pi)^3}\frac{\mathrm{d}M^2_{\mathrm{rec}}}{2\pi} \times \frac{\mathrm{d}^3 k_{\mathrm{rec}}}{2k^0_{\mathrm{rec}}(2\pi)^3}(2\pi)^4\delta^{(4)}(q-k-k_{\mathrm{rec}})\mathrm{d}\Phi_{\mathrm{rec}}. \tag{1.105}$$

On the other hand, following the same arguments that led to Eq. (1.75), we can split the barred Born phase space into a two-body phase space and the phase space of the system recoiling against the emitting parton

$$\mathrm{d}\overline{\Phi}_n = \frac{\mathrm{d}\overline{M}^2_{\mathrm{rec}}}{2\pi}\frac{\mathrm{d}^3\vec{\overline{k}}_n}{2\overline{k}^0_n(2\pi)^3}\frac{\mathrm{d}^3\vec{\overline{k}}_{\mathrm{rec}}}{2\overline{k}^0_{\mathrm{rec}}(2\pi)^3} \times (2\pi)^4\delta^{(4)}(q-\overline{k}_n-\overline{k}_{\mathrm{rec}})\mathrm{d}\overline{\Phi}_{rec}. \tag{1.106}$$

Since $\overline{k}_n = q - \Lambda k_{\mathrm{rec}}$, the delta function in Eq. (1.106) constrains the value of $\overline{k}_{\mathrm{rec}}$ to be

$$\overline{k}_{\mathrm{rec}} = \Lambda k_{\mathrm{rec}}. \tag{1.107}$$

Then, exploiting the Lorentz invariance of the phase space element, we have

$$\frac{\mathrm{d}M^2_{\mathrm{rec}}}{2\pi}\frac{\mathrm{d}^3\vec{k}_{\mathrm{rec}}}{2k^0_{\mathrm{rec}}(2\pi)^3}(2\pi)^4\delta^{(4)}(q-k-k_{\mathrm{rec}})\mathrm{d}\Phi_{\mathrm{rec}} = \frac{\mathrm{d}\overline{M}^2_{\mathrm{rec}}}{2\pi}\frac{\mathrm{d}^3\vec{\overline{k}}_{\mathrm{rec}}}{2\overline{k}^0_{\mathrm{rec}}(2\pi)^3}(2\pi)^4\delta^{(4)}(q-\overline{k}_n-\overline{k}_{\mathrm{rec}})\mathrm{d}\overline{\Phi}_{\mathrm{rec}}, \tag{1.108}$$

where the r.h.s and the l.h.s are related by the boost transformation Λ. In particular, we observe that

$$\Lambda(q-k) = \Lambda k_{\mathrm{rec}} = q - \overline{k}_n, \tag{1.109}$$

so that the boost maps the argument of the delta function in the r.h.s into that of the delta function in the l.h.s. Inserting Eq.(1.105) and Eq.(1.106) into Eq.(1.100) and using Eq.(1.108), we get

$$\frac{q^2}{(4\pi)^3}\xi \mathrm{d}\xi\, \mathrm{d}\cos\alpha\, \mathrm{d}\phi \frac{\underline{k}^2 \mathrm{d}\underline{k}\mathrm{d}\Omega}{2k^0_n(2\pi)^3} = J(\xi,y,\phi)\mathrm{d}\xi\, \mathrm{d}y\, \mathrm{d}\phi \frac{\mathrm{d}^3\overline{k}_n}{2\overline{k}^0_n(2\pi)^3}. \tag{1.110}$$

By virtue of the mapping, the vectors $\vec{k}$ and $\vec{\overline{k}}_n$ are parallel so that in polar coordinates their angular elements are equal, $d\Omega = d\overline{\Omega}_n$. Then, from Eq. (1.110) we have

$$\frac{q^2}{(4\pi)^3}\xi\frac{\underline{k}^2}{k^0_n}\mathrm{d}\cos\alpha\, \mathrm{d}\underline{k} = J(\xi,y,\phi)\frac{\overline{\underline{k}}^2_n}{\overline{k}^0_n}\,\mathrm{d}y\, \mathrm{d}\overline{\underline{k}}_n. \tag{1.111}$$

and we are left with the computation of the Jacobian of the two-variable-transformation

$$J^{(2)} = \begin{vmatrix} \frac{\partial \bar{\underline{k}}_n}{\partial \underline{k}} & \frac{\partial y}{\partial \underline{k}} \\ \frac{\partial \bar{\underline{k}}_n}{\partial \cos\alpha} & \frac{\partial y}{\partial \cos\alpha} \end{vmatrix} . \tag{1.112}$$

This transformation is implicitly defined by the relations

$$\begin{aligned} \underline{k}_n &= \sqrt{\underline{k}^2 + \underline{k}_{n+1}^2 - 2\underline{k}\,\underline{k}_{n+1}\cos\alpha}, \quad & y &= \frac{\underline{k}^2 - \underline{k}_n^2 - \underline{k}_{n+1}^2}{2\underline{k}_n\,\underline{k}_{n+1}}, \\ M_{\mathrm{rec}}^2 &= (q^0 - k_n^0 - \underline{k}_{n+1})^2 - \underline{k}^2, \quad & \bar{\underline{k}}_n &= \frac{\lambda^{1/2}(q^2, M_{\mathrm{rec}}^2, m^2)}{2q^0}, \end{aligned} \tag{1.113}$$

where λ is the kinematic Kallen function:

$$\lambda(x, y, z) = x^2 + y^2 + z^2 - 2xy - 2xz - 2yz. \tag{1.114}$$

Applying the chain-rule for the derivative, it is straightforward to compute the Jacobian. We get

$$J^{(2)} = \frac{1}{\underline{k}_n^3} \frac{\underline{k}^2}{\bar{\underline{k}}_n} \frac{\bar{k}_n^0}{k_n^0} \left[k_n^0 (\bar{k}_n^0 - \underline{k}_{n+1}) - m^2 (1 - \underline{k}_{n+1}/q^0) \right] \tag{1.115}$$

The final expression for the full Jacobian J is thus

$$\begin{aligned} J(\xi, y, \phi) &= \frac{q^2}{(4\pi)^3} \xi \frac{\underline{k}_n^3}{\bar{\underline{k}}_n} \frac{1}{k_n^0 (\bar{k}_n^0 - \underline{k}_{n+1}) - m^2 (1 - \underline{k}_{n+1}/q^0)} \\ &= \frac{q^2}{(4\pi)^3} \xi \frac{\underline{k}_n^3}{\bar{\underline{k}}_n} \frac{2}{k_n^0 (2\bar{k}_n^0 - q^0 \xi) - m^2 (2 - \xi)} \end{aligned} \tag{1.116}$$

Note that the denominator of J vanishes in two regions:

- when approaching the curve $\xi = \xi(0)$ for $y > 0$, behaving as $\xi(0) - \xi$
- when approaching the curve $\xi = \xi(y)$, as $\sqrt{\xi(y) - \xi}$.

In the first case, the k_n^3 term in the numerator vanishes simultaneously as $(\xi(0) - \xi)^3$. It follows that the Jacobian vanishes as $J \sim (\xi(0) - \xi)^2$ for $\xi \to \xi(0)$ at fixed $y > 0$. This result is coherent with what has been argued above regarding the degenerate points corresponding to the configuration with the emitter parton at rest in the partonic centre-of-mass frame. In the second region, the Jacobian develops an integrable singularity, that can be dealt with by importance sampling techniques in Monte Carlo integration.

1.4 Application: heavy quark radiation in NLO+PS `POWHEG` generators

Having a mass much larger than the typical hadronic scales, bottom quark hadroproduction is calculable in perturbative QCD. Nonetheless, in cases when the transverse momentum involved in the production is large compared to its mass, as, for example, in high-energy e^+e^- annihilation, or in production at large transverse momentum in hadronic collisions, bottom can behave as a light parton, and give rise to a hadronic jet. Techniques for dealing with these regimes have been developed in the past [65], and have been applied to the LHC case [71]. They allow for the computation of the transverse momentum spectrum of promptly produced b quarks at next-to-leading order in QCD, including the resummation of large logarithms of the ratio of the transverse momentum over the bottom mass up to next-to-leading-logarithmic accuracy. These large logarithms can arise both from initial state radiation, when, for instance, an incoming gluon splits into a $b\bar{b}$ pair, with one of the b undergoing a large-momentum-transfer collision with a parton from the target, and from final state radiation. In the last case, an outgoing gluon can split into a $b\bar{b}$ pair, or a directly produced b quark can emit a collinear gluon.

In next-to-leading order (NLO) calculations matched to Shower generators (NLO+PS) for heavy flavour production [72, 73], one generally treats the heavy flavour as being very heavy. The heavy quark mass thus acts as a cut-off on collinear singularities, that are thus not resummed. This approach has in fact proven to be quite viable in heavy flavour production even at relatively large momentum transfer [71]. Consider, for example, heavy quark pair production in a POWHEG framework. By neglecting collinear singularities from heavy quarks, the only singular region that we have to consider has to do with initial state radiation involving only light partons. Since the POWHEG procedure guarantees that the matrix elements are given correctly for up to one hard radiation, gluon splitting, flavour excitation and radiation from the heavy flavour are included, so that the logarithmically enhanced terms are correctly reproduced at first order. Higher order leading logarithms, however, are not treated correctly. In particular, there are reasons to give an adequate treatment to final state radiation from a high transverse momentum bottom quark. In fact, this radiation process is intimately related to the physics of the bottom fragmentation function, and may have important effects in processes of considerable interest, like for example in top decay.

The purpose of the present work is twofold:

- we present a new algorithm, based on the massive FKS mapping developed in Sec. 1.3, for radiation from a heavy quark, that has proven superior to the available implementation [55] (Sec. 1.4.1);
- we perform a thorough investigation of the behaviour of this component of the POWHEG generator, also by comparing the two methods, both in the framework of bottom quarks generated in top decay, and in inclusive bottom quark pair production. In the last case, such a study was never carried out (Sec. 1.4.2).

1.4.1 Generation of radiation

We recall the POWHEG master formula for the generation of radiation [24, 74] is

$$d\sigma_{\rm NLO} = \overline{B}(\Phi_n)d\Phi_n\left[\Delta_{\rm NLO}(\Phi_n, t_{\rm min}) + \sum_\alpha \frac{\left[d\Phi_{\rm rad}\Delta_{\rm NLO}(\Phi_n, K_\perp(\Phi_{n+1}))R(\Phi_{n+1})\right]_\alpha^{\overline{\Phi}_n^\alpha=\Phi_n}}{B(\Phi_n)}\right], \tag{1.117}$$

where $t_{\rm min}$ is an infrared cutoff, and the NLO Sudakov form factor is given by

$$\Delta_{\rm NLO}(\Phi_n, p_T) = \theta(p_T - t_{\rm min})\exp\left[-\sum_\alpha\int\frac{\left[d\Phi_{\rm rad}R(\Phi_{n+1})\Theta(K_\perp(\Phi_{n+1}) - p_T)\right]_\alpha^{\overline{\Phi}_n^\alpha=\Phi_n}}{B(\Phi_n)}\right]. \tag{1.118}$$

In the case of a massless emitter, $K_\perp$ is a smooth function of the radiation variables, which is required to reduce to the transverse momentum in approaching the soft and collinear limits.

For the massive case, in ref. [55] the following definition was proposed

$$K_{\perp}^{2} = 2\frac{k^0}{p^0} p \cdot k = \frac{q^2}{2}\xi^2(1 - \beta y_{\text{phy}}). \tag{1.119}$$

y_{phy} denotes the cosine of the physical angle between the emitter and the emitted parton.[3] Eq. (1.119) has the remarkable property of reducing continuously to the transverse momentum in the massless limit. We assume it as our default scale choice.

According to the standard veto method, we look for a suitable upper bound function U of the integrand in the NLO Sudakov form factor, namely

$$U(\xi, y) d\xi dy \geq \frac{R}{B} J(\xi, y) d\xi dy. \tag{1.120}$$

For the sake of simplicity, we have omitted the integration on the azimuthal angle $d\phi$, which results in a constant 2π factor.
We model the upper bound function on the asymptotic singular behavior of the real matrix element near the soft and collinear singularities. We recall that the Jacobian of the mapping has a divergent behaviour near the curve $\xi = \bar{\xi}(y)$. The upper bound function should have a behaviour not weaker than the Jacobian near the singular regions, and furthermore, it should be simple enough to allow us to perform an analytical integration in the constrained radiation phase space given by the cut $K_T^2 > t$.
It is convenient to perform a change of integration variables from ξ, y to ξ, K_T^2. Indeed, it turns out that K_T^2 is a monotonic decreasing function of y at fixed ξ, i.e. $\partial K_T^2/\partial y < 0$.
The inversion of this mapping is too complex to be performed analytically,[4] but easy to perform numerically. We find that the associated Jacobian $\partial K_T^2/\partial y$ has a behaviour similar to that of the Jacobian of the mapping J:

$$\sim \quad \frac{1}{\sqrt{\bar{\xi}(y) - \xi}} \quad \text{when} \quad \xi \to \bar{\xi}(y); \tag{1.121}$$

$$\sim \quad (\bar{\xi}(0) - \xi)^2 \quad \text{when} \quad \xi \to \bar{\xi}(0) \quad \text{for} \quad y \geq 0. \tag{1.122}$$

We now write

$$U = \frac{\partial K_T^2}{\partial y} U', \tag{1.123}$$

so that in the new integration variables the integrand becomes U'

$$\int d\xi \, dy \, \Theta(K_T^2 - t) U = \int d\xi dK_T^2 \Theta(K_T^2 - t) U'. \tag{1.124}$$

U' must have a simple form, and must have the appropriate behaviour to act as an upper bound for the soft and collinear singularities of the real matrix element.

[3] y_{phy} must not be confused with the y variable of the mapping. More specifically, in the region $\bar{\xi}(0) \leq \xi \leq \xi_{\max}$, $y > 0$ we have $y_{\text{phy}} = -y$, while in all the remaining region $y_{\text{phy}} = y$.

[4] In fact, rather than proving analytically that K_T^2 is a monotonic decreasing function of y at fixed ξ, we demonstrated it numerically by checking it a large number of times for random values of the input parameters.

Upper bound function

The singular behaviour of the real matrix element squared is universal and can be extracted in a straightforward manner by means of the eikonal approximation. In terms of the radiation variables, we get

$$\frac{R}{B} \sim \frac{N}{\xi^2(1-\beta y_{\text{phy}})} = \frac{N}{K_T^2}, \tag{1.125}$$

with N a suitable normalization constant. On the other hand, in the soft limit, the Jacobian of the mapping behaves as

$$J(\xi, y) \sim N'\xi. \tag{1.126}$$

We must also take into account the behaviour in the soft limit of the Jacobian term factorized in U:

$$\frac{\partial K_T^2}{\partial y} \sim N''\xi^2. \tag{1.127}$$

Putting all the three contributions together, we obtain the following expression of the upper bound function U'

$$U'(\xi, K_T^2) = \frac{1}{K_T^2} \times \xi \times \frac{1}{\xi^2} = \frac{1}{\xi K_T^2}. \tag{1.128}$$

A more complete analysis shows that mapping J is enhanced (although not divergent) at large ξ for $y \to -1$. In order to get a more efficient upper bound, we add the factor $\frac{1}{1-K_T^2/q^2}$ to the previous expression. Hence, our final choice for the upper bound function U' is

$$U'(\xi, K_T^2) = \frac{1}{\xi K_T^2(1-K_T^2/q^2)}. \tag{1.129}$$

Integral of the upper bound function

In order to integrate the upper bound function analytically, its domain of integration has to be suitably enlarged. This can be done by interpreting the R/B expression as being defined in the larger domain, but as vanishing outside of the physical domain. Since the veto procedure prescribes that a point generated according to the upper bound function should be accepted with a probability proportional to the value of the radiation function divided by the upper bound function, points generated outside the physical domain should always be vetoed according to the above interpretation. From Eq. (1.119), we find the upper bound

$$K_T^2 < K_{\max}^2 \equiv \frac{q^2}{2}\xi_{\max}^2(1+\beta_0), \tag{1.130}$$

where β_0 is the velocity of the emitter in the underlying Born configuration (this follows from the fact that we always have $\beta \leq \beta_0$), and we also find

$$\frac{2K_T^2}{(1+\beta_0)} < \xi^2 < \frac{2K_T^2}{(1-\beta_0)}, \tag{1.131}$$

We thus take as our domain of integration the region in K_T and ξ such that eqs. (1.130) and (1.131) are satisfied. We notice that in this way ξ can even become larger than 1. In practice, however, adding also the $\xi < 1$ or $\xi < \xi_{\max}$ limit would render the integration more difficult, so we prefer to deal with it by vetoing. Defining

$$\xi_{\substack{M\\m}}(K_t^2) \equiv \sqrt{\frac{2K_T^2}{q^2(1\mp\beta_0)}}, \tag{1.132}$$

the integral of the upper bound function is then

$$I(t) = \int_t^{K^2_{\max}} \frac{dK_T^2}{K_T^2(1-K_T^2/q^2)} \int_{\xi_m(K_t^2)}^{\xi_M(K_t^2)} \frac{d\xi}{\xi} = \ln\left[\frac{K^2_{\rm max}}{q^2-K^2_{\rm max}}\frac{q^2-t}{t}\right] y_0, \tag{1.133}$$

where $y_0 \equiv (1/2)\ln[(1+\beta_0)/(1-\beta_0)]$ is the rapidity of the emitter in the underlying Born configuration. Given a number $0 < r < 1$, the t value generated by solving the equation $r = \exp[-2\pi N I(t)]$ is

$$t = \frac{A}{1+A}q^2, \quad A = \frac{K^2_{\rm max}}{q^2-K^2_{\rm max}} \exp\left[\frac{\log r}{2\pi N y_0}\right]. \tag{1.134}$$

Generation of radiation kinematics

The algorithm for generating the radiation variables proceeds as follows:

1. We set the initial scale $t_0 = K^2_{\rm max}$.
2. We generate a uniform random number

   $$0 < r < \exp[-2\pi N I(t_0)],$$

   and get t from Eq. (1.134). If t is below $t_{\rm min}$, no radiation is generated, and the event is emitted as is.
3. We pick a new uniform random number $0 < r' < 1$ and we generate a value for ξ as

   $$\xi = \xi_{\rm m}(t)\exp(y_0 r'). \tag{1.135}$$

   This is consistent with the distribution of ξ at fixed K_T^2 according to Eq. (1.133).
4. If $\xi > \xi_{\rm max}$, we set $t_0 = t$, and go back to the step 2.
5. If the veto condition is passed, given t and ξ, we solve numerically for y the implicit equation

   $$K_T^2(\xi, y) = t. \tag{1.136}$$

   If a solution does not exist, we set $t = t_0$ and go back to step 2.
6. Now that ξ and y are available, we generate a random ϕ, and compute the ratio $R = [R/BJ(\xi,y)]/U(\xi,y)]$, with U given in terms of U' in Eq. (1.123), and generate a new random number $0 < r''' < 1$. If $r''' > R$ we set $t_0 = t$ and go back to the step 2. Otherwise, the event is accepted.

1.4.2 Phenomenology

Comparison in the `bb4l` case

We have compared results obtained with the new method presented here, with those obtained with the default `POWHEG` settings for the `bb4l` generator of ref. [75]. We found remarkable agreement between the two results for all the distributions that we have examined. Here we show only two of them, to convey the idea of the quality of the agreement. These results were obtained for the 8TeV LHC collider, using the MSTW2008 PDF [76] set for reference only (other sets could be used as well [77, 78]). In our simulations we make the B hadrons stable. Jets are reconstructed using the Fastjet [79] implementation of the anti-$k_{\rm T}$ algorithm [80] with $R = 0.5$. We denote as B ($\bar{B}$) the hardest (i.e. largest $p_{\rm T}$) b ($\bar{b}$) flavoured hadron. The B ($\bar{B}$) jet j_B ($j_{\bar{B}}$) is defined to be the jet that contains the hardest B ($\bar{B}$). We discard events where the j_B and $j_{\bar{B}}$ coincide. The hardest e^+ (μ^-) and the hardest ν_e ($\bar{\nu}_\mu$) are paired to reconstruct the W^+ (W^-). The reconstructed top (antitop) quark is identified with the corresponding $W^+ j_B$ ($W^- j_{\bar{B}}$) pair. We show the invariant mass of the $W - b$-jet system (Fig. 1.5) and the B fragmentation function in top decay (Fig. 1.6), as defined in ref. [75], i.e.

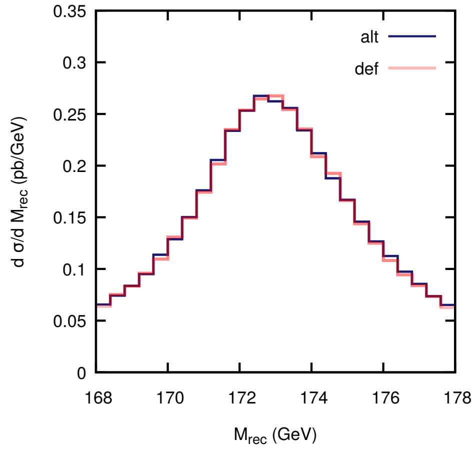

FIGURE 1.5: Invariant mass distribution of the reconstructed top quark mass, defined as the mass of the $W^+ j_B$ or $W^- j_{\bar{B}}$ system, produced with the `bb4l` generator, at the 8 TeV LHC. The two distributions are obtained with the default implementation of radiation from b quarks (def), and with the new implementation presented here (alt).

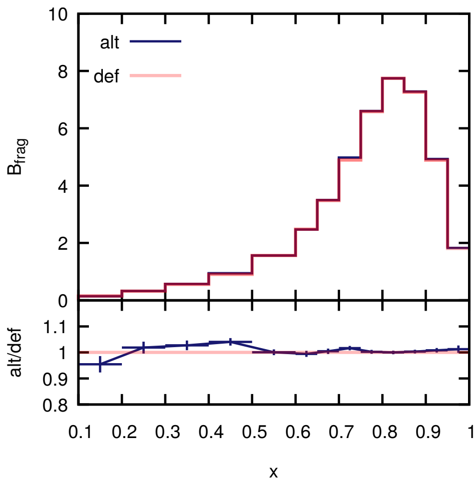

FIGURE 1.6: B fragmentation function in top quark decay as defined in ref. [75], produced with the `bb4l` generator for the 8 TeV LHC. The default and alternative implementation of radiation from b quarks are compared.

the the B energy in the reconstructed top rest frame normalized to the maximum value that it can attain at the given top virtuality. In the curves, the `alt` (for "alternative") label stands for our new implementation, while `def` (for "default") is the current `POWHEG` default. As one can see, the agreement is very good. This also shows that details in the implementation of radiation from the b quark in top decays do not seem to have important impact on physical observables.

We found that the efficiency and the generation rate of the new implementation are comparable with those of the `POWHEG` default.

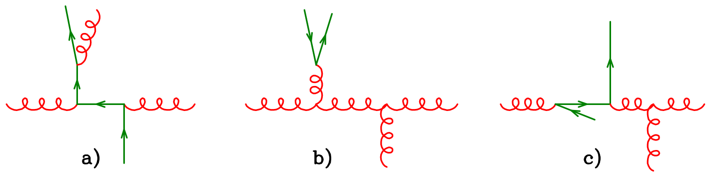

FIGURE 1.7: Example diagrams for the three mechanism that give rise to log-enhanced contributions in heavy flavour production: a) final state radiation from a quark; b) gluon splitting; c) flavour excitation.

b production in hadronic collisions

In this section we study the available `POWHEG` implementations of radiation from massive quarks for the `hvq` generator [73], i.e. the default `POWHEG` implementation and our new one. In spite of the fact that the default formalism has been available for quite some time [55], no such study has been performed so far. We thus discuss it in this work, where we can also compare with our new implementation.

The `hvq` generator has been available for quite some time as a tool to generate top, bottom and charm pairs in hadronic collisions. It is designed to simulate correctly the production of a heavy flavour pair when the logarithm of the ratio of the transverse momentum of the heavy quark divided by its mass is not too large. This limitation arises because there are three mechanisms, depicted in figure 1.7, involving radiation from the final state quark, production of a heavy quark-antiquark pair via final state gluon splitting and the splitting of an initial state gluon into a heavy quark-antiquark pair (where one of the two quarks is scattered at large transverse momentum), that can generate large logarithms involving the mass of the heavy quark. In the inclusive cross section for the production of a heavy quark with a given p_T, for example, they generate logarithms of p_T/m (see ref. [81], Eq. (5.1)). The last two mechanisms are commonly referred to as gluon splitting and flavour excitation. In spite of this, the `hvq` generator has also been used to model relatively large transverse momentum production of heavy flavours, as in ref. [71]. There, the transverse momentum distribution of the heavy flavoured hadron in `hvq` was compared with the more accurate (but less exclusive) `FONLL` prediction [65]. It was found to be in rather good agreement. However, the large uncertainties related to the non-perturbative fragmentation of the heavy quark leads to the suspect that such agreement is at least in part accidental.

We will now compare the results obtained with the default `hvq` generator, that we will label `nol` (for "no light", meaning that the heavy quark is treated as very heavy), that treats as singular regions only the radiation from massless partons (i.e. initial state radiation); `hvq` with the inclusion of the radiation from the heavy quark as a singular region will be labeled `asl` (for "as light", meaning that the heavy quark is treated as a light parton). Furthermore, the default treatment of the heavy quark radiation region will be denoted as `def`, while the new implementation presented here will be called `alt`. In Fig. 1.8, we show a comparison of `def` and `alt`. We can immediately see that we do not find important differences between the two methods, consistently with what was found in the `bb4l` case. The settings are similar to the `bb4l` case: we make the B hadrons stable, and define the b ($\bar{b}$) jets as the jets containing the hardest b ($\bar{b}$) flavoured hadron, with the jets defined as in the `bb4l` case. However, we do not exclude the case when both hardest b-flavoured hadrons are in the same jet. We perform the calculation for the LHC at 8 TeV, using `NNPDF30_nlo_as_0118` pdf set [78]. As one can see, the two implementations are in excellent agreement. Observe the jump at 10 GeV in the j_B mass. It is due to the case in which the b and $\bar{b}$ flavoured hadrons are both in the jet cone. From figure 1.8 we also see that for jet masses above 10 GeV the gluon splitting configuration dominates.

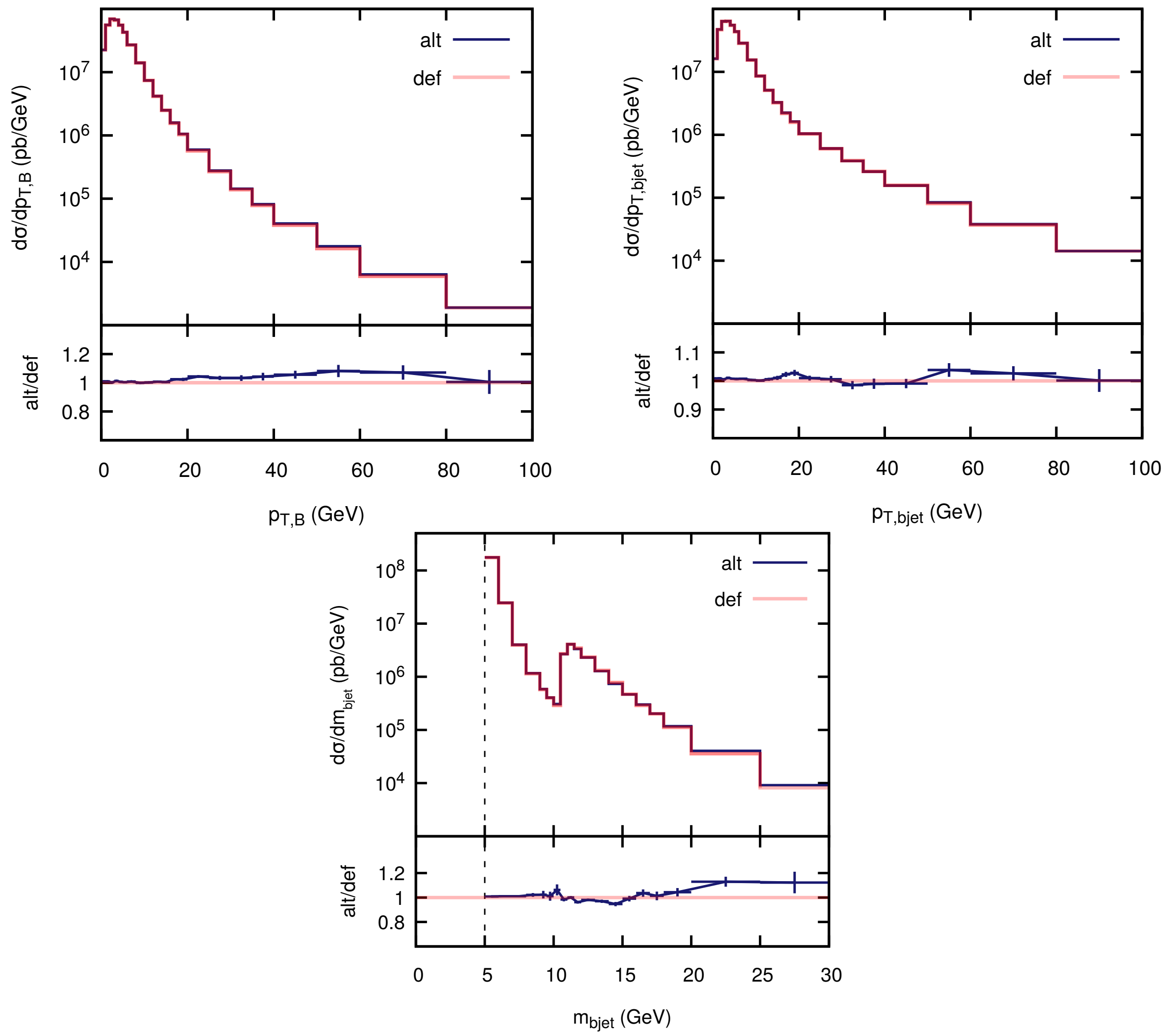

FIGURE 1.8: Comparison of `alt` and `def` for the transverse momentum distribution of the B hadron (top left), for the transverse momentum distribution of the b-jet (top right) and for the b-jet mass (bottom) at the 8TeV LHC.

We found that the new implementation has a generation efficiency, which is estimated from the numbers of vetoes in FSR generation, three times greater than the default one. This leads to a generation rate of 1316 events per minute, against the 298 events per minute of the `POWHEG` default, which corresponds to a gain more than a factor of 4.

We now show in the left panels of Fig. 1.9, the comparison among the `alt` and `nol`. Here we see considerable differences, especially in the large-momentum tail of the B and j_B transverse momentum distribution, the `alt` ones being much harder. The mass of the b jet is also remarkably different. The large difference above 10 GeV hints to the fact that heavy quark pair production via the splitting of a large transverse momentum gluon is treated in a very different way in the two cases, and that this difference may be the cause of the large discrepancy in the transverse momentum distribution of the b hadron.

The difference between the `alt` and `nol` cases should not come as a surprise. The generation of radiation is performed in the `nol` case according to the formula

$$d\sigma \;=\; d\Phi_B \tilde{B}(\Phi_B) \exp\left[\int \frac{R(\Phi_B, \Phi'_{\rm rad})}{B(\Phi_B)} \theta(k'_t - k_t) d\Phi'_{\rm rad} \right] \times \frac{R(\Phi_B, \Phi_{\rm rad})}{B(\Phi_B)} d\Phi_{\rm rad} \,,$$

where k_t is the transverse momentum of the emitted gluon with respect to the beam axis,

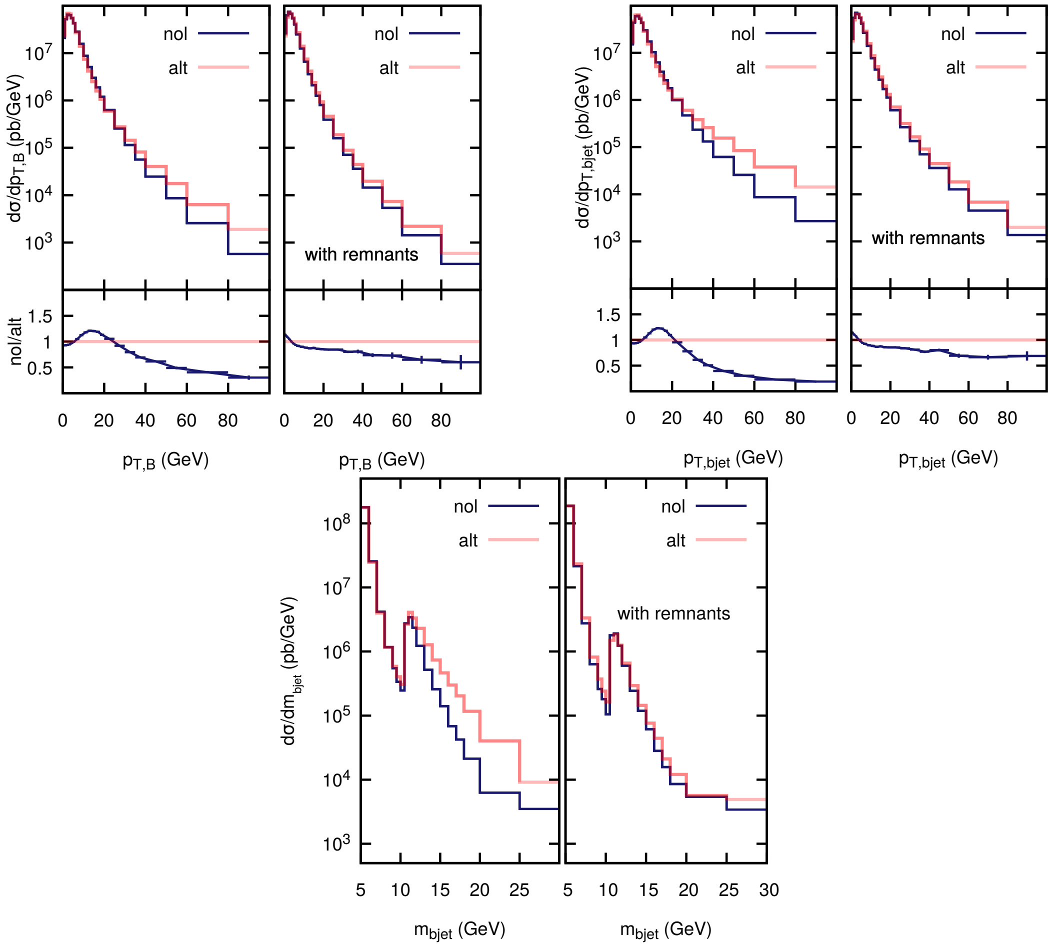

FIGURE 1.9: Left panels: comparison of `alt` and `nol` for the transverse momentum distribution of the B hadron (top left), for the transverse momentum distribution of the b-jet (top right) and for the b-jet mass (bottom) at 8TeV LHC. Right panel: same comparison with the treatment of the enhanced regions using remnants, as discussed in the text.

since the only singular regions that are considered there are the initial-state radiation (ISR) ones. The strong coupling constant and the parton densities are evaluated by default at a scale equal to the transverse mass of the heavy quark at the level of the underlying Born kinematics

$$\mu_f = \mu_r = \sqrt{k_{t,q}^2 + m_q^2} \tag{1.137}$$

in the $\tilde{B}$ function, while they are evaluated at a scale k_t (or k'_t) in the R/B ratios appearing in formula (1.137). Since $\tilde{B}$ and B are of order α_S^2, while R is of order α_S^3, this means that in practice two powers of the strong coupling are evaluated at the scale of Eq. (1.137), while one power is evaluated at a scale k_t. The mismatch in the scale used in $\tilde{B}$ and in the B appearing in the ratios, combined with the exponential, leads as usual to the correct Sudakov form factor for initial state emission.

Problematic regions

In case the transverse momentum of the gluon is small, the scale assignments and the Sudakov form factor describe the process appropriately. It can happen however, that the real emission kinematics is near the gluon splitting, flavour excitation or quark radiation regimes. In these cases the gluon transverse momentum is not small. Furthermore, the numerator R in the integrand may be enhanced with respect to the denominator, thus yielding a damping of the real cross section that is not justified. Also the scale choices are not appropriate. For example, in the case of production of a high transverse momentum heavy quark pair according to the gluon splitting mechanism, the appropriate scale should correspond to two powers of α_S evaluated at the gluon transverse momentum, and one power of α_S evaluated at the scale of the order of the invariant mass of the heavy quark pair.

The adoption of the methods illustrated in ref. [55] and in the present work for dealing with radiation from a heavy quark leads to the correct treatment of the radiation from the heavy, quark provided all remaining regions are treated correctly. This is in fact what happens in the case of the `bb4l` generator, where there is only one enhanced region, but it is not the case for the `asl` generator, that does not treat in a proper way the two regions of gluon splitting and flavour excitation. Thus, the `nol` and the `asl` generators will end up treating the enhanced regions in different (and in both cases incorrect) ways. In fact, while in the `nol` case the enhanced regions will all be treated as if they were ISR processes, in the `asl` case they will be split, and treated in part as ISR processes, and in part as radiation from the heavy quarks. In order to test this hypothesis, and in order to explore possible strategies to deal with this problem, we proceed as follows. It is possible in `POWHEG` to further separate out the real cross section into two terms, such that only one term has singular behaviour, while the remaining term, being finite, can be integrated independently. In the `hvq` case, this means

$$R = R^{(s)} + R^{(r)} . \tag{1.138}$$

Eq. (1.137) is then replaced by

$$\begin{aligned} d\sigma = {} & d\Phi_B \tilde{B}^{(s)}(\Phi_B) \exp\left[\int \frac{R^{(s)}(\Phi_B, \Phi'_{\rm rad})}{B(\Phi_B)} \theta(k'_t - k_t) d\Phi'_{\rm rad}\right] \\ & \times \frac{R^{(s)}(\Phi_B, \Phi_{\rm rad})}{B(\Phi_B)} d\Phi_{\rm rad} + \int d\Phi_B d\Phi_{\rm rad} R^{(r)}(\Phi_B, \Phi_{\rm rad}) . \end{aligned} \tag{1.139}$$

We can exploit this mechanism in order to separate out the enhanced regions, in such a way that we can treat them in a more uniform way with our generators. In particular, we separate out the gluon splitting and flavour excitation processes in all cases. In the `nol` case we also separate out the regions of radiation from the heavy quarks, in such a way that they are treated in a more transparent way. Observe that in performing this separation we rely upon the fact that the three enhanced region are not really singular, since the quark mass cuts off the collinear singularities, and thus the remnant term is actually finite.

We define the distance of a real configuration from a given enhanced region as follows

$$\begin{aligned} d_{\rm isr} &= k_t^2, & d_{\rm glsp} &= 2k_q \cdot k_{\bar{q}} \frac{k_q^0 k_{\bar{q}}^0}{(k_q^0 + k_{\bar{q}}^0)^2}, \\ d_q &= 2k_q \cdot k \frac{k^0}{k_q^0} + m_q^2, & d_{\bar{q}} &= 2k_{\bar{q}} \cdot k \frac{k^0}{k_{\bar{q}}^0} + m_q^2, \\ d_{q,\rm flex} &= k_{\bar{q},\perp}^2 + m_q^2, & d_{\bar{q},\rm flex} &= k_{q,\perp}^2 + m_q^2, \end{aligned} \tag{1.140}$$

where in the first line the distances for ISR and gluon splitting are given, in the second line those for radiation from the heavy quarks, and in the last line the ones for flavour excitation.

We then define, for the `nol` generator

$$
\begin{aligned}
D &= \frac{d_{\rm isr}^{-1}}{d_{\rm isr}^{-1}+d_{\rm glsp}^{-1}+d_{q}^{-1}+d_{\bar q}^{-1}+d_{q,\rm flex}^{-1}+d_{\bar q,\rm flex}^{-1}},\\
R^{(s)} &= RD, \qquad R^{(r)} = R(1-D)\,.
\end{aligned} \tag{1.141}
$$

For the `alt` and `def` generators, we define

$$
D = \frac{d_{\rm isr}^{-1}+d_{q}^{-1}+d_{\bar q}^{-1}}{d_{\rm isr}^{-1}+d_{\rm glsp}^{-1}+d_{q}^{-1}+d_{\bar q}^{-1}+d_{q,\rm flex}^{-1}+d_{\bar q,\rm flex}^{-1}} \tag{1.142}
$$

$$
R_i^{(s)} = R_i D, \qquad R_i^{(r)} = R_i(1-D)\,, \tag{1.143}
$$

where the index i labels the three singular regions that `POWHEG` is handling. In this case, the cross section is damped if the kinematics is near a singular region that is nether ISR nor FSR, i.e. only gluon splitting and flavour excitation kinematics are separated into the (r) component.

There is one more issue that needs to be considered when using a damping factor in `POWHEG`. By default, when evaluating the $R^{(r)}$ component (called "real remnant"), the scale choice is the same as for $\tilde{B}$, i.e. it is Eq. (1.137) applied to the underlying Born kinematics, that depends upon the considered singular region. This would lead to a different scale choice for the remnants in `nol` and `asl`. In order to avoid that, we should set the scale on the basis of the real kinematics. This can be done in `POWHEG` by setting appropriate flags and by modifying the code that computes the scales for the process. Our scale choice is

$$
\mu_f = \mu_r = \frac{1}{2}\left[\sqrt{k_{t,q}^2+m_q^2}+\sqrt{k_{t,\bar q}^2+m_{\bar q}^2}+k_t\right], \tag{1.144}
$$

that has the correct limit to the underlying Born scale both in the ISR and in the FSR case.

The result of this procedure is shown in the right panels of Fig. 1.9. We notice a remarkable improvement in the agreement, although some important differences do remain. This is not unexpected, since in the two cases radiation from the heavy quark is treated in a very different way. It is interesting to notice that the B and the $j_{\rm B}$ spectra computed with the `nol` *without* remnants (which is the default in the standard `hvq` generator), is in fair agreement with the `alt` one when the enhanced regions are separated using the remnants. Since the default `hvq` program gives a description of the transverse momentum distribution of B hadrons that is in fair agreement with the FONLL calculation, we infer that also the `alt` prediction will display a similar agreement, provided the gluon splitting and flavour excitation region are treated separately as remnants.

The `alt` (or equivalently the `def` generator), with the remnant separation discussed above, seems to be at this point the generator that may give the best description of b production data at hadron collider. We should not forget, however, that some flexibility still remains in the treatment of the remnant (in this work we have made a definite scale choice for the remnants in order to have a clearer comparison with the `nol` generator). We also notice from Fig. 1.9 that after the remnants are introduced, the B-hadron and b-jet p_T spectra become softer. This seems to be in contrast with the discussion at the beginning of sec. 1.4.2. On the other hand, this result may be due to the particular scale choice that we have performed for the real graphs, and that `POWHEG` applies automatically also to the remnants. This scale turns out to be higher than the typical scale involved in the region discussed at the beginning of sec. 1.4.2. A better approach would be to introduce the possibility of alternative scale choices in the remnants, including the possibility of performing a different scale choice depending upon which enhanced region one is considering.

In order to make progress in this direction, we have started a systematic comparison with data on single inclusive b-hadron and b-jet production (see ref. [82–84] and references therein) and on correlations of $b\bar{b}$ pairs [85, 86]. The analyses are still ongoing and will be the topic of a dedicated work.

Chapter 2

NNLO QCD with qt subtraction

The development of general-purpose subtraction schemes as dipoles subtraction and FKS, together with a great boost in techniques used to compute tree and one-loop amplitudes has allowed to achieve a high level of automation in the calculation of NLO QCD (and, as it will be discussed in Chapter 4, NLO EW) corrections. This opened the door to the so called "NLO revolution". With this, it is meant that the problem to compute NLO corrections for any process can be considered solved. In practice, the only limitation is related to the computational load needed for processes with large number of external legs.

In view of the precision physics program undergoing at LHC and future colliders, going beyond the NLO is highly desirable. As a rule of thumb, the theoretical uncertainty associated to a NLO prediction is around $10-30\%$ and one usual starts to see the convergence and the stability of the perturbative expansion at NNLO, with a reduction of the uncertainty to order $\mathcal{O}(5-10\%)$. In this context, one of the main bottleneck is given by the computation of the two-loop virtual amplitudes. This topic is beyond the scope of this work and it will not be discussed further.

In this chapter, we briefly address the problems we find to extend the subtraction formalism to NNLO. Indeed, despite the great effort of different groups, a general-purpose subtraction algorithm similar to those available at NLO is still missing. We focus on a different approach that is possible when one relaxes the condition to have fully local counterterms. In particular, we review the main aspects of the non-local q_T subtraction formalism as it will be our starting point to develop a suitable scheme to handle the infrared singularities for mixed QCD-QED corrections in Chapter 3.

2.1 NNLO corrections within the subtraction formalism

At NNLO, one must include in the computation real emission processes with up two extra partons. The Feynman diagrams contributing to this order are then classified accordingly to the number of extra partons in the final state: two-loop amplitude to be interfered with the LO one and the squared of one-loop amplitude with no extra partons (double-virtual $\mathcal{VV}$), the interference of the one-loop amplitude with 1 extra parton with the corresponding tree-level (real-virt $\mathcal{RV}$), the squared tree-level amplitude with 2 extra partons (double-real $\mathcal{RR}$). In Fig. 2.1, we show an illustrative example of the three classes of contributions occurring in the hadroproduction of an electroweak gauge boson W/Z in the diagonal quark-antiquark annihilation channel at NNLO.

The contribution of NNLO corrections $\delta\sigma_{\rm NNLO} \equiv \sigma_{\rm NNLO} - \sigma_{\rm NLO}$ can then be written as

$$\delta\sigma_{\rm NNLO} = \int d\Phi_n \mathcal{VV}(\Phi_n) + \int d\Phi_{n+1} \mathcal{RV}(\Phi_{n+1}) + \int d\Phi_{n+2} \mathcal{RR}(\Phi_{n+2}) \,, \tag{2.1}$$

for a generic process starting with n parton in the final state at LO. We assume here that the loop diagrams have already been renormalized leading to UV finite quantities. Similarly to what happens at NLO, virtual and real corrections develop infrared singularities associated

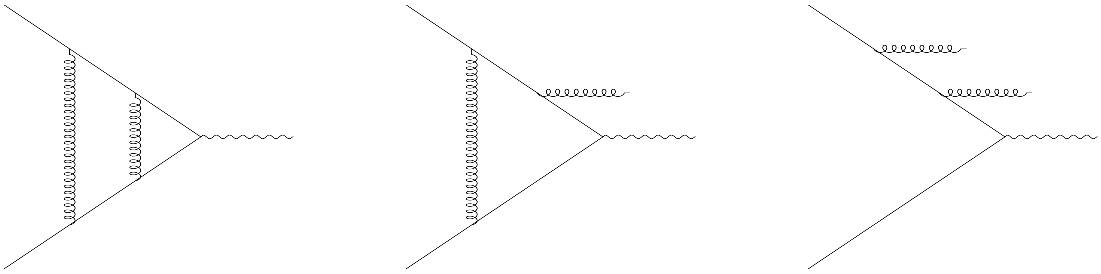

FIGURE 2.1: Illustrative Feynman diagrams for the three classes of contributions to the hadroproduction of a electroweak gauge boson at NNLO in the diagonal $q\bar{q}$ channel: double virtual (left), real virt (center) and double real (right). One-loop diagrams squared also belong to the first class.

to the soft and collinear limits. In case the partons are all massless, the maximally singular configuration corresponds to two soft and collinear singularities. This means that we have up to poles of degree four in the dimensional regulator ϵ. Factorization together with the KLN theorem ensures the cancellation of the IR divergences for infrared-safe observables. In practice, as in the NLO case, the situation is complicated by the fact that the divergences are implicit in the real radiation corrections. They only appear after integration over the phase space as opposed to the explicit pole structure in ϵ in the virtual corrections:

- two-loop virtual corrections

$$\int d\Phi_n \mathcal{VV}(\Phi_n) = \int d\Phi_n \left(\frac{VV_4}{\epsilon^4} + \frac{VV_3}{\epsilon^3} + \frac{VV_2}{\epsilon^2} + \frac{VV_1}{\epsilon} + VV_0 \right) ; \tag{2.2}$$

- one-loop real emission corrections

$$\int d\Phi_{n+1} \mathcal{RV}(\Phi_{n+1}) = \int d\Phi_{n+1} \left(\frac{RV_2}{\epsilon^2} + \frac{RV_1}{\epsilon} + RV_0 \right) ; \tag{2.3}$$

- double real emissions corrections

$$\int d\Phi_{n+2} \mathcal{RR}(\Phi_{n+2}) = \int d\Phi_{n+2} RR_0 \,. \tag{2.4}$$

Formally, it is natural and straightforward to extend the idea of the subtraction formalism at NNLO:

1. introduce two new classes of countertems to deal with double and single real emission processes respectively;
2. integrate analytically the counterterms over the corresponding radiation phase space (double and single, respectively).

Schematically, the generic form of a NNLO subtraction scheme reads

$$\begin{aligned} \delta\sigma_{\text{NNLO}} = &\int d\Phi_n \mathcal{VV}(\Phi_n + \int d\Phi_{n+1} C_{\mathcal{RV}}(\Phi_{n+1}) + \int d\Phi_n C_{\mathcal{RR}}(\Phi_{n+2}) \\ &+ \int d\Phi_{n+1} \left[\mathcal{RV}(\Phi_{n+1}) - C_{\mathcal{RV}}(\Phi_{n+1}) \right] + \int d\Phi_{n+2} \left[\mathcal{RR}(\Phi_{n+2}) - C_{\mathcal{RR}}(\Phi_{n+2}) \right] . \end{aligned} \tag{2.5}$$

For the sake of simplicity, we have omitted in the above formula the collinear remainders coming from the factorization of initial-state collinear singularities. While the program appears well defined, building an actual implementation of a NNLO subtraction is a highly non-trivial task and, despite the great efforts profused by different groups in the last several years, a general-purpose algorithm comparable to what we have at NLO is not yet available. The reason rests on the fact that the structure of the IR singularities is much richer and more involved at NNLO with respect to the NLO case. In the double real emission phase space, there are now two types of singular configurations: a single parton can become soft and/or collinear (*single unresolved* limit) or both the extra partons become soft and/or collinear (*double unresolved* limit), leading to a proliferation of possible overlapping singular configurations (triple-collinear, double-collinear, double-soft, single-soft, soft+collinear, etc.).

In general, one should introduce two classes of counterterms, one responsible for the cancellation of singularities of the double real squared matrix element in the double unresolved limits, that we denote collectively as $\mathcal{A}^{(2)}$, and the other in the single unresolved limits, $\mathcal{A}^{(1)}$. Suppose to build the counterterm along the main ideas of the dipole formalism. Schematically, this means to promote suitable factorization formulae, which approximate the matrix elements in specific singular limits, to the whole real phase space through momentum mappings chosen in a such a way to achieve the exact factorization of the phase space. At NLO, this is sufficient to build the subtraction scheme. At NNLO, the situation is complicated by the fact that the kernel itself of such counterterms may be divergent approaching a different singular limit from the one they cancel. For example, a counterterm in the class $\mathcal{A}^{(2)}$, responsible for the cancellation of a double unresolved limit, can become divergent in one of the single unresolved limit, and a similar situation can occur for the counterterms in the class $\mathcal{A}^{(1)}$. If one wants to proceed in this direction, additional counterterms must be subtracted to single out these "spurious" singularities, leading to a proliferation of terms to be defined and to be integrated analytically. We point out that the $\mathcal{A}^{(1)}$ class must be integrated over the 1-particle phase space to be combined with the real-virtual contribution, as it is required to cancel the explicit poles of the one-loop real-virtual matrix element.

In the "dipole"-style approach sketched above, the construction of the counterterms is completely independent from the treatment of the space space. A different strategy consists in partitioning the phase space via suitable measurement functions. This allows to disentangle the singular limits and simplify the structure of the counterterms needed in each "sub-sector", following an approach inspired by the FKS subtraction scheme. The counterterms are defined only in the specific sub-sector corresponding to a given singular limit that they are required to cancel.

Both approaches have been pursued. ColorFull subtraction [87] can be thought as a generalization of the dipoles scheme and, so far, it has been completed for processes involving no identified hadrons in the initial state [88–90]. Improved sector decomposition [91] and nested soft-collinear subtraction [92] instead belong to the class of FKS-inspired subtractions. They have been used in NNLO computations for relevant processes at the LHC [93–99]. Among other viable approaches, also the antenna subtraction scheme [100] has been successfully employed for several important calculations [101–106].

For the sake of completeness, we conclude this general section mentioning the development of other schemes based on a combination of dipoles and FKS approaches [107] and on a geometric approach [108].

2.1.1 Non-local subtraction and slicing

All the subtraction schemes listed in the previous section attempt to build a realization of the **local** subtraction formalism as presented in the previous chapter. By local, we mean that the

cancellation of the IR divergences in the real corrections occurs pointwise at the integrand level. From the numerical point of view, this approach is very robust and efficient, since the resulting subtracted integrand is a harmless function, which contains at most integrable singularities in the real emission phase space. On the other hand, as already discussed, the construction of local counterterms is very involved due to the many overlapping singularities occurring at NNLO, which have to be isolated by means of suitable phase-space parametrizations. At the same time, the counterterms should remain simple enough to allow one to perform their analytical integration over the radiation phase-space and to extract the IR poles in the ϵ regulator.
A different approach is possible if one relaxes the requirement to have local counterterms. The key observations here are the following:

1. the single unresolved regions can be separated from the double unresolved ones by defining a suitable resolution variable X (non negative), such that for $X > 0$ at most one parton can become soft and/or collinear, while the double unresolved limit occurs only at $X = 0$. Furthermore, the resolution variable X is a physical infrared safe observable.

   Then, the structure of the divergences greatly simplifies: in the region $X > 0$, there are only NLO-type singularities (that can be handled by standard NLO subtraction algorithms); in the region $X = 0$, there are the genuine NNLO-type of singularities.

2. The cross section $d\sigma/d\Phi_n dX$, differential with respect to the Born configuration Φ_n and the resolution variable X, can be *easily* computed up to (at least) NNLO in the unresolved region $X = 0$. By easily, we mean that either it is already available or it is calculable with well established techniques. More in details, we formally split the differential cross section into a regular and a singular part

$$\frac{d\sigma}{d\Phi_n dX} = \frac{d\sigma^{\text{reg}}}{d\Phi_n dX} + \frac{d\sigma^{\text{sing}}}{d\Phi_n dX}\,. \tag{2.6}$$

   The singular part of the X spectrum contains all the contributions that are singular in the $X \to 0$ limit, i.e. all the contributions which are either proportional to $\delta(X)$ or that behaves as $\ln^k X/X$ for vanishing X. This logarithmic structure of the singular contributions is a general result which follows directly from the IR structure of QCD amplitudes [109, 110], the KLN theorem, and the fact that the resolution variable X is a physical infrared safe observable. Since in the unresolved region, the phase-space reduces to the Born one, $d\sigma^{\text{sing}}/d\Phi_n dX$ can only depend on the lowest-order configurations Φ_n. Hence, it can be written as

$$\frac{d\sigma^{\text{sing}}}{d\Phi_n dX}(\Phi_N) = \mathcal{H}(\Phi_n)\delta(X) + \sum_{k\geq 0} \mathcal{C}_k(\Phi_n)\left[\theta(X)\frac{\ln^k X}{X}\right]_+ \tag{2.7}$$

   in terms of usual plus distributions. In this form, it is manifest the cancellation between real and virtual IR divergences, with the finite remnant of the virtual contributions, after the cancellation has taken place, contained in the coefficient $\mathcal{H}(\Phi_n)$ of the $\delta(X)$ term. The coefficient functions appearing in Eq. (2.7) admit a perturbative expansion in the strong coupling constant

$$\mathcal{H} = \sum_{m\geq 0} \alpha_s^m \mathcal{H}^{(m)}, \quad \mathcal{C}_k = \sum_{m\geq 0} \alpha_s^m \mathcal{C}_k^{(m)} \tag{2.8}$$

and Eq. (2.7) can be recast in the form:

$$\frac{d\sigma^{\text{sing}}}{d\Phi_n dX}(\Phi_N) = \sum_{m\geq 0} \alpha_s^m \left[\mathcal{H}^{(m)}(\Phi_n)\delta(X) + \sum_{k=0}^{2m-1} \mathcal{C}_k^{(m)}(\Phi_n) \left[\theta(X) \frac{\ln^k X}{X} \right]_+ \right]. \tag{2.9}$$

At a given order m in the perturbative expansion, real emission processes of up to m extra partons are included in the computation. The maximally IR singular configuration corresponds to all the extra partons approaching simultaneously the soft and collinear limits. The degree of the singularity is therefore $2m$ and this explains the maximum value of the exponent $k = 2m - 1$ in Eq. (2.9). Indeed, after integrating over the X variable, it produces a logarithmic divergent term raised to the power of $2m$, $\log^{2m} X$.

Having defined the singular part, the regular is formally defined as the difference

$$\frac{d\sigma^{\text{reg}}}{d\Phi_n dX} = \frac{d\sigma}{d\Phi_n dX} - \frac{d\sigma^{\text{sing}}}{d\Phi_n dX}. \tag{2.10}$$

and, by construction it satisfies the property

$$\lim_{X_0 \to 0} \int_0^{X_0} dX \frac{d\sigma^{\text{reg}}}{d\Phi_n dX} = 0 \tag{2.11}$$

What it is actually demanded is the knowledge of just the singular part, i.e. the determination of the coefficient functions in Eq. (2.9) up to the desired perturbative order.

In the following, we will detail how it is possible to build a subtraction procedure for the NNLO corrections starting from the above observations. As first step, we split the contribution of the real emission processes in Eq. (2.1) in the two regions $X < X_{\text{min}}$ and $X > X_{\text{min}}$

$$\begin{aligned} \delta\sigma_{\text{NNLO}} = &\int d\Phi_n \mathcal{VV}(\Phi_n) + \int d\Phi_{n+1} \mathcal{RV}(\Phi_{n+1})\Theta^< + \int d\Phi_{n+2} \mathcal{RR}(\Phi_{n+2})\Theta^< \\ &+ \int d\Phi_{n+1} \mathcal{RV}(\Phi_{n+1})\Theta^> + \int d\Phi_{n+2} \mathcal{RR}(\Phi_{n+2})\Theta^>, \end{aligned} \tag{2.12}$$

where $\Theta^< \equiv \Theta(X_{\text{min}} - X)$ and $\Theta^> \equiv \Theta(X - X_{\text{min}})$. X_{min} plays the role of a small but finite resolution cut-off. The three contributions in the first line of the r.h.s. of Eq. (2.12) live in the unresolved region, so they can be formally re-combined to yield the total NNLO correction below X_{min}

$$\begin{aligned} &\int d\Phi_n \mathcal{VV}(\Phi_n) + \int d\Phi_{n+1} \mathcal{RV}(\Phi_{n+1})\Theta^< + \int d\Phi_{n+2} \mathcal{RR}(\Phi_{n+2})\Theta^< \\ &= \int d\Phi_n dX \frac{d(\delta\sigma_{\text{NNLO}})}{d\Phi_n dX}\Theta^< = \int d\Phi_n dX \left[\frac{d(\delta\sigma^{\text{sing}}_{\text{NNLO}})}{d\Phi_n dX} + \frac{d(\delta\sigma^{\text{reg}}_{\text{NNLO}})}{d\Phi_n dX} \right]\Theta^< \\ &= \int d\Phi_n dX \frac{d(\delta\sigma^{\text{sing}}_{\text{NNLO}})}{d\Phi_n dX}\Theta^< + O(X^l_{\text{min}}). \end{aligned} \tag{2.13}$$

In the above, we have used the decomposition into singular and regular part, Eq. (2.6), and in the last step we have neglected the integral of the regular contribution, as it vanishes in the $X_{\text{min}} \to 0$ limit according to Eq. (2.11). Therefore, the error associated to this approximation is **power suppressed**, modulo logarithmic enhancements, in the resolution cut-off X_{min}.

The real contributions in the second line of the r.h.s. of Eq. (2.12) live in the resolved region. This means that one of the real partons is always resolved so that they can be effectively viewed as the NLO corrections to the process given by the LO one plus one extra jet. The structure of the singularities is then one order less and by applying one of the NLO subtraction schemes (as dipoles or FKS), the quantity in the second line of Eq. 2.12

$$\begin{aligned}&\int d\Phi_{n+1}\mathcal{RV}(\Phi_{n+1})\Theta^{>}+\int d\Phi_{n+2}\mathcal{RR}(\Phi_{n+2})\Theta^{>}\\&=\int d\Phi_{n+1}\left[\mathcal{RV}(\Phi_{n+1})+\overline{\mathcal{C}}^{NLO}(\Phi_{n+1})\right]\Theta^{>}+\int d\Phi_{n+2}\left[\mathcal{RR}(\Phi_{n+2})-\mathcal{C}^{NLO}(\Phi_{n+2})\right]\Theta^{>}\,,\end{aligned}\tag{2.14}$$

is finite as long as X_{min} is non-vanishing. It can be integrated numerically and provides a fully differential description for infrared safe observables. In the above, we have introduced the NLO counterterm, schematically denoted as $\mathcal{C}^{NLO}(\Phi_{n+2})$, and its integrated version $\overline{\mathcal{C}}^{NLO}(\Phi_{n+1})$. The latter term, living in the $n+1$-phase space, is combined with the real-virtual contribution. In the sum, the explicit poles in the ϵ regulator, Eq. (2.3), cancel. Then, Eq. (2.12) becomes

$$\begin{aligned}\delta\sigma_{\text{NNLO}}=&\int d\Phi_n dX\frac{d(\delta\sigma^{\text{sing}}_{\text{NNLO}})}{d\Phi_n dX}\Theta^{<}+\int d\Phi_{n+1}\left[\mathcal{RV}(\Phi_{n+1})+\overline{\mathcal{C}}^{NLO}(\Phi_{n+1})\right]\Theta^{>}\\&+\int d\Phi_{n+2}\left[\mathcal{RR}(\Phi_{n+2})-\mathcal{C}^{NLO}(\Phi_{n+2})\right]\Theta^{>}+O(X^{l}_{\text{min}})\,,\end{aligned}\tag{2.15}$$

which gives a well-defined *phase-spacing slicing* [111–113] numerical scheme suitable for NNLO QCD computations. All the integral can be performed numerically and the computation is fully differential with respect to any infrared safe observables. The IR divergences manifest themselves as large logarithmic enhancements in the resolution parameter X_{min} **after integrating** over the phase space both in the unresolved and in the resolved regions. These two contributions exactly match with opposite sign so that the real-virt cancellation takes place and the final result reproduces the NNLO correction up to power corrections in the resolution parameter X_{min}.

We can formally recast Eq. (2.15) in a form closer to a subtraction scheme by writing the integral in the unresolved region as

$$\begin{aligned}\int d\Phi_n dX\frac{d(\delta\sigma^{\text{sing}}_{\text{NNLO}})}{d\Phi_n dX}\Theta^{<}=&\int d\Phi_n dX\frac{d(\delta\sigma^{\text{sing}}_{\text{NNLO}})}{d\Phi_n dX}\Theta(X_{\text{max}}-X)\\&-\int d\Phi_n dX\frac{d(\delta\sigma^{\text{sing}}_{\text{NNLO}})}{d\Phi_n dX}\Theta^{>}\Theta(X_{\text{max}}-X)\end{aligned}\tag{2.16}$$

for an arbitrary $X_{\text{max}} > X_{\text{min}}$, so that

$$\begin{aligned}\delta\sigma_{\text{NNLO}}=&\int d\Phi_n dX\frac{d(\delta\sigma^{\text{sing}}_{\text{NNLO}})}{d\Phi_n dX}\Theta(X_{\text{max}}-X)\\&+\left[\int d\Phi_{n+1}\left[\mathcal{RV}(\Phi_{n+1})+\overline{\mathcal{C}}^{NLO}(\Phi_{n+1})\right]\Theta^{>}+\int d\Phi_{n+2}\left\{\mathcal{RR}(\Phi_{n+2})-\mathcal{C}^{NLO}(\Phi_{n+2})\right]\Theta^{>}\right.\\&\left.-\int d\Phi_n dX\frac{d(\delta\sigma^{\text{sing}}_{\text{NNLO}})}{d\Phi_n dX}\Theta^{>}\Theta(X_{\text{max}}-X)\right\}+O(X^{l}_{\text{min}})\,.\end{aligned}\tag{2.17}$$

In Eq. (2.17), the logarithmic enhancements in the cut-off $X_{\min}$ cancel between the real contributions and the term

$$\int d\Phi_n dX \frac{d(\delta\sigma^{\mathrm{sing}}_{\mathrm{NNLO}})}{d\Phi_n dX} \Theta^{>} \Theta(X_{\max} - X) \tag{2.18}$$

which plays the role of a non-local counterterm since it is not fully differential in the radiation variables. The first term in the r.h.s. of Eq. (2.17) can be viewed then as the contribution given by the virtual terms (sitting at $X = 0$) and the integrated counterterm. From the above formula, one can derive a numerical scheme which is different from a pure phase-space slicing. Indeed, with an appropriate choice of the space mapping in the Monte Carlo integration, it is possible to integrate the real and the counterterm together mimicking what happens in a local subtraction scheme. In this context, the parameter $X_{\min}$ assumes the role of a technical cutoff for the numerical integration, which is still necessary because the integrand is given by the difference of two divergent integrands. As for the power corrections, the two formulae Eq. (2.15) and Eq. (2.17) are completely equivalent.
Summarizing, as compared to a local subtraction scheme, the slicing/non-local formalism based on the introduction of a suitable resolution parameter X allows in practice

- to lower the order of the computation, from NNLO to NLO, but for the small unresolved region, where the cross section can be computed by other techniques (resummation, effective field theory) up to NNLO,

with the drawbacks that

- the logarithmic enhancements associated to the IR singularities in the unresolved region globally cancel only after the integration over the phase space (*large global cancellations*);
- while the method is exact in the limit of a vanishing resolution cutoff $X_{\min} \to 0$, the latter cannot be set to zero introducing a dependence in the computation in the form of power corrections (modulo logarithmic enhancements).

Despite these drawbacks, q_T and N-jettiness [114, 115] subtraction formalisms are two examples of non-local schemes that have been successfully employed to compute the NNLO QCD corrections to a variety of processes relevant at the LHC. In this work, our focus is on the q_T subtraction method.

2.2 q_T subtraction formalism

2.2.1 Color singlet case

In the last section, we have outlined the general aspects of a non-local subtraction formalism to deal with NNLO corrections. Here, we focus on the specific case given by q_T subtraction, reviewing its construction. Originally, the method has been formulated to deal with the IR divergences associated to the QCD corrections to the process of hadroproduction of a color singlet system, as an electroweak gauge boson W/Z or the Higgs boson. We can generically consider the reaction

$$h_1(P_1) + h_2(P_2) \to F(\{q_i\}) + X \tag{2.19}$$

for a color singlet system F possibly made of n particles with momenta $\{q_i\}_{i=1}^{n}$. The total momentum of the system F as a whole is denoted as $q = \sum_{i=1}^{n} q_i$. At the lowest order in perturbation theory, this class of reactions is initiated only by two partonic subprocesses:

FIGURE 2.2: Feynman diagrams contributing to the NLO real corrections in the hadroproduction of an electroweak gauge boson W/Z.

- the annihilation of a quark-antiquark pair $q(p_1) + \bar{q}(p_2) \to F(q)$ (as in the case of W/Z production),
- the fusion of two gluons $g(p_1) + g(p_2) \to F(q)$ (as in the case of Higgs boson production in the "heavy-top" Higgs Effective Theory [116, 117]).

as all the other partonic subprocesses are vanishing for color conservation.

To understand the main idea, consider the class of real corrections shown in Fig. 2.2, which start to contribute at NLO. To be definite, we have considered explicitly the case of the hadroproduction of an electroweak boson W/Z, but the following reasoning applies for any color singlet objects in the final state as well. The IR divergences of the real emission Feynman diagrams correspond to the configurations where the t-channel propagator is singular. In the partonic center-of-mass frame, we can parametrize the initial state momenta as

$$p_1 = \frac{\sqrt{s}}{2}(1,0,0,1), \quad p_2 = \frac{\sqrt{s}}{2}(1,0,0,-1) \tag{2.20}$$

being s the center-of-mass energy, and the final state particles are back-to-back, $\mathbf{k} = -\mathbf{q}$. Then, the t-channel propagator can be parametrized in terms of the transverse momentum q_T of the color object F as

$$\frac{1}{2p_1 \cdot k} = \frac{1}{\sqrt{s}} \frac{1}{k^0 - k^3} = \frac{1}{\sqrt{s}} \frac{k^0 + k^3}{(k^0)^2 - (k^3)^2} = \frac{1}{\sqrt{s}} \frac{k^0 + k^3}{q_T^2}. \tag{2.21}$$

We see that the variable q_T is a **good resolution variable** in the sense of the previous section:

- for $q_T > 0$ the propagator cannot be divergent. The real corrections are then finite and they have the IR structure of a LO (one order less) computation;
- all the IR divergences are contained in the small q_T limit.

Similarly, going one order higher, the transverse momentum of the q_T color singlet object separates the region with at least one resolved final state parton, as long as $q_T > 0$, from the unresolved region at $q_T = 0$. In the former region, the NNLO corrections are equivalent to the NLO corrections to the process $F + 1$ jet with an extra resolved jet in the final state.

The q_T subtraction formalism cannot handle partonic processes with final-state collinear singularities as in reactions involving the production of QCD jets. To clarify this statement, we follow the same reasoning as before and consider the NLO real correction to the process $V + 1$ jet ($V = W/Z$) depicted in Fig. 2.3. In this case, we focus on the fermion propagator carrying the momentum $k = k_1 + k_2$. Adopting the parametrization in terms of the transverse momentum p_T, the rapidity y and the azimuthal angle ϕ,

$$k_i = k_{i,T}(\cosh y_i, \cos \phi_i, \sin \phi_i, \sinh y_i), \quad i = 1, 2, \tag{2.22}$$

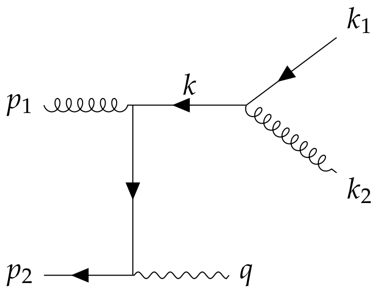

FIGURE 2.3: Feynman diagrams contributing to the NLO real corrections in associated hadroproduction of an electroweak gauge boson W/Z with a QCD jet.

the propagator can be written as

$$\frac{1}{2k_1 \cdot k_2} = \frac{1}{2k_{1,T}k_{2,T}(\cosh(y_1 - y_2) - \cos(\phi_1 - \phi_2))} = \frac{1}{2k_{1,T}|q_T - k_{1,T}|}\frac{1}{\cosh \Delta y - \cos \Delta\phi}\,, \tag{2.23}$$

where in the last step we exploit the tri-momentum conservation in the partonic center-of-mass frame, $\mathbf{k_{1,T}} + \mathbf{k_{2,T}} + \mathbf{q_T} = \mathbf{0}$. Hence, we see that the final-state propagator blows up in the collinear limit $\Delta y = \Delta\phi = 0$ for any values of the transverse momentum q_T. In this situation, the transverse momentum cannot play the role of the resolution variable and one should look for another observable as the 1-jettiness [118, 119].

The fact that the q_T observable is a good resolution variable for the process in Eq. (2.19) is not sufficient alone to fully define a subtraction scheme. According to the discussion in the previous section, the other fundamental ingredient is provided by the knowledge of the singular part of the q_T spectrum in the $q_T \to 0$ limit. In the case the produced final-state system is composed of non-QCD particles, the behavior of the q_T distribution in the small q_T limit has a universal structure that has been extensively studied, through the formalism of the transverse momentum resummation both in QCD [120–123] and in Soft and Collinear Effective Theory (SCET) [124–128], and it is explicitly known up to the NNLO level. In particular, the result on transverse-momentum resummation are sufficient to fully specify the q_T subtraction formalism for this entire class of processes.

Small-q_T behavior in the transverse-momentum resummation formalism

In the following, we detail the construction of the q_T subtraction scheme as an explicit realization of the non local subtraction formalism, generically described by Eq. (2.17). To this aim, we first briefly recall the main results of the transverse-resummation for the q_T distribution in the hadroproduction of a color singlet system. Let us introduce the fully differential cross section for the generic process in Eq. (2.19)

$$\frac{d\sigma_F}{d^2\mathbf{q}_T dM^2 dy d\mathbf{\Omega}}(P_1, P_2; \mathbf{q}_T, M, y, \mathbf{\Omega})\,, \tag{2.24}$$

which depends on the total momentum of the system F, i.e. on its invariant mass $M^2 = q^2$, rapidity y and the set $\mathbf{\Omega} = \{\Omega_A, \Omega_B, \dots\}$ of additional variables that control the kinematics of the particles in the system F. This represents the explicit form of the differential cross section $d\sigma/d\Phi_n dX$ introduced in the previous section for the specific case under consideration. In this context, it is assumed that the kinematic variables $\{\Omega_A, \Omega_B, \dots\}$ do not depend on $\mathbf{q}_T$, M^2 and y and that the set of variable $\{\mathbf{q}_T, M^2, y, \mathbf{\Omega}\}$ completely determines the kinematic configurations of the particles in the system F. The hadronic cross section in Eq. (2.24)

is obtained as the convolution of partonic cross sections and the customary scale-dependent parton distributions $f_{a/h}(x,\mu_F^2)$, being $a = q_f, \bar{q}_f, g$ the parton label of the colliding hadrons. As it is customary in QCD calculations, it is assumed that the parton densities are defined in the $\overline{MS}$ factorization scheme and the strong coupling $\alpha_s(q^2)$ corresponds to the QCD running coupling in the $\overline{MS}$ renormalization scheme.
We then decompose the fully differential cross section into a regular and a singular part as in Eq. (2.6). In particular, we recall that the partonic cross section entering the singular component contains all the contributions that are enhanced at small q_T, i.e. either contribution proportional to $\delta^{(2)}(\mathbf{q}_T)$ or to large logarithms of the type $1/q_T^2 \ln^k M^2/q_T^2$. Within the transverse-momentum resummation formalism, only the singular component is considered, which represents what is needed to develop the subtraction scheme. The main result is encoded in the resummation formula which predicts a universal structure for the singular component in all-order perturbation theory. It explicitly reads [120, 129]

$$\frac{d\sigma_F^{\text{sing}}}{d^2\mathbf{q}_T dM^2 dy d\mathbf{\Omega}}(P_1,P_2;\mathbf{q}_T,M,y,\mathbf{\Omega}) = \frac{M^2}{S}\sum_{c=q,\bar{q},g}\frac{d\hat{\sigma}^{(0)}_{c\bar{c},F}}{dM^2 d\mathbf{\Omega}}(P_1,P_2;M,\mathbf{\Omega})$$
$$\times \int \frac{d^2\mathbf{b}}{(2\pi)^2} e^{i\mathbf{b}\cdot\mathbf{q}_T} S_c(M,b) \sum_{a_1,a_2}\int_{x_1}^1 \frac{dz_1}{z_1}\int_{x_2}^1\frac{dz_2}{z_2}[H^F C_1 C_2]_{c\bar{c};a_1,a_2} f_{a_1/h_1}(x_1,b_0^2/b^2) f_{a_2/h_2}(x_2,b_0^2/b^2)\,, \tag{2.25}$$

where $b_0 = 2e^{-\gamma_E}$, ($\gamma_E = 0.5772\ldots$ is the Euler constant) is a numerical coefficient, $S = 2P_1 \cdot P_2$ is the energy in the hadronic system, and the kinematic variables x_1 and x_2 are

$$x_1 = \frac{M}{\sqrt{S}}e^{y}, \quad x_2 = \frac{M}{\sqrt{S}}e^{-y}\,. \tag{2.26}$$

We highlight the main features of the resummation formula in Eq. (2.25):

- it factorizes the lowest order partonic cross section $d\hat{\sigma}^{(0)}_{c\bar{c},F}$, which introduces a trivial process dependence due to the Born scattering amplitude of the partonic process $c\bar{c} \to F$;
- it involves the Fourier transformation with respect to the *impact parameter* $\mathbf{b}$, which represents the Fourier conjugate variable of the transverse momentum $\mathbf{q}_T$. Therefore, the region $q_T/M \ll 1$ corresponds to $Mb \gg 1$;
- the function $S_c(M,b)$, which depends only on the type ($c = q$ or $c = g$) of colliding partons, is the Sudakov form factor whose all-order expression is [120]

$$S_c(M,b) = \exp\left\{-\int_{b_0^2/b^2}^{M^2}\frac{dq^2}{q^2}\left[A_c(\alpha_s(q^2))\ln\frac{M^2}{q^2} + B_c(\alpha_s(q^2))\right]\right\}. \tag{2.27}$$

  in terms of the perturbative functions

$$A_c(\alpha_s) = \sum_{n=1}^{\infty}\left(\frac{\alpha_s}{\pi}\right)^n A_c^{(n)}, \quad B_c(\alpha_s) = \sum_{n=1}^{\infty}\left(\frac{\alpha_s}{\pi}\right)^n B_c^{(n)}\,. \tag{2.28}$$

  As stated in Eq. (2.27), it is responsible for the resummation of the large logarithmically-enhanced contributions;
- the parton densities are evaluated at the scale of b_0^2/b^2 which depends on the impact parameter;

- the *hard-collinear* term $[H^F C_1 C_2]_{c\bar{c};a_1,a_2}$ embodies the remaining process dependence of the resummation formula related to the virtual corrections proportional to $\delta(q_T^2)$.

The idea to build the subtraction is now quite simple. In practice, what we need are the coefficient functions in Eq. (2.9). By comparing it with the fixed order expansion of the resummation formula, we can express such coefficient functions in terms of the resummation coefficients. If the latter are known up to the required order, then the subtraction will directly follow. Before going on in this direction, we discuss further the hard collinear term and the universality structure of the resummation formula. This is an important point to understand to what extent the subtraction scheme will be process-independent (remaining, of course in the class of color singlet processes we are dealing with).

The first comment is that the structure of the hard collinear function is different for processes initiated at the Born level by the quark-anti quark annihilation channel and the ones initiated by the gluon fusion channel. In the latter case, indeed, the physics of the small-q_T region has a richer structure due to the non-trivial spin dependence of the collinear splittings. Collinear radiation from the colliding gluons leads to spin and azimuthal correlations [123, 130] which are embodied in the hard-collinear function. For ease of reading and since, in view of the application to the mixed corrections to the Drell-Yan processes, we are mainly interested in the quark-anti quark channel, in the following we specialize the discussion to this case. Then, in the case of processes initiated at the Born level by the quark-anti quark channel, the symbolic hard-collinear function is explicitly given by the product

$$[H^F C_1 C_2]_{q\bar{q};a_1,a_2} = H_q^F C_{qa_1} C_{\bar{q}a_2} \tag{2.29}$$

of two scalar functions, H_q^F and C_{qa_1}, which admit a perturbative expansion in powers of the strong coupling α_s. Notice that in the above, we do not specify the argument of these functions on purpose. The reason is the following: the resummation formula in Eq. (2.25) is invariant under the following renormalization-group transformation [129]

$$H_c^F(\alpha_s) \to H_c^F(\alpha_s)[h_c(\alpha_s)]^{-1}, \tag{2.30}$$

$$B_c(\alpha_s) \to B_c(\alpha_s) - \beta(\alpha_s)\frac{d\ln h_c(\alpha_s)}{d\ln(\alpha_s)}, \tag{2.31}$$

$$C_{cb}(\alpha_s) \to C_{cb}(\alpha_s)[h_c(\alpha_s)]^{1/2}, \tag{2.32}$$

$$\tag{2.33}$$

where $h_c(\alpha_s) = 1 + \mathcal{O}(\alpha_s)$ is an arbitrary perturbative function, and $\beta(\alpha_s)$ denotes the QCD β-function

$$\frac{d\ln\alpha_s(q^2)}{d\ln q^2} = \beta(\alpha_s(q^2)), \tag{2.34}$$

$$\beta(\alpha_S) = -\beta_0\,\alpha_S - \beta_1\,\alpha_S^2 + \mathcal{O}(\alpha_S^3), \tag{2.35}$$

$$\beta_0 = \frac{11C_A - 2N_f}{12\pi}\;, \quad \beta_1 = \frac{17C_A^2 - 5C_A N_f - 3C_F N_f}{24\pi^2}\;, \tag{2.36}$$

where N_f is the number of quark flavours, N_c is the number of colours, and the colour factors are $C_F = (N_c^2-1)/(2N_c)$ and $C_A = N_c$ in $SU(N_c)$ QCD. This means that the resummation factors H_c^F, S_c and C_{cb} are not unambiguously defined and according to the prescription used to uniquely fix their definition one will end up with a different resummation scheme. In particular, the process dependence can be shifted among the three factors and this is the reason why we omit the arguments in Eq. (2.29). One of the result of Ref. [129] is the fact

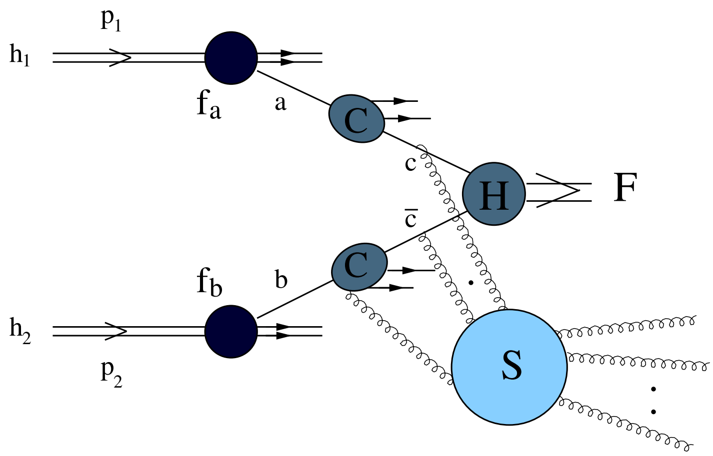

FIGURE 2.4: Diagrammatic representation of the different factors entering the resummation formula in the hadroprodution of a color singlet object.

that, employing this freedom, one can define a scheme, dubbed *hard scheme*[1], in which all the process dependence is contained just in one coefficient, namely the hard coefficient H^F_c, while both the resummation factors S_c and C_{cb} are universal and process-independent. In this scheme, Eq.(2.29) explicitly reads [129]

$$[H^F C_1 C_2]_{q\bar{q};a_1,a_2} = H^F_q(x_1P_1, x_2P_2; \mathbf{\Omega}; \alpha_s(M^2))C_{qa_1}(z_1; \alpha_s(b_0^2/b^2))C_{\bar{q}a_2}(z_2; \alpha_s(b_0^2/b^2)), \quad (2.37)$$

where we highlight that the difference in the scales at which the strong coupling is evaluated (M^2 in the case of H^F_q and b_0^2/b^2 in the case of C_{qa}) is a crucial result of the factorization of the short distance and process-dependent physics contained in the hard function from the long-distance and process-independent physics embodied in the universal factors S_c and C_{cb}. The specification of the hard scheme (or any other schemes) is not a fundamental one, in the sense that the q_T cross section, its all-order resummation formula (2.25) and any consistent perturbative truncation (either order-by-order in α_S or in classes of logarithmic-enhanced terms) of the latter [121, 129] does not depend on the resummation scheme at all. On the other hand, it allows a cleaner presentation and organization of the resummation factors. Indeed, in the hard scheme, the physical origin of the resummation formula emerges clearly and can be pictorial represented as in Fig. 2.4: at small-q_T, the emission of radiation accompanying the final-state system F is strongly inhibited, but for soft and collinear radiation. Then, a distinctive picture emerges characterized by three class of processes separated in the q_T *evolution*:

- the process dependent factor H^F_c embodies the hard contributions produced by virtual corrections at transverse-momentum scales $q_T \sim M$;
- the Sudakov form factor S_c describes real and virtual (through unitary) contributions associated to soft ($A_c(\alpha_s)$) and flavour-conserving collinear (B_c) radiation at scales $M \gtrsim q_T \gtrsim 1/b$;
- going at very low momentum scale, $q_T \lesssim 1/b$, real and virtual soft-gluon corrections cancel among each other as the cross section is infrared safe. The left over is provided by initial-state collinear radiation associated to the proton activity and is embodied in the coefficient functions C_{ab}.

[1]More precisely, the *hard scheme* is the scheme in which, order-by-order in perturbation theory, the coefficients $C^{(n)}_{ab}(z)$ with $n \geq 1$ do not contain any $\delta(1-z)$ term.

q_T subtraction formula

In this section, we present and discuss the q_T subtraction formula for the color singlet case. We follow Ref. [121] and introduce the compact notation for the resummation formula in Eq. (2.25)

$$\frac{d\sigma_F}{dq_T dM^2 dy d\mathbf{\Omega}}(P_1, P_2; q_T, M, y, \mathbf{\Omega}) = \frac{M^2}{S} \int db \frac{b}{2} J_0(bq_T) W^F(b, M, y, \mathbf{\Omega}) \,. \tag{2.38}$$

which has been specialized for the case of processes initiated by the quark-anti quark annihilation channel. The integrand in the resummation formula for this class of processes depends only on the modulo of the impact parameter **b**. This factorizes the integration over the angle in the **b**-space

$$\int \frac{d^2\mathbf{b}}{(2\pi)^2} e^{i\mathbf{b}\cdot\mathbf{q_T}} = \int \frac{bdbd\phi}{(2\pi)^2} e^{ibq_T\cos\phi} = \int db \frac{b}{2}\frac{1}{\pi}(J_0 bq_T)\,, \tag{2.39}$$

with $J_0(x)$ the customary 0th-order Bessel function. As already mentioned before, the idea is to expand the resummation formula at fixed order in α_s and to identify the coefficients of the logarithmic enhanced contributions and of the contact delta term in Eq. (2.9).

Since the resummation formula is expressed in the impact parameter space, the large logarithms in the small q_T limit corresponds to large logarithms in the $b \to \infty$ limit of the type $\ln M^2 b^2$. Some degree of arbitrariness remains in the definition of the argument of the logarithm as we are allowed to rescale it as $\ln M^2 b^2 = \ln Q^2 b^2 + \ln M^2/Q^2$ provided Q is independent on b and $\ln M^2/Q^2 = \mathcal{O}(1)$ in the limit $bM \gg 1$. The *resummation* scale $Q \sim M$ plays in the resummation program the same role assumed by the renormalization μ_R and factorization μ_F scales respectively in the context of renormalization and factorization. While the all-order resummation formula is independent on this scale, its truncation at some level of logarithmic accuracy (to be not confused with the fixed order expansion in the strong coupling) will show a residual dependence on Q which can be interpreted as a measure of the uncertainty associated to missing higher order terms.

In the application to the subtraction, the final result cannot depend on Q at any fixed order. In this context, the resummation scale Q can be either neglected or considered as an additional free parameter that can be used to check the implementation or to shift part of the corrections from the counterterm to the hard-collinear part. In the following presentation, we retain the dependence on Q for the sake of generality. Then, we parametrize the large logarithmic expansion parameter L as

$$L \equiv \ln \frac{Q^2 b}{b_0^2}. \tag{2.40}$$

A second comment regard the behavior of L at small-b (large-q_T). Also in this limit, L diverges logarithmically. In order to avoid the resummation of this enhanced contribution, the simplest strategy is given by the introduction of an hard cut-off $b_{\rm min}$ (corresponding to a maximum value $q_{T,\rm max}$). In Ref. [121] a different approach is proposed with the aim to obtain a procedure to match the fixed order calculation with the resummed one without introducing any arbitrary matching scale (uniform/smooth scaleless matching). The strategy consists in replacing L with

$$\tilde{L} = \ln\left(\frac{Q^2 b}{b_0^2} + 1\right). \tag{2.41}$$

The above replacement, which has the effect to reduce the impact of the resummed contribution in the small-b region (where the resummation is not justified), is legitimate in the sense explained above, the difference between L and $\tilde{L}$ being of order $O(1/(Qb)^2)$ and so negligible in the large-b limit. In particular, we observe that $\tilde{L}$ is integrable for $b \to 0$ so that we can effectively push $b_{\min}$ to 0, or equivalently $q_{T,\max} = \infty$. It is then customary in this context to organize the fixed order expansion in terms of the perturbative coefficients $\tilde{\Sigma}^{(n)}$ implicitly defined as

$$\begin{aligned}\mathcal{W}^F_{ab}(b, M, \hat{s}; \alpha_S, \mu_R^2, \mu_F^2, Q^2) = \sum_c \frac{d\hat{\sigma}^{(0)}_{c\bar{c},F}}{dM^2 d\mathbf{\Omega}}(P_1, P_2; M, \mathbf{\Omega}) \Big\{ \delta_{ca}\, \delta_{\bar{c}b}\, \delta(1-z) \\ + \sum_{n=1}^{\infty} \left(\frac{\alpha_S}{\pi}\right)^n \left[\tilde{\Sigma}^{F\,(n)}_{c\bar{c}\leftarrow ab}\left(z, \tilde{L}; \frac{M^2}{\mu_R^2}, \frac{M^2}{\mu_F^2}, \frac{M^2}{Q^2}\right) \right. \\ \left. + \mathcal{H}^{F\,(n)}_{c\bar{c}\leftarrow ab}\left(z; \frac{M^2}{\mu_R^2}, \frac{M^2}{\mu_F^2}, \frac{M^2}{Q^2}\right)\right] \Big\} \,,\end{aligned} \tag{2.42}$$

where the resummed factor $\mathcal{W}^F_{ab}$ is related to the factor W^F in Eq. (2.38) by the relation

$$W^F_N(b, M) = \sum_{a,b} \mathcal{W}^F_{ab,\,N}(b, M; \alpha_S(\mu_R^2), \mu_R^2, \mu_F^2)\; f_{a/h_1,N}(\mu_F^2)\; f_{b/h_2,N}(\mu_F^2) \;. \tag{2.43}$$

In particular, for $n = 1, 2$ we have explicitly

$$\tilde{\Sigma}^{F\,(1)}_{c\bar{c}\leftarrow ab}(z, \tilde{L}) = \Sigma^{F\,(1;2)}_{c\bar{c}\leftarrow ab}(z)\; \tilde{L}^2 + \Sigma^{F\,(1;1)}_{c\bar{c}\leftarrow ab}(z)\; \tilde{L}\,, \tag{2.44}$$

$$\tilde{\Sigma}^{F\,(2)}_{c\bar{c}\leftarrow ab}(z, \tilde{L}) = \Sigma^{F\,(2;4)}_{c\bar{c}\leftarrow ab}(z)\; \tilde{L}^4 + \Sigma^{F\,(2;3)}_{c\bar{c}\leftarrow ab}(z)\; \tilde{L}^3 + \Sigma^{F\,(2;2)}_{c\bar{c}\leftarrow ab}(z)\; \tilde{L}^2 + \Sigma^{F\,(2;1)}_{c\bar{c}\leftarrow ab}(z)\; \tilde{L}\,, \tag{2.45}$$

where the dependence on the scale ratios $M^2/\mu_R^2, M^2/\mu_F^2$ and M^2/Q^2 is understood. The notation $c\bar{c} \leftarrow ab$ denotes the transition from the incoming partons a, on the first leg, and b, on the second leg, to the $c\bar{c}$ partons entering the hard scattering process. The NNLO truncation of Eq. (2.42), supplemented with Eqs. (2.44)-(2.45), represents the explicit form of Eq. (2.9) in the case of q_T subtraction formalism. In this context, $X = q_T/Q$ and the logarithmic terms in Eq. (2.9), are replaced by the more involved functions given by the Bessel transformation from the b- to the q_T-space of the $\tilde{L}^n$ powers

$$\tilde{I}_n(q_T/Q) = Q^2 \int_0^{\infty} db\, \frac{b}{2}\, J_0(bq_T)\; \ln^n\left(\frac{Q^2b^2}{b_0^2} + 1\right) \;. \tag{2.46}$$

whose properties are detailed in Appendix B of Ref. [121]. The q_T subtraction formula for the parton level differential cross section in the hadroproduction of a color singlet system F can be written with obvious notation in the following compact form

$$d\hat{\sigma}^F_{\text{(N)NLO}} = \mathcal{H}^F_{\text{(N)NLO}} \otimes d\sigma^F_{\text{LO}} + \left[d\sigma^{F+\text{jets}}_{(N)LO} - d\hat{\sigma}^{\text{CT}}_{\text{(N)NLO}}\right]_{\frac{q_T}{Q} > r_{\text{cut}}} \,, \tag{2.47}$$

where the symbol $\otimes$ denotes convolutions with respect to the longitudinal-momentum fractions z_1 and z_2 of the colliding partons and the counterterm reads

$$d\hat{\sigma}^{\text{CT}} = d\hat{\sigma}^F_{\text{LO}} \otimes \tilde{\Sigma}\left(\frac{q_T}{Q}\right). \tag{2.48}$$

We stress that Eq. (2.47) must be interpreted as explicitly stated in Eq. (2.17) for a generic non-local subtraction scheme, with $X_{\max} \to \infty$, i.e. the counterterm for large q_T is integrated up to infinity. In the small-q_T region instead, since the counterterm does not act locally, the

difference in the square bracket is integrated up to $q_T/M = r_{\rm cut} > 0$, $r_{\rm cut}$ being a dimensionless cut-off parameter.
Having given the basic structure of the subtraction, the explicit form of the perturbative b-independent coefficients $\Sigma^{F\,(1;k)}(z)$, $\mathcal{H}^{F\,(1)}(z)$, $\Sigma^{F\,(2;k)}(z)$ and $\mathcal{H}^{F\,(2)}(z)$, required to performed the computation up to NNLO, is presented in the following formulae in terms of the perturbative resummation coefficients. The results are more easily presented in terms of the N-moments with respect to the variable z[2]. We have

$$\Sigma^{F\,(1;2)}_{c\bar{c}\leftarrow ab,\,N} = -\frac{1}{2} A_c^{(1)}\;\delta_{ca}\delta_{\bar{c}b}\;, \tag{2.49}$$

$$\Sigma^{F\,(1;1)}_{c\bar{c}\leftarrow ab,\,N}(M^2/Q^2) = -\left[\delta_{ca}\delta_{\bar{c}b}\;\left(B_c^{(1)} + A_c^{(1)}\,\ell_Q\right) + \delta_{ca}\gamma^{(1)}_{\bar{c}b,\,N} + \delta_{\bar{c}b}\gamma^{(1)}_{ca,\,N}\right]\;, \tag{2.50}$$

$$\begin{aligned}\mathcal{H}^{F\,(1)}_{c\bar{c}\leftarrow ab,\,N}\left(\frac{M^2}{\mu_R^2},\frac{M^2}{\mu_F^2},\frac{M^2}{Q^2}\right) \;&=\; \delta_{ca}\delta_{\bar{c}b}\left[H_c^{F\,(1)} - \left(B_c^{(1)} + \frac{1}{2}A_c^{(1)}\ell_Q\right)\ell_Q - p_{cF}\beta_0\ell_R\right]\\ &\quad+\delta_{ca}C^{(1)}_{\bar{c}b,\,N} + \delta_{\bar{c}b}C^{(1)}_{ca,\,N} + \left(\delta_{ca}\gamma^{(1)}_{\bar{c}b,\,N} + \delta_{\bar{c}b}\gamma^{(1)}_{ca,\,N}\right)(\ell_F - \ell_Q)\;,\end{aligned} \tag{2.51}$$

$$\Sigma^{F\,(2;4)}_{c\bar{c}\leftarrow ab,\,N} = \frac{1}{8}\left(A_c^{(1)}\right)^2\;\delta_{ca}\delta_{\bar{c}b}\;, \tag{2.52}$$

$$\Sigma^{F\,(2;3)}_{c\bar{c}\leftarrow ab,\,N}(M^2/Q^2) = -\,A_c^{(1)}\left[\frac{1}{3}\beta_0\;\delta_{ca}\delta_{\bar{c}b} + \frac{1}{2}\Sigma^{F\,(1;1)}_{c\bar{c}\leftarrow ab,\,N}(M^2/Q^2)\right]\;, \tag{2.53}$$

$$\begin{aligned}\Sigma^{F\,(2;2)}_{c\bar{c}\leftarrow ab,\,N}\left(\frac{M^2}{\mu_R^2},\frac{M^2}{\mu_F^2},\frac{M^2}{Q^2}\right) \;&=\; -\frac{1}{2}A_c^{(1)}\left[\mathcal{H}^{F\,(1)}_{c\bar{c}\leftarrow ab,\,N}\left(\frac{M^2}{\mu_R^2},\frac{M^2}{\mu_F^2},\frac{M^2}{Q^2}\right) - \beta_0\;\delta_{ca}\delta_{\bar{c}b}\,(\ell_R - \ell_Q)\right]\\ &\quad-\;\frac{1}{2}\sum_{a_1,b_1}\Sigma^{F\,(1;1)}_{c\bar{c}\leftarrow a_1b_1,\,N}(M^2/Q^2)\left[\delta_{a_1a}\gamma^{(1)}_{b_1b,\,N} + \delta_{b_1b}\gamma^{(1)}_{a_1a,\,N}\right]\\ &\quad-\;\frac{1}{2}\left[A_c^{(2)}\;\delta_{ca}\delta_{\bar{c}b} + \left(B_c^{(1)} + A_c^{(1)}\,\ell_Q - \beta_0\right)\Sigma^{F\,(1;1)}_{c\bar{c}\leftarrow ab,\,N}(M^2/Q^2)\right]\;,\end{aligned} \tag{2.54}$$

$$\begin{aligned}\Sigma^{F\,(2;1)}_{c\bar{c}\leftarrow ab,\,N}&\left(\frac{M^2}{\mu_R^2},\frac{M^2}{\mu_F^2},\frac{M^2}{Q^2}\right) = \Sigma^{F\,(1;1)}_{c\bar{c}\leftarrow ab,\,N}(M^2/Q^2)\,\beta_0\,(\ell_Q - \ell_R)\\ &-\;\sum_{a_1,b_1}\mathcal{H}^{F\,(1)}_{c\bar{c}\leftarrow a_1b_1,\,N}\left(\frac{M^2}{\mu_R^2},\frac{M^2}{\mu_F^2},\frac{M^2}{Q^2}\right)\left[\delta_{a_1a}\delta_{b_1b}\left(B_c^{(1)} + A_c^{(1)}\,\ell_Q\right) + \delta_{a_1a}\gamma^{(1)}_{b_1b,\,N} + \delta_{b_1b}\gamma^{(1)}_{a_1a,\,N}\right]\\ &-\;\left[\delta_{ca}\delta_{\bar{c}b}\left(B_c^{(2)} + A_c^{(2)}\,\ell_Q\right) - \beta_0\left(\delta_{ca}C^{(1)}_{\bar{c}b,\,N} + \delta_{\bar{c}b}C^{(1)}_{ca,\,N}\right) + \delta_{ca}\gamma^{(2)}_{\bar{c}b,\,N} + \delta_{\bar{c}b}\gamma^{(2)}_{ca,\,N}\right]\;,\end{aligned} \tag{2.55}$$

[2] In this work, we define the N-moments f_N of any function $f(z)$ of the variable z as $f_N = \int_0^1 dz\,z^{N-1}\,f(z)$.

$$
\begin{aligned}
&\mathcal{H}^{F\,(2)}_{c\bar{c}\leftarrow ab,\,N}\left(\frac{M^2}{\mu_R^2},\frac{M^2}{\mu_F^2},\frac{M^2}{Q^2}\right) = \delta_{ca}\delta_{\bar{c}b}\,H_c^{F\,(2)} + \delta_{ca}\,C^{(2)}_{\bar{c}b,\,N} + \delta_{\bar{c}b}\,C^{(2)}_{ca,\,N} + C^{(1)}_{ca,\,N}\,C^{(1)}_{\bar{c}b,\,N} \\
&+\; H_c^{F\,(1)}\left(\delta_{ca}\,C^{(1)}_{\bar{c}b,\,N} + \delta_{\bar{c}b}\,C^{(1)}_{ca,\,N}\right) + \frac{1}{6}\,A_c^{(1)}\,\beta_0\,\ell_Q^3\,\delta_{ca}\delta_{\bar{c}b} + \frac{1}{2}\left[A_c^{(2)}\,\delta_{ca}\delta_{\bar{c}b} + \beta_0\,\Sigma^{F\,(1;1)}_{c\bar{c}\leftarrow ab,\,N}(M^2/Q^2)\right]\ell_Q^2 \\
&-\; \left[\delta_{ca}\delta_{\bar{c}b}\left(B_c^{(2)} + A_c^{(2)}\,\ell_Q\right) - \beta_0\left(\delta_{ca}C^{(1)}_{\bar{c}b,\,N} + \delta_{\bar{c}b}C^{(1)}_{ca,\,N}\right) + \delta_{ca}\gamma^{(2)}_{\bar{c}b,\,N} + \delta_{\bar{c}b}\gamma^{(2)}_{ca,\,N}\right]\ell_Q \\
&+\; \frac{1}{2}\,\beta_0\left(\delta_{ca}\gamma^{(1)}_{\bar{c}b,\,N} + \delta_{\bar{c}b}\gamma^{(1)}_{ca,\,N}\right)\ell_F^2 + \left(\delta_{ca}\gamma^{(2)}_{\bar{c}b,\,N} + \delta_{\bar{c}b}\gamma^{(2)}_{ca,\,N}\right)\ell_F - \mathcal{H}^{F\,(1)}_{c\bar{c}\leftarrow ab,\,N}\left(\frac{M^2}{\mu_R^2},\frac{M^2}{\mu_F^2},\frac{M^2}{Q^2}\right)\beta_0\ell_R \\
&+\; \frac{1}{2}\sum_{a_1,b_1}\left[\mathcal{H}^{F\,(1)}_{c\bar{c}\leftarrow a_1b_1,\,N}\left(\frac{M^2}{\mu_R^2},\frac{M^2}{\mu_F^2},\frac{M^2}{Q^2}\right) + \delta_{ca_1}\delta_{\bar{c}b_1}\,H_c^{F\,(1)} + \delta_{ca_1}\,C^{(1)}_{\bar{c}b_1,\,N} + \delta_{\bar{c}b_1}\,C^{(1)}_{ca_1,\,N}\right] \\
&\times\; \left[\left(\delta_{a_1a}\gamma^{(1)}_{b_1b,\,N} + \delta_{b_1b}\gamma^{(1)}_{a_1a,\,N}\right)(\ell_F - \ell_Q) - \delta_{a_1a}\delta_{b_1b}\left(\left(B_c^{(1)} + \frac{1}{2}\,A_c^{(1)}\,\ell_Q\right)\ell_Q + p_{cF}\,\beta_0\,\ell_R\right)\right] \\
&-\; \delta_{ca}\delta_{\bar{c}b}\,p_{cF}\left(\frac{1}{2}\,\beta_0^2\,\ell_R^2 + \beta_1\,\ell_R\right)\;.
\end{aligned}
\tag{2.56}
$$

In the above formulae, p_{cF} is the power of the α_s^n factor in the LO partonic process, we have defined

$$
\ell_R = \ln\frac{M^2}{\mu_R^2}\;,\quad \ell_F = \ln\frac{M^2}{\mu_F^2}\;,\quad \ell_Q = \ln\frac{M^2}{Q^2}\;. \tag{2.57}
$$

and $\gamma_{ab,\,N}(\alpha_S)$ are the parton anomalous dimensions or, more precisely, the N-moments of the customary Altarelli–Parisi splitting functions $P_{ab}(\alpha_S, z)$ [70, 131–133]:

$$
\gamma_{ab,\,N}(\alpha_S) = \int_0^1 dz\, z^{N-1}\,P_{ab}(\alpha_S, z) = \sum_{n=1}^{\infty}\left(\frac{\alpha_S}{\pi}\right)^n \gamma^{(n)}_{ab,\,N}\;. \tag{2.58}
$$

We observe that the required ingredients for

- a NLO order computation are the universal resummation coefficients $A_c^{(1)}$, $B_c^{(1)}$, $C_{ab}^{(1)}$, the perturbative coefficient β_0 of the QCD β-function, the process-dependent hard-virtual function $H_c^{F(1)}$ and the LO Altarelli-Parisi splitting functions;
- a NNLO order computation are, in addition to the previous ones, the universal resummation coefficients $A_c^{(2)}$, $B_c^{(2)}$, $C_{ab}^{(2)}$, the perturbative coefficient β_1 of the QCD β-function, the NLO Altarelli-Parisi splitting functions.

It is worth to mention that in terms of the logarithmic accuracy, the $A_c^{(1)}$ coefficient controls the Leading-Log (LL), then $B_c^{(1)}$ and $A_c^{(2)}$ enter the computation at Next-to-Leading-Log (NLL) and the coefficient $B_c^{(2)}$ starts to appear at Next-to-Next-to-Leading-Log (NNLL). All the ingredients required for a NNLO computation are known and for ease of reading we collect them in Appendix A.

Before concluding this section, we comment on the universality of the q_T subtraction formula. Since the perturbative coefficient functions $A_c^{(n)}$, $B_c^{(n)}$, $C_{ab}^{(n)}$ are universal, they can be computed once and for all in a specific process and then they are fixed for the entire class of processes to which it belongs. In particular, this means that one has to carry out explicitly the computation for one process initiated by the quark-anti quark annihilation channel and another one initiated by the gluon fusion channel to fully specify the counterterm for the entire class of color-singlet processes. By *explicitly carry out* we mean that it is really needed to perform the integration of the total cross section at small-q_T analytically, as it has been done in Ref. [134] (vector boson) and Ref.[135] (Higgs), in order to extract the expressions of the these universal coefficients.

In the hard scheme, the hard-virtual coefficient H_c^F contains all the process-dependent contributions due to virtual corrections. In principle, one should compute it process-by-process performing the integration of the cross section as discussed before, making the extension to a new process (in the same class of reactions for which all the other universal coefficients are know) cumbersome. On the other hand, multi-loop virtual scattering amplitudes can be computed independently exploiting other strategies and are usually the ingredients required in local subtraction formalism. It arises naturally the question whether it is possible to relate the multi-loop virtual amplitudes to the hard-virtual function in such a way that from the knowledge of the former it is possible to get the latter. The answer to this question is affermative and it is the main result of Ref. [136]. In practice, starting from the on-shell multi-loop virtual amplitude $\mathcal{M}_{c\bar{c}\to F}$ renormalized in the $\overline{MS}$ scheme (UV finite, IR divergent), one introduces an auxiliary amplitude $\widetilde{\mathcal{M}}_{c\bar{c}\to F}$ by means of the following factorization formula

$$\widetilde{\mathcal{M}}_{c\bar{c}\to F}(\hat{p}_1,\hat{p}_2;\{q_i\}) = \left[1-\tilde{I}_c(\epsilon,M^2)\right]\mathcal{M}_{c\bar{c}\to F}(\hat{p}_1,\hat{p}_2;\{q_i\}) \ , \tag{2.59}$$

with

$$\begin{aligned}\tilde{I}_c(\epsilon,M^2) &= \frac{\alpha_S(\mu_R^2)}{2\pi}\,\tilde{I}_c^{(1)}(\epsilon,M^2/\mu_R^2) + \left(\frac{\alpha_S(\mu_R^2)}{2\pi}\right)^2 \tilde{I}_c^{(2)}(\epsilon,M^2/\mu_R^2)\\ &+\sum_{n=3}^{\infty}\left(\frac{\alpha_S(\mu_R^2)}{2\pi}\right)^n \tilde{I}_c^{(n)}(\epsilon,M^2/\mu_R^2)\,.\end{aligned} \tag{2.60}$$

The *subtraction factor* $\tilde{I}_c(\epsilon,M^2)$ removes from the original $\mathcal{M}_{c\bar{c}\to F}$ the IR divergent poles plus some *definite* amount of IR finite terms, which specifically depend on the transverse-momentum cross section in Eq. (2.19) but are otherwise process-independent. We report the explicit expression of the coefficients $\tilde{I}_c^{(1)}(\epsilon,M^2/\mu_R^2)$ and $\tilde{I}_c^{(2)}(\epsilon,M^2/\mu_R^2)$ in Appendix A. What it is worth noticing is that to fix the structure of the subtraction operator, at least up to the second order, it is sufficient to use only one process, either initiated at LO by the quark-anti quark channel or by the gluon fusion, as the dependence on the parton c factorizes and, hence, can be easily derived from one case to the other. In particular, this holds for the finite part of $\tilde{I}_c^{(2)}(\epsilon,M^2/\mu_R^2)$, for which all the dependence on the parton c is contained in the overall color charge factor C_c ($C_q = C_F$, $C_g = C_A$) (see Eq. (A.59)). This represents one of main results of the universality of the transverse-momentum resummation.
The process-dependent resummation coefficients H_c^F can then be written as follows

$$\alpha_S^{p_{cF}}(M^2)\,H_q^F(x_1P_1,x_2P_2;\mathbf{\Omega};\alpha_S(M^2)) = \frac{|\widetilde{\mathcal{M}}_{q\bar{q}\to F}(x_1p_1,x_2p_2;\{q_i\})|^2}{|\mathcal{M}^{(0)}_{q\bar{q}\to F}(x_1p_1,x_2p_2;\{q_i\})|^2}\,. \tag{2.61}$$

in the case of processes initiated by quark-anti quark annihilation.

2.2.2 Heavy-quark production

The q_T subtraction formalism is not limited to the color-singlet case. In the previous section, we have argued that the q_T observable does not act as a good resolution variable for processes involving jets in the final state. We recall that the reason is that the q_T does not control the collinear final-state singular limit, so that a radiated (and massless) parton can become collinear to another massless parton in the finale-state regardless q_T is vanishing or not. We observe that, in order to develop collinear final-state singularities, massless partons must appear in the lowest order partonic subprocesses, because otherwise the mass acts

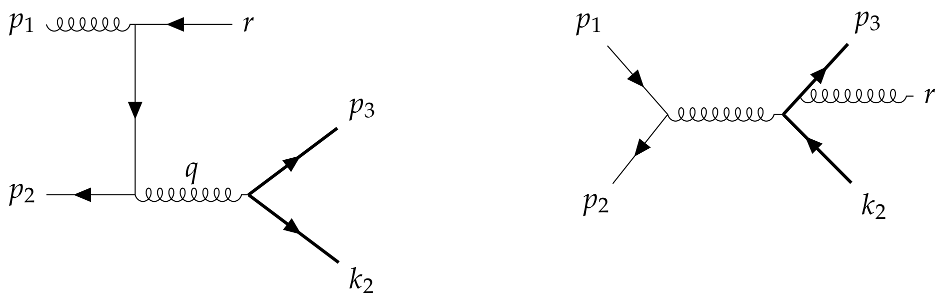

FIGURE 2.5: Feynman diagrams contributing to the NLO real corrections in the hadroproduction of a heavy-quark pair: initial-state radiation (left), final-state radiation (right).

as a physical regulator of these divergences. Therefore we can think to look at processes involving massive coloured final-state systems.
In particular, consider the inclusive process of hadroprodution of a heavy-quark pair

$$h_1(P_1) + h_2(P_2) \to Q(p_3) + \bar{Q}(k_2) + X \tag{2.62}$$

At lowest order, both the quark-anti quark annihilation $q\bar{q} \to Q\bar{Q}$ and the gluon fusion $gg \to Q\bar{Q}$ partonic channels are possible. In the following, we argue that the transverse momentum q_T of the heavy-quark pair can be used as a resolution variable for this case. In Fig. 2.5, we report two illustrative Feynman diagrams of real corrections to the quark-anti quark annihilation channel:

- initial-state radiation (left panel of Fig. 2.5): the situation is perfectly analogous to that of color singlet in Fig. 2.2. The IR divergences are associated to the t-channel propagator and the kinematics is the same. Therefore, we conclude that q_T acts as a resolution variable for this case.

- final-state radiation (right panel of Fig. 2.5): the situation is similar to the $V + 1\,\text{jet}$ in Fig. 2.3, with the fundamental difference that now the quark is massive. We consider the massive propagator carrying the momentum $k = p_3 + r$ and use again the parametrization of the momenta in terms of transverse momentum, rapidity and azimuthal angle:

$$p_3 = (E_{3,T}\cosh y_3, p_{3,T}\cos\phi_1, p_{3,T}\sin\phi_1, E_{3,T}\sinh y_1), \quad E_{3,T} = \sqrt{m_Q^2 + p_{3,T}^2}, \tag{2.63}$$

$$r = (q_T\cosh y_r, q_T\cos\phi_r, q_T\sin\phi_r, q_T\sinh y_r), \tag{2.64}$$

where m_Q is the mass of the heavy quark and we have exploited the conservation of the tri-momentum, so that $r_T = q_T$. Then, the propagator can be written as

$$\frac{1}{2p_3 \cdot r} = \frac{1}{2q_T\left[E_{3,T}\cosh(y_3 - y_r) - p_{3,T}\cos(\phi_1 - \phi_r)\right]} = \frac{1}{2q_T}\frac{1}{\left[E_{3,T}\cosh\Delta y - p_{3,T}\cos\Delta\phi\right]}\,. \tag{2.65}$$

As long as m_Q is not vanishing, the quantity $[E_{1,T}\cosh\Delta y - k_{1,T}\cos\Delta\phi]$ is finite and the propagator is divergent if and only if $q_T = 0$. We conclude that also in this case, the q_T variable is a good resolution variable.

Transverse-momentum resummation and q_T subtraction formula at NLO

In the last few years, thanks to the formulation of transverse-momentum resummation for heavy-quark production [44–48] the q_T subtraction formalism has been extended and applied to the production of top-quark pairs [49–51]. In this section, we will briefly review the main results and present explicitly the q_T subtraction formula at NLO accuracy.
Adopting the same notation of the previous section, the all-order transverse momentum resummation formula reads [46]

$$\frac{d\sigma^{\text{sing}}_{Q\bar{Q}}}{d^2\mathbf{q}_T dM^2 dy d\mathbf{\Omega}}(P_1,P_2;\mathbf{q}_T,M,y,\mathbf{\Omega}) = \frac{M^2}{S}\sum_{c=q,\bar{q},g}\frac{d\hat{\sigma}^{(0)}_{c\bar{c},Q\bar{Q}}}{dM^2 d\mathbf{\Omega}}(P_1,P_2;M,\mathbf{\Omega})$$
$$\times\int\frac{d^2\mathbf{b}}{(2\pi)^2}e^{i\mathbf{b}\cdot\mathbf{q}_T}S_c(M,b)\sum_{a_1,a_2}\int_{x_1}^1\frac{dz_1}{z_1}\int_{x_2}^1\frac{dz_2}{z_2}[\mathbf{H\Delta}C_1C_2]_{c\bar{c};a_1,a_2}f_{a_1/h_1}(x_1,b_0^2/b^2)f_{a_2/h_2}(x_2,b_0^2/b^2)\,. \tag{2.66}$$

Compared to the color singlet case, Eq. (2.25), we see that the structure is similar. The important difference is all enclosed in the symbolic notation $[\mathbf{H\Delta}C_1C_2]_{c\bar{c};a_1,a_2}$. In particular, the factor $\mathbf{\Delta}$ embodies the new contributions due to the accompanying soft-parton radiation in $Q\bar{Q}$ production. Formally, this means that the color-singlet case can be recovered setting $\mathbf{\Delta}=1$. To be more precise, the analog of Eq. (2.37) for the quark-anti quark annihilation channels is

$$[(\mathbf{H}\,\mathbf{\Delta})\,C_1C_2]_{c\bar{c};a_1a_2} = (\mathbf{H}\,\mathbf{\Delta})_{c\bar{c}}\;\;C_{c\,a_1}(z_1;\alpha_S(b_0^2/b^2))\;\;C_{\bar{c}\,a_2}(z_2;\alpha_S(b_0^2/b^2))\;\;,\quad (c=q,\bar{q})\;\;, \tag{2.67}$$

which makes manifest that the collinear coefficient functions C_{ab} are the same of the color singlet case.

The factors $(\mathbf{H}\,\mathbf{\Delta})$ in Eq. (2.67) depend on $\mathbf{b}$, M and on the kinematic variables of the elastic partonic process

$$c(p_1)+\bar{c}(p_2)\to Q(p_3)+\bar{Q}(p_4)\,, \tag{2.68}$$

In the shorthand notation $(\mathbf{H}\,\mathbf{\Delta})$ for the contribution of the factors $\mathbf{H}$ and $\mathbf{\Delta}$, it is hidden the non-trivial dependence on the colour structure (and colour indices) of the elastic partonic process. To take into account the colour dependence, the colour space formalism of Ref. [137] is used: the colour-index dependence of the scattering amplitude $\mathcal{M}$ of the process in Eq. (2.68) is represented by a vector $|\,\mathcal{M}\,\rangle$ in colour space, and colour matrices are represented by colour operators acting onto $|\,\mathcal{M}\,\rangle$. Using the colour space formalism, we can write the explicit representation of $(\mathbf{H}\,\mathbf{\Delta})$. In the case of the quark-anti quark annihilation channel, we have

$$(\mathbf{H}\,\mathbf{\Delta})_{c\bar{c}} = \frac{\langle\,\widetilde{\mathcal{M}}_{c\bar{c}\to Q\bar{Q}}\,|\,\mathbf{\Delta}\,|\,\widetilde{\mathcal{M}}_{c\bar{c}\to Q\bar{Q}}\,\rangle}{\alpha_S^2(M^2)\;|\mathcal{M}^{(0)}_{c\bar{c}\to Q\bar{Q}}(p_1,p_2;p_3,p_4)|^2}\;\;,\quad (c=q,\bar{q})\;\;. \tag{2.69}$$

In the above, the IR finite auxiliary hard-virtual amplitude $\widetilde{\mathcal{M}}_{c\bar{c}\to Q\bar{Q}}$ is defined by an extension of Eq. (A.52):

$$|\,\widetilde{\mathcal{M}}_{c\bar{c}\to Q\bar{Q}}(p_1,p_2;p_3,p_4)\rangle = \left[1-\widetilde{\mathbf{I}}_{c\bar{c}\to Q\bar{Q}}(\alpha_S(M^2),\epsilon)\right]\;|\mathcal{M}_{c\bar{c}\to Q\bar{Q}}(p_1,p_2;p_3,p_4)\rangle\;\;, \tag{2.70}$$

in terms of a suitable subtraction operator for heavy-quark $\widetilde{\mathbf{I}}_{c\bar{c}\to Q\bar{Q}}(\alpha_S(M^2),\epsilon)$, which is calculable order by order by order in perturbation theory:

$$\widetilde{\mathbf{I}}_{c\bar{c}\to Q\bar{Q}}(\alpha_S(M^2),\epsilon) = \frac{\alpha_S(\mu_R^2)}{2\pi}\,\widetilde{\mathbf{I}}^{(1)}_{c\bar{c}\to Q\bar{Q}}(\epsilon, M^2/\mu_R^2) + \sum_{n=2}^{\infty}\left(\frac{\alpha_S(\mu_R^2)}{2\pi}\right)^n \widetilde{\mathbf{I}}^{(n)}_{c\bar{c}\to Q\bar{Q}}(\epsilon, M^2/\mu_R^2) \ . \tag{2.71}$$

The factor $\mathbf{\Delta}$ depends on the impact parameter $\mathbf{b}$, on M and on the kinematics of the partonic process in Eq. 2.68. The kinematic dependence is specified by the rapidity difference $y_{34} = y_3 - y_4$ between $Q(p_3)$ and $\bar{Q}(p_4)$ and the azimuthal angle ϕ_3 of the quark $Q(p_3)$. The all-order structure of $\mathbf{\Delta}$ is

$$\mathbf{\Delta}(\mathbf{b}, M; y_{34}, \phi_3) = \mathbf{V}^{\dagger}(b, M; y_{34})\ \ \mathbf{D}(\alpha_S(b_0^2/b^2); \phi_{3b}, y_{34})\ \mathbf{V}(b, M; y_{34}) \ , \tag{2.72}$$

where

$$\mathbf{V}(b, M; y_{34}) = \overline{P}_q\ \exp\left\{-\int_{b_0^2/b^2}^{M^2}\frac{dq^2}{q^2}\,\mathbf{\Gamma}_t(\alpha_S(q^2); y_{34})\right\} \ , \tag{2.73}$$

$$\mathbf{\Gamma}_t(\alpha_S; y_{34}) = \frac{\alpha_S}{\pi}\,\mathbf{\Gamma}_t^{(1)}(y_{34}) + \left(\frac{\alpha_S}{\pi}\right)^2 \mathbf{\Gamma}_t^{(2)}(y_{34}) + \sum_{n=3}^{\infty}\left(\frac{\alpha_S}{\pi}\right)^n \mathbf{\Gamma}_t^{(n)}(y_{34}) \ , \tag{2.74}$$

$$\mathbf{D}(\alpha_S; \phi_{3b}, y_{34}) = 1 + \frac{\alpha_S}{\pi}\,\mathbf{D}^{(1)}(\phi_{3b}, y_{34}) + \sum_{n=2}^{\infty}\left(\frac{\alpha_S}{\pi}\right)^n \mathbf{D}^{(n)}(\phi_{3b}, y_{34}) \ . \tag{2.75}$$

We remark that

- The colour operator (matrix) $\mathbf{\Gamma}_t$ is the **soft anomalous dimension matrix**, specific of transverse-momentum resummation for $Q\bar{Q}$ production. This quantity is computable order-by-order in α_S as in Eq. (2.74) and embodies the non-trivial colour correlations induced by soft-parton radiation. The first two coefficient functions $\mathbf{\Gamma}_t^{(1)}(y_{34})$ and $\mathbf{\Gamma}_t^{(2)}(y_{34})$ are directly related to the IR structure of the virtual amplitude $|\mathcal{M}_{c\bar{c}\to Q\bar{Q}}(p_1, p_2; p_3, p_4)\rangle$ [138–140].

- $\mathbf{V}$ is an evolution operator which resums large logarithmic terms $\alpha_S^n(M^2)\ln^k(Mb)$ (with $k \leq n$). According to Eq. (2.73) it is obtained by the exponentiation of the integral of the soft anomalous dimension. The symbol $\overline{P}_q$ in Eq. (2.73) denotes the anti path-ordering of the exponential matrix with respect to the integration variable q^2.

- The colour operator $\mathbf{D}$ in Eq. (2.72), computable as a powers series expansion in $\alpha_S(b_0^2/b^2)$ (see Eq. (2.75)), embodies azimuthal correlations, specific of the heavy-quark pair production process, at scale $q_T \sim 1/b$.

The physical interpretation is as follows (see Fig. 2.6): aside the common structure shared with the color singlet case, the new factor $\mathbf{\Delta}$, specific of $Q\bar{Q}$ production, is due to QCD radiation of soft non-collinear (at wide angles with respect to the direction of the initial-state partons) partons from the underlying subprocess $c\bar{c} \to Q\bar{Q}$. $\mathbf{\Delta}$ embodies the effect of soft radiation from the $Q\bar{Q}$ final state and from initial-state and final-state interference at scales $1/b \lesssim q_T \lesssim M$. Therefore, $\mathbf{\Delta}$ resums additional NLL logarithmic terms $\alpha_S^n \ln^k(Mb)$. Moreover, soft-parton radiation at the scale $q_T \sim 1/b$ has a ‘special’ physical role, since it is eventually responsible for azimuthal correlations.

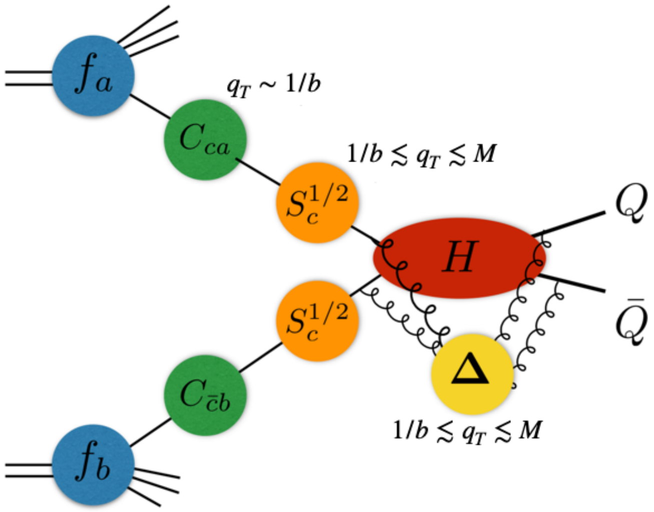

FIGURE 2.6: Diagrammatic representation of the different factors entering the resummation formula in the hadroprodution of a heavy-quark pair.

For the application to the NLO subtraction, we report here the explicit expressions of the coefficient functions (colour matrix) $\mathbf{\Gamma}_t^{(1)}(y_{34})$ and $\widetilde{\mathbf{I}}^{(1)}_{c\bar{c}\to Q\bar{Q}}(\epsilon, M^2/\mu_R^2)$ [46]:

$$\mathbf{\Gamma}_t^{(1)}(y_{34}) = -\frac{1}{4}\left\{ (\mathbf{T}_3^2 + \mathbf{T}_4^2)\,(1 - i\pi) + \sum_{\substack{i=1,2\\ j=3,4}} \mathbf{T}_i \cdot \mathbf{T}_j \ln\frac{(2p_i \cdot p_j)^2}{M^2 m^2} \right. \\ \left. + 2\,\mathbf{T}_3 \cdot \mathbf{T}_4 \left[\frac{1}{2v} \ln\left(\frac{1+v}{1-v}\right) - i\pi\left(\frac{1}{v} + 1\right)\right]\right\} \;, \tag{2.76}$$

where $\mathbf{T}_i$ are the color charge matrices in the colour space formalism of Ref. [137], m is the heavy-quark mass, M is the invariant mass of the heavy-quark pair , and

$$\widetilde{\mathbf{I}}^{(1)}_{c\bar{c}\to Q\bar{Q}}\left(\epsilon, \frac{M^2}{\mu_R^2}\right) = -\frac{1}{2}\left(\frac{M^2}{\mu_R^2}\right)^{-\epsilon} \left\{ \left(\frac{1}{\epsilon^2} + i\pi\frac{1}{\epsilon} - \frac{\pi^2}{12}\right)(\mathbf{T}_1^2 + \mathbf{T}_2^2) + \frac{2}{\epsilon}\gamma_c \right. \\ \left. - \frac{4}{\epsilon}\,\mathbf{\Gamma}_t^{(1)}(y_{34}) + \mathbf{F}_t^{(1)}(y_{34}) \right\}, \tag{2.77}$$

where

$$v = \sqrt{1 - \frac{m^4}{(p_3 \cdot p_4})^2} = \sqrt{1 - \left(\frac{2m^2}{M^2 - 2m^2}\right)^2} \tag{2.78}$$

is the relative velocity of Q and $\bar{Q}$ in the partonic center-of-mass frame.
The flavour dependent coefficients γ_c ($c = q, \bar{q}, g$) originate from collinear radiation: the explicit values of these coefficients are $\gamma_q = \gamma_{\bar{q}} = 3C_F/2$ and $\gamma_g = (11C_A - 2N_f)/6$, and N_f is the number of flavours of massless quarks (e.g., $N_f = 5$ in the case of $t\bar{t}$ production). The

IR finite contribution $\mathbf{F}_t^{(1)}$ in Eq. (A.54) is

$$\mathbf{F}_t^{(1)}(y_{34}) = (\mathbf{T}_3^2 + \mathbf{T}_4^2)\ \ln\left(\frac{m_T^2}{m^2}\right) + \ (\mathbf{T}_3 + \mathbf{T}_4)^2\ \mathrm{Li}_2\left(-\frac{\mathbf{p}_\mathbf{T}^2}{m^2}\right) + \mathbf{T}_3 \cdot \mathbf{T}_4\ \frac{1}{v}\ L_{34}\ , \tag{2.79}$$

where the function L_{34} is

$$\begin{aligned} L_{34} = &\ln\left(\frac{1+v}{1-v}\right)\ \ln\left(\frac{m_T^2}{m^2}\right) - 2\,\mathrm{Li}_2\left(\frac{2v}{1+v}\right) - \frac{1}{4}\ln^2\left(\frac{1+v}{1-v}\right) \\ &+ 2\left[\mathrm{Li}_2\left(1-\sqrt{\frac{1-v}{1+v}}\,e^{y_{34}}\right) + \mathrm{Li}_2\left(1-\sqrt{\frac{1-v}{1+v}}\,e^{-y_{34}}\right) + \frac{1}{2}\,y_{34}^2\right] \end{aligned} \tag{2.80}$$

and Li_2 is the customary dilogarithm function, $\mathrm{Li}_2(z) = -\int_0^z \frac{dt}{t}\ \ln(1-t)$.
According to the q_T subtraction formalism, the parton level differential cross section $d\sigma_{NLO}^{Q\bar{Q}}$ for the inclusive production process $pp \to Q\bar{Q} + X$ can be written as

$$d\hat{\sigma}_{NLO}^{Q\bar{Q}} = \mathcal{H}_{NLO}^{Q\bar{Q}} \otimes d\hat{\sigma}_{LO}^{Q\bar{Q}} + \left[d\hat{\sigma}_{(N)LO}^{Q\bar{Q}+\mathrm{jet}} - d\hat{\sigma}_{(N)NLO}^{Q\bar{Q},\,CT}\right], \tag{2.81}$$

where $d\hat{\sigma}_{LO}^{Q\bar{Q}+\mathrm{jet}}$ is the $Q\bar{Q}$+jet cross section at LO accuracy. As usual, the square bracket term of Eq. (2.81) is IR finite in the limit $q_T \to 0$, but its individual contributions, $d\hat{\sigma}_{(N)LO}^{Q\bar{Q}+\mathrm{jet}}$ and $d\hat{\sigma}_{(N)NLO}^{Q\bar{Q},\,CT}$, are separately divergent.
The explicit expression of $d\hat{\sigma}_{NLO}^{Q\bar{Q},\,CT}$ in the partonic channel $ab \to Q\bar{Q} + X$ reads [49]

$$d\hat{\sigma}_{NLO\,ab}^{Q\bar{Q},\,CT} = \sum_{c=q,\bar{q},g} \frac{\alpha_S}{\pi}\,\tilde{\Sigma}_{c\bar{c}\leftarrow ab}^{Q\bar{Q}(1)} \otimes d\hat{\sigma}_{LO\,c\bar{c}}^{Q\bar{Q}}\,\frac{dq_T^2}{M^2}\ , \tag{2.82}$$

where M is the invariant mass of the $Q\bar{Q}$ pair and the symbol $\otimes$ denotes convolutions with respect to the longitudinal-momentum fractions z_1 and z_2 of the colliding partons. The functions $\widetilde{\Sigma}_{c\bar{c}\leftarrow ab}^{Q\bar{Q}(1)}$ in Eq. (4.21) can be written as

$$\Sigma_{c\bar{c}\leftarrow ab}^{Q\bar{Q}(1)}(z_1, z_2; r) = \Sigma_{c\bar{c}\leftarrow ab}^{Q\bar{Q}(1,2)}(z_1, z_2)\tilde{I}_2(r) + \Sigma_{c\bar{c}\leftarrow ab}^{Q\bar{Q}(1,1)}(z_1, z_2)\tilde{I}_1(r) \tag{2.83}$$

where $r = q_T/M$, and the coefficients $\Sigma_{c\bar{c}\leftarrow ab}^{Q\bar{Q}(1,k)}(z_1, z_2)$ $(k = 1, 2)$ read

$$\Sigma_{c\bar{c}\leftarrow ab}^{Q\bar{Q}(1,2)}(z_1, z_2) = \Sigma_{c\bar{c}\leftarrow ab}^{F(1,2)}(z_1, z_2) \tag{2.84}$$

$$\begin{aligned} \Sigma_{c\bar{c}\leftarrow ab}^{Q\bar{Q}(1,1)}(z_1, z_2) = &\,\Sigma_{c\bar{c}\leftarrow ab}^{F(1,1)}(z_1, z_2) \\ &- \delta_{ca}\delta_{\bar{c}b}\delta(1-z_1)\delta(1-z_2)\frac{\langle \mathcal{M}_{c\bar{c}\to Q\bar{Q}}|\left(\mathbf{\Gamma}_t^{(1)} + \mathbf{\Gamma}_t^{(1)\dagger}\right)|\mathcal{M}_{c\bar{c}\to Q\bar{Q}}\rangle}{|\mathcal{M}_{c\bar{c}\to Q\bar{Q}}|^2}\,. \end{aligned} \tag{2.85}$$

The coefficient $\Sigma_{c\bar{c}\leftarrow ab}^{Q\bar{Q}(1,2)}(z_1, z_2)$ in Eq. (2.84) controls the leading logarithmic contribution at small q_T, while the coefficient $\Sigma_{c\bar{c}\leftarrow ab}^{Q\bar{Q}(1,1)}(z_1, z_2)$ in Eq. (2.85) controls the next-to-leading logarithmic term. Since final-state soft-parton radiation starts to contribute at NLL, the former coincides with the color singlet coefficient $\Sigma_{c\bar{c}\leftarrow ab}^{F(1,1)}(z_1, z_2)$, Eq. (2.49). The latter has a first term (first line in Eq. (2.85)) which is identical to what we have in the case of the production of a colour singlet, Eq. (2.50). The second term (second line in Eq. (2.85)) is due to soft-parton radiation and it is the additional term that is specific of the q_T subtraction method for the case of heavy-quark pair production [49]. The first-order hard-collinear coefficients $\mathcal{H}^{Q\bar{Q}}_{NLO}$ in Eq. (2.81) are also completely known [44–46].

Chapter 3

Mixed QCD-QED corrections to on-shell Z production

So far, the q_T subtraction formalism has been applied only to handle QCD corrections. This is easily understood as the main focus has been in applications to hadronic collider physics, where the uncertainties are dominated by the modeling of strong interactions. In the introduction chapter, we have already discussed the relevance and the physical motivations to include EW corrections for the precision physics program at LHC and future colliders.

In general, virtual EW corrections are more involved than the QCD counterpart, as we will briefly discuss in the next chapter. From the point of view of the subtraction, the situation is simpler as the IR divergences are associated either to the propagation of virtual or to the emission of real photons. Indeed, for electroweak corrections involving massive Z and W bosons, the mass of the vector boson regulates the IR divergences. Therefore the structure of the IR counterterms needed for EW corrections can be put in correspondence with the abelian subset of those needed for the QCD case. This means that, while in the loops virtual (massive) electroweak bosons can propagate, we only consider real emission processes with additional (massless) photons in the final state.

We briefly comment that, at energies much larger than the electro-weak boson masses, the IR sensitivity yields the well known large logarithmic enhancements of the ratio of the vector boson mass over the partonic center of mass energy. It is questionable whether to naively add also the real emission process of a massive vector boson. Indeed, both virtual and real corrections give rise to such large logarithms, which cancel in fully inclusive observables according to the KLN theorem. At variance with the case of massless gauge theories, however, there are two main differences: first, for massive gauge bosons, both virtual and real contributions, which usually lead to two different experimental signatures, are separately finite, so that there is no need to combine them for physical observables. Second, even if the measurement is completely inclusive over the final state, the initial beams of colliders are typically not $SEE(2)$ singlets, such that one can never respect the conditions of the KLN theorem. In this work, we do not discuss further these aspects.

In principle, there is no limitation in the adaption of an existing QCD subtraction scheme to the case of the EW corrections in the sense discussed above. For applications to NLO EW corrections, the preferable choice is naturally given by general-purpose local subtraction schemes, as dipole or FKS. On the other hand, the extension of the q_T subtraction formalism to the EW case will make possible to develop a suitable subtraction scheme to deal with higher order corrections, as the mixed QCD-EW(or QED) and the NNLO EW ones.

In this chapter, we will outline the strategy adopted to extend the q_T subtraction method to the EW case focusing on initial-state radiation. We have applied the new formalism to compute the mixed QCD-QED correction to on-shell Z production. All the ingredients required to carry out this computation are available, including the two-loop virtual amplitude and, furthermore, the total cross section is known in analytic form [13]. This provides us with a perfect playground and a very stringent way to test our construction in all its part and to study its numerical efficiency.

3.1 The q_T subtraction formalism for initial-state mixed QCD-EW corrections

3.1.1 Abelianisation procedure at NLO

Consider the production of a color singlet and neutral charge object F in hadron-hadron collisions

$$h_1(P_1) + h_2(P_2) \to F(q) + X, \tag{3.1}$$

where q denotes the total momentum of the F system and $q^2 = M^2$ is its mass. Since photons and gluons do not couple each other, mixed corrections are vanishing for the gluon fusion channel, so that we can focus to the case the reaction starts at lowest order in the quark-anti quark annihilation channel

$$q(p_1) + \bar{q}(p_2) \to F(q)\,. \tag{3.2}$$

In order to clarify the notation and explain the main ideas, we consider as first step the case of NLO EW corrections. In general, at NLO we have to consider the EW virtual corrections to the Born process in Eq. (3.2), the process of a real photon

$$q(p_1) + \bar{q}_{p_2} \to F(q) + \gamma(k)\,. \tag{3.3}$$

and the photon induced processes

$$q(p_1) + \gamma(p_2) \to F(q) + q(k), \quad \bar{q}(p_1) + \gamma(p_2) \to F(q) + \bar{q}(k)\,. \tag{3.4}$$

In a way similar to what happens for QCD corrections, new partonic channels open going to higher order in the perturbative expansion. In this context, photons are treated as partons, i.e. constituents of the protons, to which one associates a customary parton density function, the photon pdf. The precise determination of the photon content of the proton has been achieved recently [141, 142]. The resulting `LUX_QED` photon pdf have become part of the major pdf sets. The evolution from one energy scale to another is performed by solving the coupled system of DGLAP [131, 143, 144], including the photon pdf itself.

The photonic real emission processes in Eq.(3.3) and Eq. (3.4) are in one-to-one correspondence to the QCD real corrections, from which can be obtained by simply replacing the gluon with the photon, as showed in Fig. 3.1. Since the diagrams in correspondence are the same, the QCD and QED contributions differ only by an overall factor which is related only to the color and the electric charges, while it does not depend on the kinematics. This allows to map the results from one type of correction to the other by constructing a suitable list of replacement rules. The structure of the singularities is the same in the two cases, so that the same replacement rules can be applied to both the counterterm and the hard-collinear functions to obtained the EW version of the subtraction. In particular, this means the structure of the subtraction is the same as in Eq. (2.38).

To distinguish between QCD and EW, we introduce the notation (i, j), which may appear as pre-subscript or superscript, with i and j denoting the order of the QCD and EW correction respectively. Therefore, $(1, 0)$ stands for NLO QCD, (0,1) for NLO EW, (1,1) for the mixed QCD-EW and so forth. Explicitly, all the coefficient functions needed for the NLO

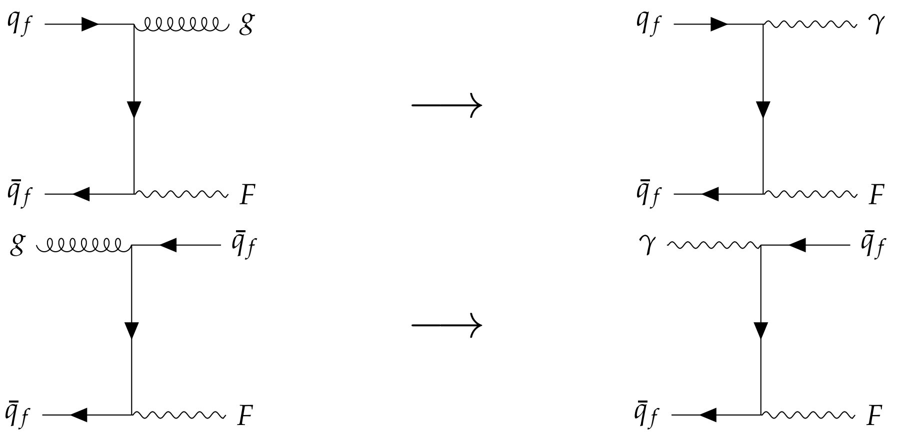

FIGURE 3.1: The photonic real corrections contributing to the NLO EW corrections in the hadroproduction of a color singlet and neutral object F (schematically depicted as an electroweak gauge boson) are obtained by replacing a gluon with a photon starting from the QCD real corrections.

EW corrections in the production of a neutral object F are:

$$ {}_{(0,1)}\Sigma^{F\,(1;2)}_{c\bar{c}\leftarrow ab,\,N} = -\frac{1}{2} A_c^{(0,1)}\ \delta_{ca}\delta_{\bar{c}b}\ , \tag{3.5} $$

$$ {}_{(0,1)}\Sigma^{F\,(1;1)}_{c\bar{c}\leftarrow ab,\,N}(M^2/Q^2) = -\left[\delta_{ca}\delta_{\bar{c}b}\ \left(B_c^{(0,1)} + A_c^{(0,1)}\ \ell_Q\right) + \delta_{ca}\gamma^{(0,1)}_{\bar{c}b,\,N} + \delta_{\bar{c}b}\gamma^{(0,1)}_{ca,\,N}\right]\ , \tag{3.6} $$

$$ \begin{aligned} {}_{(0,1)}\mathcal{H}^{F\,(0,1)}_{c\bar{c}\leftarrow ab,\,N}\left(\frac{M^2}{\mu_R^2},\frac{M^2}{\mu_F^2},\frac{M^2}{Q^2}\right) \ &= \ \delta_{ca}\delta_{\bar{c}b}\left[H_c^{F\,(0,1)} - \left(B_c^{(0,1)} + \frac{1}{2}A_c^{(0,1)}\ell_Q\right)\ell_Q - p^{\mathrm{QED}}_{cF}\beta_0^{\mathrm{QED}}\ell_R\right] \\ &+\delta_{ca}C^{(0,1)}_{\bar{c}b,\,N} + \delta_{\bar{c}b}C^{(0,1)}_{ca,\,N} + \left(\delta_{ca}\gamma^{(0,1)}_{\bar{c}b,\,N} + \delta_{\bar{c}b}\gamma^{(0,1)}_{ca,\,N}\right)(\ell_F - \ell_Q)\ , \end{aligned} \tag{3.7} $$

where it understood $c = q$. The structure is perfectly analogous to the QCD case (which can be written in this notation replacing everywhere $(0,1)$ with $(1,0)$). To completely determine the subtraction scheme, the resummation coefficients $A_c^{(0,1)}$ and $B_c^{(0,1)}$, the Altarelli-Parisi QED splitting-kernel $P_{ab}^{(0,1)}(z)$ and the the collinear functions $C_{ab}^{(0,1)}(z)$ must be supplied. Following the above reasoning, everything can be obtained starting from the QCD case and applying suitable replacement rules. To extract the latter, we consider again the two processes in Fig. 3.1 which correspond to

- qq-splitting: $q \to q(g)$
- qg-splitting: $g \to q(\bar{q})$

In the first process, the color factor, including the color average, and the electric charge associated to the two diagrams are

$$ \frac{1}{N_c^2}\mathrm{Tr}[T^aT^a] = \frac{C_F}{N_c} \longrightarrow \frac{1}{N_c^2}N_c e_f^2 = \frac{e_f^2}{N_c}\ , \tag{3.8} $$

Then, we get the replacement rule

$$ C_F \to e_f^2, \tag{3.9} $$

where f specifies the flavour of quark occurring in the splitting as the electric charge depends on this information. In other words, we are replacing the QCD color casimir charge

(C_f) with the QED electric casimir charge (e^2). This introduces a difference with the QCD case which is flavour blind. In general, we should explicitly add the dependence on the flavour index. In order to keep the notation simple and unified as much as possible, we prefer to have the flavour index implicitly defined in each parton label a which must now be understood as $a = \{a, f_a\}$. Keeping this in mind and applying the replacement rule in Eq. (3.9), we get

$$A_q^{(0,1)} = \frac{e_f^2}{C_F} A_q^{(1,0)} = e_f^2, \quad B_q^{(0,1)} = \frac{e_f^2}{C_F} B_q^{(1,0)} = -\frac{3}{2} e_f^2 \tag{3.10}$$

and for the qq Altarelli-Parisi splitting function $P_{qq}^{(0,1)}$ and the collinear function $C_{qq}^{(0,1)}$,

$$P_{qq}^{(1,0)} \to P_{qq}^{(0,1)}(z) = \frac{1}{2} \frac{e_f^2}{C_F} P_{qq}^{(1,0)}(z) = e_f^2 \left[\frac{1+z^2}{(1-z)_+} + \frac{3}{2}\delta(1-z) \right]; \tag{3.11}$$

$$C_{qq}^{(1,0)} \to C_{qq}^{(0,1)}(z) = \frac{e_f^2}{C_F} C_{qq}^{(1,0)}(z) = e_f^2 \frac{1}{2}(1-z). \tag{3.12}$$

In the same way, from the second splitting process, we have that

$$\frac{1}{N_c} \frac{1}{N_c^2 - 1} \mathrm{Tr}[T^a T^a] = \frac{T_R}{N_c} \longrightarrow \frac{1}{N_c} N_c e_f^2 = e_f^2\,, \tag{3.13}$$

which corresponds to the replacement rule

$$T_R \to e_f^2 N_c. \tag{3.14}$$

Then, the $q\gamma$ Altarelli-Parisi splitting function $P_{q\gamma}^{(0,1)}$ and the collinear remnant $C_{q\gamma}^{(0,1)}$ read:

$$P_{qg}^{(1,0)} \to P_{q\gamma}^{(0,1)}(z) = \frac{e_f^2 N_C}{T_R} P_{qg}^{(1,0)}(z) = \frac{1}{2} e_f^2 N_c (1 - 2z + 2z^2) \tag{3.15}$$

$$C_{qg}^{(1,0)} \to C_{q\gamma}^{(0,1)}(z) = \frac{e_f^2 N_C}{T_R} C_{qg}^{(1,0)}(z) = e_f^2 N_c z(z-1) \tag{3.16}$$

For completeness, we report also the results for the γq splitting ($q \to \gamma(q)$)

$$P_{gq}^{(1,0)} \to P_{\gamma q}^{(0,1)}(z) = \frac{1}{2} \frac{e_f^2}{C_F} P_{qq}^{(1,0)}(z) = e_f^2 \frac{1+(1-z)^2}{z}; \tag{3.17}$$

$$C_{gq}^{(1,0)} \to C_{\gamma q}^{(0,1)}(z) = \frac{e_f^2}{C_F} C_{qq}^{(1,0)}(z) = e_f^2 \frac{1}{2} z. \tag{3.18}$$

This splitting is relevant, for example, in the hadroproduction of a dilepton pair via the Drell-Yan mechanism

$$h_1(P_1) + h_2(P_2) \to l^+(p_3) + l^-(p_4) \tag{3.19}$$

that will be discussed in the next chapter. In this case, at Born level, the process can be initiated, beside by the quark-anti quark annihilation channel, also by the photon-photon partonic process $\gamma + \gamma \to l^+ + l^-$. In Fig. 3.2, we show the Feynman diagram associated to the real correction containing the γq splitting.

Before concluding, we comment on the treatment of the photon pdf within our formalism. Since the collinear mass singularities is subtracted in the same way as in the QCD case, it must be understood that we are using a $\overline{MS}$ factorization prescription also for the photon

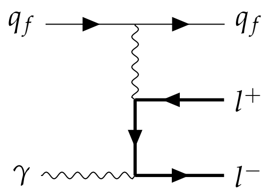

FIGURE 3.2: Example of Feynman diagram contributing to the NLO real corrections in the hadroproduction of a massive dilepton pair containing the γq splitting.

PDF. Therefore, the input photon pdf used should be consistently defined and evolved in the same scheme. In general, the conversion to another factorization scheme can be computed order-by-order in perturbation theory [70]. It should be kept in mind that even if formally equivalent at any fixed order accuracy, the result given by two different schemes can be numerical different as they organize the perturbative series in a peculiar way which can lead to a different impact of the high order contributions. The conversion to the DIS scheme, which is the other common choice, at NLO accuracy in the electromagnetic coupling can be found in the Appendix A of Ref. [145].

3.1.2 Abelianisation for mixed QCD-EW corrections

The procedure outlined in the previous section can be extended to higher order corrections. In particular, starting from the q_T subtraction formula at NNLO in QCD one can derive the structure both for the mixed corrections QCD-EW and for the pure NNLO EW (or QED). At this order, the correspondence between the QCD and the QED diagrams associated to the radiative corrections to the quark-anti quark annihilation channel is a bit more involved as the contributions due to the non-abelian component of QCD start to appear in the game. In this context, one more specifically talks about *abelianisation* referring to the procedure aiming at determine the abelian subset of the QCD computation in order to extract the results for the EW/QED case.

This strategy is nowadays well established in the literature and it has proved itself successful and useful in a number of applications highly related to our study case: the derivation of order $\mathcal{O}(\alpha)$, $\mathcal{O}(\alpha^2)$ and $\mathcal{O}(\alpha_s\alpha)$ Altarelli-Parisi splitting kernels [52, 146], the extension of the transverse-resummation formalism to the neutral Z boson production [147] combining QED and QCD corrections, the computation of mixed corrections to the inclusive on-shell Z production [13], the first computation at the differential level of the mixed corrections to the hadroproduction of a dilepton pair via the Drell-Yan mechanism in the approximation of an on-shell Z within the framework of nested local subtraction [18]. In particular, in Ref.[52] the abelianisation procedure is presented in details and their results on the mixed splitting kernels are an essential ingredient to build the q_T subtraction formula for the $\mathcal{O}(\alpha_s\alpha)$ corrections.

In principle, the combined QED and QCD transverse-momentum resummation formalism of Ref. [147] represents the first step of the usual construction of the q_T subtraction formalism. In practice, this means to expand at fixed order in the couplings their results on the expansion in the large logarithms (in the small-q_T limit) of the singular component of the differential cross section. We observe that in that work the resummation program has be carried out up to LL with respect to the mixed correction, while to fully specify the subtraction also NLL subleading contributions are required. We prefer to start directly from the q_T subtraction at NNLO QCD and use the results in Ref. [147] as a non-trivial cross check, especially for some combinatorics.

Let us start from the counterterm. From the discussion in the previous section, it should be clear that it shares the same structure of the NNLO QCD counterterm, i.e.

$$d\hat{\sigma}^{F}_{\rm LO} \otimes {}_{(1,1)}\widetilde{\Sigma}^{F\,(2)}_{c\bar{c}\leftarrow ab}(z,\widetilde{L}) \tag{3.20}$$

with the explicit expression of ${}_{(1,1)}\widetilde{\Sigma}^{F\,(2)}_{c\bar{c}\leftarrow ab}(z,\widetilde{L})$ given by

$${}_{(1,1)}\widetilde{\Sigma}^{F\,(2)}_{c\bar{c}\leftarrow ab}(z,\widetilde{L}) = {}_{(1,1)}\Sigma^{F\,(2;4)}_{c\bar{c}\leftarrow ab}(z)\;\widetilde{L}^4 + {}_{(1,1)}\Sigma^{F\,(2;3)}_{c\bar{c}\leftarrow ab}(z)\;\widetilde{L}^3 + {}_{(1,1)}\Sigma^{F\,(2;2)}_{c\bar{c}\leftarrow ab}(z)\;\widetilde{L}^2 + {}_{(1,1)}\Sigma^{F\,(2;1)}_{c\bar{c}\leftarrow ab}(z)\;\widetilde{L}\,, \tag{3.21}$$

each coefficient function being associated to the power of the corresponding logarithmic divergence in the small-q_T limit. Consider first the most divergent term ${}_{(1,1)}\Sigma^{F\,(2;4)}_{c\bar{c}\leftarrow ab}(z)$. It is associated to two qq splittings becoming soft-collinear at the same time. This can only occurs for the diagonal quark-anti quark annihilation channel. The situation is better understood if one focuses on the double real corrections. The maximally singular configuration corresponds to the emission of two real soft-collinear gluons. To derive the mixed corrections, we replace one gluon with a photon. There are two ways to perform the replacements which lead to two non-equivalent contributions at variance with the QCD case for which the two gluons are indistinguishable. We recall the expression of the coefficient in QCD (Eq. (3.24))

$$\Sigma^{F\,(2;4)}_{c\bar{c}\leftarrow ab,\,N} = \frac{1}{8}\left(A_c^{(1,0)}\right)^2\;\delta_{ca}\delta_{\bar{c}b}\,. \tag{3.22}$$

The result in the r.h.s. comes from the individual contribution of the two gluon becoming soft and collinear, so that it is indeed $\left(A_c^{(1,0)}\right)^2 = A_c^{(1,0)} \times A_c^{(1,0)}$. Then, we applied the gluon-photon replacement to each of the two gluon contributions, once at time, obtaining the correspondence

$$\left(A_c^{(1,0)}\right)^2 \to A_c^{(0,1)} \times A_c^{(1,0)} + A_c^{(1,0)} \times A_c^{(0,1)} = 2A_c^{(1,0)}A_c^{(0,1)} \tag{3.23}$$

where in the last step we have exploited the basic fact that the numerical coefficients commute. We get then that

$${}_{(1,1)}\Sigma^{F\,(2;4)}_{c\bar{c}\leftarrow ab,\,N} = \frac{1}{4}A_c^{(1,0)}A_c^{(0,1)}\;\delta_{ca}\delta_{\bar{c}b}\,, \tag{3.24}$$

and we check that the combinatorics is coherent with what can be derived starting from the result in Ref. [147], so that the above replacement rules correctly takes into account the factor of two corresponding to the different photon-gluon configurations. The above reasoning can be generalized and applied to derive the structure of the coefficients of the other logarithmic terms. In pure QCD, the generic contribution to any of the coefficients has the form either $X_1^{(1,0)} \times X_2^{(1,0)}$ or $X^{(2,0)}$, where X, X_1, X_2 stand for any of the resummation coefficients, the Altarelli-Parisi kernels, the collinear functions or the hard-virtual coefficient functions. Then, the replacement rules are

- $X_1^{(1,0)} \times X_2^{(1,0)} \to X_1^{(1,0)} \times X_2^{(0,1)} + X_1^{(0,1)} \times X_2^{(1,0)}$;
- $X^{(2,0)} \to X^{(1,1)}$.

In particular, in the second case, the possible factor of two is implicitly contained in the actual expression of $X^{(1,1)}$. In addition, we observe that

- the coefficient $A^{(1,1)}$ is vanishing. This coefficient indeed has an easily interpretation (the same as its pure QCD counterpart [148]): it corresponds to the coefficient of the term in the Altarelli-Parisi splitting function $P_{qq}^{(1,1)}$ which is singular in the soft limit $z = 1$. Since $P_{qq}^{(1,1)}$ is not divergent in this limit (see Eq. (3.38)), we have $A^{(1,1)} = 0$;

- at variance with the pure QCD case, at order $\mathcal{O}(\alpha_s\alpha)$, diagrams related to the running of the coupling, both α_s and α, cannot contribute. Therefore, the terms proportional to β_0 in the pure QCD case are vanishing in this context (they will contribute instead for the NNLO EW corrections)

Applying the above considerations, we get

$$
{}_{(1,1)}\Sigma^{F\,(2;3)}_{c\bar{c}\leftarrow ab,\,N}(M^2/Q^2) = -\frac{1}{2}\,A_c^{(1,0)}\;{}_{(0,1)}\Sigma^{F\,(1;1)}_{c\bar{c}\leftarrow ab,\,N}(M^2/Q^2) - \frac{1}{2}\,A_c^{(0,1)}\;{}_{(1,0)}\Sigma^{F\,(1;1)}_{c\bar{c}\leftarrow ab,\,N}(M^2/Q^2)\,, \tag{3.25}
$$

$$
\begin{aligned}
{}_{(1,1)}\Sigma^{F\,(2;2)}_{c\bar{c}\leftarrow ab,\,N}\left(\frac{M^2}{\mu_R^2},\frac{M^2}{\mu_F^2},\frac{M^2}{Q^2}\right) = &- \frac{1}{2}\,A_c^{(1,0)}\mathcal{H}^{F\,(0,1)}_{c\bar{c}\leftarrow ab,\,N}\left(\frac{M^2}{\mu_R^2},\frac{M^2}{\mu_F^2},\frac{M^2}{Q^2}\right)\\
&- \frac{1}{2}\,A_c^{(0,1)}\mathcal{H}^{F\,(1,0)}_{c\bar{c}\leftarrow ab,\,N}\left(\frac{M^2}{\mu_R^2},\frac{M^2}{\mu_F^2},\frac{M^2}{Q^2}\right)\\
&- \frac{1}{2}\sum_{a_1,b_1}\;{}_{(0,1)}\Sigma^{F\,(1;1)}_{c\bar{c}\leftarrow a_1b_1,\,N}(M^2/Q^2)\left[\delta_{a_1a}\gamma^{(1,0)}_{b_1b,\,N}+\delta_{b_1b}\gamma^{(1,0)}_{a_1a,\,N}\right]\\
&- \frac{1}{2}\sum_{a_1,b_1}\;{}_{(1,0)}\Sigma^{F\,(1;1)}_{c\bar{c}\leftarrow a_1b_1,\,N}(M^2/Q^2)\left[\delta_{a_1a}\gamma^{(0,1)}_{b_1b,\,N}+\delta_{b_1b}\gamma^{(0,1)}_{a_1a,\,N}\right]\\
&- \frac{1}{2}\left(B_c^{(1,0)}+A_c^{(1,0)}\,\ell_Q\right)\;{}_{(0,1)}\Sigma^{F\,(1;1)}_{c\bar{c}\leftarrow ab,\,N}(M^2/Q^2)\\
&- \frac{1}{2}\left(B_c^{(0,1)}+A_c^{(0,1)}\,\ell_Q\right)\;{}_{(1,0)}\Sigma^{F\,(1;1)}_{c\bar{c}\leftarrow ab,\,N}(M^2/Q^2)\,,
\end{aligned} \tag{3.26}
$$

$$
\begin{aligned}
&{}_{(1,1)}\Sigma^{F\,(2;1)}_{c\bar{c}\leftarrow ab,\,N}\left(\frac{M^2}{\mu_R^2},\frac{M^2}{\mu_F^2},\frac{M^2}{Q^2}\right) =\\
&- \sum_{a_1,b_1}\;{}_{(0,1)}\mathcal{H}^{F\,(1)}_{c\bar{c}\leftarrow a_1b_1,\,N}\left(\frac{M^2}{\mu_R^2},\frac{M^2}{\mu_F^2},\frac{M^2}{Q^2}\right)\Big[\delta_{a_1a}\delta_{b_1b}\left(B_c^{(1,0)}+A_c^{(1,0)}\,\ell_Q\right)\\
&\qquad +\delta_{a_1a}\gamma^{(1,0)}_{b_1b,\,N}+\delta_{b_1b}\gamma^{(1,0)}_{a_1a,\,N}\Big]\\
&- \sum_{a_1,b_1}\;{}_{(1,0)}\mathcal{H}^{F\,(1)}_{c\bar{c}\leftarrow a_1b_1,\,N}\left(\frac{M^2}{\mu_R^2},\frac{M^2}{\mu_F^2},\frac{M^2}{Q^2}\right)\Big[\delta_{a_1a}\delta_{b_1b}\left(B_c^{(0,1)}+A_c^{(0,1)}\,\ell_Q\right)\\
&\qquad +\delta_{a_1a}\gamma^{(0,1)}_{b_1b,\,N}+\delta_{b_1b}\gamma^{(0,1)}_{a_1a,\,N}\Big] \qquad (3.27)\\
&- \left[\delta_{ca}\delta_{\bar{c}b}B_c^{(1,1)}+\delta_{ca}\gamma^{(1,1)}_{\bar{c}b,\,N}+\delta_{\bar{c}b}\gamma^{(1,1)}_{ca,\,N}\right]\,, \qquad (3.28)
\end{aligned}
$$

and similarly for the hard-collinear coefficient (for easy of reading we do not report the terms proportional to ℓ_Q)

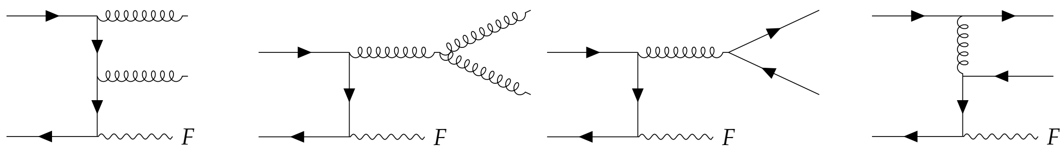

FIGURE 3.3: Classes of Feynman diagrams contributing to the double real emission corrections to the hadroproduction of a color singlet system F in the quark-anti quark annihilation channel.

$$
\begin{aligned}
\mathcal{H}^{F\,(1,1)}_{c\bar{c}\leftarrow ab,\,N}\left(\frac{M^2}{\mu_R^2},\frac{M^2}{\mu_F^2},\frac{M^2}{Q^2}\right) &= \delta_{ca}\delta_{\bar{c}b}\, H_c^{F\,(1,1)} + \delta_{ca}\, C^{(1,1)}_{\bar{c}b,\,N} + \delta_{\bar{c}b}\, C^{(1,1)}_{ca,\,N} \\
+ & \left\{ C^{(1,0)}_{ca,\,N}\, C^{(0,1)}_{\bar{c}b,\,N} + H_c^{F\,(1,0)}\left(\delta_{ca}\, C^{(0,1)}_{\bar{c}b,\,N} + \delta_{\bar{c}b}\, C^{(0,1)}_{ca,\,N}\right) + \right. \\
+ & \frac{1}{2}\sum_{a_1,b_1}\left[\mathcal{H}^{F\,(1,0)}_{c\bar{c}\leftarrow a_1b_1,\,N}\left(\frac{M^2}{\mu_R^2},\frac{M^2}{\mu_F^2},\frac{M^2}{Q^2}\right) + \delta_{ca_1}\delta_{\bar{c}b_1}\, H_c^{F\,(1,0)} + \delta_{ca_1}\, C^{(1,0)}_{\bar{c}b_1,\,N} + \delta_{\bar{c}b_1}\, C^{(1,0)}_{ca_1,\,N}\right] \\
\times & \left[\left(\delta_{a_1a}\gamma^{(0,1)}_{b_1b,\,N} + \delta_{b_1b}\gamma^{(0,1)}_{a_1a,\,N}\right)\ell_F - \delta_{a_1a}\delta_{b_1b}\, p_{cF}^{\mathrm{QED}}\, \beta_0^{\mathrm{QED}}\,\ell_R\right] \\
& \qquad \left. + \left((1,0)\leftrightarrow(0,1), \mathrm{QED}\leftrightarrow\mathrm{QCD}\right)\right\} \\
- & \delta_{ca}\delta_{\bar{c}b}\left(p_{cF}^{\mathrm{QCD}}\beta^{\mathrm{QED}}_{(1,0)} + p_{cF}^{\mathrm{QED}}\beta^{\mathrm{QCD}}_{(0,1)}\right)\ell_R \ . \qquad (3.29)
\end{aligned}
$$

In the above, a residual dependence on the running of the couplings remains according to the renormalization of the p_{cF}^{QCD} powers of α_s and of the p_{cF}^{QED} powers of α appearing at the Born level. The coefficient $\beta^{\mathrm{QED}}_{(1,0)}$ and $\beta^{\mathrm{QCD}}_{(0,1)}$ correspond respectively to the $\beta'_{(0,1)}$ and $\beta_{(0,1)}$ in Eq.(17) and Eq.(16) of Ref. [147]. They are finite contributions associated to the variation of the renormalization scale and, therefore, are suppressed by ℓ_R.

By inspection of Eqs. (3.24)-(3.29), we see that in order to fully specify the subtraction we need the resummation coefficient $B^{(1,1)}$, the mixed Altarelli-Parisi splitting kernels $P^{(1,1)}_{ab}$ and the collinear functions $C^{(1,1)}_{ab}(z)$. The $P^{(1,1)}_{ab}$ kernels are already available in Ref. [52], while we have to determine all the others. Once again, we rely on the abelianisation procedure starting from the pure QCD case. As discussed at the beginning of this section, we have to put some care to select the abelian component of the corresponding QCD coefficients in order to extract the QED result. As it will be clear in a moment, one can look at the possible colour structures and select the ones corresponding to the abelian contribution.

Let us start from the $q\bar{q}$ diagonal channel. We can focus on a particular type of contributions, for example the double real emission diagrams, as the colour structures must match the ones in the real-virtual and double virtual terms in order for the KLN cancellation to happen. In Fig.3.3, we collect illustrative example of the classes of Feynman diagrams contributing to the double real emission process. By interfering these diagrams, three different color structures arise:

- squaring the diagram (a) for two identical gluons (so it must be considered also the interference with the diagram obtained by exchanging the two gluons) we get two colour factors

$$
\frac{1}{2N_C^2}\mathrm{Tr}[T^aT^aT^bT^b] = \frac{C_F^2}{2N_c}, \quad \frac{1}{2N_C^2}\mathrm{Tr}[T^aT^bT^aT^b] = \frac{C_F}{2N_c}\left(C_F - \frac{C_A}{2}\right). \qquad (3.30)
$$

In the above we have included also the colour average and the symmetry factor 1/2 for identical gluons. The contribution proportional to $C_A C_F$ arises from the non-commutative nature of the $SU_c(3)$ colour group. Following the abelianisation procedure, we replace a gluon with a photon. There are two different ways to do the replacement leading to two diagrams, which this time are **distinguishable**. Squaring the two diagrams individually, one obtains the same colour factor

$$\frac{1}{N_C^2}\mathrm{Tr}[T^a T^a] e_{q_f}^2 = \frac{C_F e_{q_f}^2}{N_c}. \tag{3.31}$$

Comparing Eq.(3.30) and Eq. (3.31), the mixed QCD-QED result can be obtained from the QCD one by applying the following replacements

$$C_A \to 0, \quad C_F^2 \to 2C_F e_{q_f}^2\,; \tag{3.32}$$

- the diagram in (b) containing the triple gluon vertex does not have a counterpart in the mixed QCD-QED since photons and gluons do not couple each other. In the pure QCD case, this diagram gives rise to color factors proportional to the Casimir C_A so that it is possible to get rid of it by applying the replacement rule

$$C_A \to 0\,; \tag{3.33}$$

- in pure QCD, due to diagrams in (c) and (d), partonic channels initiated by quark of different flavours are possible. Furthermore, those diagrams give rise to contribution proportional to the number of light flavour N_f. From their interference, we can have either situations with two dis-jointed quark lines or with only a single quark line. In the former case, the colour factor is proportional to $\mathrm{Tr}[T^a T^b]\mathrm{Tr}[T^a T^b] = C_F T_R$. When a gluon is replaced with a photon, we get colour traces with only one colour generator, $\mathrm{Tr}[T^a]\mathrm{Tr}[T^a]$, which are vanishing. For this reason partonic processes initiated by quarks of different flavours do non contribute to the mixed correction. Terms proportional to the colour structure $C_F T_R$ in the QCD computation have to be removed. This can be achieved by applying the replacement rule

$$T_R \to 0. \tag{3.34}$$

  In Fig. 3.4, we show an example of an interference which leads to a single quark line. In this case, the mixed correction is non-vanishing. We compute the corresponding colour factors:

$$\frac{1}{N_C^2}\mathrm{Tr}[T^a T^b T^a T^b] = \frac{C_F}{N_c}\left(C_F - \frac{C_A}{2}\right) \to \frac{2}{N_C^2}\mathrm{Tr}[T^a T^a] e_{q_f}^2 = \frac{2C_F e_{q_f}}{N_c} \tag{3.35}$$

  where the factor of two in the mixed case takes into account the two possible interferences (at variance with the QCD case where there is only one interference). Then we get again the replacement rules in Eq.(3.32). Similar contributions come also from the the collisions of identical (anti)quark-(anti)quark, and the same replacement rule still applies.

We conclude that for processes initiated by same flavour quark-anti quark and identical (anti)quark-(anti)quark collisions, the abelianisation procedure is carried out by applying the following replacement rules

$$C_A \to 0, \quad T_R = 0, \quad C_F^2 \to 2C_F e_{q_f}\,. \tag{3.36}$$

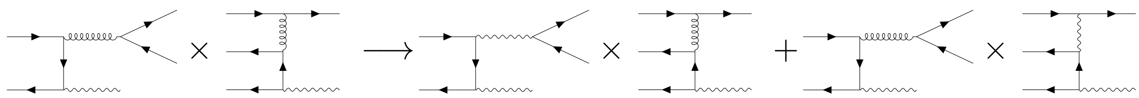

FIGURE 3.4: Non-vanishing interference contributing to the mixed correction.

In the following we give the explicit expression of the resummation coefficient $B_q^{(1,1)}$, the qq and $q\bar{q}$ Altarelli-Parisi splitting kernels (in the notation of Ref. [52]) and the corresponding collinear coefficients:

$$B_q^{(1,1)} = (-3 + 24\zeta_2 - 48\zeta_3) 2 C_F e_{q_f}^2, \tag{3.37}$$

$$\begin{aligned} P_{qq}^{S(1,1)} &= P_{q\bar{q}}^{S(1,1)} = 0\,, && (3.38)\\ P_{qq}^{V(1,1)} &= -2\, C_F\, e_q^2 \left[\left(2 \ln 1 - x + \frac{3}{2} \right) \ln x\, p_{qq}(x) + \frac{3+7x}{2} \ln x + \frac{1+x}{2} \ln^2(x) \right.\\ &+ \left. 5(1-x) + \left(\frac{\pi^2}{2} - \frac{3}{8} - 6\zeta_3 \right) \delta(1-x) \right], && (3.39)\\ P_{q\bar{q}}^{V(1,1)} &= 2\, C_F\, e_q^2 \left[4(1-x) + 2(1+x) \ln x + 2 p_{qq}(-x) S_2(x) \right], && (3.40) \end{aligned}$$

with

$$p_{qq}(z) = \frac{1+z^2}{(1-z)_+}, \tag{3.41}$$

and

$$\begin{aligned} S_2(x) &= \int_{\frac{x}{1+x}}^{\frac{1}{1+x}} \frac{dz}{z} \ln \frac{1-z}{z} = \mathrm{Li}_2\left(-\frac{1}{x}\right) - \mathrm{Li}_2(-x)\\ &+ \ln^2\left(\frac{x}{1+x}\right) - \ln^2\left(\frac{1}{1+x}\right). && (3.42) \end{aligned}$$

$$\begin{aligned} C_{qq}^{(1,1)} = \frac{2 C_F e_{q_f}^2}{48(1-z)} \Big[& 12\left(z^2+1\right) \mathrm{Li}_3(1-z) - 60 z^2 \mathrm{Li}_3(z) + 12 \mathrm{Li}_2(z) \left(\left(z^2+1\right) \log(1-z) \right.\\ & \left. + 3\left(z^2+1\right) \log(z) - 2(z-1)^2 \right) - 60 \mathrm{Li}_3(z) + 60 z^2 \zeta(3) + 10\pi^2 z^2 - 114 z^2 - z^2 \log^3(z)\\ & - 6z^2 \log^2(z) + 6z^2 \log(1-z) \log^2(z) + 18 z^2 \log^2(1-z) \log(z) + 96 z^2 \log(z)\\ & - 36 z^2 \log(1-z) \log(z) - 2\pi^2 z^2 \log(1-z) + 6z^2 \log(1-z) - 20\pi^2 z + 228 z + \log^3(z)\\ & + 6z \log^2(z) + 6 \log(1-z) \log^2(z) + 9 \log^2(z) + 18 \log^2(1-z) \log(z) - 78 z \log(z)\\ & + 72 z \log(1-z) \log(z) - 36 \log(1-z) \log(z) + 30 \log(z) - 6z \log(1-z)\\ & - 2\pi^2 \log(1-z) + 60\zeta(3) + 10\pi^2 - 114 \Big]. \end{aligned} \tag{3.43}$$

$$
\begin{aligned}
C_{q\bar{q}}^{(1,1)} = & -\frac{2C_F e_{q_f}^2}{24(z+1)}\Bigg[12z^2\mathrm{Li}_3(z) - 9z^2\mathrm{Li}_3\left(z^2\right) - 9\mathrm{Li}_3\left(z^2\right) - 24z^2\mathrm{Li}_3\left(\frac{1}{z+1}\right) \\
& + 6\mathrm{Li}_2\left(z^2\right)\left(\left(z^2+1\right)\log(z) + (z+1)^2\right) - 24(z+1)\mathrm{Li}_2(z) + 12\mathrm{Li}_3(z) - 24\mathrm{Li}_3\left(\frac{1}{z+1}\right) \\
& + 18z^2\zeta_3 - \pi^2 z^2 + 45z^2 + z^2\log^3(z) + 4z^2\log^3(z+1) - 6z^2\log(z+1)\log^2(z) \\
& - 33z^2\log(z) + 12z^2\log(1-z)\log(z) + 12z^2\log(z+1)\log(z) - 2\pi^2 z^2\log(z+1) \\
& + 2\pi^2 z + \log^3(z) + 4\log^3(z+1) - 6\log(z+1)\log^2(z) - 42z\log(z) \\
& + 24z\log(z+1)\log(z) - 9\log(z) - 2\pi^2\log(z+1) + 24\log(z)\tanh^{-1}(z) \\
& + 18Z3 + 3\pi^2 - 45\Bigg]\,.
\end{aligned}
\tag{3.44}
$$

With this approach, we can obtain also the hard-virtual coefficient $H_{q,DY}^{(1,1)}$ needed for the mixed QCD-QED correction to on-shell Z boson production starting from the corresponding $H_{q,DY}^{(2,0)}$. We get

$$
H_{q,DY}^{(1,1)} = \frac{1}{4}2C_F e_{q_f}^2\left(-15\zeta_3 + \frac{511}{16} - \frac{67\pi^2}{12} + \frac{17}{45}\right)\,. \tag{3.45}
$$

The same reasoning can be applied for the quark-gluon, quark-photon and gluon-photon channels. The latter is trivial: it opens for the fist time at the level of the mixed corrections and only requires NLO coefficients. We briefly comment on the first two. For these channels, the qg and $q\gamma$ splitting and collinear functions are relevant. In NNLO QCD there is only the qg splitting, which gives rise to two colour structures, one proportional to $C_F T_R$ and the other to $C_A T_R$. In the abelian limit only the first one survives, while, taking into account also the difference in the colour average factor, we have now two different replacement rules for the qg and $q\gamma$ splittings:

$$
C_F \to e_{q_f}^2 \quad \text{for } qg \text{ splitting,} \qquad T_R \to N_C e_{q_f}^2 \quad \text{for } q\gamma \text{ splitting.} \tag{3.46}
$$

In particular, we observe that this time there are not any factors of two, since there is no issue with indistinguishable processes. Then, introducing the quantities

$$
\begin{aligned}
p_{qv}^{(1,1)} &= \frac{1}{2}\Bigg\{4 - 9x - (1-4x)\ln x - (1-2x)\ln^2(x) + 4\ln 1 - x \\
&+ \quad p_{qg}(x)\left[2\ln^2\left(\frac{1-x}{x}\right) - 4\ln\frac{1-x}{x} - \frac{2\pi^2}{3} + 10\right]\Bigg\}\,,
\end{aligned}
\tag{3.47}
$$

with

$$
p_{qq}(z) = z^2 + (1-z)^2\,, \tag{3.48}
$$

and

$$
\begin{aligned}
c_{qv}^{(1,1)} = \frac{1}{96}\Big[& -48z^2\mathrm{Li}_3(1-z) - 48z^2\mathrm{Li}_3(z) + 24\left(2z^2-2z+1\right)\mathrm{Li}_2(1-z)\log(1-z) \\
& + 24\left(2z^2-2z+1\right)\mathrm{Li}_2(z)\log(z) + 48z\mathrm{Li}_3(1-z) - 24\mathrm{Li}_3(1-z) + 48z\mathrm{Li}_3(z) - 24\mathrm{Li}_3(z) \\
& + 384z^2\zeta_3 - 16\pi^2z^2 - 240z^2 - 8z^2\log^3(1-z) - 8z^2\log^3(z) - 24z^2\log^2(1-z) \\
& + 24z^2\log(z)\log^2(1-z) + 24z^2\log^2(z)\log(1-z) - 24z^2\log^2(z) + 48z^2\log(z)\log(1-z) \\
& + 96z^2\tanh^{-1}(1-2z) - 384z\zeta_3 + 16\pi^2 z + 258z + 8z\log^3(1-z) - 4\log^3(1-z) \\
& + 4z\log^3(z) - 2\log^3(z) + 24z\log^2(1-z) - 24z\log(z)\log^2(1-z) + 12\log(z)\log^2(1-z) \\
& - 24z\log^2(z)\log(1-z) + 12\log^2(z)\log(1-z) + 36z\log^2(z) + 3\log^2(z) - 36z\log(1-z) \\
& - 48z\log(z)\log(1-z) + 90z\log(z) + 48\log(z) + 192\zeta_3 - 78\Big]
\end{aligned}
\tag{3.49}
$$

we can express the Altarelli-Parisi $P_{qg}^{(1,1)}$ and $P_{q\gamma}^{(1,1)}$ as

$$
P_{qg}^{(1,1)} = T_R e_{q_f}^2 p_{qv}^{(1,1)}, \quad P_{q\gamma}^{(1,1)} = C_F e_{q_f}^2 N_c p_{qv}^{(1,1)}, \tag{3.50}
$$

and the collinear functions $C_{qg}^{(1,1)}$ and $C_{q\gamma}^{(1,1)}$ as

$$
C_{qg}^{(1,1)} = T_R e_{q_f}^2 c_{qv}^{(1,1)}, \quad C_{q\gamma}^{(1,1)} = C_F e_{q_f}^2 N_c c_{qv}^{(1,1)}. \tag{3.51}
$$

This completes the list of ingredients needed to specify the subtraction to handle the mixed corrections in the initial-state.

3.2 Numerical Validation: mixed QCD-QED corrections to on-shell Z boson production

In this section, we present a collection of numerical results to validate the q_T subtraction formula developed in the previous section. To this aim we focus on the mixed QCD-QED corrections to on-shell Z boson production in proton-proton collisions since

- the hard virtual term $H_{q,DY}^{F\,(1,1)}$, related to the two-loop virtual amplitude, is known in this case, its analytic expression given in Eq. (3.45) as obtained via the abelianisation of the $H_{c,DY}^{F\,(2,0)}$ coefficient in pure QCD;
- the inclusive result is available in the literature [13], in the form of a one-fold integral to be convoluted with the proton pdf.

We have implemented all the formulae in Ref. [13] in a Mathematica [149] notebook. The package `ManeParse` [150] has been used to link the pdf into Mathematica and the Vegas [151] implementation provided by the Cuba [152, 153] library has been used for the actual integration to obtain the total cross section. Our calculation is carried out by using an extension of the numerical program of Ref. [7]. To have a better control of all the contributions, in the actual implementation we prefer to treat the q_T subtraction as a slicing. We rely on MCFM-8.2 [154, 155] and MATRIX [56], suitably adapted for our purposes, to address the most time consuming task, i.e. the integration of the subtracted double real and real-virtual contributions with the constraint $q_T > Mr_{\mathrm{cut}}$. In this region, we treat the remaining NLO-type IR divergences using dipoles subtraction.

	$\Delta^{(1,1)}_{q\bar{q}}$ [pb]	$\Delta^{(1,1)}_{Qg}$ [pb]	$\Delta^{(1,1)}_{Q\gamma}$ [pb]	$\Delta^{(1,1)}_{g\gamma}$ [pb]	$\Delta^{(1,1)}_{qq+\bar{q}\bar{q}}$ [pb]
analytic	57.46 ± 0.02	-39.5 ± 0.2	-1.576 ± 0.009	0.6496 ± 0.0016	0.594 ± 0.001
q_T subtraction	56.9 ± 0.6	-39.8 ± 0.5	-1.575 ± 0.013	0.646 ± 0.008	0.594 ± 0.003

TABLE 3.1: Mixed QCD-QED correction to on-shell Z boson production in proton-proton collisions at $\sqrt{S} = 14$ TeV, split into the different partonic channels. We compare our results obtained with the numerical implementation of the q_T subtraction method with the "analytic" computation of Ref. [13]

	2 TeV	14 TeV		
$\Delta^{(1,1)}_{q\bar{q}}$ $[pb]$	6.66 ± 0.06	57.46 ± 0.02	349 ± 3	analytic
$\Delta^{(1,1)}_{q\bar{q}}$ $[pb]$	6.59 ± 0.12	56.9 ± 0.6	348 ± 7	q_T subtraction

TABLE 3.2: Mixed QCD-QED correction to on-shell Z boson production in the diagonal quark-anti quark channel in proton-proton collisions at different collider energies. We compare our results obtained with the numerical implementation of the q_T subtraction method with the "analytic" computation of Ref. [13]

In the following we use the notation $\Delta^{(1,1)}$ to denote the mixed correction. We decompose this contribution according to the initial partonic channels:

$$\Delta^{(1,1)} = \Delta^{(1,1)}_{q\bar{q}} + \Delta^{(1,1)}_{Qg} + \Delta^{(1,1)}_{Q\bar{\gamma}} + \Delta^{(1,1)}_{g\bar{\gamma}} + \Delta^{(1,1)}_{qq+\bar{q}\bar{q}} \tag{3.52}$$

where Q stands for all quarks and anti quarks. The last channel corresponds to the contribution due to identical quark-quark and anti quark-anti quark interactions. We consider the following setup: collider energy $\sqrt{s} = 14$ TeV, mass of the Z boson $M_Z = 91.1876$, effective electromagnetic coupling at LO $\alpha = 0.00754757036825847 \sim 1/132.5$, electromagnetic coupling associated to the radiative corrections $\alpha(M_Z) \sim 1/128 = 0.0078125$, strong coupling constant $\alpha_s(M_Z) = 0.11800$. We use `NNPDF31_nnlo_as_0118_luxqed` [78] pdf set which includes the `LUX_QED` [141, 142] photon pdf, and we consider the contribution of all the quarks but the quark top. We set the renormalization scale and the factorization scale equal to each other, with their common value being the mass of Z boson $\mu_F = \mu_R = M_Z$.

In Tab. 3.1, we report the comparison between the results obtained with the analytic computation of Ref [13] and with the q_T subtraction formula, obtained at the fixed value of the cut-off $r_{\text{cut}} = 0.8\%$, as motivated in the next section. We see that we get a good agreement, within 1σ with a precision of $1-2\%$.

The hard-virtual coefficient $H^{F\,(1,1)}_{c,DY}$ appears only in the corrections to the diagonal channel $\Delta^{(1,1)}_{q\bar{q}}$. We have found that the numerical impact of the hard-collinear coefficient in this channel, which contains the contribution proportional to $\delta(q_T)$ and hence also the $H^{F\,(1,1)}_{c,DY}$ term, is very small, being of the order of the numerical error of the entire correction. To have a more stringent test of this contribution, we have consider two more points at well separated collider energies, $\sqrt{s} = 2$ TeV and $\sqrt{s} = 100$ TeV. The results are shown in Tab. 3.2. We got a good agreement even though we find that the contribution of the hard-collinear component is very small also in those cases. Given the stability of the result to this large variation in the collider energy, we can reasonably conclude that the implementation has been tested with positive results and it is very unlikely that some of the terms are wrong.

3.2.1 Dependence on $r_{\rm cut}$

As discussed in the previous chapter, the q_T subtraction formula is affected by power corrections in the $r_{\rm cut}$ regulator modulo logarithmic enhancements. We study the stability of the prediction for the total cross section by varying $r_{\rm cut}$ in the nominal range $[0.01, 1]\%$ for all the partonic channels but the diagonal quark-anti quark channel for which we restrict the exploration range to the interval $[0.1, 1]\%$ where we have a good numerical control. In Fig. 3.5, we plot the mixed correction $\Delta^{(1,1)}$ for all the partonic channels as a function of $r_{\rm cut}$ normalised to the $r_{\rm cut}$-independent result given by the the "analytic" computation of Ref. [13]. The behavior is nicely flat in all the partonic channels and it motivates our choice of the cut-off, $r_{\rm cut} = 0.8\%$. This result is consistent with what expected from the $r_{\rm cut}$ analysis on the color-singlet production in pure QCD, where the dependence on $r_{\rm cut}$ is known to be quadratic [39, 56].

3.2.2 Differential distributions

We conclude this chapter showing results for the relevant kinematic distributions, the rapidity y_Z and the transverse momentum $p_{T,Z}$ of the Z boson. This analysis is meant to be a technical study more than a phenomenological one. For this reason, we just focus on the behavior of the reference central value scale $\mu_F = \mu_R = M_Z$ without performing a complete analysis including scale variations and we do not push the computation further in the direction to include also the decay of the Z boson into a lepton pair, that can be treated consistently in the narrow-width approximation. For an on-shell Z, such computation has already been performed in Ref. [18], providing a detailed phenomenological study for physical fiducial cross sections.

In that work, results on the inclusive cross sections are also given. This allows us to perform a tuned comparison which provides us a completely independent validation of our computation. The setup is very similar to the one in the previous section apart for the hadronic center-of-mass energy: collider energy $\sqrt{s} = 13\,\text{TeV}$, mass of the Z boson $M_Z = 91.1876$, effective electromagnetic coupling at LO $\alpha = 0.0075563839074311188 \sim 1/132.3$, electromagnetic coupling associated to the radiative corrections $\alpha(M_Z) \sim 1/128 = 0.0078125$, strong coupling constant $\alpha_s(M_Z) = 0.11800$, `NNPDF31_nnlo_as_0118_luxqed` with five active flavours.
Following Ref. [18], we introduce the relative corrections

$$\Delta_r^{(i,j)} = \frac{\Delta^{(i,j)}}{\sigma_{ref}} \tag{3.53}$$

with respect to the reference cross section given by the NLO QCD cross section

$$\sigma_{ref} = \sigma^{(0,0)} + \sigma^{(1,0)}. \tag{3.54}$$

We obtain the following results for the NLO QED, the NNLO QCD and the mixed QCD-QED corrections

$$\Delta_r^{(0,1)} = (3.228 \pm 0.004) \times 10^{-3}, \quad \Delta_r^{(2,0)} = -(6.34 \pm 0.14) \times 10^{-3}, \quad \Delta_r^{(1,1)} = (3.0 \pm 0.1) \times 10^{-4}, \tag{3.55}$$

which are in very good agreement with the results in Eq.(3.1) of Ref [18]. In particular, the order $\mathcal{O}(\alpha)$ and $\mathcal{O}(\alpha_s\alpha)$ results represent a check of our new computation. The NNLO QCD, which we computed with the well-established code in Ref. [7], is quoted here just as reference value to get an idea of the relative importance of the other corrections.

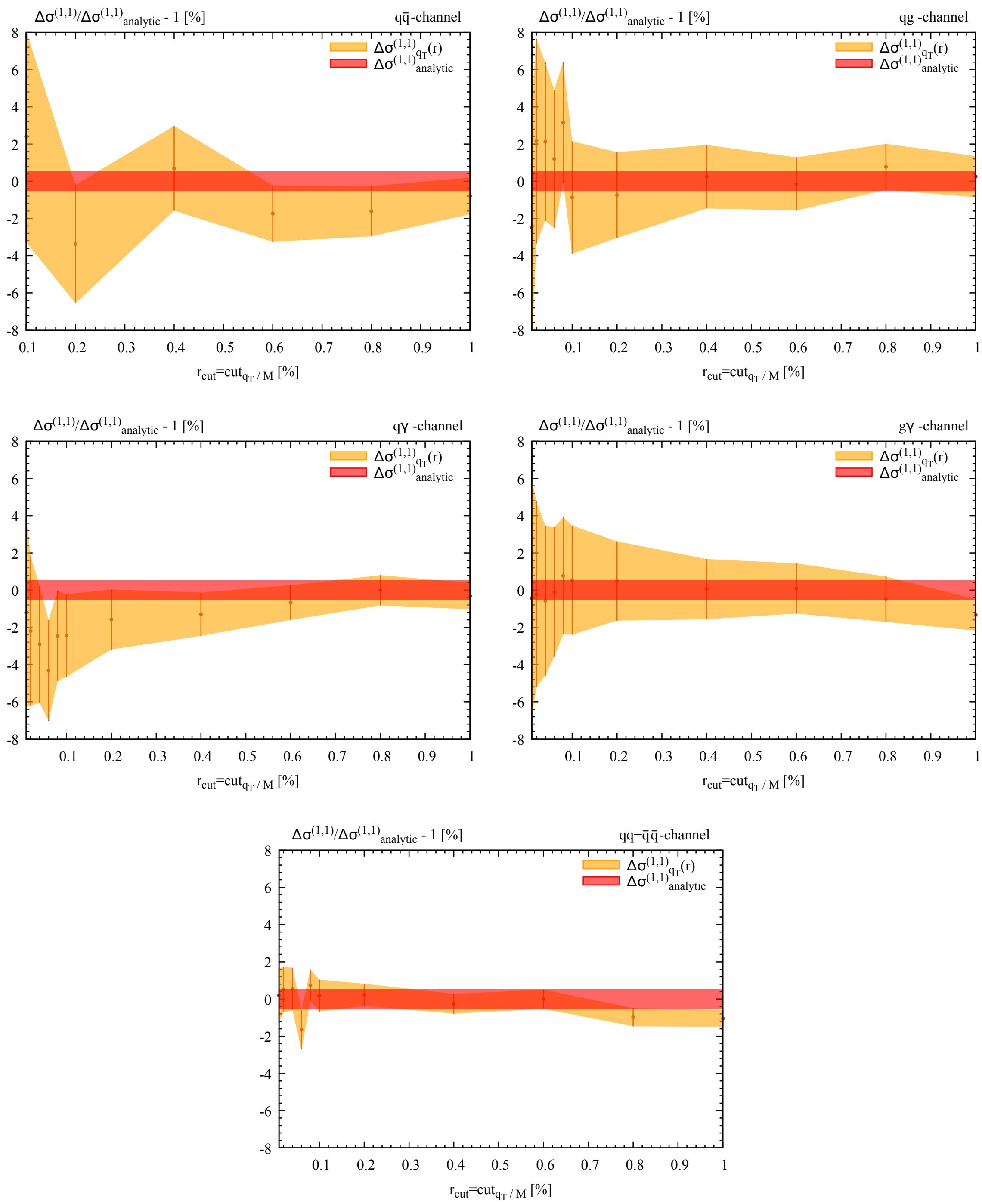

FIGURE 3.5: Mixed correction as a function of r_{cut} in all the partonic channel defined in the main text in proton-proton collisions at 14 TeV. The result is normalised to the r_{cut}-independent cross section given by the "analytic" computation of Ref. [13].

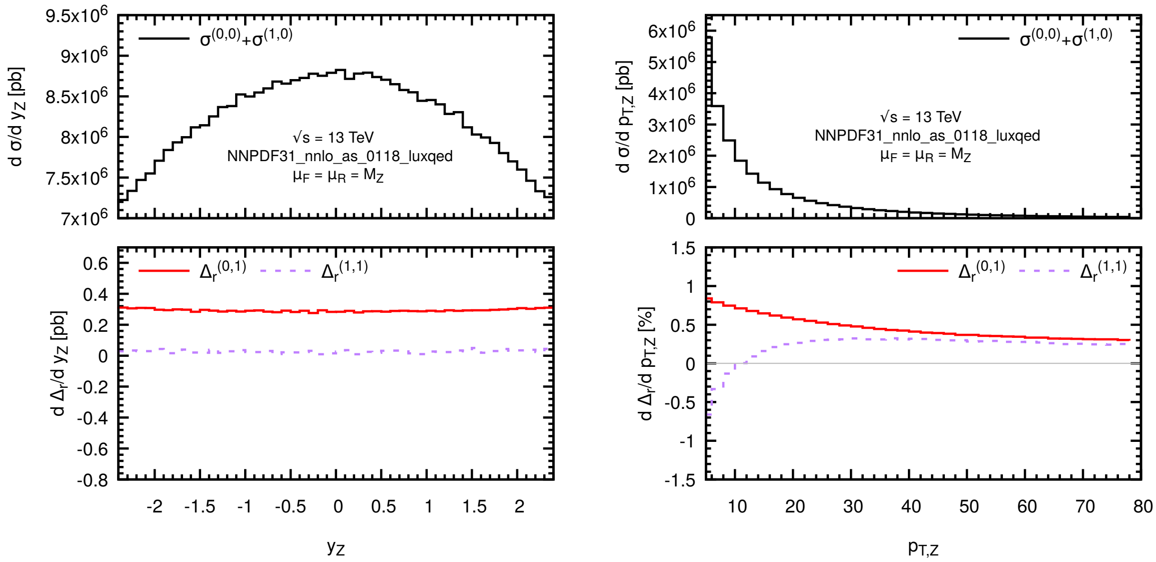

FIGURE 3.6: Rapidity y_Z (left panel) and transverse momentum $p_{T,Z}$ (right panel) of the Z boson produced in proton-proton collisions at $\sqrt{S} = 13\,\text{TeV}$. In the upper panels, we plot the NLO QCD cross section, in the lower panels, the relative corrections $\mathcal{O}(\alpha)$, $\mathcal{O}(\alpha_s^2)$ and $\mathcal{O}(\alpha_s\alpha)$ as defined in Eq. (3.53).

In Fig. 3.6, we look at the behavior of the relative corrections $\Delta_r^{(0,1)}$ and $\Delta_r^{(1,1)}$ with the rapidity (left panel) and with the transverse momentum (right panel) of the Z boson, which are the relevant kinematic distributions that can be studied for this 2-to-1 reaction. We recall that at LO, the p_T distribution reduces to a delta function at $p_T = 0$, while a non trivial p_T spectrum starts to appear when the NLO correction is included. This means that the accuracy of the p_T distribution is one order less than the accuracy of the computation, (N)LO for a (N)NLO computation, while the rapidity contains genuine (N)NLO effects.

Looking at the rapidity distribution, we observe that both corrections have a flat behavior, as it is usually expected, and give us the information about their relative importance. Both corrections are positive with the mixed correction, as already seen in Eq. (3.54), smaller by a factor of 10 than the NLO QED as expected by the naive power counting of the couplings. As pointed out in Ref. [18], the relative importance of the mixed correction is rather sensitive to the input parameters as at this energies, of relevance for the LHC physics, a large cancellation occurs between the $q\bar{q}$ and the Qg channels, as shown in Fig. 3.7.

As for the p_T spectrum, we observe a rather flat behavior of the K-factor at moderate and large p_T, where the fix-order prediction is reliable. Going towards small p_T, one starts to observe the logarithmic divergence of the two contributions, especially for the mixed correction due to the higher logarithmic powers. Indeed, lowering the p_T, the mixed correction turns negative as expected from a NNLO correction.

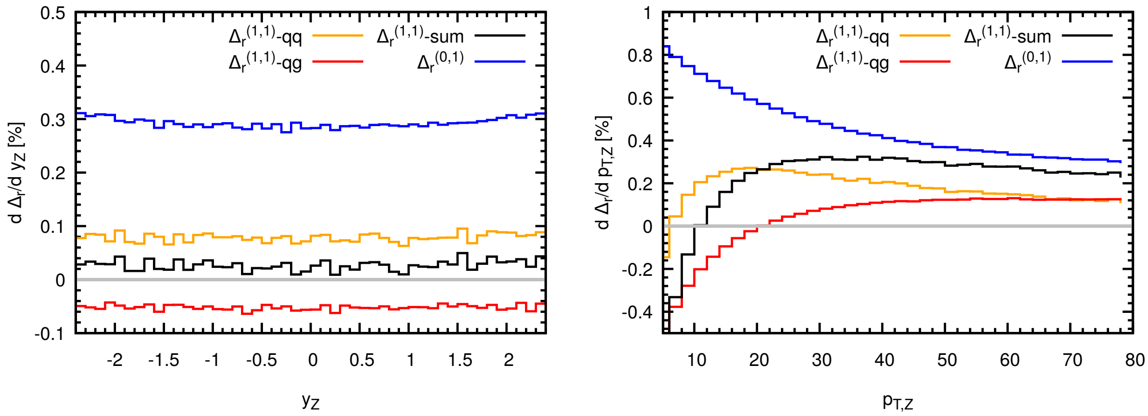

FIGURE 3.7: Impact of the dominant $q\bar{q}$ and Qg channels for the relative mixed correction as a function of the rapidity y_Z (left panel) and of the transverse momentum $p_{T,Z}$ (right panel) of the Z boson produced in proton-proton collisions at $\sqrt{S} = 13\,\text{TeV}$.

Chapter 4

NLO EW and power Suppressed terms

In this chapter, we focus on the first application of the q_T subtraction formalism to the full set of NLO EW radiative corrections including final-state radiation for both the neutral- and charged-current Drell-Yan processes in hadronic collisions. To deal with the new structure of soft divergences arising from the square of final-state diagrams and the interference between initial and final-state ones, we take the abelian limit of the corresponding contributions in the NLO q_T subtraction formula for heavy quark production reviewed in Sec. 2.2.2. While the abelianisation is straightforward, the efficiency of the method is crucial to achieve the level of accuracy required by the applications of precision physics we are interested in. From the study of the heavy-quark hadroproduction, indeed, it is known that the convergence of the q_T subtraction formula is challenged by the presence of final-state radiation.

At NLO, the r_{cut} dependence is numerically found to be linear [50, 51, 60] at variance with the case of the production of a color singlet/ neutral charged object [39]. The analytical structure of the power corrections to the latter case has been recently established [58, 59]. A similar analysis for final-state radiation was missing in the literature. In the view of the applications to EW and mixed radiative corrections, we have analytically computed the power corrections for a simplified pure QED case including for the first time the effects of final-state radiation. We investigate the origin of the observed linear behavior at the level of the inclusive cross section. This analysis completes the study of the r_{cut} dependence of the NLO q_T subtraction formula. Nonetheless, the proposed approach, being limited to inclusive observables, does not provide an effective way to improve the convergence of the subtraction. Based on the fact that power corrections are free of divergences, we have developed a procedure to remove from the NLO q_T subtraction formula the linear r_{cut} dependence associated to final-state radiation.

The mass of the colored/charged final-state particle acts as a regulator of the collinear singularities and it cannot be set to zero within the q_T subtraction formalism. The q_T variable, indeed, is not able to resolve the singularities associated to radiation emitted collinear to final state particles. So far, the formalism for heavy quark pair hadroproduction has been successfully applied only to the case of a very heavy fermion, namely the top quark [49–51]. In the limit of vanishing mass, the amplitudes develop singularities in the form of logarithms of the mass, which might lead to numerical instabilities. For the NLO EW applications we are interested in, this is of primary importance since really light fermions, as electron and muons, are involved. To this aim, we have investigated the small mass behavior of the q_T subtraction formula pushing our implementation up to the physical case of the muon mass $m \approx 105\,\text{MeV}$.

The chapter is organized into two parts. In the first part, we focus on the NLO EW corrections to the neutral- and charged-current Drell-Yan lepton hadroproduction within the q_T subtraction formalism. EW radiative corrections are usually more involved than QCD ones and present some specific technical aspects concerning renormalization/input schemes and the treatment of unstable particles. Therefore, in the first section, we briefly review the main aspects intended for the practitioners of the EW radiative corrections. We then discuss in

Sec. 4.2 the implementation of the NLO EW corrections within the q_T subtraction formalism giving the main formulas, and we report a numerical validation for a heavy lepton of mass $m_l = 10\,\text{GeV}$. We then detail the treatment of small masses in Sec. 4.2.3 and we show a tuned comparison for fiducial cross sections and differential distributions for the relevant physical case provided by muon hadroproduction. In the second part, we present the computation and the results for the analytical structure of the power correction associated to final-state radiation for the inclusive total partonic cross section, Sec. 4.3. We then discuss in Sec. 4.6, a viable strategy to go beyond inclusive observables with the aim to develop an "improved" q_T subtraction formula for final-state radiation.

4.1 Survey of NLO EW corrections

Compared to QCD, the Lagrangian of the EW in the SM involves many terms and gives rise to a large set of Feynman rules, rendering calculations of EW corrections more tedious. Nonetheless, the ingredients required to perform one-loop corrections are the same in the two cases and in the last decades have received a great boost: the treatment of soft and collinear divergences (in dimensional regularization and/or mass regularization), the reduction of tensor integral (Passarino-Veltman [156], OPP [157–160]), the evaluation of the scalar master integral [161–166], analytical and numerical helicity methods. The progresses achieved have allowed to obtain a complete automation of the computation of QCD corrections. Going to EW case, the complexity increases due to the mixing of QCD and EW corrections, the increasing number of contributions, and the presence of more and very different mass scales. Additional complications arise from the chiral structure of the EW interactions and the instability of many SM particles. Recently an increasing number of one-loop providers, as for example, RECOLA [167, 168], GoSam [169, 170], MadLoop [171, 172], OPENLOOPS [173], NLOX [174], have been developed to deal with EW one loop corrections as well, making it possible to compute the EW radiative corrections for a great number of processes relevant at high energy hadronic and leptonic colliders [172, 175].

The focus of this work is on the subtraction procedure needed to tame the soft and collinear singularities associated to the real corrections in such a way to ensure the cancellation of the infrared singularities between virtual and real corrections. In our numerical implementation, we rely on the aforementioned automated tool for the computation of one-loop virtual amplitudes. In what follows, we want to briefly convey two general aspects concerning the EW radiative corrections from the point of view of the practical computation: the choice of the EW input scheme and the treatment of the unstable intermediate resonances.

4.1.1 EW input schemes

The EW Standard Model, being a non-abelian gauge theory, is renormalizable [68, 176–179]. We mean that all the UV divergences can be absorbed into renormalization constants associated to the renormalization of the independent input parameters and the fields and/or external wave functions. To fulfill the renormalization procedure a set of independent parameters has to be chosen. In this way, one defines a customary *renormalization scheme*.

At variance with QCD, where one usually relies on the Minimum Subtraction (MS) prescription, the common choice for EW is provided by the On Shell (OS) renormalization scheme [180–183]. In the OS scheme, the renormalization constants are fixed imposing the renormalization conditions directly in the physical basis of the mass eigenstates. In such a scheme, the renormalized masses of the gauge bosons, of the Higgs bosons, and of the fermions are set equal to the physical masses, defined as the locations of the poles of the propagators. The renormalized electric charge can be set to be equal to the Thomson limit, which corresponds to the low-energy Compton scattering of on-shell particles. This choice is natural in the sense that the input parameters are directly related to observables which are measured with high accuracy. In this context, the renormalization of the parameters together with the renormalization of only the external wave functions, as dictated by the correct normalization of S-matrix elements, is sufficient to obtain UV-finite predictions without any additional fields renormalization [156, 181]. The latter are required to obtain finite Green functions. We do not enter the details of the EW renormalization, which are beyond the scope of this work.

Here, we discuss the choice of the input parameters, which define the so called *input scheme* within the context of the OS renormalization scheme. It is indeed fundamental to consider as input parameters a set of independent quantities to preserve gauge invariance and the internal consistency of the results. Furthermore, as we discuss in the following, the choice of the input scheme allows one to incorporate, on a process-by-process basis, parts of (universal) electroweak corrections in the definition of the input parameters reducing the impact of higher order corrections. As already stated, in the OS renormalization, the input-parameters set is given by the the electromagnetic coupling constant α, the Higgs mass M_H, the weak-gauge boson masses M_W and M_Z, the fermion masses m_f and the element of the CKM matrix. In the EW sector the masses of the particles are conveniently defined as *pole masses*. This does not apply to light quarks for which is preferred to consider a running $\overline{MS}$ mass defined at some convenient scale.

The definition of the CKM is in general a non trivial task. For high-energy scattering, the approximation to consider all the quark but the top (and possibly the bottom) massless and ignoring mixing with the third generation is appropriate. Within this approximation, the CKM reduces to the identity matrix but for charged-current processes, such as the quark-antiquark annihilation channels in Drell-Yan-like W-boson production, where it leads to global factors $|V_{ij}|^2$ in partonic cross sections with $q_i\bar{q}_j$ or $q_j\bar{q}_i$ initial states. This result holds also including NLO EW corrections because of the mass degeneracy between the first two quark generations.

The boson masses M_W, M_Z and M_H, are usually set to on-shell real values. With this choice of the input-parameters set, the Weinberg angle θ_w is not an independent quantity and it is usually defined via the relation

$$c_w \equiv \cos\theta_w = \frac{M_W}{M_Z}\,, \quad c_w \equiv \sin\theta_w = \sqrt{1-c_w^2}\,. \tag{4.1}$$

In particular, it is not consistent to use an independent value for s_w as provided, for example, by the effective mixing angle $\sin^2\theta_{W,eff}$ extracted from measurements of the various asymmetries of the Z resonance [184].

As for the value of the electromagnetic coupling constant, three input values are usually used in the applications:

- $\alpha(0)$-*scheme*: the value of α is set to the low-energy *Thomson limit*, $\alpha(0) \approx 1/137$;
- $\alpha(M_Z^2)$-*scheme*: the value of α is set to the effective coupling at the Z pole due to the running from $Q^2 = 0$ to $Q^2 = M_Z^2$, $\alpha(M_Z^2) \approx 1/128$;
- G_μ-*scheme*: the value of α is set to the effective coupling $\alpha_{G_\mu} = \sqrt{2}/\pi G_\mu M_W^2 \left(1 - M_W^2/M_Z^2\right) \approx 1/132$, where G_μ is the Fermi constant as measured in the muon decay $\mu^- \to e^-\bar{\nu}_e\nu_\mu$.

The difference between them ranges between $2-6\%$ and represents an important part of the input scheme. Indeed, while at LO this choice represents only a modification of an input parameter, at NLO it affects also the charge renormalization in a consistent way. To

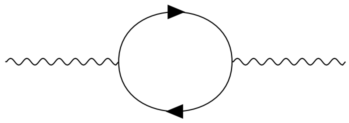

FIGURE 4.1: Fermion insertions in the photon propagator give rise to logarithms of the fermion masses.

understand the idea underlying, let us start from the $\alpha(0)$-scheme, which represent the most natural choice at low energies. When applied to processes at energies of the EW gauge bosons or above, this scheme leads to the appearence in the radiative corrections of large logarithmic enhacements of the ratio of the fermion masses over the characteristic energy scale of the reaction s. It is well understood that such logarithms are associated to the running of the electromagnetic coupling from $Q^2 = 0$ to $Q^2 = s \gtrsim M_Z^2$ and can be reabsorbed in the numerical value of the coupling. The resummation of this enhanced contributions at the leading logarithmic accuracy can indeed be achieved by employing standard Renormalization Group techniques, leading to the relation for the running of the coupling

$$\alpha(M_Z^2) = \frac{\alpha(0)}{1 - \Delta\alpha(M_Z^2)} \tag{4.2}$$

where $\Delta\alpha(M_Z^2)$ is provided by the renormalization of the vacuum polarization of the photon. In the $\alpha(0)$-scheme, this quantity contains logarithms of the fermion masses associated to the one-loop diagram in Fig. 4.1

$$\Delta\alpha(M_Z^2) = \frac{\alpha(0)}{3\pi} \sum_f N_C^2 Q_f^2 \left(\ln \frac{M_Z^2}{m_f^2} - \frac{5}{3} \right) + \mathcal{O}\left(\frac{m_f^2}{M_Z^2} \right), \tag{4.3}$$

with the color number $N_C^q = 3$ for quarks and $N_C^l = 1$ for leptons, and Q_f the electric charge of the fermion f in unit of the electron electric charge e. We observe that $\Delta\alpha(M_Z^2)$ is sensitive to the values of the light quark masses which are not well defined quantities in perturbation theory. Therefore, $\alpha(M_Z^2)$ is non-perturbative. The hadronic contribution to the running is extracted from experimental data in electron-positron annihilation into hadrons and tao lepton hadronic decays using theoretical arguments based on dispersion relations [185].

Replacing $\alpha(0)$ with $\alpha(M_Z^2)$, i.e. passing to the $\alpha(M_Z^2)$-scheme, in the LO predictions effectively removes $\Delta\alpha(M_Z^2)$ from the EW corrections. In doing so, the logarithms of the fermion masses (and in particular the non-perturbative one associated to the light quark) nicely disappear from the computation, and this cancellation holds at each loop order in α, effectively resumming the dominant effects of the running. To implement the $\alpha(M_Z^2)$-scheme, beside the modification of the input values of the electromagnetic coupling constant, one should care to change the renormalization constant in order to properly subtract the $\Delta\alpha(M_Z^2)$ contribution. From the above discussion, it follows that the $\alpha(M_Z^2)$-scheme is preferred for processes at high energies.

When external photons are present, the situation is different. Indeed, the renormalization of the photon wave function compensates the charge renormalization as a consequence of the Ward identities. In this case, mass-singularities in the form of (non perturbative) logarithmic enhancements do not occur signalling that external photons effectively couple at $Q^2 \approx 0$. The $\alpha(0) - scheme$ must be preferred in such cases.

One can accommodate more complex situations by applying in a consistent way different input-schemes for each of the different electromagnetic couplings appearing in the process (*mixed* input-scheme). As an illustrative example, consider the NLO EW corrections to the hadroproduction of a dilepton pair through the Drell-Yan mechanism. At LO, the process contains two powers of the electromagnetic coupling. The characteristic energy is given by the mass of the Z boson M_Z^2, so that the $\alpha(M_Z^2)$-scheme seems appropriate in the light of the virtual EW corrections. On the other hand, as the real corrections are concerned, an $\alpha(0)$ factor should be associated to the coupling of the real photon emission vertex. In these situations, one can use an hybrid scheme, separating the α^2 factor occurring at LO from the extra α factor associated to the NLO EW corrections. In practice, this means to compute the virtual corrections within the $\alpha(M_Z^2)$-scheme (in particular taking into account the modified prescription for the charge renormalization constant), while setting the value of the NLO electromagnetic coupling to $\alpha(0)$ both in real and virtual corrections. The last point is important for self-consistency, otherwise the use of different couplings for real and virtual contributions will spoil the cancellation of the infrared singularities. With this *hybrid* choice, the NLO cross section will be proportional to $\alpha(0) \times \alpha^2(M_Z^2)$.

In a similar manner, the introduction of the G_μ-scheme is motivated by the attempt to reabsorb an other class of universal EW radiative corrections which are related to the renormalization of the weak mixing angle. At NLO, the G_μ and $\alpha(0)$ schemes are related according to

$$\alpha_{G_\mu} = \frac{\sqrt{2} G_\mu M_W^2}{\pi} \left(1 - \frac{M_W^2}{M_Z^2}\right) = \alpha(0)(1 + \Delta r^{(1)}) + \mathcal{O}(\alpha^3)\,, \tag{4.4}$$

where $\Delta r^{(1)}$ parametrizes the NLO EW correction to muon decay [181, 186, 187]. In turn, the quantity $\Delta r^{(1)}$ can be further decomposed

$$\Delta r^{(1)} = \Delta\alpha(M_Z^2) - \Delta\rho^{(1)} \frac{c_W^2}{s_w^2} + \Delta r_{\text{rem}} \tag{4.5}$$

in terms of $\Delta\alpha(M_Z^2)$, the universal correction to the ρ parameter [188–190]

$$\Delta\rho^{(1)} = \frac{3\alpha(0) m_t^2}{16\pi s_w^2 M_W^2}, \tag{4.6}$$

which shows the distinctive quadratic growth in the top mass, and a small remainder Δr_{rem}. From Eq. (4.5), we see that the G_μ-scheme and the $\alpha(M_Z^2)$-scheme behaves similarly as the running of the coupling is concerned. In addition, the G_μ-scheme takes into account the leading EW correction to mixing angle. Indeed, a s_w factor involved in an EW coupling (for example a vertex $W f \bar{f}$) will receive an universal correction $s_W^2 \to s_w^2 + \Delta\rho^{(1)} c_W^2$ due to the OS renormalization of the weak mixing angle. In the G_μ scheme such contribution is subtracted by the corresponding contribution proportional to $\Delta\rho^{(1)}$ in Eq. (4.5). This is particularly effective for processes involving the W boson. Nonetheless, also for the Z, which introduces a c_w factor, some part of the corrections are reabsorbed, so that it is preferable to use this scheme whenever an electro-weak boson is involved. A detailed numerical study on the impact of the different input schemes for the charged- and neutral-current Drell-Yan leptons hadroproduction can be found in Ref. [145, 191].

4.1.2 Unstable particles

Unstable particles, as the EW gauge bosons and the Higgs, deserve a dedicated treatment, especially when EW radiative corrections are concerned. From the theoretical point of view, the presence of resonances leads to complications in the formulation of perturbation theory, where stable asymptotic states are used to build the S-matrix. An unstable particle P of OS mass M_P should only appear in internal lines in Feynman diagrams. Nonetheless, even in this case, the presence of a massive propagator $(p^2 - M_P^2)^{-1}$ is dangerous and may develop a spurious singularity at any fixed order in perturbation theory when the momentum transfer p becomes close to its pole. The solution to this problem is non perturbative and relies on the Dyson resummation of the self energy corrections near the singularity. In terms of the renormalized self-energies $\Sigma_R(p^2)$ of P, the resummed propagator reads

$$G_p(p^2) = \frac{i}{p^2 - M_P^2} + \frac{i}{p^2 - M_P^2} i\Sigma_R(p^2) \frac{i}{p^2 - M_P^2} + \cdots = \frac{i}{p^2 - M_P^2 + \Sigma_R(p^2)} . \tag{4.7}$$

The all orders result in Eq. (4.7) shows that radiative corrections may lead to a change in the location of the pole of the full propagator. In OS renormalization, the renormalization condition $Re(\Sigma_R) = 0$ ensures that the real part of the pole stay unchanged and, hence, the mass M_R does not get corrections. In this context, the difference between a stable and an unstable particle rests on the fact whether $\Sigma_R(p^2)$ develops an imaginary part or not, as a consequence of the optical theorem [192]:

- for a stable particle, $\Sigma_R(p^2)$ is real and the resummed propagator asymptotically behaves as the LO propagator $G_p \sim i(p^2 - M_P)^{-1}$ near the pole;
- for an unstable particle, which can decay into other final state particles, $\Sigma_R(p^2)$ develops an imaginary part, and the resummed propagator behaves as

$$G_p(p^2) \sim \frac{i}{p^2 - M_P^2 + iM_P\Gamma_P} \tag{4.8}$$

  where $\Gamma_P > 0$ is related to the width of the unstable particle. The sign of Γ_P is dictated by causality (as given by the Feynman prescription) and guarantees that the resonance decays with exponential law propagating forward in time.

While the Dyson summation provides a clean and straightforward framework to deal with resonances, its use in practical applications is very limited. Indeed, this procedure gets invalidated by the truncation of the perturbative series, which is required to compute corrections that are not of self-energy type (as irreducible vertex functions). The reason is that consistency relations from gauge invariance and unitarity usually hold order by order and get violated in perturbative orders that are not completely taken into account. In particular, we stress the importance of preserving gauge invariance. Beside being independent on the gauge-fixing procedure and, hence, on the gauge parameters, gauge invariance ensures the validity of the Ward identities. This guarantees that the resulting amplitudes will behaves correctly in the high-energy limit.

Narrow-width-approximation and naive LO treatment

The simplest (and crudest) way to deal with resonances is provided by the *narrow-width-approximation* (NWA) which consists in the separation of the full process into the production of an OS particle P and its decay to some finale state. The approximation is asymptotically exact in the limit of a "stable"resonance, $\Gamma_P \to 0$, where the square of the propagator of the resonance behaves as

$$\frac{i}{|p^2 - M_P^2 + iM_P\Gamma_P|^2} \sim \frac{\pi}{M_P\Gamma_P}\delta(p^2 - M_P^2) + \mathcal{O}\left(\frac{\Gamma_P}{M_P}\right) , \tag{4.9}$$

neglecting, in doing the above replacement, off-shell effects of order $\mathcal{O}(\Gamma_P/M_P)$. In this context, the quantity Γ_P is given by

$$\Gamma_P = \sum_X \Gamma_{P\to X}, \tag{4.10}$$

where the $\Gamma_{P\to X}$ is the partial decay width in the final state or channel X and it is computable in perturbation theory as

$$\Gamma_{P\to X} = \frac{1}{2M_P}\int d\Phi_X |\mathcal{M}_{P\to X}| \tag{4.11}$$

where $\mathcal{M}_{P\to X}$ is the matrix element for the process $P \to X$ and Φ_X is the phase space element associated to the final state X. The ratio between the partial decay width $\Gamma_{P\to X}$ and the total width Γ_P defines the *branching ration* $BR(P \to X)$ into the channel X.

If the intermediate resonant state carries a non-trivial quantum spin number, spin correlations between initial and final states may appear in kinematic distributions and when cuts on the decaying particles are imposed. Such correlations are neglected in the simplest implementations of the NWA, which rely upon unpolarized cross sections. This naive description can be improved by using instead a combination of production and decay parts for definite polarization states of the unstable particle. In this way, spin correlations are fully taken into account.

Within the NWA, radiative corrections can be approximately accommodated. Following the separation of the decay process, radiative corrections to the production and to the relevant BR are computed separately, neglecting off-shell effects of order $\mathcal{O}(\Gamma_P/M_P)$ due to the off-shell tail of the resonance and to non-resonant contributions. Restoring the full NLO accuracy requires going beyond the NWA. An improved description which adds such effects on top of the NWA is possible, but limited to the resonance region. Furthermore, the NWA cannot describe observables which resolve the resonance since, by construction, the resonance is integrated over. A full description of a resonance process, keeping the full differential information of the kinematics of the decay products, must be based on complete matrix elements for the full process, including both resonant and non- resonant diagrams. At LO, the simplest prescription to deal with the resonant state is given by the following modification of the propagator of the unstable particle

$$\frac{i}{p^2 - M_P^2} \to \frac{i}{p^2 - M_P^2 + iM_P\Gamma_P(p^2)} \tag{4.12}$$

which takes into account the imaginary part of the Dyson summed self-energy. In particular, we observe that the square of the above propagator gives raise to the characteristic Breit-Wigner shape in the cross sections. Two alternative choices of $\Gamma_P^2(p^2)$ have been commonly used in practice:

- *Fixed width (FW)*: $\Gamma_P(p^2) = \Gamma_P = const$. The pole of the propagator is displaced in the complex plane and is given by the complex squared mass

$$\mu_P^2 = M_P^2 - iM_P\Gamma_P\,. \tag{4.13}$$

- *Running width (RW)*:

$$\Gamma_P(p^2) = \Gamma_P\frac{p^2}{M_P^2}\theta(p^2), \tag{4.14}$$

  with the aim to mimic the p^2 dependence of the imaginary part of the one-loop self-energy of a vector particle P that exclusively decays into pairs of massless fermions, as it approximately applies to EW gauge bosons. In particular, the factor $\theta(p^2)$ switches off the imaginary part below the kinematic decay threshold, as demanded by causality and unitarity.

From a theoretical point of view, none of the above schemes appear satisfactory since they introduce gauge dependent quantities. In practice, it has been observed that the FW scheme works well for W/Z [193–195], while the RW, used for the analysis at the Z resonance [184], can lead to totally wrong results, especially at high energies [196]. The reason can be traced back to the p^2 dependence in $\Gamma_P(p^2)$, which is responsible for an enhancement of gauge-invariant-breaking terms. Beyond LO, this issues becomes even more severe and they deserve a proper treatment within suitable computational schemes.

Complex-mass scheme, input parameters and relations with OS quantities

In this work, we adopt the complex-mass scheme [193, 197, 198], which relies on the introduction of the complex pole μ_P^2 in Eq. (4.13). Within this framework, the mass squared of each unstable particle P is identified with μ_P^2 not only in the propagator of P but also in the couplings, which in turn become complex quantities. In particular, the weak mixing angle is promoted into the complex domain via the relation

$$c_w^2 = 1 - s_w^2 = \frac{\mu_W^2}{\mu_Z^2}\,. \tag{4.15}$$

The procedure outlined above is sufficient to fully specify the complex-mass scheme at LO. At NLO, the renormalization procedure follows directly the standard machinery for stable particles but for few modifications. The complex-mass scheme does not change the underlying theory. Instead, it provides a procedure to systematically rearrange the perturbative expansion avoiding double counting. This can be easily understood if one think that the imaginary parts appearing in the complex masses are associated to higher-order contributions in the standard perturbation theory for stable particles. We refer to Ref. [199] (and reference therein) for a description of the necessary changes in the renormalization procedure in the complex-mass scheme.

Here, we limit ourselves to list the main advantages given by this approach:

- gauge invariance is automatically preserved because the gauge boson masses are modified only by an analytic continuation. In particular, since the pole location μ_P^2 is an intrinsic property of the S-matrix, the complex mass renormalization constants and the parametrization of S-matrix elements in terms of μ_P^2 are gauge independent. On the other hand, the OS scheme involves gauge dependences starting from the two-loop level [200];

- NLO accuracy is uniformly reached both in resonant and non-resonant regions of the phase space;

- the introduction of imaginary parts spoils unitary as expressed by standard cutting relations at the amplitude level [201]. This is harmless within this approach since this effect is formally of one order higher than the one of the computation (NLO for a LO computation, NNLO for a NLO one). Unitary cancellations are therefore respected and this is sufficient to prevent the appearing of unphysical and spurious enhancements.

The choice of the input parameters within the complex-mass scheme deserves some clarifications. In particular, we remark that the width of the unstable particle Γ_P, despite the fact that μ_P^2 is promoted to the level of complex renormalized constant, is not an independent quantity. This follows directly from the condition that μ_P^2 corresponds to the location of the pole of the propagator of P, which reads

$$\mu_P^2 - M_{0,P}^2 + \Sigma(\mu_p^2) = 0, \tag{4.16}$$

in terms of the bare mass $M_{0,P}^2$ and the unrenormalized self-energy $\Sigma(p^2)$. Replacing Eq. (4.13) in Eq. (4.16) and equating the imaginary part, we obtain the relation

$$M_P\Gamma_P = \Im\Sigma(M_P^2 - iM_P^2\Gamma_P)\,, \tag{4.17}$$

that can be iteratively solved for Γ_P. From the above equation, it follows that if the self-energy is known at NLO, the accuracy in the prediction of the width will be only LO. This is a consequence of unitary cuts, which relate the imaginary part of the one-loop insertions to corresponding tree-level real emission processes. In the proximity of the resonance, the offshellness of the propagator is of the same size of the width, $|p^2 - M_P^2| = \mathcal{O}(M_P^2\Gamma_P)$, requiring to go one order higher in the computation of the width in order to achieve full NLO accuracy. From the above discussion, it follows that, in the view of a NLO computation, we need to use as "input" the Γ_P as provided by the solution of Eq. (4.17) using self energy corrections up to two-loop level or equivalently computing the relative decay amplitudes at NLO. While there is a requirement regarding the lower accuracy at which the width should be computed, actually it is allowed to go beyond NLO or even take an empirical value for it. We mean that this choice for the width, and more generally for any other input parameters (real or complex), does not introduce any inconsistencies such as violating gauge invariance or unitarity cancellation.

An other important example is given by the electromagnetic coupling. Within the complex-mass scheme, also this parameter becomes complex because of loop corrections that enter the charge renormalization constant. Again, the imaginary part of the charge e is not a free input parameter being determined by the charge renormalization in the same way the width is determined by Eq. (4.17). In this case, the imaginary parts start to appear at two-loop (the charge renormalization only involves self-energies contributions that are evaluated at zero momentum transfer, which do not develop imaginary parts for real internal masses). For this reason, it is allowed to put to zero the imaginary part of e within the NLO accuracy. Moreover, we observe that a complex imaginary part in the virtual corrections would introduce a mismatch in the cancellation of IR divergences between reals and virtuals. The different α-input schemes described in Sec. 4.1.1 can be accommodated straightforwardly.

The complex-mass scheme provides a theoretically well-motivated framework to deal with unstable particles and renormalization in EW SM. However, historically, the W and Z masses and widths were experimentally determined at LEP, Tevatron, and the LHC in the OS scheme. The definitions of *pole* masses and widths in the complex-mass scheme differ from the one in OS scheme and they are related by the following relations [194, 202]

$$M_P = \frac{M_{P,OS}}{\sqrt{1+\frac{\Gamma_{P,OS}^2}{M_{P,OS}^2}}}, \quad \Gamma_P = \frac{\Gamma_{P,OS}}{\sqrt{1+\frac{\Gamma_{P,OS}^2}{M_{P,OS}^2}}} \tag{4.18}$$

where $M_{P,OS}$ and $\Gamma_{P,OS}$ are quantities in the OS scheme. For W and Z bosons, the mass difference between the pole and OS definitions is

$$M_{W,OS} - M_W \approx 27\,\mathrm{MeV} \quad M_{Z,OS} - M_Z \approx 34\,\mathrm{MeV} \tag{4.19}$$

so that scheme differences are much larger than the current experimental uncertainties.

4.2 NLO EW for Drell-Yan lepton hadroproduction

4.2.1 q_T subtraction formula

We focus on the processes of hadroproduction of a dilepton l^+l^- pair and lepton-neutrino $l^+\nu_l$ $(l^-\bar{\nu}_l)$ pair, namely $pp \to l^+l^- + X$ and $pp \to l^+\nu_l\,(l^-\bar{\nu}_l) + X$. We can give an unified treatment of the two processes and consider the general reaction $pp \to l_1 l_2 + X$ in terms of generic leptons l_1 and l_2 carrying electric charges e_3 and e_4 respectively. The NLO EW q_T subtraction formula for the partonic cross section has again the familiar structure

$$d\hat{\sigma}^{l_1l_2}_{NLO} = \mathcal{H}^{l_1l_2}_{NLO} \otimes d\hat{\sigma}^{l_1l_2}_{LO} + \left[d\hat{\sigma}^{l_1l_2+\text{jet}}_{LO} - d\hat{\sigma}^{l_1l_2,CT}_{NLO} \right] , \tag{4.20}$$

where, as already specified before, we include in the definition of jet also the photon. Let us start the discussion from the IR subtraction counterterm $d\hat{\sigma}^{l_1l_2,CT}_{NLO}$. Its explicit expression in the partonic channel $ab \to l_1l_2 + X$ reads

$$d\hat{\sigma}^{l_1l_2,CT}_{NLO\,ab} = \sum_{c=q,\bar{q},\gamma} \frac{\alpha}{\pi}\, \Sigma^{(1)}_{c\bar{c}\leftarrow ab} \otimes d\hat{\sigma}^{l_1l_2}_{LO\,c\bar{c}}\, \frac{dq_T^2}{M^2} \;, \tag{4.21}$$

where M is the invariant mass of the l_1l_2 pair and the symbol $\otimes$ denotes convolutions with respect to the longitudinal-momentum fractions z_1 and z_2 of the colliding partons. As in the previous chapter, we suppressed the dependence on the flavour of the parton for ease of notation, i.e. a generic partonic index a must be understood as $a \equiv \{a, f_a\}$. As usual, the functions $\Sigma^{(1)}_{c\bar{c}\leftarrow ab}$ in Eq. (4.21) can be written as

$$\Sigma^{(1)}_{c\bar{c}\leftarrow ab}(z_1, z_2; r) = \Sigma^{(1,2)}_{c\bar{c}\leftarrow ab}(z_1, z_2)\tilde{I}_2(r) + \Sigma^{(1,1)}_{c\bar{c}\leftarrow ab}(z_1, z_2)\tilde{I}_1(r) \tag{4.22}$$

where $r = q_T/M$. Now, we observe that the structure of the IR subtraction counterterm can be decomposed as

- the Drell-Yan-like contribution due to the square of Feynman diagrams associated to initial-state radiation only;
- all the new contributions due to the presence of final state radiation.

Since final-state radiation can only develop a single soft singularity, the coefficient $\Sigma^{(1,2)}_{c\bar{c}\leftarrow ab}(z_1, z_2)$ reduces to the pure Drell-Yan one

$$\Sigma^{(1,2)}_{c\bar{c}\leftarrow ab}(z_1, z_2) = {}_{(0,1)}\Sigma^{(1,2)}_{c\bar{c}\leftarrow ab}(z_1, z_2) \tag{4.23}$$

as given in Eq. (3.5), while the coefficient $\Sigma^{(1,1)}_{c\bar{c}\leftarrow ab}(z_1, z_2)$ will get an additive contribution $\Sigma^{(1,1),l_1l_2}_{c\bar{c}\leftarrow ab}(z_1, z_2)$

$$\Sigma^{(1,1)}_{c\bar{c}\leftarrow ab}(z_1, z_2) = {}_{(0,1)}\Sigma^{(1,1)}_{c\bar{c}\leftarrow ab}(z_1, z_2) + \Sigma^{(1,1),l_1l_2}_{c\bar{c}\leftarrow ab}(z_1, z_2) \,. \tag{4.24}$$

The coefficient $\Sigma^{(1,1),l_1l_2}_{c\bar{c}\leftarrow ab}(z_1, z_2)$ is obtained by taking the abelian limit of the customary coefficient for heavy-quark production, Eq. (2.85). For ease of reference, we report here the latter

$$\Sigma^{(1,1),Q\bar{Q}}_{c\bar{c}\leftarrow ab}(z_1, z_2) = -\delta_{ca}\delta_{\bar{c}b}\delta(1-z_1)\delta(1-z_2) \frac{\langle \mathcal{M}_{c\bar{c}\to Q\bar{Q}} | \left(\mathbf{\Gamma}^{(1)}_t + \mathbf{\Gamma}^{(1)\dagger}_t \right) | \mathcal{M}_{c\bar{c}\to Q\bar{Q}} \rangle}{|\mathcal{M}_{c\bar{c}\to Q\bar{Q}}|^2} \,, \tag{4.25}$$

which is controlled by the first-order contribution to the soft anomalous dimension for transverse-momentum resummation in heavy-quark production $\mathbf{\Gamma}_t^{(1)}$, whose explicit expression is (Eq. (2.76))

$$\begin{aligned}\mathbf{\Gamma}_t^{(1)} = -\frac{1}{4}\Big\{&(\mathbf{T}_3^2+\mathbf{T}_4^2)(1-i\pi) + \sum_{i=1,2;j=3,4} \mathbf{T}_i\cdot\mathbf{T}_j \ln\frac{(2p_i\cdot p_j)^2}{M^2m^2}\} \\ &+ 2\mathbf{T}_3\cdot\mathbf{T}_4\left[\frac{1}{2v}\ln\left(\frac{1+v}{1-v}\right) - i\pi\left(\frac{1}{v}+1\right)\right]\Big\}.\end{aligned} \tag{4.26}$$

The abelian limit is simply obtained by replacing the QCD charges, given by the color matrices $\mathbf{T}_i$, with the corresponding scalar electric charges

$$\mathbf{T}_i \to e_i\mathbf{I}, \tag{4.27}$$

and taking care of the modifications in the kinematics in the case of different lepton masses $m_{l_1} \neq m_{l_2}$. Therefore, the structure in color space becomes trivial, while a dependence on the flavour of the fermions is introduced. The $\Sigma_{c\bar{c}\leftarrow ab}^{(1,1),l_1l_2}(z_1,z_2)$ coefficient reads

$$\Sigma_{c\bar{c}\leftarrow ab}^{(1,1),l_1l_2}(z_1,z_2) = -\delta_{ca}\delta_{\bar{c}b}\delta(1-z_1)\delta(1-z_2)2\Re\Gamma_t^{(1),l_1l_2}, \tag{4.28}$$

where $\Gamma_t^{(1),l_1l_2}$ can be interpreted as the customary first-order contribution to the QED soft anomalous dimension for transverse-momentum resummation in dilepton production. We specialize its explicit expression for the neutral-current dilepton pair production

$$\begin{aligned}\Gamma_t^{(1),l^+l^-} = -\frac{1}{4}\Big\{&(e_3^2+e_4^2)(1-i\pi) + \sum_{i=1,2;j=3,4} e_ie_j \ln\frac{(2p_i\cdot p_j)^2}{M^2m_l^2}\} \\ &+ 2e_3e_4\left[\frac{1}{2v}\ln\left(\frac{1+v}{1-v}\right) - i\pi\left(\frac{1}{v}+1\right)\right]\Big\},\end{aligned} \tag{4.29}$$

and for the charged-current lepton-neutrino pair production

$$\Gamma_t^{(1),l^+\nu_l} = \Gamma_t^{(1),l^-\bar{\nu}_l} = -\frac{1}{4}\Big\{e_3^2(1-i\pi) + \sum_{i=1,2;} e_ie_3 \ln\frac{(2p_i\cdot p_j)^2}{M^2m_l^2}\}\Big\}. \tag{4.30}$$

Similarly, the hard-collinear coefficient $\mathcal{H}_{NLO}^{l_1l_2}$ is made of three contributions

- the process-dependent hard-virtual function $H^{(1),l_1l_2}$ associated to the one-loop EW virtual corrections.
- the universal Drell-Yan-like collinear remainder;
- the customary first-order contribution to the soft function $F_t^{(1),l_1l_2}$.

The latter term represents the new contribution at $q_T = 0$ (i.e. proportional to $\delta(q_T^2)$) arising from soft final state radiation. Again, it can be obtained by taking the abelian limit of the corresponding soft function in heavy-quark production, i.e. by applying the replacement in Eq.(2.79). Its explicit expression reads

$$F_t^{(1),l_1l_2} = \begin{cases}(e_3^2+e_4^2)\ln\frac{m_{l,T}^2}{m_l^2} + e_3e_4\frac{1}{v}L_{34} & (\text{neutral-current } l_1 = l^+, l_2 = l^-) \\ e_3^2\left[\ln\frac{m_{l,T}^2}{m_l^2} + \mathrm{Li}_2\left(-\frac{\mathbf{p}_\mathrm{T}^2}{\mathrm{m}_\mathrm{l}^2}\right)\right] & (\text{charged-current } l_1 = l^+(l^-), l_2 = \nu_l(\bar{\nu}_l))\end{cases} \tag{4.31}$$

with the function L_{34} as given by Eq. (2.80). For the sake of completeness, we report the full expression of the hard-collinear coefficient $\mathcal{H}^{l_1 l_2}_{NLO}$

$$\begin{aligned}\mathcal{H}^{l_1 l_2}_{NLO} = \delta_{ca}\delta_{\bar{c}b}\delta(1-z_1)\delta(1-z_2)\left[H^{(1),l_1 l_2} + F_t^{(1),l_1 l_2}\right] \\ + \delta_{ca}\delta(1-z_1)C^{(1)}_{\bar{c}b}(z_2) + \delta_{\bar{c}b}\delta(1-z_2)C^{(1)}_{ca}(z_1) \\ + \left[\delta_{ca}\delta(1-z_1)\,P^{(1)}_{\bar{c}b}(z_2) + \delta_{\bar{c}b}\delta(1-z_2)\,P^{(1)}_{ca}(z_1)\right] L_F\end{aligned} \tag{4.32}$$

with $L_F = \mu_F^2/M^2$.

4.2.2 Numerical validation for a heavy lepton

We report here a numerical validation of the subtraction formalism developed in the previous section. To be definite, we consider the hadroproduction of a dilepton pair through the Drell-Yan mechanism. In order to avoid at this stage the appearance of large logarithmic terms in the lepton mass, which may complicate the numerical convergence, we set the mass of the final-state lepton to $m_l = 10$ GeV. We postpone the discussion of the small mass behavior to the following section. Our calculation is carried out by using an extension of the numerical program of Ref. [7]. All the required tree level matrix elements are computed analytically while the virtual EW corrections for $q\bar{q} \to l^+l^-$, which include vertex and box diagrams, are obtained by using GoSam [169, 170].

Let us start setting the notation used to label the different contributions to the cross section. At LO (i.e. $\mathcal{O}(\alpha^2)$) both the resonant $q\bar{q}$ and the non-resonant $\gamma\gamma$ partonic channels contribute and we can write for the hadronic cross section

$$\sigma_{LO} = \sigma^{q\bar{q}}_{LO} + \sigma^{\gamma\gamma}_{LO}\,, \tag{4.33}$$

where $\sigma^{q\bar{q}}_{LO}$ and $\sigma^{\gamma\gamma}_{LO}$ are the Born level cross sections in the $q\bar{q}$ and $\gamma\gamma$ channels, respectively. At NLO EW we can write

$$\sigma_{NLO} = \sigma^{q\bar{q}}_{LO} + \sigma^{\gamma\gamma}_{LO} + \Delta\sigma_{q\bar{q}} + \Delta\sigma_{q\gamma} + \Delta\sigma_{\gamma\gamma} \tag{4.34}$$

where we have introduced the $\mathcal{O}(\alpha^3)$ correction in the $q\bar{q}$ channel, $\Delta\sigma_{q\bar{q}}$, the corresponding correction in the $q(\bar{q})\gamma$ channel, $\Delta\sigma_{q\gamma}$, and the correction in the $\gamma\gamma$ channel, $\Delta\sigma_{\gamma\gamma}$. Since the $\gamma\gamma$ channel provides only a very small contribution to the Drell-Yan cross section, $\Delta\sigma_{\gamma\gamma}$ will be neglected in the following discussion.

We use the setup of Ref. [145], and, in particular, we work in the G_μ scheme with

$$G_F = 1.16637 \times 10^{-5}\ \text{GeV}^{-2} \qquad \alpha(0) = 1/137.03599911 \tag{4.35}$$
$$M_{W,OS} = 80.403\ \text{GeV} \qquad M_{Z,OS} = 91.1876\ \text{GeV} \tag{4.36}$$
$$\Gamma_{W,OS} = 2.141\ \text{GeV} \qquad \Gamma_{Z,OS} = 2.4952\ \text{GeV} \tag{4.37}$$

and use the complex-mass scheme [197] throughout. More precisely, as explained in Sec. 4.1.1, we adopt a mixed scheme in which real and virtual photons emissions are controlled by $\alpha(0)$, while the α^2 in the LO cross section is derived from G_F, m_Z and m_W and the charge renormalization includes the Δr contribution. The conversion from the OS widths and masses to the corresponding pole definitions is performed by using the relations in Eq. (4.18). Following Ref. [145], the MRST2004qed [203] parton distribution functions (PDFs) are used. The following set of cuts are applied

$$m_{ll} > 50\ \text{GeV} \qquad p_{T,l} > 25\ \text{GeV} \qquad |y_l| < 2.5\,. \tag{4.38}$$

To validate our implementation, we have repeated our calculation by using the dipole subtraction method [21] and the independent matrix-element generator RECOLA [167, 168] for the virtual corrections. In Table 4.1 we report our result for the lowest order cross sections $\sigma_{LO}^{q\bar{q}}$ and $\sigma_{LO}^{\gamma\gamma}$, and the NLO EW corrections in the $q\bar{q}$ and $q\gamma$ channels, $\Delta\sigma_{q\bar{q}}$ and $\Delta\sigma_{q\gamma}$. The NLO correction $\Delta\sigma_{q\bar{q}}$ is obtained performing the calculation at different values of $r_{\rm cut}$ and extrapolating to $r_{\rm cut} \to 0$ through a linear fit. Our results are compared with the corresponding results obtained with dipole subtraction (CS+RECOLA). We see that the two results are in perfect agreement.

	q_T + GoSam	CS+RECOLA
$\sigma_{LO}^{q\bar{q}}$ (pb)	683.53 ± 0.03	
$\Delta\sigma_{q\bar{q}}$ (pb)	-5.920 ± 0.034	-5.919 ± 0.008
$\sigma_{LO}^{\gamma\gamma}$ (pb)	1.1524 ± 0.0004	
$\Delta\sigma_{q\gamma}$ (pb)	-0.6694 ± 0.0008	-0.6690 ± 0.0005

TABLE 4.1: Comparison of NLO EW corrections to the Drell-Yan process computed with q_T subtraction and dipole subtraction. In the $q\bar{q}$ channel the q_T result is obtained with a linear extrapolation in the $r_{\rm cut} \to 0$ limit (see Fig. 4.2), while in the $q(\bar{q})\gamma$ channel it is obtained at $r_{\rm cut} = 0.01\%$. The LO result in the $q\bar{q}$ and $\gamma\gamma$ channels is also reported for reference.

Dependence on $r_{\rm cut}$

We have studied the dependence of the NLO corrections for the fiducial cross section on $r_{\rm cut}$. We have varied $r_{\rm cut}$ in the range $0.01\% \le r_{\rm cut} \le 1\%$ and we have used the $r_{\rm cut}$-independent cross section computed with our inhouse implementation of the dipole subtraction method as normalisation. The results for the $r_{\rm cut}$ dependent correction $\delta_{q_T} = \Delta\sigma/\sigma_{LO}^{q\bar{q}}$ in the $q\bar{q}$ and $q\gamma$ channels are shown in Fig, 4.2. A distinctive linear behavior in the dominant $q\bar{q}$-annihilation channel emerges. Nonetheless, as reported in Ref. [56], it is known that symmetric cuts on the transverse momenta of the final state leptons challenge the convergence of q_T-subtraction leading to a stronger dependence on $r_{\rm cut}$ even in the case in which a charge-neutral final state is produced. In Fig. 4.3 we show the dependence of the NLO corrections for the inclusive cross section on $r_{\rm cut}$ when no cuts are applied. Again a distinct linear behavior in the dominant $q\bar{q}$-annihilation channel emerges, in agreement with what has already been observed for the case of the $t\bar{t}$ cross section [50], which can be clearly interpreted as a genuine new effect due to the emission of radiation off the massive final-state leptons.

4.2.3 Physical lepton masses: small-mass limit and muon production

A finite lepton mass regulates the collinear divergence associated to the emission of a collinear photon off the final-state charged lepton. Radiation emitted at small angles with respect the direction of the emitter particle is suppressed and the resulting *dead cone* region has an angular aperture of order of the lepton mass divided by the lepton energy. Heavier the lepton, bigger will be the angular separation with the emitted photon that, in turn will be more easily resolved as an isolated particle. In the limit of vanishing lepton mass, the collinear singularity manifests itself in the form of asymptotically divergent logarithms of the ratio of the mass divided by the characteristic energy scale of the process Q, and the size of the *dead cone* region reduces, even below the experimental resolution. The KLN theorem guarantees

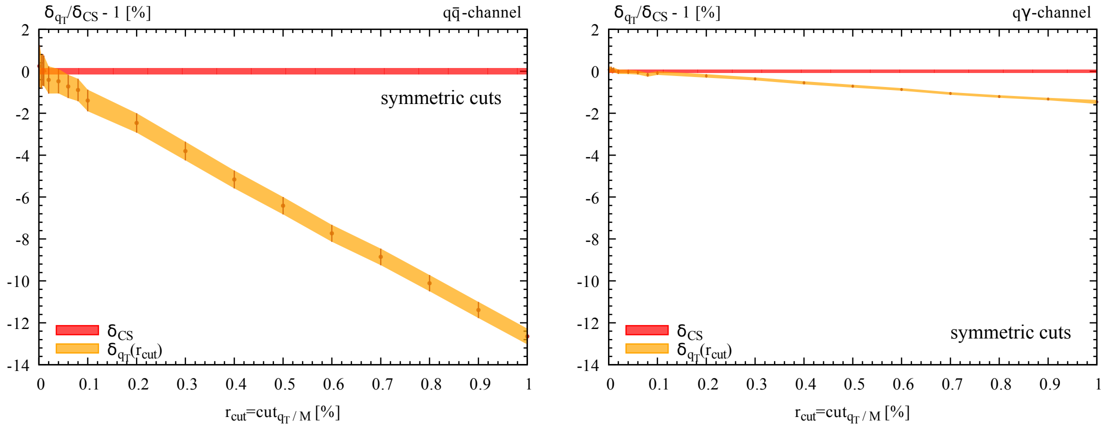

FIGURE 4.2: NLO EW correction as a function of r_{cut} in the dominant $q\bar{q}$ diagonal channel (left panel) and in the off-diagonal $q(\bar{q})\gamma$ channel (right panel) at 14 TeV. The NLO result is normalised to the r_{cut}-independent cross section computed with dipole subtraction. The lepton mass is fixed to $m_l = 10\,\text{GeV}$. The fiducial cuts in Eq. (4.38) are applied.

that these logarithms cancel if photons collinear to the lepton are treated fully inclusively. However, this picture can be spoiled by the application of phase-space cuts on the lepton momenta. Indeed, events with a photon emitted in a small collinear cone around the momenta of the lepton might not pass the cuts, leading to an imbalance of the logarithmic divergent contributions between reals and virtuals. This is due to the fact that the cuts assume perfect isolation of photons from the leptons. Fiducial cross sections of this kind are not *infrared safe*. We stress that this situation is a general consequence of fixed order perturbation theory in Quantum Field Theory and does not depend on the particular subtraction scheme employed to handle the IR singularities.

The problem rests on the application of the phase-space cuts on the *bare* leptons as given by the partonic description. Experimentally it is not possible to distinguish between a single electron and an electron accompanied by a collinear photon. Therefore, the concept of a bare lepton is not realistic for electrons, while it is phenomenologically relevant for muon final states. Cross sections defined in terms of *dressed leptons*, which include the accompanied collinear photon radiation, restore the infrared safety in a way similar to jet cross sections in QCD. In practice, *dressed leptons* are defined by a simple *recombination procedure* [145, 191]

1. Photons with a rapidity $|y_\gamma| > 3$, which are close to the beams, are considered part of the proton remnant and are not recombined with the lepton.

2. For each photon passing the first step, we compute the resolution R between the photon and the generic charged lepton l in the final state as

$$R = \sqrt{(y_l - y_\gamma)^2 + \Delta\phi_{l\gamma}^2} \tag{4.39}$$

where ϕ is the azimuthal angle in the transverse plane.

3. If $R \leq 0.1$, the photon is recombined with the lepton l, i.e. the momenta of the photon and of the lepton l are added and associated with the momentum of l, and the photon is discarded.

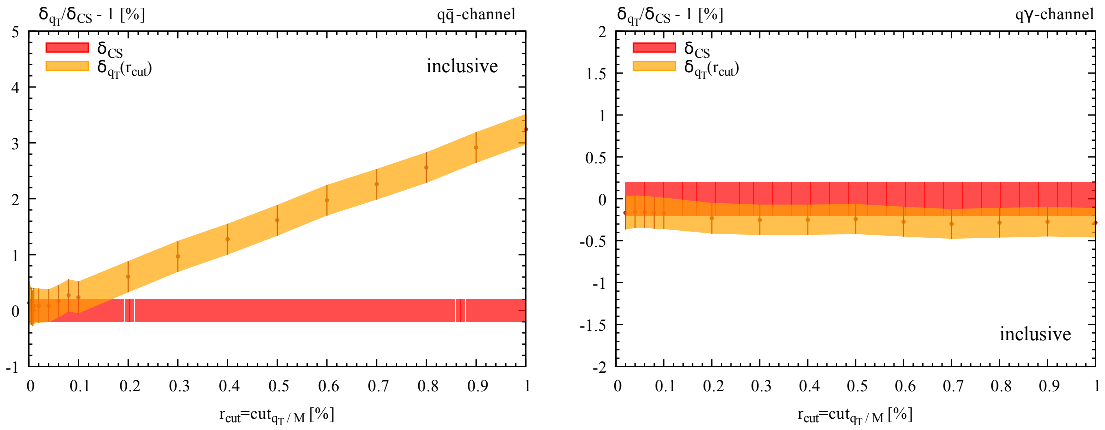

FIGURE 4.3: NLO EW correction as a function of $r_{\rm cut}$ in the dominant $q\bar{q}$ diagonal channel (left panel) and in the off-diagonal $q(\bar{q})\gamma$ channel (right panel) at 14 TeV. The NLO result is normalised to the $r_{\rm cut}$-independent cross section computed with dipole subtraction. The lepton mass is fixed to $m_l = 10\,$GeV. No cuts are applied.

The cuts are then applied on the *dressed or recombined* leptons. While the electroweak corrections differ for final-state electrons and muons without photon recombination, the corrections become universal in the presence of photon recombination, since the lepton-mass logarithms cancel in this case, in accordance with the KLN theorem.

So far, the discussion has been general, without entering the details of specific subtraction schemes. The cancellation of the large logarithms ensured by the KLN theorem is non-trivial in a numerical differential calculation. This is due to the fact that, while in the virtual corrections the lepton-mass logarithms are usually known analytically (or can be evaluated numerically with high accuracy), in the real contribution they arise only after performing the integration over the radiation phase space. This might lead to numerical instabilities when the lepton mass gets very small values. In a local subtraction scheme, the choice of suitable counterterms allows to "shift" the logarithmic enhanced contributions from the real cross section to the virtual one in such a way to ensure their analytical cancellation for infrared safe observables. As an example, this occurs employing the massive dipoles of Ref. [21], which have the remarkable property of reducing to their massless counterparts in the limit of vanishing masses. Then, the subtracted integrand (the real term minus the contribution of counterterms) is a smooth function for all space points in the real kinematics and can be efficiently integrated with standard Monte Carlo methods, while the lepton-mass logarithms are contained in the integrated counterterms in an analytic form. Of course, this approach is effective also for *bare leptons*, when the cancellation is not complete, thanks to the analytical treatment of the logs.

The situation is different for a slicing formalism, where one has really to perform the numerical integration of the real contribution as it is. Formally, a finite lepton mass makes the real integrand finite in the final-state collinear limit and, therefore, integrable. When the mass gets smaller, the integrand function asymptotically approaches the divergent behavior in the massless limit. This means that in the proximity of the quasi-collinear singularity, the integral function has a steep gradient, so that even a small slice close to this end-point can give a non-negligible contribution to the integral. In practice, this challenges the convergence of the Monte Carlo numerical integration to the exact or true result. What happens here is that the Monte Carlo estimate becomes dependent on the number of points used to sample the phase-space, which in turn corresponds to the resolution of the exploration. Indeed, if the sample is not sufficiently wide, the region associated to the logarithmic enhancement might be not 'resolved". In this situation, the Monte Carlo average is systematically shifted from the true result and the Monte Carlo error tends to underestimate the uncertainty associated to the numerical integration. We recall that the Monte Carlo uncertainty is reliable under the assumption that the integrand function is square integrable. This result is not contradicted in our case, since the integrand function behaves effectively as a divergent function.

In conclusion, the numerical integration of the reals becomes highly inefficient, requiring huge sample points in phase space for each integration step. Within the q_T subtraction formalism, this represents the main source of numerical inefficiency when the computation is pushed to the case of very light fermions, especially in combination with very small values of the $r_{\rm cut}$ regulator. Indeed, the dependence on the mass of the final state emitter particle in the IR subtraction counterterm and in the hard-collinear function is harmless, being contained only in the coefficient functions Γ_t and F_t respectively, in closed analytical form. In particular, it is known the full dependence on the the leading logarithmic behavior in the fermion mass. This provides a great control over the numerics, and it allows to use analytical expansions whenever it is required to improve the numerical implementation. To give an example, we notice that the function L_{34} in Eq. (2.80), needed to compute the soft function F_t for dilepton pair production, gets numerical instabilities for very small letpon masses. This occurs when the lepton velocity v, which behaves asymptotically as $v \sim 1 + \mathcal{O}((m_l/M)^4)$, cannot be distinguished from 1 within the finite machine representation of floating numbers, usually set to double precision (16 digits). In this case, one can either promote the computation to higher precision (as the quad precision) or use a truncated power series expansion for L_{34}, as

$$\begin{aligned} L_{34} &= \frac{\pi^2}{3} + y_{34} + \ln\frac{m_l^2}{M^2}\ln\frac{m_l^2 M^2}{m_{l,T}^4} \\ &+ 2\frac{m^2}{M^2}\left[e^{y_{34}}\left(1+\ln\frac{m_l^2}{M^2} - y_{34}\right) + e^{-y_{34}}\left(1+\ln\frac{m_l^2}{M^2}+y_{34}\right)\right] + \mathcal{O}\left(\frac{m_l^4}{M^4}\right). \end{aligned} \tag{4.40}$$

From the formal point of view, we can conclude that there are no limitations, intrinsic to the method, which prevent the use of the q_T subtraction formalism for light fermions (as long as they have a finite mass). The main problem rests on the numerical integration of the real contribution. Nonetheless, knowing its origin, one can develop different strategies to improve this aspect, which eventually rely on an efficient way to generate points in phase-space. In our opinion, indeed, the importance sampling method represents the best way to make the integrand suitable for the Monte Carlo integration. This can be combined with smart techniques of multi-channel generation to further improve the numerical efficiency.

To this aim, we employ a strategy similar to the FKS separation described in Sec. 1.2. By means of suitable projection operators, we separate the initial-state and the final-state regions and we apply a different phase-space mapping in the two cases. In particular, we rely on the massive FKS mapping presented in Sec. 1.3 to treat the final-state region. In this parametrization, the quasi-collinear singularity in the real matrix element squared behaves as $(1-\beta y)^{-1}$. Then, we can generate the angular variable y according to the above distribution so that the integrand becomes a smooth function whose integral can be accommodated by the standard Monte Carlo algorithm.

In the following, we show a tuned comparison of fiducial cross sections and a selected collection of differential distributions for muon hadroproduction processes, via both the neutral- and the charged-current Drell-Yan mechanism, obtained with our implementation

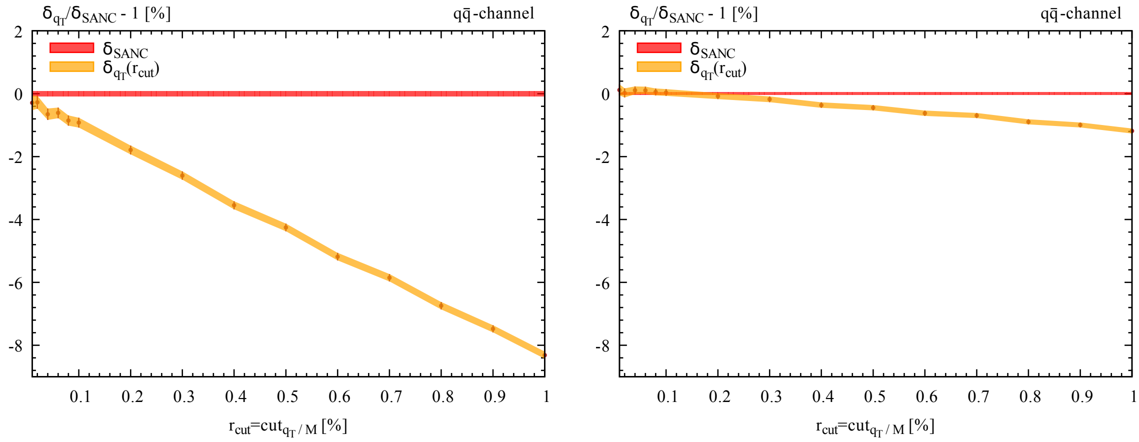

FIGURE 4.4: NLO EW correction to the neutral-current Drell-Yan process as a function of r_{cut} in the dominant $q\bar{q}$ diagonal channel (left panel) and in the off-diagonal $q(\bar{q})\gamma$ channel (right panel) at 14 TeV. The NLO result is normalised to the r_{cut}-independent cross section computed with SANC. The lepton mass is fixed to the muon mass, $m_l = m_\mu = 105.658369$ MeV. The fiducial cuts in Eq. (4.38) are applied.

of the q_T subtraction formalism and with the well-established public generator SANC [204].

Neutral-current

We stick with the same setup given in Sec. 4.2.2 for the numerical validation of the NLO EW q_T subtraction formula for a heavy lepton, with the EW input parameters given in Eq. (4.35)-(4.37) and the fiducial cuts in Eq. (4.38). Here, we set the lepton mass to the physical muon value, $m_l = 105.658369$ MeV, and we consider *bare* leptons.

We discuss first the fiducial cross section. We focus on the total NLO EW corrections, given by the sum of the corrections in the $q\bar{q}$ and $q\gamma$ channels, $\Delta\sigma_{q\bar{q}}$ and $\Delta\sigma_{q\gamma}$ respectively. The NLO correction $\Delta\sigma_{q\bar{q}}$ is obtained performing the calculation at different values of r_{cut} and extrapolating to $r_{\mathrm{cut}} \to 0$ through a linear fit. In Tab. 4.2, we report the comparison of our result with the one obtained with SANC. The agreement on the NLO correction, which in turn amounts to a 4% effect compared to the LO, is pretty good, at the *per mille* level. In Fig. 4.4, we show the r_{cut}-dependence of the NLO correction to the fiducial cross section, normalized to SANC. The behavior of both $\Delta\sigma_{q\bar{q}}$ and $\Delta\sigma_{q\gamma}$ are consistent to what has been observed for the case of the heavy lepton, Fig. 4.2. This nicely demonstrates that, apart from the numerical issues discussed in the previous section, the use of the q_T-subtraction formalism is not restricted to heavy fermions.

	q_T + GoSam	SANC
$\Delta\sigma_{q\bar{q}} + \Delta\sigma_{q\gamma}$ (pb)	-29.95 ± 0.04	-29.99 ± 0.02

TABLE 4.2: Tuned comparison for NLO EW corrections to the Drell-Yan process with $m_l = m_\mu = 105.658369$ MeV with the SANC generator. The q_T result is the limiting value for $r_{\mathrm{cut}} \to 0$ obtained with a linear fit for the NLO correction in the diagonal $q\bar{q}$-annihilation channel, and it is the value at $r_{\mathrm{cut}} = 0.01\%$ for the off-diagonal $q(\bar{q})\gamma$ channel.

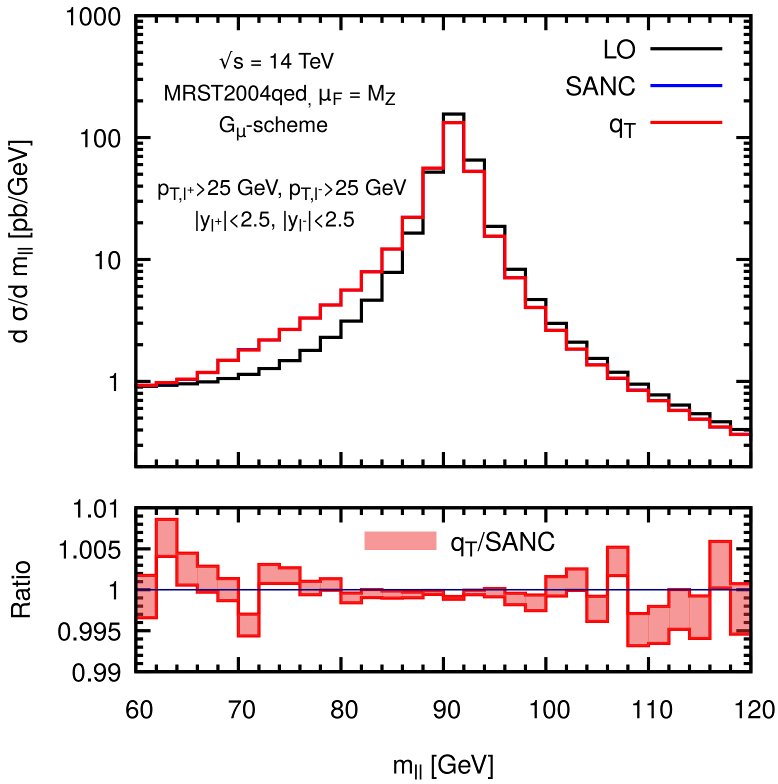

FIGURE 4.5: Tuned comparison for the dilepton invariant mass with the SANC generator. The q_T result is obtained by fixing $r_{\mathrm{cut}} = 0.01\%$ and with $m_l = m_\mu = 105.653869$ MeV. In black the LO prediction.

According to Fig. 4.4, the residual power corrections in r_{cut} can be safely neglected for $r_{\mathrm{cut}} \lesssim 0.01\%$. Setting $r_{\mathrm{cut}} = 0.01\%$, we have computed a collection of phenomenological relevant kinematic distributions: the dilepton invariant mass, the lepton transverse momentum and rapidity, the dilepton transverse momentum and rapidity. In Figs.4.5-4.7, we report the comparison with SANC. We see that, for all the observables considered, the agreement is within few per mille, which is appropriate for phenomenology.

Charged-current

In this section, we show results for the charge-current Drell-Yan process $pp \to \mu^+\nu_\mu$. The setup is similar to the neutral-current case of the previous section apart for the fiducial cuts. We use the same selection cuts as in Ref.[191]:

$$p_{T,\mu^+} > 25\,\mathrm{GeV} \qquad p_{T,\nu_\mu} > 25\,\mathrm{GeV} \qquad |y_\mu^+| < 1.2\,. \tag{4.41}$$

For simplicity, we assume a unit CKM matrix. In Fig. 4.8, we show the dependence of the fiducial cross section as function of the r_{cut} parameter. The behavior in the $q\bar{q}$ channel exhibits the usual linear shape, while the one in the $q\gamma$ is pretty flat. This is consistent with the fact that this time the rapidity cuts on the two leptons are not symmetric. In Figs 4.9, we show the comparison with SANC for the most relevant distributions: the transverse-momentum of the charged lepton and the transverse mass of the W boson. Again, we have an excellent agreement.

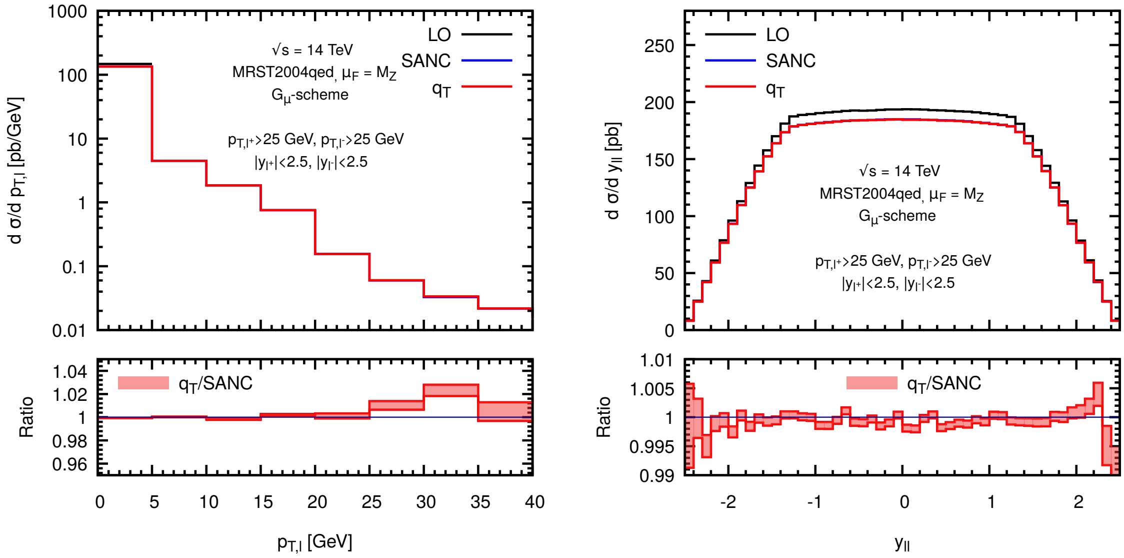

FIGURE 4.6: Tuned comparison for the dilepton transverse momentum distribution (left) and rapidity distribution (right) with the SANC generator. The q_T result is obtained by fixing $r_{\rm cut} = 0.01\%$ and with $m_l = m_\mu = 105.653869$ MeV. In black the LO prediction.

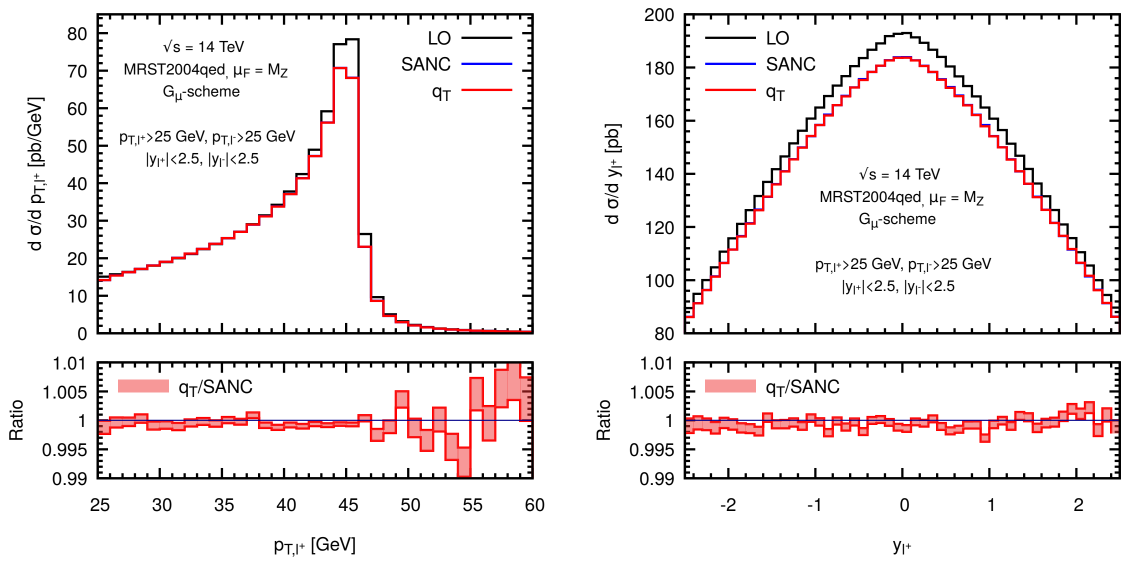

FIGURE 4.7: Tuned comparison for the transverse momentum distribution of the positively charged lepton (left) and rapidity distribution (right) with the SANC generator. The q_T result is obtained by fixing $r_{\rm cut} = 0.01\%$ and with $m_l = m_\mu = 105.653869$ MeV. In black the LO prediction.

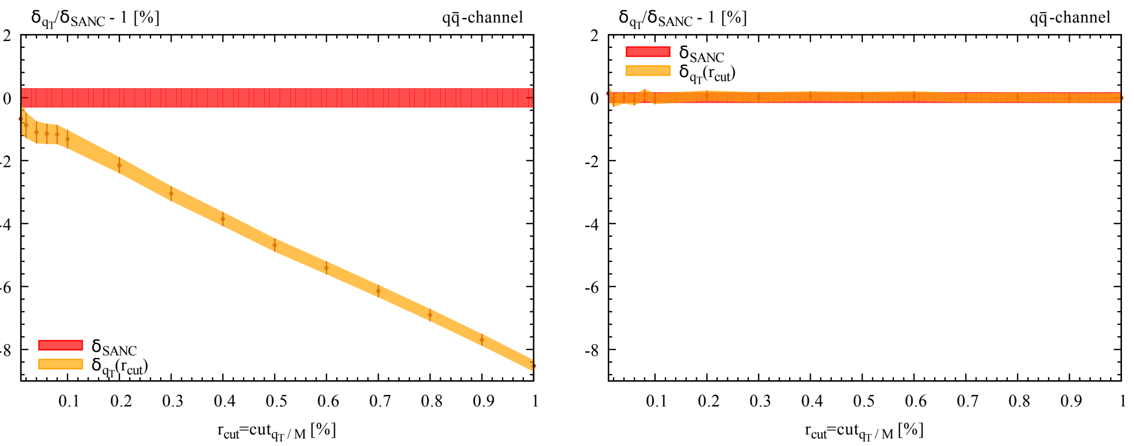

FIGURE 4.8: NLO EW correction to the charged-current Drell-Yan process as a function of r_{cut} in the dominant $q\bar{q}$ diagonal channel (left panel) and in the off-diagonal $q(\bar{q})\gamma$ channel (right panel) at 14 TeV. The NLO result is normalised to the r_{cut}-independent cross section computed with SANC. The lepton mass is fixed to the muon mass, $m_l = m_\mu = 105.658369$ MeV. The fiducial cuts in Eq. (4.41) are applied.

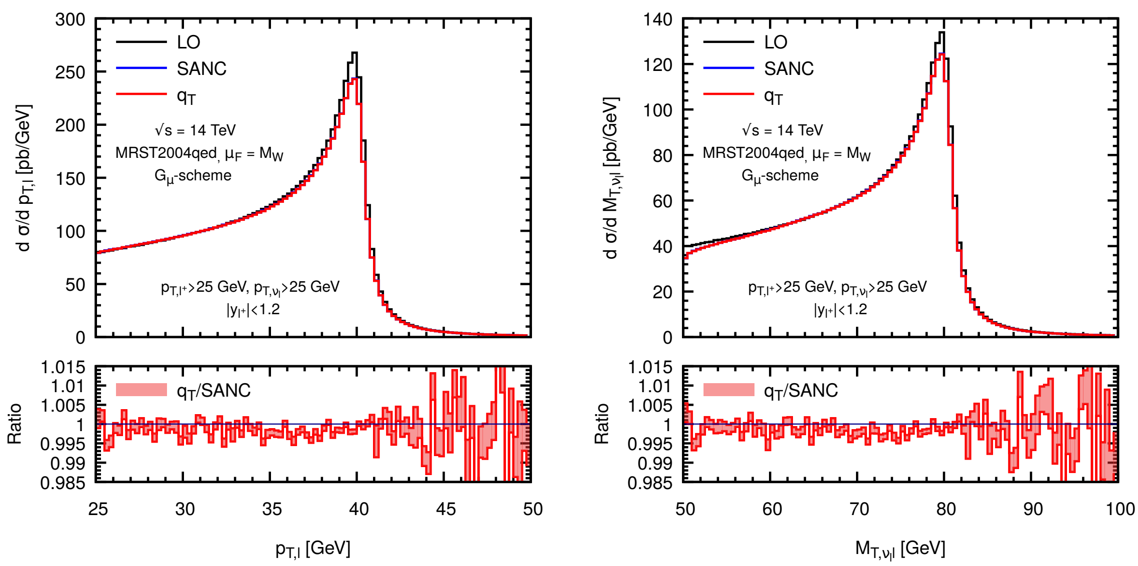

FIGURE 4.9: Tuned comparison for the transverse momentum distribution of the positively charged lepton (left) and transverse mass distribution of the W boson (right) with the SANC generator. The q_T result is obtained by fixing $r_{\text{cut}} = 0.01\%$ and with $m_l = m_\mu = 105.653869$ MeV. In black the LO prediction.

4.3 Power corrections

The numerical results in Section 4.2.2 on the r_{cut} dependence of NLO cross sections computed with q_T subtraction clearly show the change in the power correction from quadratic to linear passing from the production of a color singlet/neutral system to that one of a colorful/charged massive final state. Here, we investigate the origin of the observed linear behavior through a fully analytical computation. To this purpose, we focus on a simplified process: the production of a massive lepton pair in pure QED in the diagonal channel

$$q(p_1) + \bar{q}(p_2) \to l^+(p_3) l^-(p_4) + \gamma(k) \tag{4.42}$$

with $p_3^2 = p_4^2 = m^2$. While it allows for a great simplification in the computation, pure QED already contains the relevant physical aspects involved in this effect without introducing any additional complications (as a more involved gauge group), which might obscure the interpretation of the results. For these reasons, this process represents for us a perfect playground to deal with.

The power suppressed terms arise by the integration of real emission cross section and the counterterm. Since we keep r_{cut} finite, we can consider their contributions separately. We start our discussion from the contribution of the counterterm. From Eq. (4.21) we have

$$d\hat{\sigma}_{ab}^{CT}(r_{\text{cut}}) = \sum_{c=q,\bar{q},\gamma} \int_{r_{\text{cut}}}^{\infty} 2rdr\, \frac{\alpha_S}{\pi} \Sigma^{(1)}_{c\bar{c}\leftarrow ab} \otimes d\hat{\sigma}^{l^+l^-}_{LO\, c\bar{c}}\,. \tag{4.43}$$

The NLO coefficient $\Sigma^{(1)}_{c\bar{c}\leftarrow ab}$ depends on $r = q_T/M$ only through the functions $\tilde{I}_i(r)$. Therefore we have

$$\frac{d\hat{\sigma}_{ab}^{CT}(r_{\text{cut}})}{dr_{\text{cut}}} = -2r_{\text{cut}} \frac{\alpha_S}{\pi} \left(\Sigma^{(1,2)}_{c\bar{c}\leftarrow ab} \tilde{I}_2(r_{\text{cut}}) + \Sigma^{(1,1)}_{c\bar{c}\leftarrow ab} \tilde{I}_1(r_{\text{cut}}) \right) \otimes d\hat{\sigma}^{l^+l^-}_{LO\, c\bar{c}}\,. \tag{4.44}$$

In the small r limit the integrals $\tilde{I}_1(r)$ and $\tilde{I}_2(r)$ read

$$\begin{aligned}
\tilde{I}_1(r) &= -\frac{1}{r^2} + \frac{b_0^2}{4}(1 - 2\ln r) + O(r^2), \\
\tilde{I}_2(r) &= \frac{4\ln r}{r^2} + \frac{b_0^2}{2}\left(-1 + 2\ln^2 r\right) + O(r^2)\,,
\end{aligned} \tag{4.45}$$

i.e., they depend quadratically on r modulo logarithmic terms. This results holds also at NNLO and beyond. It follows that the leading power corrections from the counterterm are always quadratic in r_{cut}, independently on the perturbative order. Moreover, given the factorised form of the counterterm (2.48), this result is fully differential with respect the Born variable and, thus, it holds even when fiducial cuts are applied. As a consequence, the linear behavior with r_{cut} that we observe in heavy-quark production and in the EW corrections to dilepton production must be due to the real emission only. In the following we analytically compute the real-emission contribution at small values of r_{cut}.

4.4 Outline of the computation

The r_{cut} dependence is contained in the constraint applied to the integration region, namely

$$\hat{\sigma}_{q\bar{q}}(s; r_{\text{cut}}) = \int d\Phi_3 |\mathcal{M}^2| \Theta\left(\frac{q_T}{M} - r_{\text{cut}}\right) \tag{4.46}$$

where $s = (p_1 + p_2)^2$ is the partonic center-of-mass energy, $d\Phi_3$ the 3-body phase space element and $\mathcal{M}$ the corresponding real emission matrix element. Our strategy is based on the following simple idea: the treatment of the constraint becomes trivial if q_T explicitly appears among the integration variables. This amounts to parametrize in a smart way the phase space. We consider the following parametrization

$$R_3 = \frac{1}{16}\frac{1}{(2\pi)^4}\int dM^2 dq_T^2 \frac{1}{\sqrt{(s-M^2)^2 - 4sq_T^2}}\sqrt{1-\frac{4m^2}{M^2}}\int d\Omega. \tag{4.47}$$

in terms of the variables

$$M^2 = (p_3 + p_4)^2 \quad t = (p_1 - k)^2 \quad u = (p_2 - k)^2 \quad q_T^2 = ft/s \tag{4.48}$$

and the angular integral is defined in the centre-of-mass frame of the final-state leptons. The derivation of Eq. (**??**) and further details on the kinematics are given in Appendix B. Then, introducing the energy fraction

$$z = M^2/s\,, \tag{4.49}$$

the double differential real emission cross section can be written in the following form

$$\frac{d^2\hat{\sigma}_{q\bar{q}}}{dM^2 dq_T^2} = \frac{1}{32s^2}\frac{1}{(2\pi)^4}\frac{1}{\sqrt{(1-z)^2 - 4zq_T^2/M^2}}\sqrt{1-\frac{4m^2}{M^2}}\int d\Omega |\mathcal{M}|^2 \tag{4.50}$$

By integrating Eq. (4.50) over q_T^2 and M^2 and keeping into account the phase space constraints Eq. (B.11) we obtain

$$\frac{d\hat{\sigma}_{q\bar{q}}}{dr_{\rm cut}^2} = -\frac{1}{32}\frac{1}{(2\pi)^4}\int_{z_{\rm min}}^{z_{\rm max}} \frac{z\,dz}{\sqrt{(1-z)^2 - 4zr_{\rm cut}^2}}\sqrt{1-\frac{z_{\rm min}}{z}}\int d\Omega |\mathcal{M}|^2. \tag{4.51}$$

where

$$z_{\rm min} = \frac{4m^2}{s} \qquad z_{\rm max} = 1 - 2r_{\rm cut}\sqrt{1+r_{\rm cut}^2} + 2r_{\rm cut}^2\,. \tag{4.52}$$

Eq. (4.51) represents our master formula for the $r_{\rm cut}$ dependence of the real emission cross section. According to this formula, we are left with two integrations: first the angular integration in the rest frame of the lepton pair, second the integration over the energy fraction z. We profit of the fact that the matrix element squared $|\mathcal{M}|^2$ can be divided into three separate gauge invariant contributions: final state radiation, initial state radiation and interference. We split the computation accordingly and we treat the three contributions separately. We further observe that interference contribution is odd under the exchange $p_3 \leftrightarrow p_4$ and therefore vanishes after angular integration. Thus, we are left with only the final- and initial-state contributions.

4.4.1 Angular integration

In the calculation of the real emission process in Eq. (4.42), we introduce the following ten invariants

$$\begin{aligned} s &= (p_1 + p_2)^2 \\ s_2 &= (p_3 + p_4)^2 = 2m^2 + 2p_3 \cdot p_4 \\ u &= (p_2 - k)^2 = -2p_2 \cdot k \\ t &= (p_1 - k)^2 = -2p_1 \cdot k \\ u_1 &= (p_1 - p_4)^2 - m^2 = -2p_1 \cdot p_4 \\ t_1 &= (p_2 - p_4)^2 - m^2 = -2p_2 \cdot p_4 \\ s_3 &= (k - p_4)^2 - m^2 = -2k \cdot p_4 \\ s_4 &= (k - p_3)^2 - m^2 = -2k \cdot p_3 \\ u_6 &= (p_2 - p_3)^2 - m^2 = -2p_2 \cdot p_3 \\ u_7 &= (p_1 - p_3)^2 - m^2 = -2p_1 \cdot p_3. \end{aligned} \tag{4.53}$$

Since we are considering a $2 \to 3$ process, only five of the invariants are linearly independent. In particular, the following relations among the invariants

$$u_6 = -s - t_1 - u, \tag{4.54}$$

$$u_7 = -s - u_1 - t, \tag{4.55}$$

$$u_1 = -s_2 - t_1 - s_3 = -s - t_1 + s_4, \tag{4.56}$$

allow us to express u_1, u_6, u_7 in terms of the others. We notice that the invariants u, t, s_2 do not depend on the leptons angular variables ϑ_1, ϑ_2. Thus, the dependence upon ϑ_1, ϑ_2 is contained only in t_1, s_3, s_4. By means of the relation of partial fraction

$$\frac{1}{s_3 s_4} = \frac{1}{s - s_2}\left(\frac{1}{s_3} + \frac{1}{s_4}\right) \tag{4.57}$$

we can organize the expression of $|\mathcal{M}|^2$ in such a way that, in each of its terms, the dependence on ϑ_1, ϑ_2 is of the form either $t_1^k s_3^l$ or $t_1^{k'} s_4^{l'}$. Then, the required angular integrals belong to the family of integrals

$$I^{(k,l)} = \int_0^\pi \sin\vartheta_1 d\vartheta_1 \int_0^\pi d\vartheta_2 (a + b\cos\vartheta_1)^{-k} (A + B\cos\vartheta_1 + C\sin\vartheta_1\cos\vartheta_2)^{-j} \tag{4.58}$$

where the coefficients a, b, A, B, C are functions of the invariants s, s_2, u, t. The integrals relevant for our computation are known since long and are available in the literature [205–207]. In the case of initial-state radiation they trivial. We list here for completeness only the ones needed for the case of final-state radiation:

$$I^{(0,1)} = \frac{\pi}{\sqrt{B^2+C^2}} \ln\left(\frac{A+\sqrt{B^2+C^2}}{A-\sqrt{B^2+C^2}}\right), \tag{4.59}$$

$$I^{(0,2)} = \frac{2\pi}{A^2-B^2-C^2}, \tag{4.60}$$

$$I^{(-1,1)} = \pi\left[\frac{2bB}{B^2+C^2} + \frac{a(B^2+C^2)-bAB}{(B^2+C^2)^{3/}} \ln\left(\frac{A+\sqrt{B^2+C^2}}{A-\sqrt{B^2+C^2}}\right)\right], \tag{4.61}$$

$$I^{(-1,2)} = \pi\left[\frac{2[a(B^2+C^2)-bAB]}{(B^2+C^2)(A^2-B^2-C^2)} + \frac{bB}{(B^2+C^2)^{3/}} \ln\left(\frac{A+\sqrt{B^2+C^2}}{A-\sqrt{B^2+C^2}}\right)\right] \tag{4.62}$$

$$\begin{aligned} I^{(-2,1)} = \pi\Bigg[&\frac{4abB}{B^2+C^2} + \frac{b^2A(C^2-2B^2)}{(B^2+C^2)^2} \\ &+ \frac{2[a(B^2+C^2)-bAB]^2 - b^2C^2(A^2-B^2-C^2)}{2(B^2+C^2)^{5/2}} \ln\left(\frac{A+\sqrt{B^2+C^2}}{A-\sqrt{B^2+C^2}}\right)\Bigg] \end{aligned} \tag{4.63}$$

$$\begin{aligned} I^{(-2,2)} = \pi\Bigg[&\frac{2b^2(B^2-C^2)}{(B^2+C^2)^2} + \frac{2[a(B^2+C^2)-bAB]^2}{(A^2-B^2-C^2)(B^2+C^2)^2} \\ &+ \frac{2bB[a(B^2+C^2)-bAB]+b^2AC^2}{(B^2+C^2)^{5/2}} \ln\left(\frac{A+\sqrt{B^2+C^2}}{A-\sqrt{B^2+C^2}}\right)\Bigg] \end{aligned} \tag{4.64}$$

The algebraic manipulations, the book-keeping of the substitutions and the simplifications required in performing the angular integration have been performed in Mathematica. As sanity check of the computation, we have considered different sets of input parameters and have compared the direct numerical integration with our analytical expressions for the angular integration, finding perfect agreement within the double precision accuracy.

4.4.2 Expansion in $r_{\rm cut}$

After the angular integration, we are left with a further one-dimensional integral in the z variable, see Eq. (4.51). The presence of different square root factors makes the analytical integration a very hard task. Nonetheless, since we are interested in extracting the small-$r_{\rm cut}$ behavior of the integral, we do not need to compute it exactly.

Some care must be taken in performing the $r_{\rm cut}$ expansion. To this purpose, we notice indeed that the dependence on $r_{\rm cut}$ is contained both in the upper integration limit $z_{\rm max}(r_{\rm cut})$ and in the integrand function. The angular integration of the matrix element gives rise to an analytic function in $r^2_{\rm cut}$ while it is divergent in z when approaching the soft limit $z \to 1$. The most problematic term is the Jacobian square root factor, $\sqrt{(1-z)^2 - 4zr^2_{\rm cut}}$. Since the integral is ill-defined in the limit $r_{\rm cut} \to 0$, we cannot employ a simple expansion in Taylor series. Even attempting to expand the integrand function only in power series does not help. Indeed, the expansion of the Jacobian square root factor leads to a tower of more and more divergent terms at $z = 1$: each term will contribute, after integrating over z, to the same order in $r_{\rm cut}$ requiring for the resummation of the series.

An effective strategy consists in introducing suitable $r_{\rm cut}$-dependent distributions, defined in the interval $[0,1]$, and expand them in power series in $r_{\rm cut}$. We proceed as follows:

1. after performing the angular integration, we expand the matrix element (without the Jacobian square root) in power series of $r_{\rm cut}$;

2. in each term of the expansion, we extract a coefficient function which is regular at $z = 1$;

3. the remaining part together with the product of theta function defining the integration limits, $\Theta(z_{\max}(r_{\text{cut}}) - z) \times \Theta(z - z_{\min})$, is interpreted as distribution;

4. we expand the distribution in power series in r_{cut} up to the order relevant to compute the leading power and next-to-leading power contribution.

In the last step, we rely on standard mathematical techniques as the introduction of generalized plus distributions and the Mellin transform.

4.5 Results

We discuss separately the case of final-state and initial-state radiation. Before giving the final expression for the partonic cross section, we present some intermediate results obtained following the procedure outlined above.

4.5.1 Final-state radiation

We report for completeness the expression of the unpolarized matrix element squared, averaged over the initial colors and the spins degrees of freedom and summed over the final ones in terms of the invariants in Eq. (4.53)

$$\begin{aligned}|\mathcal{M}|^2 = \frac{4e^6 e_q^2}{3s^2}\Bigg[&-\frac{4m^4 s}{s_3^2} - \frac{8m^4 s}{s_3 s_4} - \frac{4m^4 s}{s_4^2} + \frac{4m^2 s s_2}{s_3 s_4} - \frac{2m^2 t u_6}{s_3^2} - \frac{2m^2 t_1 u_7}{s_3^2} - \frac{2m^2 u u_7}{s_3^2} \\ &- \frac{2m^2 u_1 u_6}{s_3^2} - \frac{2m^2 t t_1}{s_3 s_4} - \frac{4m^2 t u}{s_3 s_4} - \frac{2m^2 t u_6}{s_3 s_4} - \frac{4m^2 t_1 u_7}{s_3 s_4} - \frac{2m^2 u u_1}{s_3 s_4} - \frac{2m^2 u u_7}{s_3 s_4} \\ &- \frac{4m^2 u_1 u_6}{s_3 s_4} - \frac{2m^2 t t_1}{s_4^2} - \frac{2m^2 t_1 u_7}{s_4^2} - \frac{2m^2 u u_1}{s_4^2} - \frac{2m^2 u_1 u_6}{s_4^2} + \frac{s_2 t t_1}{s_3 s_4} + \frac{s_2 t u_6}{s_3 s_4} \\ &+ \frac{2 s_2 t_1 u_7}{s_3 s_4} + \frac{s_2 u u_1}{s_3 s_4} + \frac{s_2 u u_7}{s_3 s_4} + \frac{2 s_2 u_1 u_6}{s_3 s_4} + \frac{t u_6}{s_3} - \frac{2 t_1 u_1}{s_3} + \frac{t_1 u_7}{s_3} + \frac{u u_7}{s_3} + \frac{u_1 u_6}{s_3} \\ &+ \frac{t t_1}{s_4} + \frac{t_1 u_7}{s_4} + \frac{u u_1}{s_4} + \frac{u_1 u_6}{s_4} - \frac{2 u_6 u_7}{s_4}\Bigg]\end{aligned} \tag{4.65}$$

After performing the angular integration, the ensuing contribution to $d\hat{\sigma}_{q\bar{q}}/dr_{\text{cut}}^2$ can be expressed in the following form

$$\frac{d\hat{\sigma}_{q\bar{q}}^{\text{FS}}}{dr_{\text{cut}}^2} = -\frac{4\alpha^3 e_q^2}{3s}\int_{z_{\min}}^{z_{\max}} dz \left[\frac{K_1(z;z_{\min})}{(1-z)^2\sqrt{(1-z)^2 - 4zr_{\text{cut}}^2}} + \frac{K_2(z;z_{\min})r_{\text{cut}}^2}{(1-z)^4\sqrt{(1-z)^2 - 4zr_{\text{cut}}^2}}\right] \tag{4.66}$$

in terms of two coefficient functions, K_1 and K_2, regular at $z = 1$ (soft limit) and independent on the cut-off parameter $r_{\rm cut}$:

$$
\begin{aligned}
K_1(z; z_{\rm min}) = &-\left[z_{\rm min} z^2 + z(1+z)^2\right] \sqrt{1-\frac{z_{\rm min}}{z}} \\
&+ z(1+z^2+z_{\rm min} z - \frac{z_{\rm min}^2}{2}) \ln \frac{1+\sqrt{1-\frac{z_{\rm min}}{z}}}{1-\sqrt{1-\frac{z_{\rm min}}{z}}},
\end{aligned}
\tag{4.67}
$$

and

$$
\begin{aligned}
K_2(z; z_{\rm min}) = 2z^2 \Bigg\{ &\left[1+z(6+z)+z_{\rm min} z\right] \sqrt{1-\frac{z_{\rm min}}{z}} \\
&- \left(1+z^2+z_{\rm min}(2+z)-\frac{z_{\rm min}^2}{2}\right) \ln \frac{1+\sqrt{1-\frac{z_{\rm min}}{z}}}{1-\sqrt{1-\frac{z_{\rm min}}{z}}} \Bigg\}.
\end{aligned}
\tag{4.68}
$$

In the small-$r_{\rm cut}$ limit the integral in Eq. (4.66) can be computed by using the expansions

$$
\begin{aligned}
\frac{\Theta(z_{\rm max}-z)\Theta(z-z_{\rm min})}{(1-z)^2\sqrt{(1-z)^2-4zr_{\rm cut}^2}} &= \frac{1}{4}\delta(1-z)\frac{1}{r_{\rm cut}^2} + \frac{\pi}{8}\left[\delta(1-z)+2\delta'(1-z)\right]\frac{1}{r_{\rm cut}} + \mathcal{O}(1) \\
\frac{\Theta(z_{\rm max}-z)\Theta(z-z_{\rm min})r_{\rm cut}^2}{(1-z)^4\sqrt{(1-z)^2-4zr_{\rm cut}^2}} &= \frac{1}{24}\delta(1-z)\frac{1}{r_{\rm cut}^2} + \frac{\pi}{64}\left[3\delta(1-z)+2\delta'(1-z)\right]\frac{1}{r_{\rm cut}} + \mathcal{O}(1)
\end{aligned}
\tag{4.69}
$$

We observe that up to the considered order the lower limit $z_{\rm min}$ does not enter in the expansion. Then, we obtain for the $r_{\rm cut}$ dependence of the partonic cross section

$$
\begin{aligned}
\hat{\sigma}^{\rm FS}_{q\bar{q}}(s; r_{\rm cut}) = &\,\sigma_0(s)\frac{\alpha}{2\pi}\Bigg\{\left[2-\frac{(1+\beta^2)}{\beta}\ln\frac{1+\beta}{1-\beta}\right]\ln(r_{\rm cut}^2) \\
&- \frac{3\pi}{8}\left[\frac{6(5-\beta^2)}{3-\beta^2}+\frac{-47+8\beta^2+3\beta^4}{\beta(3-\beta^2)}\ln\frac{1+\beta}{1-\beta}\right] r_{\rm cut}\Bigg\} + O(r_{\rm cut}^2) \\
\equiv &\,\hat{\sigma}^{\rm FS}_{\rm LP}(s; r_{\rm cut}) + \hat{\sigma}^{\rm FS}_{\rm NLP}(s; r_{\rm cut}) + O(r_{\rm cut}^2)
\end{aligned}
\tag{4.70}
$$

where we have dropped terms which do not depend on $r_{\rm cut}$ (which cannot be obtained following our strategy) and we have introduced the Born cross section

$$
\sigma_0(s) = \frac{2\pi}{9s}\alpha^2 e_q^2 \beta(3-\beta^2)
\tag{4.71}
$$

with $\beta = \sqrt{1-\frac{4m^2}{s}}$.

Eq. (4.70) shows that the final-state contribution to the NLO cross section, integrated down to $r_{\rm cut}$, contains the expected single logarithmic term in $r_{\rm cut}$ associated to the soft emission. This divergent contribution is exactly cancelled by the corresponding term in the subtraction counterterm controlled by the soft anomalous dimension for transverse momentum resummation $\mathbf{\Gamma}_T$. The main result concerns the next-to-leading power contribution $\hat{\sigma}^{\rm FS}_{\rm NLP}(s; r_{\rm cut})$. We have found that it is linear, thus explaining the source of the behavior shown in Figs. 4.3 and, for the case under investigation, we have computed its coefficient analytically.

4.5.2 Initial-state radiation

The integration of the matrix element squared corresponding to initial-state radiation over the angular variables is straightforward and we obtain

$$\frac{d\hat{\sigma}^{\mathrm{IS}}_{q\bar{q}}}{dr^2_{\mathrm{cut}}} = -\frac{4\alpha^3 e_q^4}{9s}\int_{z_{\mathrm{min}}}^{z_{\mathrm{max}}} dz \left[\frac{K_3(z;z_{\mathrm{min}})}{r^2_{\mathrm{cut}}\sqrt{(1-z)^2-4zr^2_{\mathrm{cut}}}} + \frac{K_4(z;z_{\mathrm{min}})}{\sqrt{(1-z)^2-4zr^2_{\mathrm{cut}}}}\right] \tag{4.72}$$

where the coefficient functions K_3 and K_4 now read

$$K_3(z;z_{\mathrm{min}}) = \sqrt{1-\frac{z_{\mathrm{min}}}{z}}\left(z+\frac{z_{\mathrm{min}}}{2}\right)\frac{1+z^2}{z^2} \qquad K_4(z;z_{\mathrm{min}}) = -2K_3(z;z_{\mathrm{min}})\frac{z}{1+z^2}\,. \tag{4.73}$$

The coefficient function $K_3(z;z_{\mathrm{min}})$ controls the most singular term, and is proportional to the Altarelli-Parisi splitting function. In order to evaluate the integral in Eq. (4.72) we have to expand the distribution

$$T(z,r_{\mathrm{cut}},z_{\mathrm{min}}) = \frac{\Theta(z-z_{\mathrm{min}})\Theta(z_{\mathrm{max}}-z)}{\sqrt{(1-z)^2-4zr^2_{\mathrm{cut}}}} \tag{4.74}$$

in the small r_{cut} limit. Since we already know that linear terms in r_{cut} are absent, we have to expand up to $\mathcal{O}(r^2_{\mathrm{cut}})$. This time, at variance with the case of final-state radiation, the expansion is complicated by the treatment of the lower integration z_{min}. To this aim, we observe indeed, that the coefficient functions $K_3(z;z_{\mathrm{min}})$ and $K_4(z;z_{\mathrm{min}})$ contain a square root which vanishes at $z=z_{\mathrm{min}}$. This will lead to spurious singularities when the distributions appearing in the expansion involve derivatives at $z=z_{\mathrm{min}}$. In order to overcome this issue, we found it convenient to split the integration over z as follows

$$\int_{z_{\mathrm{min}}}^{z_{\mathrm{max}}} dz = \int_{z_{\mathrm{min}}}^{a} dz + \int_{a}^{z_{\mathrm{max}}} dz, \quad z_{\mathrm{min}} < a < z_{\mathrm{max}}\,. \tag{4.75}$$

The integral from z_{min} to a can be safely computed by expanding the integrand function in r_{cut} and truncating the expansion at the desired order, $\mathcal{O}(r^2_{\mathrm{cut}})$. The integral from a to z_{max} can be computed by using our procedure and expand in power series the distribution $T(z,r_{\mathrm{cut}},a)$ in Eq. 4.74, where z_{min} has been replaced by a. We can safely carry out the expansion in the Mellin N-momentum space and we get

$$\begin{aligned} T_N(r_{\mathrm{cut}},a) &\equiv \int_0^1 z^{N-1}T(z,r_{\mathrm{cut}},a) \\ &= T_N^{(0,L)}(a)\log r^2_{\mathrm{cut}} + T_N^{(0)}(a) + T_N^{(2,L)}(a) r^2_{\mathrm{cut}}\log r^2_{\mathrm{cut}} + T_N^{(2)}(a) r^2_{\mathrm{cut}} + \mathcal{O}(r^2_{\mathrm{cut}}), \end{aligned} \tag{4.76}$$

with

$$T_N^{(0,L)}(a) = -\frac{1}{2}, \tag{4.77}$$

$$T_N^{(0)}(a) = \frac{1}{N} - H_N - B(a;N,0), \tag{4.78}$$

$$T_N^{(2,L)}(a) = -\frac{1}{2}N(N-1) \tag{4.79}$$

$$T_N^{(2)}(a) = N^2 - \frac{1}{N} - N(N-1)H_N - a^N \sum_{k=1}^{\infty} \frac{(k+1)!}{(k-1)!}\frac{a^k}{N+k} \tag{4.80}$$

In the above, H_N is the harmonic number

$$H_N = \sum_{k=1}^{N} \frac{1}{k}, \tag{4.81}$$

and B is the incomplete beta function

$$B(z;x,y) = \int_0^z dt t^{x-1}(1-t)^{y-1}. \tag{4.82}$$

The inversion of the Mellin transform into the real z-space, although quite technical and lengthy, is straightforward. We get

$$\begin{aligned} T(z, r_{\rm cut}, a) = & -\frac{1}{2}\delta(1-z)\ln r_{\rm cut}^2 + \left(\frac{1}{1-z}\right)_a + \ln(1-a)\delta(1-z) \\ & -\frac{1}{2}\left(\delta^{(2)}(1-z) - 2\delta^{(1)}(1-z)\right) r_{\rm cut}^2 \ln r_{\rm cut}^2 \\ & + \Bigg[(1+\ln(1-a))\,\delta^{(2)}(1-z) - [1+2\ln(1-a)]\delta^{(1)}(1-z) - \frac{1}{2}\delta(1-z) \\ & + \frac{1-2a}{(1-a)^2}\delta(z-a) - \frac{a}{1-a}\delta^{(1)}(z-a) + D^{(2)}(z,a) + 2D^{(1)}(z,a)\Bigg] r_{\rm cut}^2 + \mathcal{O}(r_{\rm cut}^4). \end{aligned} \tag{4.83}$$

where we have defined the distributions $\delta^{(n)}(z-b)$, $\left(\frac{1}{1-z}\right)_a$, $D^{(1)}(z,a)$ and $D^{(2)}(z,a)$ through their action on a test function $f(z)$ as

$$\int_0^1 dz f(z)\delta^{(n)}(z-b) = (-1)^n f^{(n)}(b), \quad b \in [0,1], \tag{4.84}$$

$$\int_0^1 dz f(z)\left(\frac{1}{1-z}\right)_a = \int_a^1 dz \frac{f(z)-f(1)}{1-z}, \tag{4.85}$$

$$\int_0^1 dz f(z) D^{(1)}(z,a) = \int_a^1 dz \frac{f^{(1)}(z)-f^{(1)}(1)}{1-z}, \tag{4.86}$$

$$\int_0^1 dz f(z) D^{(2)}(z,a) = \int_a^1 dz \frac{z f^{(2)}(z)-f^{(2)}(1)}{1-z}\,. \tag{4.87}$$

By combining the two contributions $z_{\rm min} < z < a$ and $a < z < z_{\rm max}$ the dependence on a cancels out and we obtain for the $r_{\rm cut}$ dependence of the partonic cross section

$$\begin{aligned}
\hat{\sigma}^{\rm IS}_{q\bar{q}}(s;r_{\rm cut}) &= \sigma_0(s)\frac{\alpha}{2\pi}e_q^2\Bigg\{\ln^2 r^2_{\rm cut} - 4\left(2\ln 2 - \frac{4}{3} - \ln\frac{1-\beta^2}{\beta^2} - \frac{1}{\beta(3-\beta^2)}\ln\frac{1+\beta}{1-\beta}\right)\ln r^2_{\rm cut} \\
&\quad - \frac{3}{2}\frac{(1+\beta^2)(1-\beta^2)^2}{\beta^4(3-\beta^2)}\left(1 - 4\ln 2 + 2\ln\frac{(1-\beta^2)r_{\rm cut}}{\beta^2}\right)r^2_{\rm cut}\Bigg\} + \ldots\ldots\ldots \\
&\equiv \hat{\sigma}^{\rm IS}_{\rm LP}(s;r_{\rm cut}) + \hat{\sigma}^{\rm IS}_{\rm NLP}(s;r_{\rm cut}) + \ldots\ldots\ldots
\end{aligned} \tag{4.88}$$

where we have dropped terms which do not depend on $r_{\rm cut}$ and the dots stand for terms that vanish faster than $r^2_{\rm cut}$ as $r_{\rm cut} \to 0$. At variance with Eq. (4.70), Eq. (4.88) contains a double and a single logarithmic term in $r_{\rm cut}$, which will be cancelled by the subtraction counterterm. As expected, the next-to-leading power contribution $\hat{\sigma}^{\rm IS}_{\rm NLP}(s;r_{\rm cut})$ is quadratic in $r_{\rm cut}$, modulo logarithmic enhancements.

Check: color singlet production

The structure of the power corrections to the inclusive production of a color-singlet (or neutral) massive vector boson can be reobtained as a byproduct of our calculation. In what follows, we show explicitly that we are able to reproduce the structure of the $r_{\rm cut}$ dependence of the vector boson production in the diagonal annihilation channel computed in Ref. [59] up to and including the quadratic terms, which represents a non-trivial test of our calculation. To get rid of the decay into the lepton pair, it is sufficient to take the limit for a vanishing lepton mass $m \to 0$ while the constraint on the mass of the vector boson M eliminates the integration over the z variable. The former requirement corresponds to take the limit $a \to 0$ inside the expansion of the distributions in Eq. 4.77-4.80. Inverting in real z-space, we have

$$T^{(0,L)}(z) = -\frac{1}{2}\delta(1-z), \tag{4.89}$$

$$T^{(0)}(z) = \left(\frac{1}{1-z}\right)_+, \tag{4.90}$$

$$T^{(2,L)}(z) = -\frac{1}{2}[\delta^{(2)}(1-z) - 2\delta^{(1)}(1-z)], \tag{4.91}$$

$$T^{(2)}(z) = \delta^{(2)}(1-z) - 3\delta^{(1)}(1-z) + \frac{1}{2}\delta(1-z) + D_0^{(2)}(z) + 2D_0^{(1)}(z), \tag{4.92}$$

where we have introduced the two auxiliary distributions

$$\int_0^1 dz f(z) D_0^{(1)}(z) = \int_0^1 dz \frac{z^2 f^{(1)}(z) - f^{(1)}(1)}{1-z}, \tag{4.93}$$

$$\int_0^1 dz f(z) D_0^{(2)}(z) = \int_0^1 dz \frac{z^3 f^{(2)}(z) - f^{(2)}(1)}{1-z}, \tag{4.94}$$

Due to the second requirement, we interpret now the partonic cross section as a distribution over which acts on the parton luminosity, as function of the variable $z = M^2/S$, S being the total energy available in the hadronic center-of-mass frame. To match the computation given in Ref. [59], we collect out a factor $1/z$. Then, apart from an overall constant normalization factor, we get the following structure for the $r_{\rm cut}$ dependence

a) contribution from K_3

$$
\begin{aligned}
&-(1+z^2)\left[\frac{T^{(0,L)}(z)}{2}\log^2 r_{\rm cut}^2 + T^{(0)}(z)\log r_{\rm cut}^2 + T^{(2,L)}(z) r_{\rm cut}^2 \log r_{\rm cut}^2\right. \\
&\qquad\qquad \left. + \left(T^{(2)}(z) - T^{(2,L)}(z)\right) r_{\rm cut}^2\right] \\
&= \frac{1}{2}\log^2 r_{\rm cut}^2 - \frac{1+z^2}{(1-z)_+}\log r_{\rm cut}^2 + \left[\delta^{(2)}(1-z) - 4\delta^{(1)}(1-z) + 3\delta(1-z)\right] r_{\rm cut}^2 \log r_{\rm cut}^2 \\
&- \left[3\delta^{(2)}(1-z) + 14\delta^{(1)}(1-z) + 12\delta(1-z) + (1+z^2)D_0^{(2)}(z) + 2(1+z^2)D_0^{(1)}(z)\right] r_{\rm cut}^2
\end{aligned}
\tag{4.95}
$$

which, apart from an overall factor of 2, matches the structure of the coefficient function $\hat{g}^{U(1)}_{q\bar{q}}$, eq.(4.7) of Ref. [59]. In particular, we have checked that the expression proportional to the quadratic term defines the same distribution as that reported in the reference work.

a) contribution from K_4

$$
\begin{aligned}
&2z\left[T^{(0,L)}(z) r_{\rm cut}^2 \log r_{\rm cut}^2 + \left(T^{(0)}(z) - T^{(0,L)}(z)\right) r_{\rm cut}^2\right] \\
&= -\delta(1-z) r_{\rm cut}^2 \log r_{\rm cut}^2 + \left[\frac{2z}{(1-z)_+} + \delta(1-z)\right] r_{\rm cut}^2,
\end{aligned}
\tag{4.96}
$$

which, apart from an overall factor of 2, matches exactly the structure of the coefficient function $\hat{g}^{R(1)}_{q\bar{q}}$, Eq. (4.8) of Ref. [59].

4.5.3 Numerical validation

In order to check the results presented in Secs. 4.5.1, 4.5.2 we have numerically implemented the exact real emission contribution to the cross section and the expansions in Eqs. (4.70) and (4.88).

In Fig. 4.10 we report the exact real emission partonic cross section in the $q\bar{q}$ channel for $\beta = 0.6$ as a function of $r_{\rm cut}$ from which we have subtracted the leading-power contribution (black curve) and both the leading and next-to-leading power contributions (red curve). The numerical computation is separately carried out for the final-state radiation (left panel) and initial-state radiation (right panel) contributions. Both for final-state radiation and initial-state radiation the leading-power contribution exactly matches the divergent behavior of the real emission cross section which is finite in the small-$r_{\rm cut}$ limit. The subtraction of the leading-power contribution exactly corresponds (up to quadratic terms in $r_{\rm cut}$, see Eqs. (4.45) to the second term on the right hand side of Eq. (4.20) and it is thus what is usually done in the standard q_T subtraction procedure. In the case of final-state radiation (left panel) the subtracted cross section exhibits the expected linear behavior, while for initial-state radiation (right panel) the subtracted cross section scales quadratically with $r_{\rm cut}$. When besides the leading-power contribution, also the next-to-leading power (linear) term is subtracted the final-state subtracted cross section (red curve) behaves quadratically with $r_{\rm cut}$, consistently with the result in Eq. (4.70). In the case of initial-state radiation, the additional subtraction of the next-to-leading power (quadratic) term makes the subtracted cross section almost independent on $r_{\rm cut}$.

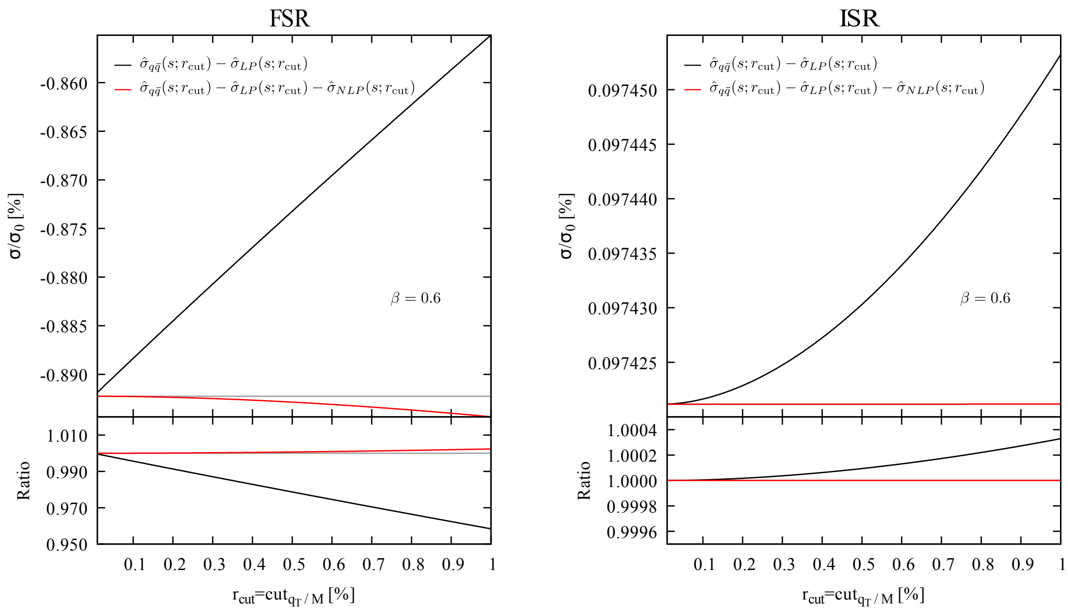

FIGURE 4.10: Subtracted partonic cross section for final-state radiation (left panel) and initial-state radiation (right panel). The solid lines represent the subtraction of the leading-power term, while the red solid line is obtained by subtracting also the next-to-leading power terms in Eq. (4.70) and Eq. (4.88), respectively. The upper panels show the result normalised to the Born cross section, while the lower panels show the result normalised to the $r_{\rm cut} \to 0$ limit. The computation is carried out at fixed $\beta = 0.6$.

4.5.4 Hadronic cross section

Before concluding this section, we briefly comment upon the behavior of the hadronic cross section. Indeed, as we will show in the following, a residual dependence on $r_{\rm cut}$ is contained in the convolution integral with the PDFs, which can potentially lead to an additional linear term in $r_{\rm cut}$. In the case of final-state radiation such contribution could modify the parton level result. In the case of initial-state radiation such contribution could potentially change the power counting, by making the power correction linear. In what follows, we show that this is not the case and that, thanks to the analicity of the cross section such additional term vanishes both for final-state and initial-state radiation.

The real contribution to the hadronic cross section reads

$$\sigma(S, r_{\rm cut}) = \sum_{a,b} \int_0^1 dx_1 \int_0^1 dx_2 f_a(x_1, \mu_F) f_b(x_2, \mu_F) \hat{\sigma}_{ab}(s, r_{\rm cut}) \delta(x_1 x_2 S - s) \tag{4.97}$$

where S is the hadronic CM-energy. The presence of a finite $r_{\rm cut}$ implies that

$$s > \frac{4m^2}{z_{\rm max}}. \tag{4.98}$$

where $z_{\rm max}$, defined in Eq. (4.52), behaves linearly with $r_{\rm cut}$

$$z_{\rm max} = 1 - 2r_{\rm cut} + \mathcal{O}(r_{\rm cut}^2)\,. \tag{4.99}$$

The hadronic cross section in Eq. (4.97) can be rewritten as

$$\begin{aligned}
\sigma(S, r_{\rm cut}) &= \sum_{a,b} \int_0^1 dx_1 \int_0^1 dx_2 f_a(x_1, \mu_F) f_b(x_2, \mu_F) \Theta\left(x_1 x_2 S - \frac{4m^2}{z_{\rm max}}\right) \hat{\sigma}_{ab}\left(s = x_1 x_2 S, r_{\rm cut}\right) \\
&= z_0 \sum_{a,b} \int_{z_0}^{z_{\rm max}} \frac{dz}{z^2} \int_{\ln\sqrt{z_0/z}}^{-\ln\sqrt{z_0/z}} dy f_a\left(\sqrt{\frac{z_0}{z}} e^y, \mu_F\right) f_b\left(\sqrt{\frac{z_0}{z}} e^{-y}, \mu_F\right) \hat{\sigma}_{ab}\left(s = \frac{4m^2}{z}, r_{\rm cut}\right) \\
&\equiv \sum_{a,b} \int_{z_0}^{z_{\rm max}} dz\, \mathcal{L}_{ab}(z, z_0; \mu_F)\, \hat{\sigma}_{ab}\left(s = \frac{4m^2}{z}, r_{\rm cut}\right) \qquad (4.100)
\end{aligned}$$

where in the last step, we have performed the change of variables

$$x_1 = \sqrt{\frac{z_0}{z}} e^y, \qquad x_2 = \sqrt{\frac{z_0}{z}} e^{-y}, \qquad z_0 \equiv \frac{4m^2}{S}\,. \qquad (4.101)$$

Hence, the presence of $z_{\rm max}$ as an upper integration limit in Eq. (4.100) could potentially induce an additional linear term in $r_{\rm cut}$ when the hadronic cross section is evaluated. However, the partonic cross section vanishes at the kinematic limit $z = z_{\rm max}$

$$\hat{\sigma}_{ab}\left(s = \frac{4m^2}{z_{\rm max}}, r_{\rm cut}\right) = 0\,. \qquad (4.102)$$

This is a sufficient mathematical condition to prevent the appearance of a further linear term through integration. We thus conclude that, as anticipated, in the case of final-state radiation the linear term in $r_{\rm cut}$ is completely driven by the parton level result, while for initial-state radiation the convolution with PDFs will not produce linear terms in $r_{\rm cut}$.

4.6 Final-state radiation at next-to-leading power: beyond inclusive observables

The results presented in Sec. 4.5 have been obtained for the most inclusive observable, the total partonic cross section without any fiducial cuts. This has been a crucial point in order to perform the computation analytically. Given this limitation, the result cannot be employed in practise to improve the efficiency of the subtraction when fiducial cuts are applied and when one is interested in distributions. It is tempting to extend the analysis for such cases and to show a viable approach at least at NLO level. In what follows we outline a strategy to remove the final-state linear power suppressed contribution from the q_T subtraction formula at NLO at differential level.
Let us start from Eq. (2.81) at NLO

$$d\hat{\sigma}^F_{NLO} = \mathcal{H}^F_{NLO} \otimes d\hat{\sigma}^F_{LO} + \left[d\hat{\sigma}^{F+\rm jet}_{LO} - d\hat{\sigma}^{F,CT}_{NLO}\right] \Theta\left(\frac{q_T}{M} - r_{\rm cut}\right), \qquad (4.103)$$

where we have written explicitly the $r_{\rm cut}$ constraint. Consider the following extension

$$\begin{aligned}
d\hat{\sigma}^F_{NLO} = \mathcal{H}^F_{NLO} \otimes d\hat{\sigma}^F_{LO} &+ \left[d\hat{\sigma}^{F+\rm jet}_{LO} - d\hat{\sigma}^{F,CT}_{NLO}\right] \Theta\left(\frac{q_T}{M} - r_{\rm cut}\right) \\
&+ \left[d\hat{\sigma}^{F+\rm jet}_{FS,LO} - d\hat{\sigma}^{F,CT}_{S,NLO}\right] \Theta\left(r_{\rm cut} - \frac{q_T}{M}\right). \qquad (4.104)
\end{aligned}$$

In the above formula, $d\hat{\sigma}^{F+\text{jet}}_{FS,LO}$ is the differential cross section associated to final-state radiation only and $d\hat{\sigma}^{F,CT}_{S,NLO}$ is an arbitrary counterterm which cancels the corresponding final-state soft divergence, so that their difference is finite. The new term lives in the unresolved region below r_{cut} so that its contribution is vanishing in the limit $r_{\text{cut}} \to 0$. Thus, the first observation is that Eq.(4.103) and Eq.(4.104) differ only by power suppressed terms in r_{cut}, and therefore they are formally equivalent. The second and key observation is that, if the new counterterm, as the standard q_T subtraction one, does not introduce additional linear power corrections, then the subtraction formula in Eq (4.104) is free of linear power suppressed terms. Indeed, the linear term arising from the real emission cross section exactly cancels in the sum

$$\left[d\hat{\sigma}^{F+\text{jet}}_{LO} - d\hat{\sigma}^{F,CT}_{NLO}\right]\Theta\left(\frac{q_T}{M} - r_{\text{cut}}\right) + \left[d\hat{\sigma}^{F+\text{jet}}_{FS,LO} - d\hat{\sigma}^{F,CT}_{S,NLO}\right]\Theta\left(r_{\text{cut}} - \frac{q_T}{M}\right) = \bar{I} + \mathcal{O}(r^2_{\text{cut}}). \tag{4.105}$$

We claim that to build a counterterm satisfying the above condition, we need only the leading term in the soft expansion of the real emission cross sections, i.e. the product of the eikonal approximation for the matrix element times the soft phase space. The argument is detailed in Appendix C, where the r_{cut} dependence of the relevant soft integrals is computed. The main result is that the leading soft contribution reproduces the leading power term in r_{cut}, which is of course expected, plus power-suppressed terms whose leading behavior is quadratic. We highlight that this result is fully differential with respect the Born variables, thanks to the soft factorisation theorem. Next-to-soft contribution, then, reproduces the next-to-leading power in r_{cut}. In other words, up to the next-to-leading power, there is a one-to-one correspondence between the power counting in the r_{cut} regulator and the soft expansion.

The third and last observation is that if the soft subtraction is local, then it is effectively possible to perform the integration in the unresolved region. Therefore, to construct the additional soft counterterm we only need a soft mapping which reabsorbs the radiation into a Born-like configuration. For this purpose we rely on the massive FKS mapping presented in Chapter 1. Then, we define the local soft counterterm as

$$d\hat{\sigma}^{CT}_{S} = d\hat{\sigma}_{LO}(\Phi_B) \times \frac{e^2}{4\pi^3 s}\frac{d\xi}{\xi}dy d\phi\left[\frac{s-2m^2}{(1-\beta y_{\text{phy}})(1+\beta y_{\text{phy}})} - \frac{m^2}{(1-\beta y_{\text{phy}})^2} - \frac{m^2}{(1+\beta y_{\text{phy}})^2}\right] \tag{4.106}$$

where $\beta = \sqrt{1-4m^2/s}$.

We stress that the crucial point for this additional subtraction to be effective is that the additional counterterm in Eq. (4.106) scales like $d\xi/\xi$, thereby leading to purely logarithmic contributions in r_{cut}. We have checked that alternative local subtractions which do not fulfill this property do not lead to a cancellation of the linear term. Furthermore, an additional source of linear terms is implicitly contained in the theta function $\Theta\left(r_{\text{cut}} - \frac{q_T}{M}\right)$, since the invariant mass M of the produce final system is a function of the real kinematics. To avoid the proliferation of this spurious contribution, one must compute M using the mapped born kinematic when the cut is applied on the counterterm. In our case, this amounts to set $M = \sqrt{s}$.

We conclude this Section with few comments on the above results. The subtraction of the linear r_{cut} behavior through Eq. (4.104) does not require any analytic integration. It just requires an appropriate phase space mapping. The reader may of course argue that there is no need to introduce the modification of Eq. (4.104) to achieve a smooth cancellation of the soft singularity. Indeed, at NLO one can simply use a local subtraction scheme like FKS or dipole subtraction to carry out the fully differential computation. Nonetheless, the strategy adopted here could prove itself useful when extending the computation to the mixed QCD-EW corrections with the q_T subtraction formalism. In this case, given that we aim at the computation of an effect of the order of few *per mille*, having a quadratic instead of linear r_{cut} behavior could dramatically improve the numerical control of the $\mathcal{O}(\alpha\alpha_s)$ contribution.

4.6.1 Numerical analysis

In fig. 4.11 we report a study case for the pure QED production (no Z resonance involved). We consider the following four cases:

- fully inclusive;
- cuts on the lepton rapidities: $|y_l| < 2.5$ only;
- cuts on the lepton rapidities and transverse momenta (asymmetric): $|y_l| < 2.5$, $p_{T,l^-} > 25\,\text{GeV}$ and $p_{T,l^+} > 20\,\text{GeV}$
- cuts on the lepton rapidities and transverse momenta (symmetric): $|y_l| < 2.5$, $p_{T,l} > 25\,\text{GeV}$.

We see that in all cases there is a milder dependence on r_{cut}. In particular, in the first three, the linear dependence with r_{cut} is nicely cancelled. This does not occur completely in the last case when symmetric cuts on the lepton transverse momenta are applied. As discussed in Sec. 4.2.2, in this situation a linear dependence on r_{cut} appears in the contribution from initial-state radiation which is beyond the scope of our modification.

In fig. 4.12 we report a study case for the complete neutral current Drell-Yan process including the Z resonance. We consider the following setups:

- fully inclusive;
- cuts on the lepton rapidities and the transverse momenta (asymmetric): $|y_l| < 2.5$, $p_{T,l^-} > 25\,\text{GeV}$ and $p_{T,l^+} > 20\,\text{GeV}$

The results show up the same behavior as in the pure QED case, confirming the validity of this approach.

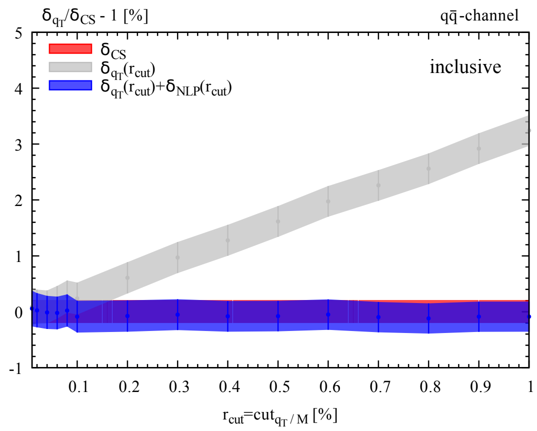

(A) Inclusive

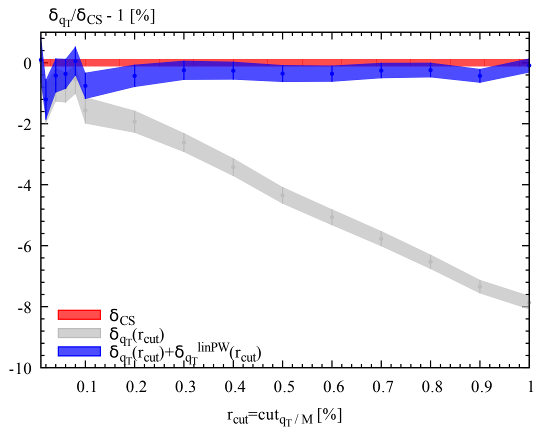

(B) $|y_l| < 2.5$

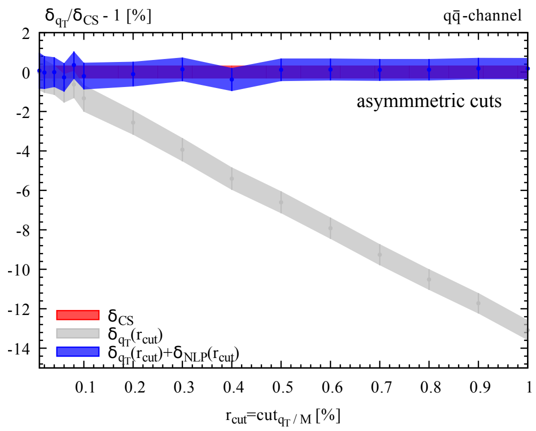

(C) $|y_l| < 2.5$,
$p_{T,l^-} > 25\,\text{GeV}$ and $p_{T,l^+} > 20\,\text{GeV}$

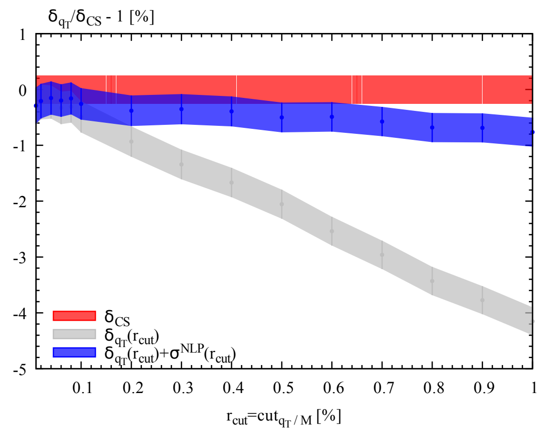

(D) $|y_l| < 2.5$, $p_{T,l} > 25\,\text{GeV}$

FIGURE 4.11: NLO QED correction as a function of r_{cut} for the pure QED (no Z boson exchange) Drell-Yan process in the dominant $q\bar{q}$ diagonal channel without cuts (a) and with cuts ((b), (c), (d)) at 7 TeV. The standard result obtained with q_T subtraction (grey band) is compared with the result obtained by including the power suppressed contribution in Eq. (4.104). The NLO result is normalised to the r_{cut}-independent cross section computed with dipole subtraction.

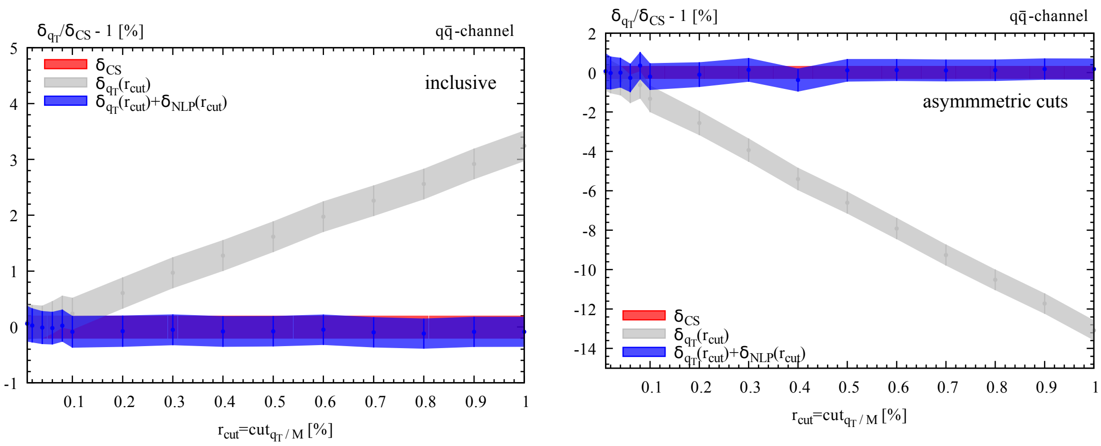

(A) Inclusive

(B) $|y_l| < 2.5$, $p_{T,l^-} > 25\,\text{GeV}$ and $p_{T,l^+} > 20\,\text{GeV}$

FIGURE 4.12: NLO EW correction as a function of r_{cut} for the complete Drell-Yan process in the dominant $q\bar{q}$ diagonal channel without cuts (left panel) and with asymmetric cuts (right panel) at 7 TeV. The standard result obtained with q_T subtraction (grey band) is compared with the result obtained by including the power suppressed contribution in Eq. (4.104). The NLO result is normalised to the r_{cut}-independent cross section computed with dipole subtraction.

Chapter 5

Conclusions

The excellent performance of the LHC offers the possibility to test the Standard Model of elementary particles at an unprecedented precision. Very clean measurements on key observables for basic processes have reached few percent accuracy and the residual uncertainties are expected to further decrease in the future. Indeed in the next years the ATLAS and CMS experiments will collect about 20 times the number of collisions they have registered so far, so that it is clear that percent accuracy will be eventually reached.

In such a situation, SM predictions at similar level of accuracy are mandatory, including radiative corrections in the strong and the EW couplings. Besides the largest and ubiquitous effects related to the QCD interaction, higher-order EW effects have an essential impact on the physics of the collisions at the LHC, in particular for the application to the production of a pair of leptons via the Drell-Yan mechanism and represent the main motivation of this work. After the computation of the second order corrections in QCD and of the first order corrections in the EW couplings, by a simple power counting argument it is clear that the third order in QCD will compete with the mixed QCD-EW corrections. First results in such computations are starting to appear in the literature.

In the theoretical study of the EW corrections at colliders, one usually retains the finite value of the very small mass of charged leptons because it represents the natural cut-off of the collinear singularities for both fixed order and shower radiation. In this scenario, the present work started by considering the description of the radiation emitted by a massive particle in the framework of the FKS NLO subtraction scheme. In the standard FKS for massless partons, the partitioning of the real phase space is driven by the collinear singularities. Nonetheless, in order to have a better control over the small-mass logarithmic enhancements, it is useful to consider also quasi-collinear regions in which, strictly speaking, only soft radiation leads to a genuine singularity. In this context, we have proposed a new FKS mapping suitable to treat the singularities of an NLO computation with massive radiators. This represents the first step towards a improved POWHEG formalism whose implementation has been fully worked out in Chapter 1. It allowed us to consistently match next-to-leading order computation to a parton shower including the resummation of subleading quasi-collinear effects. We have started the study of the phenomenology impact of such effects by comparing the predictions for bottom production at hadron colliders among different POWHEG event generators. We are currently working on a global comparison with single and double differential data available on open bottom production.

The core of the thesis was focused on the mixed QCD-EW corrections. We have moved the first steps to set up a suitable subtraction scheme that allows us to compute such corrections for Drell-Yan lepton pair production at fully differential level, by retaining the finite mass of the final-state charged leptons. We based our construction upon the q_T subtraction formalism, which has been successfully employed to compute second order QCD corrections for a large number of processes involving the hadroproduction of colorless final states, and has been extended to the computation of NNLO QCD corrections to heavy-quark pair production. The q_T subtraction formalism is a non-local subtraction in the sense discussed in Chapter 2. In particular, it relies on the introduction of a physical infrared observable, the transverse momentum of the produced system, which acts as a resolution variable for soft and collinear regions. The computation is carried out by imposing a cut-off on the resolution variable, as the cancellation of the divergences takes place only after performing the integration over the other radiation variables, thereby introducing power suppressed corrections to the q_T subtraction formula. The efficiency of the method mostly relies on the size of the power corrections, which has been one of the main aspect investigated in this work.

Since the structure of soft and collinear singularities arising from the EW corrections is due to the propagation of massless photons, the EW subtraction can be obtained applying the so called "abelianisation" procedure starting from the corresponding QCD version. The current formulation of the q_T subtraction method is sufficient to derive the structure of the subtraction for mixed QCD-EW corrections to the Drell-Yan processes. In Chapter 3, we have showed in detail the use of the abelianisation procedure for the derivation of the q_T subtraction formula to deal with QCD-EW corrections for initial-state radiation. As a first application, we have computed the mixed QCD-QED correction to the production of an on-shell Z boson at the LHC. We have studied the stability of the computation by varying the r_{cut} regulator and we have found a rather flat behavior in the nominal exploration region consistently with what is observed in the color singlet case in pure QCD, where the leading power corrections are known to be quadratic. We have verified that the fully inclusive result of our calculation is in agreement with the literature and we have produced also some illustrative differential results.

Then, the next step has been the inclusion of the final-state radiation, analyzing both the production of a Z boson decaying in a pair of charged leptons and the production of a W boson decaying into a charged lepton and a neutrino. The double virtual amplitudes, which are an essential ingredient to complete the calculation of mixed QCD-EW corrections are currently missing. Therefore, we have focused on the pure EW corrections. First of all, we have assessed the performance of the method originally proposed and applied to heavy-quark production to a process with masses as small as the muon mass. Here the numerical efficiency is challenged by a new source of power suppressed contributions, the r_{cut} dependence being linear, contrary to what happens when only initial state radiation is considered. We have computed the NLO EW corrections with the q_T subtraction formalism to both the neutral- and charged-current Drell-Yan processes. We have investigated the small-mass behavior and the dependence on r_{cut}, which in principle can compete among each others. Our results show that there is no severe interplay between the two parameters, since the q_T subtraction counterterm retains the full mass dependence at fixed r_{cut}. The numerical stability is challenged by the logarithmic enhancement in the small-mass limit, which mostly affects the integration of the real contribution. We have shown that the optimization of the sampling strategy in the Monte Carlo integration allows us to reach a good control on the numerical results, which turn out to be in nice agreement with those produced with publicly available generators. This suggests us that our method will work also in the computation of mixed QCD-EW corrections.

We have investigated for the first time the power corrections associated to the soft radiation emitted off a massive final state, in order to understand the origin of the different behavior with respect to the color-singlet case. To this extent, we have carried out the fully analytic computation of the coefficient of the leading power in the r_{cut} variable. We have established the pure soft origin of the observed linear behavior, which is due to next-to-leading order terms in the soft expansion of the q_T-spectrum produced by the final-state real emission. Inspired by our findings, we have also proposed a method to remove the linear dependence on the r_{cut} parameter from the q_T subtraction formula at NLO at differential level. Its generalization to the next order, if possible, besides being interesting from a theoretical point of view, would be very valuable in order to improve the numerical efficiency of the method.

The results presented in this work provide all the ingredients to build a subtraction scheme to deal with the full set of mixed QCD-EW corrections to both neutral- and charged-current Drell-Yan processes. We are currently working to extend the stability test on the r_{cut} and small mass dependence to the case of the mixed corrections to the charged W boson. When the two-loop QCD-EW amplitudes will be available [1], it will be possible to take the step to the evaluation of full mixed QCD-EW corrections for fiducial cross sections and differential distributions.

The successful methodology applied to extend the q_T subtraction formalism towards the mixed QCD-EW corrections is not limited to the cases considered in the present work. It can be exploited as well to compute the mixed corrections to other $2 \to 2$ reactions with massive final-state particles, as heavy-quark production, and pure NNLO EW(QED) corrections. Furthermore, we anticipate further applications to e^+e^- collider processes.

[1] There has been a recent boost in this direction with the computation of the relevant master integrals [208, 209] and the first computation of the complete set of mixed QCD-EW correction to the inclusive on-shell Z boson production [19] in the $q\bar{q}$ channel.

Appendix A

q_T subtraction formula in color singlet production

In this Appendix we collect the main formulae required to implement the q_T subtraction method for the production of a color-singlet system in processes initiated at LO by the quark-anti quark annihilation. In Sec. A.2, we briefly comment on the main differences with the gluon-fusion induced processes.

A.1 Main formulae

For ease of reading and for self-consistency, we report here the q_T subtraction formula for the hadroproduction of a colour singlet F

$$d\hat{\sigma}^F_{\text{(N)NLO}} = \mathcal{H}^F_{\text{(N)NLO}} \otimes d\sigma^F_{\text{LO}} + \left[d\sigma^{F+\text{jets}}_{(N)LO} - d\hat{\sigma}^{\text{CT}}_{\text{(N)NLO}} \right]_{\frac{q_T}{Q} > r_{\text{cut}}} , \tag{A.1}$$

where the symbol $\otimes$ denotes convolutions with respect to the longitudinal-momentum fractions z_1 and z_2 of the colliding partons. In the above, q_T is the transverse momentum of F and Q is invariant mass. $r_{\text{cut}} = q_T^{\text{min}}/Q$ is the adimensional cut-off on the transverse momentum. The counterterm reads

$$d\hat{\sigma}^{\text{CT}} = d\hat{\sigma}^F_{\text{LO}} \otimes \widetilde{\Sigma} \left(\frac{q_T}{Q} \right) . \tag{A.2}$$

The $\widetilde{\Sigma}$ function admits a fixed order expansion

$$\widetilde{\Sigma} = \sum_{n=1}^{\infty} \left(\frac{\alpha_s}{\pi} \right)^n \widetilde{\Sigma}^{F\,(n)}_{c\bar{c} \leftarrow ab}(z, q_T/Q) \tag{A.3}$$

Up to NNLO ($n = 1, 2$), we have explicitly

$$\widetilde{\Sigma}^{F\,(1)}_{c\bar{c} \leftarrow ab}(z, q_T/Q) = \Sigma^{F\,(1;2)}_{c\bar{c} \leftarrow ab}(z)\; \widetilde{I}_2(q_T/Q) + \Sigma^{F\,(1;1)}_{c\bar{c} \leftarrow ab}(z)\; \widetilde{I}_1(q_T/Q) , \tag{A.4}$$

and

$$\begin{aligned} \widetilde{\Sigma}^{F\,(2)}_{c\bar{c} \leftarrow ab}(z, q_T/Q) = {} & \Sigma^{F\,(2;4)}_{c\bar{c} \leftarrow ab}(z)\; \widetilde{I}_4(q_T/Q) + \Sigma^{F\,(2;3)}_{c\bar{c} \leftarrow ab}(z)\; \widetilde{I}_3(q_T/Q) + \Sigma^{F\,(2;2)}_{c\bar{c} \leftarrow ab}(z)\; \widetilde{I}_2(q_T/Q) \\ & + \Sigma^{F\,(2;1)}_{c\bar{c} \leftarrow ab}(z)\; \widetilde{I}_1(q_T/Q) . \end{aligned} \tag{A.5}$$

The notation $c\bar{c} \leftarrow ab$ denotes the transition from the incoming partons a, on the first leg, and b, on the second leg, to the $c\bar{c}$ partons entering the hard scattering process and the special functions $\widetilde{I}_n(q_T/Q)$ are given by the following Bessel transformation

$$\widetilde{I}_n(q_T/Q) = Q^2 \int_0^\infty db\, \frac{b}{2}\, J_0(bq_T)\; \ln^n\left(\frac{Q^2b^2}{b_0^2}+1\right)\;. \tag{A.6}$$

Having given the basic structure of the subtraction, the explicit form of the perturbative b-independent coefficients $\Sigma^{F\,(1;k)}(z), \mathcal{H}^{F\,(1)}(z), \Sigma^{F\,(2;k)}(z)$ and $\mathcal{H}^{F\,(2)}(z)$, required to performed the computation up to NNLO, is presented in the following formulae in terms of the perturbative resummation coefficients. The results are more easily presented in terms of the N-moments with respect to the variable z[1]. We have

$$\Sigma^{F\,(1;2)}_{c\bar{c}\leftarrow ab,\,N} = -\frac{1}{2}A_c^{(1)}\;\delta_{ca}\delta_{\bar{c}b}\;, \tag{A.7}$$

$$\Sigma^{F\,(1;1)}_{c\bar{c}\leftarrow ab,\,N}(M^2/Q^2) = -\left[\delta_{ca}\delta_{\bar{c}b}\;\left(B_c^{(1)}+A_c^{(1)}\,\ell_Q\right)+\delta_{ca}\gamma^{(1)}_{\bar{c}b,\,N}+\delta_{\bar{c}b}\gamma^{(1)}_{ca,\,N}\right]\;, \tag{A.8}$$

$$\begin{aligned}\mathcal{H}^{F\,(1)}_{c\bar{c}\leftarrow ab,\,N}\left(\frac{M^2}{\mu_R^2},\frac{M^2}{\mu_F^2},\frac{M^2}{Q^2}\right) \;&=\; \delta_{ca}\delta_{\bar{c}b}\left[H_c^{F\,(1)}-\left(B_c^{(1)}+\frac{1}{2}A_c^{(1)}\ell_Q\right)\ell_Q-p_{cF}\beta_0\ell_R\right]\\ &\quad+\delta_{ca}C^{(1)}_{\bar{c}b,\,N}+\delta_{\bar{c}b}C^{(1)}_{ca,\,N}+\left(\delta_{ca}\gamma^{(1)}_{\bar{c}b,\,N}+\delta_{\bar{c}b}\gamma^{(1)}_{ca,\,N}\right)(\ell_F-\ell_Q)\;,\end{aligned} \tag{A.9}$$

$$\Sigma^{F\,(2;4)}_{c\bar{c}\leftarrow ab,\,N} = \frac{1}{8}\left(A_c^{(1)}\right)^2\;\delta_{ca}\delta_{\bar{c}b}\;, \tag{A.10}$$

$$\Sigma^{F\,(2;3)}_{c\bar{c}\leftarrow ab,\,N}(M^2/Q^2) = -\,A_c^{(1)}\left[\frac{1}{3}\beta_0\;\delta_{ca}\delta_{\bar{c}b}+\frac{1}{2}\Sigma^{F\,(1;1)}_{c\bar{c}\leftarrow ab,\,N}(M^2/Q^2)\right]\;, \tag{A.11}$$

$$\begin{aligned}\Sigma^{F\,(2;2)}_{c\bar{c}\leftarrow ab,\,N}\left(\frac{M^2}{\mu_R^2},\frac{M^2}{\mu_F^2},\frac{M^2}{Q^2}\right) \;&=\; -\frac{1}{2}A_c^{(1)}\left[\mathcal{H}^{F\,(1)}_{c\bar{c}\leftarrow ab,\,N}\left(\frac{M^2}{\mu_R^2},\frac{M^2}{\mu_F^2},\frac{M^2}{Q^2}\right)-\beta_0\;\delta_{ca}\delta_{\bar{c}b}\,(\ell_R-\ell_Q)\right]\\ &\quad-\;\frac{1}{2}\sum_{a_1,b_1}\Sigma^{F\,(1;1)}_{c\bar{c}\leftarrow a_1b_1,\,N}(M^2/Q^2)\left[\delta_{a_1a}\gamma^{(1)}_{b_1b,\,N}+\delta_{b_1b}\gamma^{(1)}_{a_1a,\,N}\right]\\ &\quad-\;\frac{1}{2}\left[A_c^{(2)}\;\delta_{ca}\delta_{\bar{c}b}+\left(B_c^{(1)}+A_c^{(1)}\,\ell_Q-\beta_0\right)\Sigma^{F\,(1;1)}_{c\bar{c}\leftarrow ab,\,N}(M^2/Q^2)\right]\;,\end{aligned} \tag{A.12}$$

$$\begin{aligned}\Sigma^{F\,(2;1)}_{c\bar{c}\leftarrow ab,\,N}\left(\frac{M^2}{\mu_R^2},\frac{M^2}{\mu_F^2},\frac{M^2}{Q^2}\right) &= \Sigma^{F\,(1;1)}_{c\bar{c}\leftarrow ab,\,N}(M^2/Q^2)\,\beta_0\,(\ell_Q-\ell_R)\\ &\quad-\;\sum_{a_1,b_1}\mathcal{H}^{F\,(1)}_{c\bar{c}\leftarrow a_1b_1,\,N}\left(\frac{M^2}{\mu_R^2},\frac{M^2}{\mu_F^2},\frac{M^2}{Q^2}\right)\left[\delta_{a_1a}\delta_{b_1b}\left(B_c^{(1)}+A_c^{(1)}\,\ell_Q\right)+\delta_{a_1a}\gamma^{(1)}_{b_1b,\,N}+\delta_{b_1b}\gamma^{(1)}_{a_1a,\,N}\right]\\ &\quad-\;\left[\delta_{ca}\delta_{\bar{c}b}\;\left(B_c^{(2)}+A_c^{(2)}\,\ell_Q\right)-\beta_0\left(\delta_{ca}C^{(1)}_{\bar{c}b,\,N}+\delta_{\bar{c}b}C^{(1)}_{ca,\,N}\right)+\delta_{ca}\gamma^{(2)}_{\bar{c}b,\,N}+\delta_{\bar{c}b}\gamma^{(2)}_{ca,\,N}\right]\;,\end{aligned} \tag{A.13}$$

[1]In this work, we define the N-moments f_N of any function $f(z)$ of the variable z as $f_N = \int_0^1 dz\, z^{N-1}\, f(z)$.

$$
\begin{aligned}
&\mathcal{H}^{F\,(2)}_{c\bar{c}\leftarrow ab,\,N}\left(\frac{M^2}{\mu_R^2},\frac{M^2}{\mu_F^2},\frac{M^2}{Q^2}\right) = \delta_{ca}\delta_{\bar{c}b}\,H_c^{F\,(2)} + \delta_{ca}\,C^{(2)}_{\bar{c}b,\,N} + \delta_{\bar{c}b}\,C^{(2)}_{ca,\,N} + C^{(1)}_{ca,\,N}\,C^{(1)}_{\bar{c}b,\,N} \\
&+\; H_c^{F\,(1)}\left(\delta_{ca}\,C^{(1)}_{\bar{c}b,\,N} + \delta_{\bar{c}b}\,C^{(1)}_{ca,\,N}\right) + \frac{1}{6}\,A_c^{(1)}\,\beta_0\,\ell_Q^3\,\delta_{ca}\delta_{\bar{c}b} + \frac{1}{2}\left[A_c^{(2)}\,\delta_{ca}\delta_{\bar{c}b} + \beta_0\,\Sigma^{F\,(1;1)}_{c\bar{c}\leftarrow ab,\,N}(M^2/Q^2)\right]\ell_Q^2 \\
&-\; \left[\delta_{ca}\delta_{\bar{c}b}\,\left(B_c^{(2)} + A_c^{(2)}\,\ell_Q\right) - \beta_0\left(\delta_{ca}C^{(1)}_{\bar{c}b,\,N} + \delta_{\bar{c}b}C^{(1)}_{ca,\,N}\right) + \delta_{ca}\gamma^{(2)}_{\bar{c}b,\,N} + \delta_{\bar{c}b}\gamma^{(2)}_{ca,\,N}\right]\ell_Q \\
&+\; \frac{1}{2}\,\beta_0\left(\delta_{ca}\gamma^{(1)}_{\bar{c}b,\,N} + \delta_{\bar{c}b}\gamma^{(1)}_{ca,\,N}\right)\ell_F^2 + \left(\delta_{ca}\gamma^{(2)}_{\bar{c}b,\,N} + \delta_{\bar{c}b}\gamma^{(2)}_{ca,\,N}\right)\ell_F - \mathcal{H}^{F\,(1)}_{c\bar{c}\leftarrow ab,\,N}\left(\frac{M^2}{\mu_R^2},\frac{M^2}{\mu_F^2},\frac{M^2}{Q^2}\right)\beta_0\ell_R \\
&+\; \frac{1}{2}\sum_{a_1,b_1}\left[\mathcal{H}^{F\,(1)}_{c\bar{c}\leftarrow a_1b_1,\,N}\left(\frac{M^2}{\mu_R^2},\frac{M^2}{\mu_F^2},\frac{M^2}{Q^2}\right) + \delta_{ca_1}\delta_{\bar{c}b_1}\,H_c^{F\,(1)} + \delta_{ca_1}\,C^{(1)}_{\bar{c}b_1,\,N} + \delta_{\bar{c}b_1}\,C^{(1)}_{ca_1,\,N}\right] \\
&\times\; \left[\left(\delta_{a_1a}\gamma^{(1)}_{b_1b,\,N} + \delta_{b_1b}\gamma^{(1)}_{a_1a,\,N}\right)(\ell_F-\ell_Q) - \delta_{a_1a}\delta_{b_1b}\left(\left(B_c^{(1)} + \frac{1}{2}\,A_c^{(1)}\,\ell_Q\right)\ell_Q + p_{cF}\,\beta_0\,\ell_R\right)\right] \\
&-\; \delta_{ca}\delta_{\bar{c}b}\,p_{cF}\left(\frac{1}{2}\,\beta_0^2\,\ell_R^2 + \beta_1\,\ell_R\right)\quad .
\end{aligned}
\tag{A.14}
$$

In the above formulae, p_{cF} is the power of the α_s^n factor in the LO partonic process, we have defined

$$
\ell_R = \ln\frac{M^2}{\mu_R^2}\quad,\quad \ell_F = \ln\frac{M^2}{\mu_F^2}\quad,\quad \ell_Q = \ln\frac{M^2}{Q^2}\quad, \tag{A.15}
$$

and $\gamma_{ab,\,N}(\alpha_S)$ are the parton anomalous dimensions or, more precisely, the N-moments [2] of the customary Altarelli–Parisi splitting functions $P_{ab}(\alpha_S, z)$ [70, 131–133]

$$
\gamma_{ab,\,N}(\alpha_S) = \int_0^1 dz\, z^{N-1}\,P_{ab}(\alpha_S,z) = \sum_{n=1}^{\infty}\left(\frac{\alpha_S}{\pi}\right)^n\gamma^{(n)}_{ab,\,N}\quad . \tag{A.16}
$$

The regularized LO kernels are

$$
P^{(1)}_{qq}(z,\epsilon) = \frac{1}{2}C_F\left[\frac{1+z^2}{(1-z)_+} + \frac{3}{2}\delta(1-z) - \epsilon(1-z)\right]\,, \tag{A.17}
$$

$$
P^{(1)}_{gq}(z,\epsilon) = \frac{1}{2}C_F\left[\frac{1+(1-z)^2}{z} - \epsilon z\right]\,, \tag{A.18}
$$

$$
P^{(1)}_{qg}(z,\epsilon) = \frac{1}{2}T_R\left[1 - \frac{2z(1-z)}{1-\epsilon}\right]\,, \tag{A.19}
$$

$$
P^{(1)}_{gg}(z,\epsilon) = \frac{1}{2}2C_A\left[\frac{z}{(1-z)_+} + \frac{1-z}{z} + z(1-z)\right] + \frac{1}{2}\delta(1-z)\frac{11C_A - 4T_R n_f}{6}\,, \tag{A.20}
$$

where in $SU_c(3)$: $C_F = 4/3$, $CA = 3$, $T_R = 1/2$ and n_F is the number of active quark flavours. The NLO kernels, computed in the classic papers [132, 133], are listed in Ref. [70]. In the following, we give the explicit expressions of the the required resummation coefficients. The LL and NLL universal (i.e. independent of the process and of the factorization and resummation schemes) perturbative functions $A_c^{(1)}$ and $A_c^{(2)}$ are [210], [148]

$$
A_c^{(1)} = C_c\quad,\qquad A_c^{(2)} = \frac{1}{2}\,C_c\left[\left(\frac{67}{18} - \frac{\pi^2}{6}\right)C_A - \frac{5}{9}N_f\right]\quad, \tag{A.21}
$$

[2] Note the different normalization, α/π instead of $\alpha/(2\pi)$, in order to math the resummation formulae.

where $C_c = C_F$ if $c = q, \bar{q}$ and $C_c = C_A$ if $c = g$. The first-order $B_c^{(1)}$, $c = q, \bar{q}, g$ coefficients are [210], [148]

$$B_q^{(1)} = B_{\bar{q}}^{(1)} = -\frac{3}{2}\, C_F \ , \qquad B_g^{(1)} = -\frac{1}{6}\left(11 C_A - 2 N_f\right) \ , \tag{A.22}$$

and they are related to the coefficient of the contact term in LO Altarelli-Parisi splitting kernels, respectively $P_{qq}^{(1)}$ and $P_{gg}^{(1)}$. The second-order coefficient $B_c^{(2)}$ is resummation scheme dependent. In the hard scheme, it reads

$$B_a^{(2)} = \frac{\gamma_{a(1)}}{16} + \pi \beta_0\, C_a\, \zeta_2 \, , \tag{A.23}$$

where $\gamma_{a(1)}$ ($a = q, g$) are the coefficients of the $\delta(1-z)$ term in the NLO quark and gluon splitting functions [132, 133], which read

$$\gamma_{q\,(1)} = \gamma_{\bar{q}\,(1)} = (-3 + 24\zeta_2 - 48\zeta_3)\, C_F^2 + \left(-\frac{17}{3} - \frac{88}{3}\zeta_2 + 24\zeta_3\right) C_F C_A + \left(\frac{2}{3} + \frac{16}{3}\zeta_2\right) C_F N_f \, , \tag{A.24}$$

$$\gamma_{g\,(1)} = \left(-\frac{64}{3} - 24\zeta_3\right) C_A^2 + \frac{16}{3}\, C_A N_f + 4\, C_F N_f \, , \tag{A.25}$$

and ζ_n is the Riemann zeta-function ($\zeta_2 = \pi^2/6, \zeta_3 = 1.202\ldots, \zeta_4 = \pi^4/90$).

The first-order coefficients $C_{ab}^{(1)}(z)$ are explicitly known [211–214] and in the hard scheme[3] they read

$$C_{qq}^{(1)}(z) = \frac{1}{2} C_F (1-z) \, , \tag{A.26}$$

$$C_{gq}^{(1)}(z) = \frac{1}{2} C_F\, z \, , \tag{A.27}$$

$$C_{qg}^{(1)}(z) = \frac{1}{2} z(1-z) \, , \tag{A.28}$$

$$C_{gg}^{(1)}(z) = C_{q\bar{q}}(z) = C_{qq'}(z) = C_{q\bar{q}'}(z) = 0 \, . \tag{A.29}$$

We can give a simple interpretation of the above coefficients: they are the finite contribution arising from the O(ϵ) part of the corresponding LO Altarelli-Parisi splitting kernels in Eqs. A.17-A.20. This is not unexpected in NLO computations: such contributions usually arise as a finite remainder coming from the subtraction of the initial-state collinear singularities (see for example Eq. (2.102) in Ref. [24]).

A.1.1 Second-order collinear functions for processes initiated by quark-anti quark annihilation

In the following we give the explicit expressions of the second-order collinear functions $C_{ab}^{(2)}$ relevant for processes initiated at the LO by the quark-anti quark annihilation:

[3] The collinear coefficients $C_{ab}^{(n)}(z)$ are resummation-scheme dependent; their expressions in the hard scheme can be obtained from their corresponding expression in an arbitrary scheme by simply setting the coefficient of the $\delta(1-z)$ term to zero.

$$
\begin{aligned}
C_{qq}^{(2)} &= -\frac{1}{864(1-z)z}\Bigg[\\
&C_F^2\Big(-216(z^3+z)\mathrm{Li}_3(1-z) + 1080(z^3+z)\mathrm{Li}_3(z) - 648(z^3+z)\mathrm{Li}_2(z)\log(z) \\
&-216(z^3+z)\mathrm{Li}_2(z)\log(1-z) + 432(z-1)^2 z\mathrm{Li}_2(z) - 108(z^3+z)\log(1-z)\log^2(z) \\
&-1080z(z^2+1)\zeta(3) + 18z(z^2-1)\log^3(z) - 324z(z^2+1)\log^2(1-z)\log(z) \\
&+36z((\pi^2-3)z^2+3z+\pi^2)\log(1-z) - 36(5\pi^2-57)(z-1)^2 z \\
&+54z(2(z-1)z-3)\log^2(z) - 108z(z(16z-13)+5)\log(z) \\
&+648(z-1)^2 z\log(1-z)\log(z)\Big) \\
+\;& C_A C_F\Big(216(z^3+z)\mathrm{Li}_3(1-z) - 432(z^3+z)\mathrm{Li}_3(z) + 216(z^3+z)\mathrm{Li}_2(z)\log(z) \\
&+216(z^3+z)\mathrm{Li}_2(z)\log(1-z) - 216(z-1)^2 z\mathrm{Li}_2(z) - 108z\left(3z^2-11\right)\zeta(3) \\
&+18z(z^2+1)\log^3(z) + 216z(z^2+1)\log^2(1-z)\log(z) \\
&-36z((\pi^2-3)z^2+3z+\pi^2)\log(1-z) + 54\pi^2(z-1)^2 z + 16(z-1)z(z+100) \\
&+9z(11-(z-12)z)\log^2(z) + 12z(z(83z-36)+29)\log(z) \\
&-216(z-1)^2 z\log(1-z)\log(z)\Big) \\
+\;& C_F\Big(-144(z-1)^2 z^2\mathrm{Li}_2(z) - 144(z-1)^2\mathrm{Li}_2(z) + 72(z-1)^2 z\mathrm{Li}_2(z) \\
&+18z(z^2-1)\log^3(z) + 9z\left((5-8z)z^2+3\right)\log^2(z) \\
&+12(z-1)z(32z^2-30z+21)\log(z) - 144(z-1)^2 z^2\log(1-z)\log(z) \\
&+2(z-1)^2((143-136z)z + 6\pi^2(z(2z-1)+2) - 172) \\
&-144(z-1)^2\log(1-z)\log(z) + 72(z-1)^2 z\log(1-z)\log(z)\Big) \\
+\;& C_F n_f\Big(-18z(z^2+1)\log^2(z) - 60z(z^2+1)\log(z) - 4(z-1)z(19z+37)\Big)\Bigg]
\end{aligned}
\tag{A.30}
$$

$$
\begin{aligned}
C_{qq'}^{(2)} &= \frac{C_F}{864z}\Big[-72(2z^3-3z^2+3z-2)\mathrm{Li}_2(z) \\
&+2(z-1)(-136z^2+6\pi^2(2z^2-z+2)+143z-172) - 9z\left(8z^2+3z+3\right)\log^2(z) \\
&-12(z(-32z^2+30z-21)+6(2z^3-3z^2+3z-2)\log(1-z))\log(z) \\
&+18z(z+1)\log^3(z)\Big]
\end{aligned}
\tag{A.31}
$$

$$
\begin{aligned}
C_{qq}^{(2)} &= C_{qq'}^{(2)} \\
&+\frac{1}{24(z+1)}C_F\left(C_F-\frac{C_A}{2}\right)\Bigg[36z^2\mathrm{Li}_3(-z)+24z^2\mathrm{Li}_3(z)+24z^2\mathrm{Li}_3\left(\frac{1}{z+1}\right) \\
&-12\mathrm{Li}_2(-z)((z^2+1)\log(z)+(z+1)^2)-12\mathrm{Li}_2(z)(z^2+z^2\log(z)+\log(z)-1) \\
&+36\mathrm{Li}_3(-z)+24\mathrm{Li}_3(z)+24\mathrm{Li}_3\left(\frac{1}{z+1}\right)-18z^2\zeta(3)+\pi^2z^2-45z^2-z^2\log^3(z) \\
&-4z^2\log^3(z+1)+6z^2\log(z+1)\log^2(z)+33z^2\log(z)-12z^2\log(1-z)\log(z) \\
&-12z^2\log(z+1)\log(z)+2\pi^2z^2\log(z+1)-2\pi^2z-\log^3(z)-4\log^3(z+1) \\
&+6\log(z+1)\log^2(z)+42z\log(z)+12\log(1-z)\log(z)-24z\log(z+1)\log(z) \\
&-12\log(z+1)\log(z)+9\log(z)+2\pi^2\log(z+1)-18\zeta(3)-3\pi^2+45\Bigg]
\end{aligned}
\tag{A.32}
$$

$$
\begin{aligned}
C_{qg}^{(2)} &= \frac{1}{864z}\Bigg[\\
&+ C_FT_R\Bigg(-432z^3\mathrm{Li}_3(z)+432z^2\mathrm{Li}_3(z)-216(2(z-1)z+1)z\mathrm{Li}_3(1-z) \\
&-216z\mathrm{Li}_3(z)+432(-2(z-1)z-1)z\mathrm{Li}_2(z)\tanh^{-1}(1-2z) \\
&+864z^3\tanh^{-1}(1-2z)+3456(z-1)z^2\zeta(3)+36(1-2z)z^2\log^3(z) \\
&-216(z-1)z^2\log^2(1-z)-324z^2\log(1-z)+432(z-1)z^2\log(1-z)\log(z) \\
&+1728z\zeta(3)+18(z(-8(15+\pi^2)z+8\pi^2+129)-39)z \\
&-36(2(z-1)z+1)z\log^3(1-z)-18z\log^3(z)+27(4(3-2z)z+1)z\log^2(z) \\
&+108(2(z-1)z+1)z\log(1-z)\log^2(z)-108(2(z-1)z+1)z\log^2(1-z)\log(z) \\
&+36\pi^2(2(z-1)z+1)z\log(1-z)+54(15z+8)z\log(z)\Bigg) \\
&+ C_AT_R\Bigg(-1296z^3\mathrm{Li}_3(z)+432z^2\mathrm{Li}_3(z) \\
&+54(2z(z+1)+1)z\left(3\mathrm{Li}_3(z^2)+8\mathrm{Li}_3\left(\frac{1}{z+1}\right)\right)-864z^2\mathrm{Li}_2(z)\log(z) \\
&+216(2(z-1)z+1)z\mathrm{Li}_3(1-z)-648z\mathrm{Li}_3(z)-144(z-1)(z(11z-1)+2)\mathrm{Li}_2(z) \\
&-216z\mathrm{Li}_2(-z)(-2z(z+1)+2z(z+1)\log(z)+\log(z)) \\
&-216(-2(z-1)z-1)z\mathrm{Li}_2(z)\log(1-z)-216(6z^2+3)z\zeta(3)+72z^2\log^3(z) \\
&+216(z-1)z^2\log^2(1-z)+36(-12z+2\pi^2+9)z^2\log(1-z) \\
&+24(68z^2-30z+21)z\log(z)+144(z-1)(-11z^2+z-2)\log(1-z)\log(z) \\
&+72\pi^2\left(2z^2+1\right)z\tanh^{-1}(z)+4(z((387-298z)z-315) \\
&+6\pi^2(z(z(11z-9)+3)-2)+172)+36(2(z-1)z+1)z\log^3(1-z)+36z\log^3(z) \\
&-72(2z(z+1)+1)z\log^3(z+1)+9(8(3-11z)z-6)z\log^2(z) \\
&+216(2(z-1)z+1)z\log^2(1-z)\log(z) \\
&+36z(2\pi^2z+3\log(z)(4z(z+1)+2z(z+1)\log(z)+\log(z)))\log(z+1)\Bigg)
\end{aligned}
\tag{A.33}
$$

Convolution of LO Altarelli-Parisi splitting kernels and coefficient functions

At NNLO, two subsequent splitting processes on the same initial leg can lead to double-log singularities controlled by the convolution of two LO Altarelli-Parisi splitting kernels, $P^{(1)}_{ab} \otimes P^{(1)}_{bc}$. They contribute to the coefficient $\Sigma^{F\,(2;2)}_{c\bar{c}\leftarrow ab,\,N}$ (see second line of Eq. (A.12)). We give the expressions in real space (z-space) of the convolutions required for processes initiated by quark-anti quark annihilation at LO:

$$(P^{(1)}_{qq} \otimes P^{(1)}_{qq})(z) = C_F^2\left[2\left(\frac{\ln(1-z)}{1-z}\right)_+ + \frac{3}{2}\left(\frac{1}{1-z}\right)_+ + P_{qqqq}(z) + \frac{1}{4}\left(\frac{9}{4} - \frac{2\pi^2}{3}\right)\delta(1-z)\right] \tag{A.34}$$

with

$$P_{qqqq}(z) = \frac{1}{4}\left(-4\ln\frac{z}{1-z} - 2(1-z) + (1+z)(3\ln z - 4\ln(1-z) - 3)\right) \tag{A.35}$$

$$(P^{(1)}_{qq} \otimes P^{(1)}_{qg})(z) = \frac{1}{8}C_F T_R\left[(z^2+(1-z)^2)\ln\frac{1-z}{z} - \left(z-\frac{1}{2}\right)\ln z + z - \frac{1}{4}\right] \tag{A.36}$$

$$\begin{aligned}(P^{(1)}_{qg} \otimes P^{(1)}_{gg})(z) = C_A T_R&\left[\frac{1}{3z} + \left(z^2 - z + \frac{1}{2}\right)\ln(1-z) + \left(2z+\frac{1}{2}\right)\ln z + \frac{1}{4} + 2z - \frac{31}{12}z^2\right] \\ &+ \beta_0 P^{(1)}_{qg}\end{aligned} \tag{A.37}$$

$$(P^{(1)}_{qg} \otimes P^{(1)}_{gq})(z) = \frac{1}{8}C_F T_R\left[\frac{2}{3z} + (1+z)\ln z - \frac{2}{3}z^2 + \frac{1}{2}(1-z)\right] \tag{A.38}$$

Replacing an Altarelli-Parisi splitting kernel $P^{(1)}_{ab}$ with a collinear function $C^{(1)}_{aa}$ yields a term which controls part of the single-log singularity and, hence, contributes to the coefficient $\Sigma^{F\,(2;1)}_{c\bar{c}\leftarrow ab,\,N}$ (see second line of Eq. (A.13)). The relevant convolutions for processes initiated by quark-anti quark annihilation at LO are:

$$(C^{(1)}_{qq} \otimes P^{(1)}_{qq})(z) = \frac{1}{8}C_F^2(1-z)(4\ln(1-z) - 2\ln z - 1) \tag{A.39}$$

$$(C^{(1)}_{qq} \otimes P^{(1)}_{qg})(z) = \frac{1}{4}C_F T_R\left[-2 + z + z^2 - (1+2z)\ln z\right] \tag{A.40}$$

$$(C^{(1)}_{qg} \otimes P^{(1)}_{gg})(z) = \frac{1}{2}C_A T_R\left[2z(1-z)\ln(1-z) - 4z\ln z + \frac{1}{3z} - 1 - 5z + \frac{17}{3}z^2\right] + \beta_0 C^{(1)}_{qg} \tag{A.41}$$

$$(C^{(1)}_{qg} \otimes P^{(1)}_{gq})(z) = \frac{1}{2}C_F T_R\left[\frac{1}{3z} - 1 + \frac{2}{3}z^2 - z\ln z\right] \tag{A.42}$$

A.2 Gluon-fusion initiated processes

For gluon-fusion initiated processes (as in Higgs boson production) the hard-collinear function in Eq. 2.29 is replaced by [123]

$$\begin{aligned}\left[H^F C_1 C_2\right]_{gg;a_1a_2} &= H^F_{g;\mu_1\,\nu_1,\mu_2\,\nu_2}(x_1p_1, x_2p_2; \boldsymbol{\Omega}; \alpha_S(M^2)) \\ &\times\ C^{\mu_1\,\nu_1}_{g\,a_1}(z_1; p_1, p_2, \mathbf{b}; \alpha_S(b_0^2/b^2))\ C^{\mu_2\,\nu_2}_{g\,a_2}(z_2; p_1, p_2, \mathbf{b}; \alpha_S(b_0^2/b^2))\ ,\end{aligned} \tag{A.43}$$

where the function H^F_g has the perturbative expansion

$$\begin{aligned}H^{F\mu_1\nu_1,\mu_2\nu_2}_{g}(x_1p_1, x_2p_2; \boldsymbol{\Omega}; \alpha_S) =&H^{F(0)\mu_1\nu_1,\mu_2\nu_2}_{g}(x_1p_1, x_2p_2; \boldsymbol{\Omega}) \\ &+\sum_{n=1}^{\infty}\left(\frac{\alpha_S}{\pi}\right)^n H^{F(n)\mu_1\nu_1,\mu_2\nu_2}_{g}(x_1p_1, x_2p_2; \boldsymbol{\Omega})\ ,\end{aligned} \tag{A.44}$$

and the following lowest-order normalization:

$$H^{F(0)\mu_1\nu_1,\mu_2\nu_2}_{g}\ g_{\mu_1\nu_1}\ g_{\mu_2\nu_2} = 1\ . \tag{A.45}$$

The coefficient function $H^F_{g;\mu_1\,\nu_1,\mu_2\,\nu_2}$ depends now on the Lorentz indices (and, thus, on the spins) $\{\mu_i\,\nu_i\}$ of the colliding gluons with momenta x_ip_i $(i = 1,2)$. The Lorentz tensor coefficients $C^{\mu_i\,\nu_i}_{ga_i}$ in Eq. (A.43) depend on b^2 (through the scale of α_S) and, moreover, they also depend on the direction (i.e., the azimuthal angle) of the impact parameter vector $\mathbf{b}$ in the transverse plane and its structure is [123]

$$C^{\mu\nu}_{g\,a}(z; p_1, p_2, \mathbf{b}; \alpha_S) = d^{\,\mu\nu}(p_1, p_2)\ C_{g\,a}(z; \alpha_S) + D^{\,\mu\,\nu}(p_1, p_2; \mathbf{b})\ G_{g\,a}(z; \alpha_S)\ , \tag{A.46}$$

where

$$d^{\,\mu\nu}(p_1, p_2) = -\,g^{\mu\nu} + \frac{p_1^\mu p_2^\nu + p_2^\mu p_1^\nu}{p_1\cdot p_2}\ , \tag{A.47}$$

$$D^{\,\mu\nu}(p_1, p_2; \mathbf{b}) = d^{\,\mu\nu}(p_1, p_2) - 2\,\frac{b^\mu\,b^\nu}{\mathbf{b}^2}\ , \tag{A.48}$$

and $b^\mu = (0, \mathbf{b}, 0)$ is the two-dimensional impact parameter vector in the four-dimensional notation $(b^\mu b_\mu = -\mathbf{b}^2)$. The gluonic coefficient function $C_{g\,a}(z; \alpha_S)$ $(a = q, \bar{q}, g)$ in the right-hand side of Eq. (A.46) has the perturbative structure

$$C_{g\,a}(z; \alpha_S) = \delta_{g\,a}\ \delta(1-z) + \sum_{n=1}^{\infty}\left(\frac{\alpha_S}{\pi}\right)^n C^{(n)}_{g\,a}(z)\ . \tag{A.49}$$

In contrast, the perturbative expansion of the coefficient functions G_{ga}, which are specific to gluon-initiated processes, starts at $\mathcal{O}(\alpha_S)$, and we write

$$G_{g\,a}(z; \alpha_S) = \frac{\alpha_S}{\pi}\ G^{(1)}_{g\,a}(z) + \sum_{n=2}^{\infty}\left(\frac{\alpha_S}{\pi}\right)^n G^{(n)}_{g\,a}(z)\ . \tag{A.50}$$

The first-order coefficient $C^{(1)}_{g\,a}(z; \alpha_S)$ have been already given in Eqs. (A.27) and (A.29). The first-order coefficients $G^{(1)}_{ga}$ are resummation-scheme independent, and they read [123]

$$G^{(1)}_{g\,a}(z) = C_a\,\frac{1-z}{z} \qquad a = q, g\,, \tag{A.51}$$

where C_a is as usual the Casimir colour coefficient of the parton a with $C_q = C_F$ and $C_g = C_A$.

A.3 Hard-virtual function: subtraction operator

The auxiliary amplitude $\widetilde{\mathcal{M}}_{c\bar{c}\to F}$ required to compute the hard-virtual function is expressed by the following factorization formula

$$\widetilde{\mathcal{M}}_{c\bar{c}\to F}(\hat{p}_1, \hat{p}_2; \{q_i\}) = \left[1 - \tilde{I}_c(\epsilon, M^2)\right] \mathcal{M}_{c\bar{c}\to F}(\hat{p}_1, \hat{p}_2; \{q_i\}) \;, \tag{A.52}$$

in terms of the perturbative subtraction operator

$$\begin{aligned}\tilde{I}_c(\epsilon, M^2) &= \frac{\alpha_S(\mu_R^2)}{2\pi}\, \tilde{I}_c^{(1)}(\epsilon, M^2/\mu_R^2) + \left(\frac{\alpha_S(\mu_R^2)}{2\pi}\right)^2 \tilde{I}_c^{(2)}(\epsilon, M^2/\mu_R^2) \\ &+ \sum_{n=3}^{\infty} \left(\frac{\alpha_S(\mu_R^2)}{2\pi}\right)^n \tilde{I}_c^{(n)}(\epsilon, M^2/\mu_R^2)\,.\end{aligned} \tag{A.53}$$

The explicit expression of the first-order subtraction operator $\tilde{I}_a^{(1)}$ is

$$\tilde{I}_a^{(1)}(\epsilon, M^2/\mu_R^2) = \tilde{I}_a^{(1)\,\mathrm{soft}}(\epsilon, M^2/\mu_R^2) + \tilde{I}_a^{(1)\,\mathrm{coll}}(\epsilon, M^2/\mu_R^2)\,, \tag{A.54}$$

with

$$\tilde{I}_a^{(1)\,\mathrm{soft}}(\epsilon, M^2/\mu_R^2) = -\frac{e^{\epsilon\gamma_E}}{\Gamma(1-\epsilon)}\left(\frac{1}{\epsilon^2} + i\pi\,\frac{1}{\epsilon} + \delta^{q_T}\right) C_a \left(\frac{M^2}{\mu_R^2}\right)^{-\epsilon}\,, \tag{A.55}$$

$$\tilde{I}_a^{(1)\,\mathrm{coll}}(\epsilon, M^2/\mu_R^2) = -\frac{1}{\epsilon}\,\gamma_a \left(\frac{M^2}{\mu_R^2}\right)^{-\epsilon}\,, \tag{A.56}$$

and

$$\gamma_q = \gamma_{\bar{q}} = \frac{3}{2}\,C_F\,, \qquad \gamma_g = \frac{11}{6}\,C_A - \frac{1}{3}\,N_f\,. \tag{A.57}$$

In the hard scheme

$$\delta^{q_T} = 0\,. \tag{A.58}$$

The second-order (two-loop) subtraction operator $\tilde{I}_c^{(2)}$ is [136]

$$\begin{aligned}\tilde{I}_a^{(2)}(\epsilon, M^2/\mu_R^2) &= -\frac{1}{2}\left[\tilde{I}_a^{(1)}(\epsilon, M^2/\mu_R^2)\right]^2 + \left\{\frac{2\pi\beta_0}{\epsilon}\left[\tilde{I}_a^{(1)}(2\epsilon, M^2/\mu_R^2)\right.\right. \\ &\left.\left. - \tilde{I}_a^{(1)}(\epsilon, M^2/\mu_R^2)\right] + K\,\tilde{I}_a^{(1)\,\mathrm{soft}}(2\epsilon, M^2/\mu_R^2) + \widetilde{H}_a^{(2)}(\epsilon, M^2/\mu_R^2)\right\}\,,\end{aligned} \tag{A.59}$$

with

$$\widetilde{H}_a^{(2)}(\epsilon, M^2/\mu_R^2) = \widetilde{H}_a^{(2)\,\mathrm{coll}}(\epsilon, M^2/\mu_R^2) + \widetilde{H}_a^{(2)\,\mathrm{soft}}(\epsilon, M^2/\mu_R^2) \tag{A.60}$$

$$= \frac{1}{4\epsilon}\left(\frac{M^2}{\mu_R^2}\right)^{-2\epsilon}\left(\frac{1}{4}\,\gamma_{a\,(1)} + C_a\, d_{(1)} + \epsilon\, C_a\, \delta_{(1)}^{q_T}\right)\,. \tag{A.61}$$

The QCD coefficients K in Eq. (A.59) and $d_{(1)}$ in Eq. (A.61) (they control the IR divergences of $\tilde{I}_a^{(2)}$) are [109]

$$K = \left(\frac{67}{18} - \frac{\pi^2}{6}\right) C_A - \frac{5}{9}\,N_f\,, \tag{A.62}$$

$$d_{(1)} = \left(\frac{28}{27} - \frac{1}{3}\zeta_2\right) N_f + \left(-\frac{202}{27} + \frac{11}{6}\zeta_2 + 7\zeta_3\right) C_A\,, \tag{A.63}$$

and the coefficients $\gamma_{a\,(1)}$ ($a = q, g$) are given in Eqs. (A.24) and (A.25). In the hard scheme, the coefficient $\delta^{q_T}_{(1)}$ is

$$\delta^{q_T}_{(1)} = \frac{20}{3}\zeta_3 \pi\beta_0 + \left(-\frac{1214}{81} + \frac{67}{18}\zeta_2\right) C_A + \left(\frac{164}{81} - \frac{5}{9}\zeta_2\right) N_f\,. \tag{A.64}$$

The following formulae give the relation between the auxiliary amplitude $\widetilde{\mathcal{M}}_{c\bar{c}\to F}$ and the process resummation coefficients H^F_c:

$$\alpha_S^{2k}(M^2)\, H^F_q(x_1 p_1, x_2 p_2; \mathbf{\Omega}; \alpha_S(M^2)) = \frac{|\widetilde{\mathcal{M}}_{q\bar{q}\to F}(x_1 p_1, x_2 p_2; \{q_i\})|^2}{|\mathcal{M}^{(0)}_{q\bar{q}\to F}(x_1 p_1, x_2 p_2; \{q_i\})|^2}\,, \tag{A.65}$$

for processes initiated by quark-anti quark annihilation and

$$\alpha_S^{2k}(M^2)\, h_g^{F\,\mu_1\nu_1\mu_2\nu_2}(x_1 p_1, x_2 p_2; \mathbf{\Omega}; \alpha_S(M^2)) = \frac{\left[\widetilde{\mathcal{M}}^{\mu_1\mu_2}_{gg\to F}(x_1 p_1, x_2 p_2; \{q_i\})\right]^\dagger \widetilde{\mathcal{M}}^{\nu_1\nu_2}_{gg\to F}(x_1 p_1, x_2 p_2; \{q_i\})}{|\mathcal{M}^{(0)}_{gg\to F}(x_1 p_1, x_2 p_2; \{q_i\})|^2}\,, \tag{A.66}$$

$$H_g^{F\mu_1\nu_1\mu_2\nu_2}(x_1 p_1, x_2 p_2; \mathbf{\Omega}; \alpha_S) = d^{\,\mu_1}_{\;\;\mu_1'}\, d^{\,\nu_1}_{\;\;\nu_1'}\, d^{\,\mu_2}_{\;\;\mu_2'}\, d^{\,\nu_2}_{\;\;\nu_2'}\, h_g^{F\,\mu_1'\nu_1'\mu_2'\nu_2'}(x_1 p_1, x_2 p_2; \mathbf{\Omega}; \alpha_S)\,, \tag{A.67}$$

where $d^{\mu\nu} = d^{\mu\nu}(p_1, p_2)$ is the polarization tensor in Eq. (A.47) and it projects onto the Lorentz indices in the transverse plane, for processes initiated by gluon fusion [123]. In the above formulae, k is the power of α_s in the LO matrix element.

Remark: by inspection of Eqs. (A.59)-(A.60), we observe that the second-order subtraction coefficient $\tilde{I}_c^{(2)}$ is completely fixed computing its explicit expression for only one process, being it initiated either by quark-antiquark annihilation or by gluon fusion.

Appendix B

3-body phase space parametrization

In this Appendix, we present the derivation of the 3-body phase space parametrization employed to analytically integrate in Chapter 4 the NLO real emission cross section up to the transverse momentum cut-off r_{cut}.

We consider a variant of the parametrization outlined in [207] for the heavy-quark pair hadroproduction. The 3-body phase space can be decompose as the following chain of splittings

1. $q(k_1) + \bar{q}(k_2) \to \gamma(k_3) + R(Q)$,
2. $R(Q) \to L(p_1) + \bar{L}(p_2)$.

Formally, this is equivalent to add the following decomposition of the unity in the phase space integral

$$\int d^4Q\delta^{(4)}(Q - p_1 - p_2) = 1 \tag{B.1}$$

so that

$$\begin{aligned} R_3 &= \frac{1}{(2\pi)^5}\int d^4k_3 d^4p_1 d^4p_2 \delta^+(k_3^2)\delta^+(p_1^2 - m^2)\delta^+(p_2^2 - m^2)\delta^{(4)}(k_1 + k_2 - k_3 - p_1 - p_2) \\ &= \frac{1}{(2\pi)^5}\int d^4k_3 d^4Q\delta^+(k_3^2)\delta^{(4)}(k_1 + k_2 - k_3 - Q) \\ &\qquad \times \int d^4p_1 d^4p_2 \delta^+(p_1^2 - m^2)\delta^+(p_2^2 - m^2)\delta^{(4)}(Q - p_1 - p_2). \end{aligned}$$

We notice that each integral separately preserves Lorentz invariance. This allows to make different frame choices as long one keeps the order of the integrations. For the innermost integral, corresponding to the phase space of a decay process $1 \to 2$, we consider the center-of-mass frame of the decay products, i.e. the frame in which the two leptons are back-to-back. We get

$$\begin{aligned} R_2 &\equiv \int d^4p_1 d^4p_2 \delta^+(p_1^2 - m^2)\delta^+(p_2^2 - m^2)\delta^{(4)}(Q - p_1 - p_2) \\ &= \int d^4p_1 \delta^+(p_1^2 - m^2)\delta^+((Q - p_1)^2 - m^2) = \int \frac{d^3p_1}{2E_1}\delta^+(M^2 - 2Q\cdot p_1) \\ &= \frac{1}{8}\sqrt{1 - \frac{4m^2}{M^2}}\int d\Omega, \end{aligned}$$

with $M^2 \equiv Q^2$. Putting all together, we have

$$\begin{aligned} R_3 &= \frac{1}{(2\pi)^5} \int d^4k_3 d^4Q \delta^+(k_3^2) \delta^{(4)}(k_1 + k_2 - k_3 - p) R_2 = \frac{1}{(2\pi)^5} \int \frac{d^3k_3}{2E_3} R_2 \\ &= \frac{1}{16} \frac{1}{(2\pi)^5} \int E_3 dE_3 \int d\cos\theta \int d\varphi \sqrt{1 - \frac{4m^2}{M^2}} \int d\Omega \end{aligned}$$

where we have introduced generic polar and azimuthal angles for k_3. It is now convenient to specialize the choice of the second reference frame to the partonic center-of-mass frame. This allows to make contact with the q_T variable and to considerably simplify the expressions. As usual we orient the axes such that the third axis coincides with the beam direction,

$$k_1 = \frac{\sqrt{s}}{2}(1, 0, 0, 1), \qquad k_2 = \frac{\sqrt{s}}{2}(1, 0, 0, -1), \tag{B.2}$$

with s being the partonic center-of-mass energy. We can integrate out the azimuthal angle as the matrix element squared does not depend on it

$$R_3 = \frac{1}{16} \frac{1}{(2\pi)^4} \int E_3 dE_3 \int d\cos\theta \sqrt{1 - \frac{4m^2}{p^2}} \int d\Omega. \tag{B.3}$$

Consider now the following invariants

$$\begin{aligned} s &= (k_1 + k_2)^2 = 2k_1 \cdot k_2, \\ t &= (k_1 - k_3)^2 = -2k_1 \cdot k_3 = -\sqrt{s} E_3 (1 - \cos\theta), \\ u &= (k_2 - k_3)^2 = -2k_2 \cdot k_3 = -\sqrt{s} E_3 (1 + \cos\theta). \end{aligned}$$

We can then express E_3, $\cos\theta$ as

$$E_3 = -\frac{t + u}{2\sqrt{s}}, \qquad \cos\theta = \frac{t - u}{2, \sqrt{s} E_3} = \frac{u - t}{t + u} \tag{B.4}$$

and q_T as

$$q_T^2 = E_3^2 (1 - \cos^2\theta) = \frac{1}{4s}((t + u)^2 - (u - t)^2) = \frac{ut}{s}. \tag{B.5}$$

The Jacobian factor associated to the above change of variables reads

$$E_3 dE_3 d\cos\theta = \frac{1}{2s} dt du = \frac{1}{2u} du dq_T^2. \tag{B.6}$$

We get

$$R_3 = \frac{1}{32} \frac{1}{(2\pi)^4} \int \frac{du}{u} dq_T^2 \sqrt{1 - \frac{4m^2}{M^2}} \int d\Omega, \tag{B.7}$$

which reduces to Eq. in Ref. [] in the massless case. Introducing the change of variable from u to M^2

$$M^2 = s + u + \frac{s q_T}{u} \tag{B.8}$$

we get the following final expression for the 3-body phase space is

$$R_3 = \frac{1}{16} \frac{1}{(2\pi)^4} \int dM^2 dq_T^2 \frac{1}{\sqrt{(s - M^2)^2 - 4s q_T^2}} \sqrt{1 - \frac{4m^2}{M^2}} \int d\Omega. \tag{B.9}$$

The integration limits can be determined by looking at the points where the argument of the square roots occurring in the integrand vanish and they are given by the following relations

$$4m^2 < M^2 < s\,, \quad 0 < q_T^2 < \frac{(s-M^2)^2}{4s}\,. \tag{B.10}$$

When the lower kinematic cut r_{cut} is applied on transverse momentum divided by the mass M^2, the relations in Eq.(B.10) get modified as

$$4m^2 < M^2 < s z_{\max}(r_{\text{cut}})\,, \quad r_{\text{cut}} M^2 < q_T^2 < \frac{(s-M^2)^2}{4s}\,, \tag{B.11}$$

with $z_{\max} = (1 - 2r_{\text{cut}}\sqrt{1+r_{\text{cut}}^2} + 2r_{\text{cut}}^2)$.

B.0.1 Kinematics in the CM of the massive leptons

Here we report for completeness the expressions of the momenta for all the external particles in the frame in which the two massive leptons are back-to-back. We denote with ϑ_1 and ϑ_2 respectively the polar and azimuthal angle of the massive lepton pair. Then, we have

$$p_1 = (E, |p|\sin\vartheta_1\sin\vartheta_2, |p|\sin\vartheta_1\cos\vartheta_2, |p|\cos\vartheta_1)\,, \tag{B.12}$$

$$p_2 = (E, -|p|\sin\vartheta_1\sin\vartheta_2, -|p|\sin\vartheta_1\cos\vartheta_2, -|p|\cos\vartheta_1)\,. \tag{B.13}$$

We can write E and $|p|$ in terms of the invariant s_2:

$$s_2 = (p_1+p_2)^2 = 4E^2 \quad \Rightarrow E = \frac{\sqrt{s_2}}{2}, |p| = \sqrt{E^2 - m^2} = \frac{\sqrt{s_2}}{2}\sqrt{1 - \frac{4m^2}{s_2}}. \tag{B.14}$$

There is still some freedom in the choice of the reference frame due to rotational invariance. We fix it choosing one of the incoming momentum to be in the direction of the third axis, for example let it be k_2. We can then parameterize k_1, k_2 and k_3 in the following way

$$k_1 = (\omega_1, 0, \omega_3\sin\psi, \omega_3\cos\psi - \omega_2)\,, \tag{B.15}$$
$$k_2 = (\omega_2, 0, 0, \omega_2)\,. \tag{B.16}$$

In terms of the invariants, we have

$$\omega_1 = \frac{s_2 - u}{2\sqrt{s_2}}, \qquad \omega_2 = \frac{s+u}{2\sqrt{s_2}}, \qquad \omega_3 = \frac{s - s_2}{2\sqrt{s_2}}, \qquad \cos\psi = \frac{us_2 - ts}{(s+u)(s-s_2)}. \tag{B.17}$$

Appendix C

Soft Integrals and power counting

In this Appendix, we discuss the soft power counting for final-state radiation. In the strictly soft limit, the phase space of the emitted photon with momentum k exactly factorizes

$$d\Phi_3 = d\Phi_2 \times \frac{d^3k}{(2\pi)^3 2k^0}. \tag{C.1}$$

The leading power contribution to final-state radiation is given by the soft-factorisation formula

$$|\mathcal{M}(p_1,p_2,p_3,p_4,k)|^2_{\text{FSR}} \sim \left(e_3^2\,\mathcal{S}_{33} + e_4^2\,\mathcal{S}_{44} + 2e_3e_4\,\mathcal{S}_{34}\right)|\mathcal{M}(p_1,p_2,p_3,p_4)|^2 \tag{C.2}$$

where

$$\mathcal{S}_{ij} = \frac{p_i\cdot p_j}{(p_i\cdot k)(p_j\cdot k)}. \tag{C.3}$$

The power counting is more easily understood if we consider light-cone coordinates

$$k^{\pm} = \frac{k^0 \pm k^3}{\sqrt{2}} \qquad d^4k = dk^+dk^-d^2\mathbf{k}_\perp \tag{C.4}$$

We recall that in light cone coordinates the scalar product between two vectors takes the form

$$k\cdot p = k^+p^- + k^-p^+ - \mathbf{k}_\perp\cdot\mathbf{p}_\perp \tag{C.5}$$

and in particular the norm squared is

$$k^2 = 2k^+p^- - \mathbf{k}_\perp^2. \tag{C.6}$$

The 1-body phase space volume has the form

$$\int \frac{d^4k}{(2\pi)^3}\delta_+(k^2) = \int \frac{dk^+dk^-d^2\mathbf{k}_\perp}{(2\pi)^3}\delta_+(2k^+k^- - \mathbf{k}_\perp^2) = \frac{1}{(2\pi)^3}\int_0^\infty \frac{dk^+}{2k^+}\int d^2\mathbf{k}_\perp \tag{C.7}$$

with $k^- = \mathbf{k}_\perp^2/2k^+$. Considering first the contribution from $\mathcal{S}_{34}$, the leading power unconstrained soft integral is given by

$$\begin{aligned} I_{34}^{\text{soft}} &= \frac{1}{(2\pi)^3}\int_0^\infty \frac{dk^+}{2k^+}\int_0^\infty \frac{dk_\perp^2}{2}\int_0^{2\pi} d\theta\,\mathcal{S}_{34}\Theta(k_\perp^2 - sr_{\text{cut}}^2) \\ &= \frac{p_3\cdot p_4}{(2\pi)^3}\int_{sr_{\text{cut}}^2}^\infty \frac{dk_\perp^2}{2}\int_0^\infty \frac{dk^+}{2k^+}\int_0^{2\pi} d\theta \frac{1}{p_\perp^2 k_\perp^2}\frac{1}{(a_3-\cos\theta)(a_4+\cos\theta)} \end{aligned} \tag{C.8}$$

$$a_i = \frac{1}{p_\perp k_\perp}\left(p_i^+\frac{k_\perp^2}{2k^+} + p_i^- k^+\right). \tag{C.9}$$

In the above formula, we have enforced the soft kinematic with two back-to-back massive leptons. In particular, this means that $p_{3,\perp} = p_{4,\perp} \equiv p_\perp$. The azimuthal average is straightforward, after disentangling the product occurring in the denominator by means of the partial fraction relation

$$\frac{1}{(a_3 - \cos\theta)(a_4 + \cos\theta)} = \frac{1}{a_3 + a_4}\left(\frac{1}{a_3 - \cos\theta} + \frac{1}{a_4 + \cos\theta}\right), \tag{C.10}$$

and it gives

$$I_{34}^{\text{soft}} = \frac{p_3 \cdot p_4}{(2\pi)^2}\int_{sr_{\text{cut}}^2}^{\infty}\frac{dk_\perp^2}{2}\int_0^\infty \frac{dk^+}{2k^+}\frac{1}{p_\perp^2 k_\perp^2}\frac{1}{a_3 + a_4}\sum_{i=3,4}\frac{1}{\sqrt{a_i^2 - 1}}, \tag{C.11}$$

To make the scaling with the transverse momentum manifest, we apply the following change of variables at fixed $k_\perp$:

$$x = \left(\frac{k^+}{k_\perp}\right)^2, \quad dk^+ = k_\perp \frac{dx}{2\sqrt{x}}. \tag{C.12}$$

The soft integral becomes

$$I_{34}^{\text{soft}} = \frac{p_3 \cdot p_4}{(2\pi)^2}\frac{1}{\sqrt{2s}}\int_{sr_{\text{cut}}^2}^{\infty}\frac{dk_\perp^2}{k_\perp^2}\int_0^\infty \frac{dx}{1+2x}\sum_{i=3,4}\frac{1}{\sqrt{4(p_i^-)^2x^2 + 2(m^2 - p_\perp^2)x + (p_i^+)^2}} \tag{C.13}$$

where s is the partonic CM energy.
We can complete the calculation of the leading power contribution by performing the integration over the x variable. The relevant integrals are of the form

$$T(a,b,c) = \int_0^\infty \frac{dx}{1+2x}\frac{1}{\sqrt{ax^2 + 2bx + c}} = \frac{1}{\sqrt{a - 4b + 4c}}\ln\left[\frac{-2b + 4c + 2\sqrt{c}\sqrt{a - 4b + 4c}}{-a + 2b + \sqrt{a}\sqrt{a - 4b + 4c}}\right] \tag{C.14}$$

under the conditions $b^2 - ac < 0$ and $a, c > 0$. Then, it is straightforward to compute

$$\int_0^\infty \frac{dx}{1+2x}\sum_{i=3,4}\frac{1}{\sqrt{4(p_i^-)^2x^2 + 2(m^2 - p_\perp^2)x + (p_i^+)^2}} = \frac{1}{\sqrt{2}p}\ln\frac{1+\beta}{1-\beta}, \quad p = \sqrt{E^2 - m^2}. \tag{C.15}$$

We get the final expression

$$I_{34}^{\text{soft}} = \frac{1}{4(2\pi)^2}\frac{1+\beta^2}{\beta}\ln\frac{1+\beta}{1-\beta}\int_{sr_{\text{cut}}^2}^{\infty}\frac{dk_\perp^2}{k_\perp^2} \tag{C.16}$$

which exactly matches the coefficient of the leading logarithmic divergence proportional to the charge product $e_3 e_4 = -1$ in Eq. (4.70). The contributions from I_{33}^{soft} and I_{44}^{soft} are equal one another and can be obtained in a similar way as I_{34}^{soft}. Consider for example I_{33}^{soft}. We have

$$\begin{aligned} I_{33}^{\text{soft}} &= \frac{1}{(2\pi)^3}\int_0^\infty \frac{dk^+}{2k^+}\int_0^\infty \frac{dk_\perp^2}{2}\int_0^{2\pi} d\theta\, \mathcal{S}_{33}\Theta(k_\perp^2 - sr_{\text{cut}}^2) \\ &= \frac{m^2}{(2\pi)^3}\int_{sr_{\text{cut}}^2}^{\infty}\frac{dk_\perp^2}{2}\int_0^\infty \frac{dk^+}{2k^+}\int_0^{2\pi} d\theta \frac{1}{p_\perp^2 k_\perp^2}\frac{1}{(a_3 - \cos\theta)^2} \end{aligned} \tag{C.17}$$

After performing the azimuthal integral and the change of variable in eq. (C.12), we obtain

$$I_{33}^{\rm soft} = \frac{m^2}{(2\pi)^2}\frac{1}{2}\int_{sr_{\rm cut}^2}^{\infty}\frac{dk_\perp^2}{k_\perp^2}\int_0^\infty dx\frac{p_3^+ + 2p_3^- x}{\left[4(p_3^-)^2x^2 + 2(m^2 - p_\perp^2)x + (p_3^+)^2\right]^{3/2}} \tag{C.18}$$

where the logarithmic scaling with the transverse momentum is manifest. The relevant integral is now of the form

$$T(a,b,c) = \int_0^\infty ds\frac{a+bx}{\left[4b^2x^2 + 2cx + a^2\right]^{3/2}} = \frac{2}{2ab+c} \tag{C.19}$$

for $b > 0$. Applying the above result, it is straightforward to get

$$\int_0^\infty dx\frac{p_3^+ + 2p_3^- x}{\left[4(p_3^-)^2x^2 + 2(m^2 - p_\perp^2)x + (p_3^+)^2\right]^{3/2}} = \frac{2}{2p_3^+p_3^+ + m^2 - p_\perp^2} = \frac{1}{m^2} \tag{C.20}$$

and hence

$$I_{33}^{\rm soft} = \frac{1}{2(2\pi)^2}\int_{sr_{\rm cut}^2}^{\infty}\frac{dk_\perp^2}{k_\perp^2} \tag{C.21}$$

for the final result, which reproduces, multiplied by a factor of two to take into account the contribution of $I_{44}^{\rm soft}$, the remaining term in Eq. (4.70).

The power counting for the linear power correction follows now easily observing that the energy of the radiation scales with the transverse momentum

$$k^0 = \frac{k^+ + k^-}{\sqrt{2}} = k_\perp\sqrt{\frac{x}{2}}\left(1 + \frac{1}{2x}\right). \tag{C.22}$$

This implies that corrections to the soft approximation will produce linear terms in $r_{\rm cut}$.

Bibliography

[1] M. Baak et al. "The global electroweak fit at NNLO and prospects for the LHC and ILC". In: *Eur. Phys. J.* C74 (2014), p. 3046. DOI: 10.1140/epjc/s10052-014-3046-5. arXiv: 1407.3792 [hep-ph].

[2] Morad Aaboud et al. "Measurement of the W-boson mass in pp collisions at $\sqrt{s} = 7$ TeV with the ATLAS detector". In: *Eur. Phys. J.* C78.2 (2018). [Erratum: Eur. Phys. J.C78,no.11,898(2018)], p. 110. DOI: 10.1140/epjc/s10052-018-6354-3,10.1140/epjc/s10052-017-5475-4. arXiv: 1701.07240 [hep-ex].

[3] Guido Altarelli, R. Keith Ellis, and G. Martinelli. "Large Perturbative Corrections to the Drell-Yan Process in QCD". In: *Nucl. Phys.* B157 (1979), pp. 461–497. DOI: 10.1016/0550-3213(79)90116-0.

[4] R. Hamberg, W. L. van Neerven, and T. Matsuura. "A complete calculation of the order $\alpha - s^2$ correction to the Drell-Yan K factor". In: *Nucl. Phys.* B359 (1991). [Erratum: Nucl. Phys.B644,403(2002)], pp. 343–405. DOI: 10.1016/S0550-3213(02)00814-3,10.1016/0550-3213(91)90064-5.

[5] Charalampos Anastasiou et al. "High precision QCD at hadron colliders: Electroweak gauge boson rapidity distributions at NNLO". In: *Phys. Rev.* D69 (2004), p. 094008. DOI: 10.1103/PhysRevD.69.094008. arXiv: hep-ph/0312266 [hep-ph].

[6] Kirill Melnikov and Frank Petriello. "Electroweak gauge boson production at hadron colliders through O(alpha(s)**2)". In: *Phys. Rev.* D74 (2006), p. 114017. DOI: 10.1103/PhysRevD.74.114017. arXiv: hep-ph/0609070 [hep-ph].

[7] Stefano Catani et al. "Vector boson production at hadron colliders: a fully exclusive QCD calculation at NNLO". In: *Phys. Rev. Lett.* 103 (2009), p. 082001. DOI: 10.1103/PhysRevLett.103.082001. arXiv: 0903.2120 [hep-ph].

[8] Ryan Gavin et al. "FEWZ 2.0: A code for hadronic Z production at next-to-next-to-leading order". In: *Comput. Phys. Commun.* 182 (2011), pp. 2388–2403. DOI: 10.1016/j.cpc.2011.06.008. arXiv: 1011.3540 [hep-ph].

[9] U. Baur et al. "Electroweak radiative corrections to neutral current Drell-Yan processes at hadron colliders". In: *Phys. Rev.* D65 (2002), p. 033007. DOI: 10.1103/PhysRevD.65.033007. arXiv: hep-ph/0108274 [hep-ph].

[10] V. A. Zykunov. "Weak radiative corrections to Drell-Yan process for large invariant mass of di-lepton pair". In: *Phys. Rev.* D75 (2007), p. 073019. DOI: 10.1103/PhysRevD.75.073019. arXiv: hep-ph/0509315 [hep-ph].

[11] C. M. Carloni Calame et al. "Precision electroweak calculation of the production of a high transverse-momentum lepton pair at hadron colliders". In: *JHEP* 10 (2007), p. 109. DOI: 10.1088/1126-6708/2007/10/109. arXiv: 0710.1722 [hep-ph].

[12] A. Arbuzov et al. "One-loop corrections to the Drell–Yan process in SANC. (II). The Neutral current case". In: *Eur. Phys. J.* C54 (2008), pp. 451–460. DOI: 10.1140/epjc/s10052-008-0531-8. arXiv: 0711.0625 [hep-ph].

[13] Daniel de Florian, Manuel Der, and Ignacio Fabre. "QCD⊕QED NNLO corrections to Drell Yan production". In: *Phys. Rev.* D98.9 (2018), p. 094008. DOI: 10.1103/PhysRevD.98.094008. arXiv: 1805.12214 [hep-ph].

[14] Claude Duhr, Falko Dulat, and Bernhard Mistlberger. "The Drell-Yan cross section to third order in the strong coupling constant". In: (2020). arXiv: 2001.07717 [hep-ph].

[15] William B. Kilgore and Christian Sturm. "Two-Loop Virtual Corrections to Drell-Yan Production at order $\alpha_s \alpha^3$". In: *Phys. Rev.* D85 (2012), p. 033005. DOI: 10.1103/PhysRevD.85.033005. arXiv: 1107.4798 [hep-ph].

[16] Stefan Dittmaier, Alexander Huss, and Christian Schwinn. "Mixed QCD-electroweak $O(\alpha_s \alpha)$ corrections to Drell-Yan processes in the resonance region: pole approximation and non-factorizable corrections". In: *Nucl. Phys.* B885 (2014), pp. 318–372. DOI: 10.1016/j.nuclphysb.2014.05.027. arXiv: 1403.3216 [hep-ph].

[17] Stefan Dittmaier, Alexander Huss, and Christian Schwinn. "Dominant mixed QCD-electroweak O($\alpha_s \alpha$) corrections to Drell?Yan processes in the resonance region". In: *Nucl. Phys.* B904 (2016), pp. 216–252. DOI: 10.1016/j.nuclphysb.2016.01.006. arXiv: 1511.08016 [hep-ph].

[18] Maximilian Delto et al. "Mixed QCD⊗QED corrections to on-shell Z boson production at the LHC". In: (2019). arXiv: 1909.08428 [hep-ph].

[19] Roberto Bonciani et al. "NNLO QCD×EW corrections to Z production in the $q\bar{q}$ channel". In: (2019). arXiv: 1911.06200 [hep-ph].

[20] Federico Buccioni, Stefano Pozzorini, and Max Zoller. "On-the-fly reduction of open loops". In: *Eur. Phys. J.* C78.1 (2018), p. 70. DOI: 10.1140/epjc/s10052-018-5562-1. arXiv: 1710.11452 [hep-ph].

[21] Stefano Catani et al. "The Dipole formalism for next-to-leading order QCD calculations with massive partons". In: *Nucl. Phys.* B627 (2002), pp. 189–265. DOI: 10.1016/S0550-3213(02)00098-6. arXiv: hep-ph/0201036 [hep-ph].

[22] S. Frixione, Z. Kunszt, and A. Signer. "Three jet cross-sections to next-to-leading order". In: *Nucl. Phys.* B467 (1996), pp. 399–442. DOI: 10.1016/0550-3213(96)00110-1. arXiv: hep-ph/9512328 [hep-ph].

[23] S. Frixione. "A General approach to jet cross-sections in QCD". In: *Nucl. Phys.* B507 (1997), pp. 295–314. DOI: 10.1016/S0550-3213(97)00574-9. arXiv: hep-ph/9706545 [hep-ph].

[24] Stefano Frixione, Paolo Nason, and Carlo Oleari. "Matching NLO QCD computations with Parton Shower simulations: the POWHEG method". In: *JHEP* 11 (2007), p. 070. DOI: 10.1088/1126-6708/2007/11/070. arXiv: 0709.2092 [hep-ph].

[25] S. Laporta. "High precision calculation of multiloop Feynman integrals by difference equations". In: *Int. J. Mod. Phys.* A15 (2000), pp. 5087–5159. DOI: 10.1016/S0217-751X(00)00215-7,10.1142/S0217751X00002157. arXiv: hep-ph/0102033 [hep-ph].

[26] Andreas von Manteuffel and Robert M. Schabinger. "A novel approach to integration by parts reduction". In: *Phys. Lett.* B744 (2015), pp. 101–104. DOI: 10.1016/j.physletb.2015.03.029. arXiv: 1406.4513 [hep-ph].

[27] Tiziano Peraro. "FiniteFlow: multivariate functional reconstruction using finite fields and dataflow graphs". In: *JHEP* 07 (2019), p. 031. DOI: 10.1007/JHEP07(2019)031. arXiv: 1905.08019 [hep-ph].

[28] Stefano Catani and Massimiliano Grazzini. "An NNLO subtraction formalism in hadron collisions and its application to Higgs boson production at the LHC". In: *Phys. Rev. Lett.* 98 (2007), p. 222002. DOI: 10.1103/PhysRevLett.98.222002. arXiv: hep-ph/0703012 [hep-ph].

[29] Leandro Cieri et al. "Higgs boson production at the LHC using the q_T subtraction formalism at N^{3}LO QCD". In: *JHEP* 02 (2019), p. 096. DOI: 10.1007/JHEP02(2019)096. arXiv: 1807.11501 [hep-ph].

[30] Stefano Catani et al. "Diphoton production at hadron colliders: a fully-differential QCD calculation at NNLO". In: *Phys. Rev. Lett.* 108 (2012). [Erratum: Phys. Rev. Lett.117,no.8,089901(2 p. 072001. DOI: 10.1103/PhysRevLett.108.072001,10.1103/PhysRevLett.117.089901. arXiv: 1110.2375 [hep-ph].

[31] Stefano Catani et al. "Diphoton production at the LHC: a QCD study up to NNLO". In: *JHEP* 04 (2018), p. 142. DOI: 10.1007/JHEP04(2018)142. arXiv: 1802.02095 [hep-ph].

[32] Giancarlo Ferrera, Massimiliano Grazzini, and Francesco Tramontano. "Associated WH production at hadron colliders: a fully exclusive QCD calculation at NNLO". In: *Phys. Rev. Lett.* 107 (2011), p. 152003. DOI: 10.1103/PhysRevLett.107.152003. arXiv: 1107.1164 [hep-ph].

[33] Massimiliano Grazzini et al. "$Z\gamma$ production at hadron colliders in NNLO QCD". In: *Phys. Lett.* B731 (2014), pp. 204–207. DOI: 10.1016/j.physletb.2014.02.037. arXiv: 1309.7000 [hep-ph].

[34] Giancarlo Ferrera, Massimiliano Grazzini, and Francesco Tramontano. "Associated ZH production at hadron colliders: the fully differential NNLO QCD calculation". In: *Phys. Lett.* B740 (2015), pp. 51–55. DOI: 10.1016/j.physletb.2014.11.040. arXiv: 1407.4747 [hep-ph].

[35] Massimiliano Grazzini, Stefan Kallweit, and Dirk Rathlev. "$W\gamma$ and $Z\gamma$ production at the LHC in NNLO QCD". In: *JHEP* 07 (2015), p. 085. DOI: 10.1007/JHEP07(2015)085. arXiv: 1504.01330 [hep-ph].

[36] F. Cascioli et al. "ZZ production at hadron colliders in NNLO QCD". In: *Phys. Lett.* B735 (2014), pp. 311–313. DOI: 10.1016/j.physletb.2014.06.056. arXiv: 1405.2219 [hep-ph].

[37] T. Gehrmann et al. "W^+W^- Production at Hadron Colliders in Next to Next to Leading Order QCD". In: *Phys. Rev. Lett.* 113.21 (2014), p. 212001. DOI: 10.1103/PhysRevLett.113.212001. arXiv: 1408.5243 [hep-ph].

[38] Massimiliano Grazzini, Stefan Kallweit, and Dirk Rathlev. "ZZ production at the LHC: fiducial cross sections and distributions in NNLO QCD". In: *Phys. Lett.* B750 (2015), pp. 407–410. DOI: 10.1016/j.physletb.2015.09.055. arXiv: 1507.06257 [hep-ph].

[39] Massimiliano Grazzini et al. "W^+W production at the LHC: fiducial cross sections and distributions in NNLO QCD". In: *JHEP* 08 (2016), p. 140. DOI: 10.1007/JHEP08(2016)140. arXiv: 1605.02716 [hep-ph].

[40] Massimiliano Grazzini et al. "$W^\pm Z$ production at hadron colliders in NNLO QCD". In: *Phys. Lett.* B761 (2016), pp. 179–183. DOI: 10.1016/j.physletb.2016.08.017. arXiv: 1604.08576 [hep-ph].

[41] Massimiliano Grazzini et al. "$W^\pm Z$ production at the LHC: fiducial cross sections and distributions in NNLO QCD". In: *JHEP* 05 (2017), p. 139. DOI: 10.1007/JHEP05(2017)139. arXiv: 1703.09065 [hep-ph].

[42] Stefan Kallweit and Marius Wiesemann. "ZZ production at the LHC: NNLO predictions for $2\ell 2\nu$ and 4ℓ signatures". In: *Phys. Lett.* B786 (2018), pp. 382–389. DOI: 10.1016/j.physletb.2018.10.016. arXiv: 1806.05941 [hep-ph].

[43] Daniel de Florian et al. "Differential Higgs Boson Pair Production at Next-to-Next-to-Leading Order in QCD". In: *JHEP* 09 (2016), p. 151. DOI: 10.1007/JHEP09(2016)151. arXiv: 1606.09519 [hep-ph].

[44] Hua Xing Zhu et al. "Transverse-momentum resummation for top-quark pairs at hadron colliders". In: *Phys. Rev. Lett.* 110.8 (2013), p. 082001. DOI: 10.1103/PhysRevLett.110.082001. arXiv: 1208.5774 [hep-ph].

[45] Hai Tao Li et al. "Top quark pair production at small transverse momentum in hadronic collisions". In: *Phys. Rev.* D88 (2013), p. 074004. DOI: 10.1103/PhysRevD.88.074004. arXiv: 1307.2464 [hep-ph].

[46] Stefano Catani, Massimiliano Grazzini, and A. Torre. "Transverse-momentum resummation for heavy-quark hadroproduction". In: *Nucl. Phys.* B890 (2014), pp. 518–538. DOI: 10.1016/j.nuclphysb.2014.11.019. arXiv: 1408.4564 [hep-ph].

[47] Rene Angeles-Martinez, Micha Czakon, and Sebastian Sapeta. "NNLO soft function for top quark pair production at small transverse momentum". In: *JHEP* 10 (2018), p. 201. DOI: 10.1007/JHEP10(2018)201. arXiv: 1809.01459 [hep-ph].

[48] S. Catani, S. Devoto, M. Grazzini, J. Mazzitelli, in preparation.

[49] Roberto Bonciani et al. "The q_T subtraction method for top quark production at hadron colliders". In: *Eur. Phys. J.* C75.12 (2015), p. 581. DOI: 10.1140/epjc/s10052-015-3793-y. arXiv: 1508.03585 [hep-ph].

[50] Stefano Catani et al. "Top-quark pair hadroproduction at next-to-next-to-leading order in QCD". In: *Phys. Rev.* D99.5 (2019), p. 051501. DOI: 10.1103/PhysRevD.99.051501. arXiv: 1901.04005 [hep-ph].

[51] Stefano Catani et al. "Top-quark pair production at the LHC: Fully differential QCD predictions at NNLO". In: *JHEP* 07 (2019), p. 100. DOI: 10.1007/JHEP07(2019)100. arXiv: 1906.06535 [hep-ph].

[52] Daniel de Florian, Germán F. R. Sborlini, and Germán Rodrigo. "QED corrections to the AltarelliParisi splitting functions". In: *Eur. Phys. J.* C76.5 (2016), p. 282. DOI: 10.1140/epjc/s10052-016-4131-8. arXiv: 1512.00612 [hep-ph].

[53] S. Jadach and M. Skrzypek. "QED challenges at FCC-ee precision measurements". In: *Eur. Phys. J.* C79.9 (2019), p. 756. DOI: 10.1140/epjc/s10052-019-7255-9. arXiv: 1903.09895 [hep-ph].

[54] Massimo Alacevich et al. "Muon-electron scattering at NLO". In: *JHEP* 02 (2019), p. 155. DOI: 10.1007/JHEP02(2019)155. arXiv: 1811.06743 [hep-ph].

[55] Luca Barze et al. "Implementation of electroweak corrections in the POWHEG BOX: single W production". In: *JHEP* 04 (2012), p. 037. DOI: 10.1007/JHEP04(2012)037. arXiv: 1202.0465 [hep-ph].

[56] Massimiliano Grazzini, Stefan Kallweit, and Marius Wiesemann. "Fully differential NNLO computations with MATRIX". In: *Eur. Phys. J.* C78.7 (2018), p. 537. DOI: 10.1140/epjc/s10052-018-5771-7. arXiv: 1711.06631 [hep-ph].

[57] Markus A. Ebert and Frank J. Tackmann. "Impact of Isolation and Fiducial Cuts on q_T and N-Jettiness Subtractions". In: (2019). arXiv: 1911.08486 [hep-ph].

[58] Markus A. Ebert et al. "Subleading power rapidity divergences and power corrections for q_T". In: *JHEP* 04 (2019), p. 123. DOI: 10.1007/JHEP04(2019)123. arXiv: 1812.08189 [hep-ph].

[59] Leandro Cieri, Carlo Oleari, and Marco Rocco. "Higher-order power corrections in a transverse-momentum cut for colour-singlet production at NLO". In: *Eur. Phys. J.* C79.10 (2019), p. 852. DOI: 10.1140/epjc/s10052-019-7361-8. arXiv: 1906.09044 [hep-ph].

[60] Stefano Catani, Massimiliano Grazzini, and Hayk Sargsyan. "Azimuthal asymmetries in QCD hard scattering: infrared safe but divergent". In: *JHEP* 06 (2017), p. 017. DOI: 10.1007/JHEP06(2017)017. arXiv: 1703.08468 [hep-ph].

[61] L. Buonocore, P. Nason, and F. Tramontano. "Heavy quark radiation in NLO+PS POWHEG generators". In: *Eur. Phys. J.* C78.2 (2018), p. 151. DOI: 10.1140/epjc/s10052-018-5638-y. arXiv: 1711.06281 [hep-ph].

[62] T. Kinoshita. "Mass singularities of Feynman amplitudes". In: *J. Math. Phys.* 3 (1962), pp. 650–677. DOI: 10.1063/1.1724268.

[63] T. D. Lee and M. Nauenberg. "Degenerate Systems and Mass Singularities". In: *Phys. Rev.* 133 (1964). [,25(1964)], B1549–B1562. DOI: 10.1103/PhysRev.133.B1549.

[64] B. Mele and P. Nason. "The Fragmentation function for heavy quarks in QCD". In: *Nucl. Phys.* B361 (1991). [Erratum: Nucl. Phys.B921,841(2017)], pp. 626–644. DOI: 10.1016/0550-3213(91)90597-Q,10.1016/j.nuclphysb.2017.05.005.

[65] Matteo Cacciari, Mario Greco, and Paolo Nason. "The P(T) spectrum in heavy flavor hadroproduction". In: *JHEP* 05 (1998), p. 007. DOI: 10.1088/1126-6708/1998/05/007. arXiv: hep-ph/9803400 [hep-ph].

[66] Giovanni Ridolfi, Maria Ubiali, and Marco Zaro. "A fragmentation-based study of heavy quark production". In: (2019). arXiv: 1911.01975 [hep-ph].

[67] C. G. Bollini and J. J. Giambiagi. "Dimensional Renormalization: The Number of Dimensions as a Regularizing Parameter". In: *Nuovo Cim.* B12 (1972), pp. 20–26. DOI: 10.1007/BF02895558.

[68] In: ().

[69] R. Keith Ellis, D. A. Ross, and A. E. Terrano. "The Perturbative Calculation of Jet Structure in e+ e- Annihilation". In: *Nucl. Phys.* B178 (1981), pp. 421–456. DOI: 10.1016/0550-3213(81)90165-6.

[70] R. Keith Ellis, W. James Stirling, and B. R. Webber. "QCD and collider physics". In: *Camb. Monogr. Part. Phys. Nucl. Phys. Cosmol.* 8 (1996), pp. 1–435.

[71] Matteo Cacciari et al. "Theoretical predictions for charm and bottom production at the LHC". In: *JHEP* 10 (2012), p. 137. DOI: 10.1007/JHEP10(2012)137. arXiv: 1205.6344 [hep-ph].

[72] Stefano Frixione, Paolo Nason, and Bryan R. Webber. "Matching NLO QCD and parton showers in heavy flavor production". In: *JHEP* 08 (2003), p. 007. DOI: 10.1088/1126-6708/2003/08/007. arXiv: hep-ph/0305252 [hep-ph].

[73] Stefano Frixione, Paolo Nason, and Giovanni Ridolfi. "A Positive-weight next-to-leading-order Monte Carlo for heavy flavour hadroproduction". In: *JHEP* 09 (2007), p. 126. DOI: 10.1088/1126-6708/2007/09/126. arXiv: 0707.3088 [hep-ph].

[74] Simone Alioli et al. "A general framework for implementing NLO calculations in shower Monte Carlo programs: the POWHEG BOX". In: *JHEP* 06 (2010), p. 043. DOI: 10.1007/JHEP06(2010)043. arXiv: 1002.2581 [hep-ph].

[75] Tomá Jeo et al. "An NLO+PS generator for $t\bar{t}$ and Wt production and decay including non-resonant and interference effects". In: *Eur. Phys. J.* C76.12 (2016), p. 691. DOI: 10.1140/epjc/s10052-016-4538-2. arXiv: 1607.04538 [hep-ph].

[76] A. D. Martin et al. “Parton distributions for the LHC”. In: *Eur. Phys. J.* C63 (2009), pp. 189–285. DOI: 10.1140/epjc/s10052-009-1072-5. arXiv: 0901.0002 [hep-ph].

[77] Pavel M. Nadolsky et al. “Implications of CTEQ global analysis for collider observables”. In: *Phys. Rev.* D78 (2008), p. 013004. DOI: 10.1103/PhysRevD.78.013004. arXiv: 0802.0007 [hep-ph].

[78] Richard D. Ball et al. “Parton distributions for the LHC Run II”. In: *JHEP* 04 (2015), p. 040. DOI: 10.1007/JHEP04(2015)040. arXiv: 1410.8849 [hep-ph].

[79] Matteo Cacciari, Gavin P. Salam, and Gregory Soyez. “FastJet User Manual”. In: *Eur. Phys. J.* C72 (2012), p. 1896. DOI: 10.1140/epjc/s10052-012-1896-2. arXiv: 1111.6097 [hep-ph].

[80] Matteo Cacciari, Gavin P. Salam, and Gregory Soyez. “The Anti-k(t) jet clustering algorithm”. In: *JHEP* 04 (2008), p. 063. DOI: 10.1088/1126-6708/2008/04/063. arXiv: 0802.1189 [hep-ph].

[81] P. Nason, S. Dawson, and R. Keith Ellis. “The One Particle Inclusive Differential Cross-Section for Heavy Quark Production in Hadronic Collisions”. In: *Nucl. Phys.* B327 (1989). [Erratum: Nucl. Phys.B335,260(1990)], pp. 49–92. DOI: 10.1016/0550-3213(90)90180-L,10.1016/0550-3213(89)90286-1.

[82] Vardan Khachatryan et al. “Measurement of the B^+ Production Cross Section in pp Collisions at $\sqrt{s} = 7$ TeV”. In: *Phys. Rev. Lett.* 106 (2011), p. 112001. DOI: 10.1103/PhysRevLett.106.112001. arXiv: 1101.0131 [hep-ex].

[83] Georges Aad et al. “Measurement of the b-hadron production cross section using decays to $D^{*}\mu^{-}X$ final states in pp collisions at sqrt(s) = 7 TeV with the ATLAS detector”. In: *Nucl. Phys.* B864 (2012), pp. 341–381. DOI: 10.1016/j.nuclphysb.2012.07.009. arXiv: 1206.3122 [hep-ex].

[84] D. Acosta et al. “Measurement of the J/ψ meson and $b-$hadron production cross sections in $p\bar{p}$ collisions at $\sqrt{s} = 1960$ GeV”. In: *Phys. Rev.* D71 (2005), p. 032001. DOI: 10.1103/PhysRevD.71.032001. arXiv: hep-ex/0412071 [hep-ex].

[85] B. Abbott et al. “The $b\bar{b}$ production cross section and angular correlations in $p\bar{p}$ collisions at $\sqrt{s} = 1.8$ TeV”. In: *Phys. Lett.* B487 (2000), pp. 264–272. DOI: 10.1016/S0370-2693(00)00844-3. arXiv: hep-ex/9905024 [hep-ex].

[86] Vardan Khachatryan et al. “Measurement of $B\bar{B}$ Angular Correlations based on Secondary Vertex Reconstruction at $\sqrt{s} = 7$ TeV”. In: *JHEP* 03 (2011), p. 136. DOI: 10.1007/JHEP03(2011)136. arXiv: 1102.3194 [hep-ex].

[87] Gabor Somogyi, Zoltan Trocsanyi, and Vittorio Del Duca. “A Subtraction scheme for computing QCD jet cross sections at NNLO: Regularization of doubly-real emissions”. In: *JHEP* 01 (2007), p. 070. DOI: 10.1088/1126-6708/2007/01/070. arXiv: hep-ph/0609042 [hep-ph].

[88] Vittorio Del Duca et al. “Higgs boson decay into b-quarks at NNLO accuracy”. In: *JHEP* 04 (2015), p. 036. DOI: 10.1007/JHEP04(2015)036. arXiv: 1501.07226 [hep-ph].

[89] Vittorio Del Duca et al. “Three-Jet Production in Electron-Positron Collisions at Next-to-Next-to-Leading Order Accuracy”. In: *Phys. Rev. Lett.* 117.15 (2016), p. 152004. DOI: 10.1103/PhysRevLett.117.152004. arXiv: 1603.08927 [hep-ph].

[90] Vittorio Del Duca et al. “Jet production in the CoLoRFulNNLO method: event shapes in electron-positron collisions”. In: *Phys. Rev.* D94.7 (2016), p. 074019. DOI: 10.1103/PhysRevD.94.074019. arXiv: 1606.03453 [hep-ph].

[91] M. Czakon. "A novel subtraction scheme for double-real radiation at NNLO". In: *Phys. Lett.* B693 (2010), pp. 259–268. DOI: 10.1016/j.physletb.2010.08.036. arXiv: 1005.0274 [hep-ph].

[92] Fabrizio Caola, Kirill Melnikov, and Raoul Röntsch. "Nested soft-collinear subtractions in NNLO QCD computations". In: *Eur. Phys. J.* C77.4 (2017), p. 248. DOI: 10.1140/epjc/s10052-017-4774-0. arXiv: 1702.01352 [hep-ph].

[93] Matteo Cacciari et al. "Top-pair production at hadron colliders with next-to-next-to-leading logarithmic soft-gluon resummation". In: *Phys. Lett.* B710 (2012), pp. 612–622. DOI: 10.1016/j.physletb.2012.03.013. arXiv: 1111.5869 [hep-ph].

[94] Michal Czakon, David Heymes, and Alexander Mitov. "High-precision differential predictions for top-quark pairs at the LHC". In: *Phys. Rev. Lett.* 116.8 (2016), p. 082003. DOI: 10.1103/PhysRevLett.116.082003. arXiv: 1511.00549 [hep-ph].

[95] Michal Czakon et al. "NNLO QCD predictions for fully-differential top-quark pair production at the Tevatron". In: *JHEP* 05 (2016), p. 034. DOI: 10.1007/JHEP05(2016)034. arXiv: 1601.05375 [hep-ph].

[96] Radja Boughezal et al. "Higgs boson production in association with a jet at next-to-next-to-leading order". In: *Phys. Rev. Lett.* 115.8 (2015), p. 082003. DOI: 10.1103/PhysRevLett.115.082003. arXiv: 1504.07922 [hep-ph].

[97] Fabrizio Caola et al. "NNLO QCD corrections to associated WH production and $H \to b\bar{b}$ decay". In: *Phys. Rev.* D97.7 (2018), p. 074022. DOI: 10.1103/PhysRevD.97.074022. arXiv: 1712.06954 [hep-ph].

[98] Fabrizio Caola, Kirill Melnikov, and Raoul Röntsch. "Analytic results for color-singlet production at NNLO QCD with the nested soft-collinear subtraction scheme". In: *Eur. Phys. J.* C79.5 (2019), p. 386. DOI: 10.1140/epjc/s10052-019-6880-7. arXiv: 1902.02081 [hep-ph].

[99] Arnd Behring and Wojciech Bizo. "Higgs decay into massive b-quarks at NNLO QCD in the nested soft-collinear subtraction scheme". In: *JHEP* 01 (2020), p. 189. DOI: 10.1007/JHEP01(2020)189. arXiv: 1911.11524 [hep-ph].

[100] A. Gehrmann-De Ridder, T. Gehrmann, and E. W. Nigel Glover. "Antenna subtraction at NNLO". In: *JHEP* 09 (2005), p. 056. DOI: 10.1088/1126-6708/2005/09/056. arXiv: hep-ph/0505111 [hep-ph].

[101] X. Chen et al. "Precise QCD predictions for the production of Higgs + jet final states". In: *Phys. Lett.* B740 (2015), pp. 147–150. DOI: 10.1016/j.physletb.2014.11.021. arXiv: 1408.5325 [hep-ph].

[102] J Currie, E. W. N. Glover, and J Pires. "Next-to-Next-to Leading Order QCD Predictions for Single Jet Inclusive Production at the LHC". In: *Phys. Rev. Lett.* 118.7 (2017), p. 072002. DOI: 10.1103/PhysRevLett.118.072002. arXiv: 1611.01460 [hep-ph].

[103] James Currie et al. "Precise predictions for dijet production at the LHC". In: *Phys. Rev. Lett.* 119.15 (2017), p. 152001. DOI: 10.1103/PhysRevLett.119.152001. arXiv: 1705.10271 [hep-ph].

[104] A. Gehrmann-De Ridder et al. "Next-to-Next-to-Leading-Order QCD Corrections to the Transverse Momentum Distribution of Weak Gauge Bosons". In: *Phys. Rev. Lett.* 120.12 (2018), p. 122001. DOI: 10.1103/PhysRevLett.120.122001. arXiv: 1712.07543 [hep-ph].

[105] Wojciech Bizo et al. "Fiducial distributions in Higgs and Drell-Yan production at N^{3}LL+NNLO". In: *JHEP* 12 (2018), p. 132. DOI: 10.1007/JHEP12(2018)132. arXiv: 1805.05916 [hep-ph].

[106] R. Gauld et al. "Associated production of a Higgs boson decaying into bottom quarks and a weak vector boson decaying leptonically at NNLO in QCD". In: *JHEP* 10 (2019), p. 002. DOI: 10.1007/JHEP10(2019)002. arXiv: 1907.05836 [hep-ph].

[107] L. Magnea et al. "Local analytic sector subtraction at NNLO". In: *JHEP* 12 (2018). [Erratum: JHEP06,013(2019)], p. 107. DOI: 10.1007/JHEP06(2019)013, 10.1007/JHEP12(2018)107. arXiv: 1806.09570 [hep-ph].

[108] Franz Herzog. "Geometric IR subtraction for final state real radiation". In: *JHEP* 08 (2018), p. 006. DOI: 10.1007/JHEP08(2018)006. arXiv: 1804.07949 [hep-ph].

[109] Stefano Catani. "The Singular behavior of QCD amplitudes at two loop order". In: *Phys. Lett.* B427 (1998), pp. 161–171. DOI: 10.1016/S0370-2693(98)00332-3. arXiv: hep-ph/9802439 [hep-ph].

[110] Thomas Becher and Matthias Neubert. "On the Structure of Infrared Singularities of Gauge-Theory Amplitudes". In: *JHEP* 06 (2009). [Erratum: JHEP11,024(2013)], p. 081. DOI: 10.1088/1126-6708/2009/06/081, 10.1007/JHEP11(2013)024. arXiv: 0903.1126 [hep-ph].

[111] W. T. Giele and E. W. Nigel Glover. "Higher order corrections to jet cross-sections in e+ e- annihilation". In: *Phys. Rev.* D46 (1992), pp. 1980–2010. DOI: 10.1103/PhysRevD.46.1980.

[112] W. T. Giele, E. W. Nigel Glover, and David A. Kosower. "Higher order corrections to jet cross-sections in hadron colliders". In: *Nucl. Phys.* B403 (1993), pp. 633–670. DOI: 10.1016/0550-3213(93)90365-V. arXiv: hep-ph/9302225 [hep-ph].

[113] Stephane Keller and Eric Laenen. "Next-to-leading order cross-sections for tagged reactions". In: *Phys. Rev.* D59 (1999), p. 114004. DOI: 10.1103/PhysRevD.59.114004. arXiv: hep-ph/9812415 [hep-ph].

[114] Radja Boughezal et al. "*W*-boson production in association with a jet at next-to-next-to-leading order in perturbative QCD". In: *Phys. Rev. Lett.* 115.6 (2015), p. 062002. DOI: 10.1103/PhysRevLett.115.062002. arXiv: 1504.02131 [hep-ph].

[115] Jonathan Gaunt et al. "N-jettiness Subtractions for NNLO QCD Calculations". In: *JHEP* 09 (2015), p. 058. DOI: 10.1007/JHEP09(2015)058. arXiv: 1505.04794 [hep-ph].

[116] S. Dawson. "Radiative corrections to Higgs boson production". In: *Nucl. Phys.* B359 (1991), pp. 283–300. DOI: 10.1016/0550-3213(91)90061-2.

[117] A. Djouadi, M. Spira, and P. M. Zerwas. "Production of Higgs bosons in proton colliders: QCD corrections". In: *Phys. Lett.* B264 (1991), pp. 440–446. DOI: 10.1016/0370-2693(91)90375-Z.

[118] Radja Boughezal et al. "Z-boson production in association with a jet at next-to-next-to-leading order in perturbative QCD". In: *Phys. Rev. Lett.* 116.15 (2016), p. 152001. DOI: 10.1103/PhysRevLett.116.152001. arXiv: 1512.01291 [hep-ph].

[119] Radja Boughezal, Xiaohui Liu, and Frank Petriello. "W-boson plus jet differential distributions at NNLO in QCD". In: *Phys. Rev.* D94.11 (2016), p. 113009. DOI: 10.1103/PhysRevD.94.113009. arXiv: 1602.06965 [hep-ph].

[120] John C. Collins, Davison E. Soper, and George F. Sterman. "Transverse Momentum Distribution in Drell-Yan Pair and W and Z Boson Production". In: *Nucl. Phys.* B250 (1985), pp. 199–224. DOI: 10.1016/0550-3213(85)90479-1.

[121] Giuseppe Bozzi et al. "Transverse-momentum resummation and the spectrum of the Higgs boson at the LHC". In: *Nucl. Phys.* B737 (2006), pp. 73–120. DOI: 10.1016/j.nuclphysb.2005.12.022. arXiv: hep-ph/0508068 [hep-ph].

[122] Giuseppe Bozzi et al. “Higgs boson production at the LHC: Transverse-momentum resummation and rapidity dependence”. In: *Nucl. Phys.* B791 (2008), pp. 1–19. DOI: 10.1016/j.nuclphysb.2007.09.034. arXiv: 0705.3887 [hep-ph].

[123] Stefano Catani and Massimiliano Grazzini. “QCD transverse-momentum resummation in gluon fusion processes”. In: *Nucl. Phys.* B845 (2011), pp. 297–323. DOI: 10.1016/j.nuclphysb.2010.12.007. arXiv: 1011.3918 [hep-ph].

[124] Sonny Mantry and Frank Petriello. “Factorization and Resummation of Higgs Boson Differential Distributions in Soft-Collinear Effective Theory”. In: *Phys. Rev.* D81 (2010), p. 093007. DOI: 10.1103/PhysRevD.81.093007. arXiv: 0911.4135 [hep-ph].

[125] Sonny Mantry and Frank Petriello. “Transverse Momentum Distributions from Effective Field Theory with Numerical Results”. In: *Phys. Rev.* D83 (2011), p. 053007. DOI: 10.1103/PhysRevD.83.053007. arXiv: 1007.3773 [hep-ph].

[126] Thomas Gehrmann, Thomas Lübbert, and Li Lin Yang. “Transverse parton distribution functions at next-to-next-to-leading order: the quark-to-quark case”. In: *Phys. Rev. Lett.* 109 (2012), p. 242003. DOI: 10.1103/PhysRevLett.109.242003. arXiv: 1209.0682 [hep-ph].

[127] Thomas Becher and Matthias Neubert. “Drell-Yan Production at Small q_T, Transverse Parton Distributions and the Collinear Anomaly”. In: *Eur. Phys. J.* C71 (2011), p. 1665. DOI: 10.1140/epjc/s10052-011-1665-7. arXiv: 1007.4005 [hep-ph].

[128] Markus A. Ebert and Frank J. Tackmann. “Resummation of Transverse Momentum Distributions in Distribution Space”. In: *JHEP* 02 (2017), p. 110. DOI: 10.1007/JHEP02(2017)110. arXiv: 1611.08610 [hep-ph].

[129] Stefano Catani, Daniel de Florian, and Massimiliano Grazzini. “Universality of nonleading logarithmic contributions in transverse momentum distributions”. In: *Nucl. Phys.* B596 (2001), pp. 299–312. DOI: 10.1016/S0550-3213(00)00617-9. arXiv: hep-ph/0008184 [hep-ph].

[130] Pavel M. Nadolsky et al. “Gluon-gluon contributions to the production of continuum diphoton pairs at hadron colliders”. In: *Phys. Rev.* D76 (2007), p. 013008. DOI: 10.1103/PhysRevD.76.013008. arXiv: hep-ph/0702003 [HEP-PH].

[131] Guido Altarelli and G. Parisi. “Asymptotic Freedom in Parton Language”. In: *Nucl. Phys.* B126 (1977), pp. 298–318. DOI: 10.1016/0550-3213(77)90384-4.

[132] G. Curci, W. Furmanski, and R. Petronzio. “Evolution of Parton Densities Beyond Leading Order: The Nonsinglet Case”. In: *Nucl. Phys.* B175 (1980), pp. 27–92. DOI: 10.1016/0550-3213(80)90003-6.

[133] W. Furmanski and R. Petronzio. “Singlet Parton Densities Beyond Leading Order”. In: *Phys. Lett.* 97B (1980), pp. 437–442. DOI: 10.1016/0370-2693(80)90636-X.

[134] Stefano Catani et al. “Vector boson production at hadron colliders: hard-collinear coefficients at the NNLO”. In: *Eur. Phys. J.* C72 (2012), p. 2195. DOI: 10.1140/epjc/s10052-012-2195-7. arXiv: 1209.0158 [hep-ph].

[135] S. Catani and M. Grazzini. “Higgs Boson Production at Hadron Colliders: Hard-Collinear Coefficients at the NNLO”. In: *Eur. Phys. J.* C72 (2012). [Erratum: Eur. Phys. J. C72, 2132 (2012)], p. 2013. DOI: 10.1140/epjc/s10052-012-2013-2,10.1140/epjc/s10052-012-2132-9. arXiv: 1106.4652 [hep-ph].

[136] Stefano Catani et al. “Universality of transverse-momentum resummation and hard factors at the NNLO”. In: *Nucl. Phys.* B881 (2014), pp. 414–443. DOI: 10.1016/j.nuclphysb.2014.02.011. arXiv: 1311.1654 [hep-ph].

[137] S. Catani and M. H. Seymour. "A General algorithm for calculating jet cross-sections in NLO QCD". In: *Nucl. Phys.* B485 (1997). [Erratum: Nucl. Phys.B510,503(1998)], pp. 291–419. DOI: 10.1016/S0550-3213(96)00589-5, 10.1016/S0550-3213(98)81022-5. arXiv: hep-ph/9605323 [hep-ph].

[138] Alexander Mitov, George F. Sterman, and Ilmo Sung. "Computation of the Soft Anomalous Dimension Matrix in Coordinate Space". In: *Phys. Rev.* D82 (2010), p. 034020. DOI: 10.1103/PhysRevD.82.034020. arXiv: 1005.4646 [hep-ph].

[139] Andrea Ferroglia et al. "Two-loop divergences of scattering amplitudes with massive partons". In: *Phys. Rev. Lett.* 103 (2009), p. 201601. DOI: 10.1103/PhysRevLett.103.201601. arXiv: 0907.4791 [hep-ph].

[140] Andrea Ferroglia et al. "Two-loop divergences of massive scattering amplitudes in non-abelian gauge theories". In: *JHEP* 11 (2009), p. 062. DOI: 10.1088/1126-6708/2009/11/062. arXiv: 0908.3676 [hep-ph].

[141] Aneesh Manohar et al. "How bright is the proton? A precise determination of the photon parton distribution function". In: *Phys. Rev. Lett.* 117.24 (2016), p. 242002. DOI: 10.1103/PhysRevLett.117.242002. arXiv: 1607.04266 [hep-ph].

[142] Aneesh V. Manohar et al. "The Photon Content of the Proton". In: *JHEP* 12 (2017), p. 046. DOI: 10.1007/JHEP12(2017)046. arXiv: 1708.01256 [hep-ph].

[143] Yuri L. Dokshitzer. "Calculation of the Structure Functions for Deep Inelastic Scattering and e+ e- Annihilation by Perturbation Theory in Quantum Chromodynamics." In: *Sov. Phys. JETP* 46 (1977). [Zh. Eksp. Teor. Fiz.73,1216(1977)], pp. 641–653.

[144] V. N. Gribov and L. N. Lipatov. "Deep inelastic e p scattering in perturbation theory". In: *Sov. J. Nucl. Phys.* 15 (1972). [Yad. Fiz.15,781(1972)], pp. 438–450.

[145] Stefan Dittmaier and Max Huber. "Radiative corrections to the neutral-current Drell-Yan process in the Standard Model and its minimal supersymmetric extension". In: *JHEP* 01 (2010), p. 060. DOI: 10.1007/JHEP01(2010)060. arXiv: 0911.2329 [hep-ph].

[146] Daniel de Florian, Germán F. R. Sborlini, and Germán Rodrigo. "Two-loop QED corrections to the Altarelli-Parisi splitting functions". In: *JHEP* 10 (2016), p. 056. DOI: 10.1007/JHEP10(2016)056. arXiv: 1606.02887 [hep-ph].

[147] Leandro Cieri, Giancarlo Ferrera, and German F. R. Sborlini. "Combining QED and QCD transverse-momentum resummation for Z boson production at hadron colliders". In: *JHEP* 08 (2018), p. 165. DOI: 10.1007/JHEP08(2018)165. arXiv: 1805.11948 [hep-ph].

[148] S. Catani, E. D'Emilio, and L. Trentadue. "The Gluon Form-factor to Higher Orders: Gluon Gluon Annihilation at Small Q^-transverse". In: *Phys. Lett.* B211 (1988), pp. 335–342. DOI: 10.1016/0370-2693(88)90912-4.

[149] Wolfram Research, Inc. *Mathematica, Version 12.0*. URL: https://www.wolfram.com/mathematica.

[150] D. B. Clark, E. Godat, and F. I. Olness. "ManeParse : A Mathematica reader for Parton Distribution Functions". In: *Comput. Phys. Commun.* 216 (2017), pp. 126–137. DOI: 10.1016/j.cpc.2017.03.004. arXiv: 1605.08012 [hep-ph].

[151] G. Peter Lepage. "A New Algorithm for Adaptive Multidimensional Integration". In: *J. Comput. Phys.* 27 (1978), p. 192. DOI: 10.1016/0021-9991(78)90004-9.

[152] T. Hahn. "CUBA: A Library for multidimensional numerical integration". In: *Comput. Phys. Commun.* 168 (2005), pp. 78–95. DOI: 10.1016/j.cpc.2005.01.010. arXiv: hep-ph/0404043 [hep-ph].

[153] T. Hahn. "Concurrent Cuba". In: *Comput. Phys. Commun.* 207 (2016), pp. 341–349. DOI: 10.1016/j.cpc.2016.05.012.

[154] John M. Campbell, R. Keith Ellis, and Ciaran Williams. "Vector boson pair production at the LHC". In: *JHEP* 07 (2011), p. 018. DOI: 10.1007/JHEP07(2011)018. arXiv: 1105.0020 [hep-ph].

[155] John M. Campbell, R. Keith Ellis, and Walter T. Giele. "A Multi-Threaded Version of MCFM". In: *Eur. Phys. J.* C75.6 (2015), p. 246. DOI: 10.1140/epjc/s10052-015-3461-2. arXiv: 1503.06182 [physics.comp-ph].

[156] G. Passarino and M. J. G. Veltman. "One Loop Corrections for e+ e- Annihilation Into mu+ mu- in the Weinberg Model". In: *Nucl. Phys.* B160 (1979), pp. 151–207. DOI: 10.1016/0550-3213(79)90234-7.

[157] Giovanni Ossola, Costas G. Papadopoulos, and Roberto Pittau. "Reducing full one-loop amplitudes to scalar integrals at the integrand level". In: *Nucl. Phys.* B763 (2007), pp. 147–169. DOI: 10.1016/j.nuclphysb.2006.11.012. arXiv: hep-ph/0609007 [hep-ph].

[158] Giovanni Ossola, Costas G. Papadopoulos, and Roberto Pittau. "CutTools: A Program implementing the OPP reduction method to compute one-loop amplitudes". In: *JHEP* 03 (2008), p. 042. DOI: 10.1088/1126-6708/2008/03/042. arXiv: 0711.3596 [hep-ph].

[159] P. Mastrolia et al. "Scattering AMplitudes from Unitarity-based Reduction Algorithm at the Integrand-level". In: *JHEP* 08 (2010), p. 080. DOI: 10.1007/JHEP08(2010)080. arXiv: 1006.0710 [hep-ph].

[160] Tiziano Peraro. "Ninja: Automated Integrand Reduction via Laurent Expansion for One-Loop Amplitudes". In: *Comput. Phys. Commun.* 185 (2014), pp. 2771–2797. DOI: 10.1016/j.cpc.2014.06.017. arXiv: 1403.1229 [hep-ph].

[161] T. Hahn and M. Perez-Victoria. "Automatized one loop calculations in four-dimensions and D-dimensions". In: *Comput. Phys. Commun.* 118 (1999), pp. 153–165. DOI: 10.1016/S0010-4655(98)00173-8. arXiv: hep-ph/9807565 [hep-ph].

[162] T. Binoth et al. "Golem95: A Numerical program to calculate one-loop tensor integrals with up to six external legs". In: *Comput. Phys. Commun.* 180 (2009), pp. 2317–2330. DOI: 10.1016/j.cpc.2009.06.024. arXiv: 0810.0992 [hep-ph].

[163] G. Cullen et al. "Golem95C: A library for one-loop integrals with complex masses". In: *Comput. Phys. Commun.* 182 (2011), pp. 2276–2284. DOI: 10.1016/j.cpc.2011.05.015. arXiv: 1101.5595 [hep-ph].

[164] A. van Hameren. "OneLOop: For the evaluation of one-loop scalar functions". In: *Comput. Phys. Commun.* 182 (2011), pp. 2427–2438. DOI: 10.1016/j.cpc.2011.06.011. arXiv: 1007.4716 [hep-ph].

[165] R. Keith Ellis and Giulia Zanderighi. "Scalar one-loop integrals for QCD". In: *JHEP* 02 (2008), p. 002. DOI: 10.1088/1126-6708/2008/02/002. arXiv: 0712.1851 [hep-ph].

[166] Ansgar Denner, Stefan Dittmaier, and Lars Hofer. "Collier: a fortran-based Complex One-Loop LIbrary in Extended Regularizations". In: *Comput. Phys. Commun.* 212 (2017), pp. 220–238. DOI: 10.1016/j.cpc.2016.10.013. arXiv: 1604.06792 [hep-ph].

[167] S. Actis et al. "Recursive generation of one-loop amplitudes in the Standard Model". In: *JHEP* 04 (2013), p. 037. DOI: 10.1007/JHEP04(2013)037. arXiv: 1211.6316 [hep-ph].

[168] Stefano Actis et al. "RECOLA: REcursive Computation of One-Loop Amplitudes". In: *Comput. Phys. Commun.* 214 (2017), pp. 140–173. DOI: 10.1016/j.cpc.2017.01.004. arXiv: 1605.01090 [hep-ph].

[169] Gavin Cullen et al. "Automated One-Loop Calculations with GoSam". In: *Eur. Phys. J.* C72 (2012), p. 1889. DOI: 10.1140/epjc/s10052-012-1889-1. arXiv: 1111.2034 [hep-ph].

[170] Gavin Cullen et al. "GOSAM-2.0: a tool for automated one-loop calculations within the Standard Model and beyond". In: *Eur. Phys. J.* C74.8 (2014), p. 3001. DOI: 10.1140/epjc/s10052-014-3001-5. arXiv: 1404.7096 [hep-ph].

[171] J. Alwall et al. "The automated computation of tree-level and next-to-leading order differential cross sections, and their matching to parton shower simulations". In: *JHEP* 07 (2014), p. 079. DOI: 10.1007/JHEP07(2014)079. arXiv: 1405.0301 [hep-ph].

[172] R. Frederix et al. "The automation of next-to-leading order electroweak calculations". In: *JHEP* 07 (2018), p. 185. DOI: 10.1007/JHEP07(2018)185. arXiv: 1804.10017 [hep-ph].

[173] Fabio Cascioli, Philipp Maierhofer, and Stefano Pozzorini. "Scattering Amplitudes with Open Loops". In: *Phys. Rev. Lett.* 108 (2012), p. 111601. DOI: 10.1103/PhysRevLett.108.111601. arXiv: 1111.5206 [hep-ph].

[174] Steve Honeywell et al. "NLOX, a one-loop provider for Standard Model processes". In: (2018). arXiv: 1812.11925 [hep-ph].

[175] *Les Houches 2017: Physics at TeV Colliders Standard Model Working Group Report*. 2018. arXiv: 1803.07977 [hep-ph]. URL: http://lss.fnal.gov/archive/2018/conf/fermilab-conf-18-122-cd-t.pdf.

[176] Gerard 't Hooft. "Renormalization of Massless Yang-Mills Fields". In: *Nucl. Phys.* B33 (1971), pp. 173–199. DOI: 10.1016/0550-3213(71)90395-6.

[177] Gerard 't Hooft. "Renormalizable Lagrangians for Massive Yang-Mills Fields". In: *Nucl. Phys.* B35 (1971). [,201(1971)], pp. 167–188. DOI: 10.1016/0550-3213(71)90139-8.

[178] Benjamin W. Lee. "Renormalization of Gauge Theories: Unbroken and Broken". In: *Phys. Rev.* D9 (1974), pp. 933–946. DOI: 10.1103/PhysRevD.9.933.

[179] C. Becchi, A. Rouet, and R. Stora. "Renormalization of the Abelian Higgs-Kibble Model". In: *Commun. Math. Phys.* 42 (1975), pp. 127–162. DOI: 10.1007/BF01614158.

[180] D. A. Ross and J. C. Taylor. "Renormalization of a unified theory of weak and electromagnetic interactions". In: *Nucl. Phys.* B51 (1973). [Erratum: Nucl. Phys.B58,643(1973)], pp. 125–144. DOI: 10.1016/0550-3213(73)90608-1,10.1016/0550-3213(73)90505-1.

[181] A. Sirlin. "Radiative Corrections in the SU(2)-L x U(1) Theory: A Simple Renormalization Framework". In: *Phys. Rev.* D22 (1980), pp. 971–981. DOI: 10.1103/PhysRevD.22.971.

[182] K. I. Aoki et al. "Electroweak Theory. Framework of On-Shell Renormalization and Study of Higher Order Effects". In: *Prog. Theor. Phys. Suppl.* 73 (1982), pp. 1–225. DOI: 10.1143/PTPS.73.1.

[183] M. Bohm, H. Spiesberger, and W. Hollik. "On the One Loop Renormalization of the Electroweak Standard Model and Its Application to Leptonic Processes". In: *Fortsch. Phys.* 34 (1986), pp. 687–751. DOI: 10.1002/prop.19860341102.

[184] S. Schael et al. "Precision electroweak measurements on the Z resonance". In: *Phys. Rept.* 427 (2006), pp. 257–454. DOI: 10.1016/j.physrep.2005.12.006. arXiv: hep-ex/0509008 [hep-ex].

[185] S. Eidelman and F. Jegerlehner. "Hadronic contributions to g-2 of the leptons and to the effective fine structure constant alpha (M(z)**2)". In: *Z. Phys.* C67 (1995), pp. 585–602. DOI: 10.1007/BF01553984. arXiv: hep-ph/9502298 [hep-ph].

[186] Ansgar Denner. "Techniques for calculation of electroweak radiative corrections at the one loop level and results for W physics at LEP-200". In: *Fortsch. Phys.* 41 (1993), pp. 307–420. DOI: 10.1002/prop.2190410402. arXiv: 0709.1075 [hep-ph].

[187] W. J. Marciano and A. Sirlin. "Radiative Corrections to Neutrino Induced Neutral Current Phenomena in the SU(2)-L x U(1) Theory". In: *Phys. Rev.* D22 (1980). [Erratum: Phys. Rev.D31,213(1985)], p. 2695. DOI: 10.1103/PhysRevD.31.213,10.1103/PhysRevD.22.2695.

[188] D. A. Ross and M. J. G. Veltman. "Neutral Currents in Neutrino Experiments". In: *Nucl. Phys.* B95 (1975), pp. 135–147. DOI: 10.1016/0550-3213(75)90485-X.

[189] M. J. G. Veltman. "Limit on Mass Differences in the Weinberg Model". In: *Nucl. Phys.* B123 (1977), pp. 89–99. DOI: 10.1016/0550-3213(77)90342-X.

[190] Michael S. Chanowitz, M. A. Furman, and I. Hinchliffe. "Weak Interactions of Ultraheavy Fermions". In: *Phys. Lett.* 78B (1978), p. 285. DOI: 10.1016/0370-2693(78)90024-2.

[191] Stefan Dittmaier and Michael Krämer. "Electroweak radiative corrections to W boson production at hadron colliders". In: *Phys. Rev.* D65 (2002), p. 073007. DOI: 10.1103/PhysRevD.65.073007. arXiv: hep-ph/0109062 [hep-ph].

[192] Michael E. Peskin and Daniel V. Schroeder. *An Introduction to quantum field theory*. Reading, USA: Addison-Wesley, 1995. ISBN: 9780201503975, 0201503972. URL: http://www.slac.stanford.edu/~mpeskin/QFT.html.

[193] Ansgar Denner et al. "Predictions for all processes e+ e- —> 4 fermions + gamma". In: *Nucl. Phys.* B560 (1999), pp. 33–65. DOI: 10.1016/S0550-3213(99)00437-X. arXiv: hep-ph/9904472 [hep-ph].

[194] Wim Beenakker et al. "The Fermion loop scheme for finite width effects in e^+e^- annihilation into four fermions". In: *Nucl. Phys.* B500 (1997), pp. 255–298. DOI: 10.1016/S0550-3213(97)00316-7. arXiv: hep-ph/9612260 [hep-ph].

[195] Stefan Dittmaier and Markus Roth. "LUSIFER: A LUcid approach to six FERmion production". In: *Nucl. Phys.* B642 (2002), pp. 307–343. DOI: 10.1016/S0550-3213(02)00640-5. arXiv: hep-ph/0206070 [hep-ph].

[196] Y. Kurihara, D. Perret-Gallix, and Y. Shimizu. "e+ e- —> e- anti-electron-neutrino u anti-d from LEP to linear collider energies". In: *Phys. Lett.* B349 (1995), pp. 367–374. DOI: 10.1016/0370-2693(95)00298-Y. arXiv: hep-ph/9412215 [hep-ph].

[197] Ansgar Denner et al. "Electroweak corrections to charged-current e+ e- —> 4 fermion processes: Technical details and further results". In: *Nucl. Phys.* B724 (2005). [Erratum: Nucl. Phys.B854,504(2012)], pp. 247–294. DOI: 10.1016/j.nuclphysb.2011.09.001, 10.1016/j.nuclphysb.2005.06.033. arXiv: hep-ph/0505042 [hep-ph].

[198] Ansgar Denner and S. Dittmaier. "The Complex-mass scheme for perturbative calculations with unstable particles". In: *Nucl. Phys. Proc. Suppl.* 160 (2006). [,22(2006)], pp. 22–26. DOI: 10.1016/j.nuclphysbps.2006.09.025. arXiv: hep-ph/0605312 [hep-ph].

[199] Ansgar Denner and Stefan Dittmaier. *Electroweak Radiative Corrections for Collider Physics*. 2019. arXiv: 1912.06823 [hep-ph].

[200] A. Sirlin. "Theoretical considerations concerning the Z0 mass". In: *Phys. Rev. Lett.* 67 (1991), pp. 2127–2130. DOI: 10.1103/PhysRevLett.67.2127.

[201] R. E. Cutkosky. "Singularities and discontinuities of Feynman amplitudes". In: *J. Math. Phys.* 1 (1960), pp. 429–433. DOI: 10.1063/1.1703676.

[202] D. Yu. Bardin et al. "Energy Dependent Width Effects in e+ e- Annihilation Near the Z Boson Pole". In: *Phys. Lett.* B206 (1988), pp. 539–542. DOI: 10.1016/0370-2693(88)91627-9.

[203] A. D. Martin et al. "Parton distributions incorporating QED contributions". In: *Eur. Phys. J.* C39 (2005), pp. 155–161. DOI: 10.1140/epjc/s2004-02088-7. arXiv: hep-ph/0411040 [hep-ph].

[204] A. Andonov et al. "SANCscope - v.1.00". In: *Comput. Phys. Commun.* 174 (2006). [Erratum: Comput. Phys. Commun.177,623(2007)], pp. 481–517. DOI: 10.1016/j.cpc.2005.12.006,10.1016/j.cpc.2007.06.010. arXiv: hep-ph/0411186 [hep-ph].

[205] W. L. van Neerven. "Dimensional Regularization of Mass and Infrared Singularities in Two Loop On-shell Vertex Functions". In: *Nucl. Phys.* B268 (1986), pp. 453–488. DOI: 10.1016/0550-3213(86)90165-3.

[206] A. Devoto et al. "Analytic Calculation of the Fourth Order Quantum Chromodynamic Contribution to the Nonsinglet Quark Longitudinal Structure Function". In: *Phys. Rev.* D30 (1984), p. 541. DOI: 10.1103/PhysRevD.30.541.

[207] W. Beenakker et al. "QCD Corrections to Heavy Quark Production in p anti-p Collisions". In: *Phys. Rev.* D40 (1989), pp. 54–82. DOI: 10.1103/PhysRevD.40.54.

[208] Roberto Bonciani et al. "Two-Loop Master Integrals for the mixed EW-QCD virtual corrections to Drell-Yan scattering". In: *JHEP* 09 (2016), p. 091. DOI: 10.1007/JHEP09(2016)091. arXiv: 1604.08581 [hep-ph].

[209] Matthias Heller, Andreas von Manteuffel, and Robert M. Schabinger. "Multiple polylogarithms with algebraic arguments and the two-loop EW-QCD Drell-Yan master integrals". In: (2019). arXiv: 1907.00491 [hep-th].

[210] Jiro Kodaira and Luca Trentadue. "Single Logarithm Effects in electron-Positron Annihilation". In: *Phys. Lett.* 123B (1983), pp. 335–338. DOI: 10.1016/0370-2693(83)91213-3.

[211] C. T. H. Davies and W. James Stirling. "Nonleading Corrections to the Drell-Yan Cross-Section at Small Transverse Momentum". In: *Nucl. Phys.* B244 (1984), pp. 337–348. DOI: 10.1016/0550-3213(84)90316-X.

[212] R. P. Kauffman. "Higher order corrections to Higgs boson p(T)". In: *Phys. Rev.* D45 (1992), pp. 1512–1517. DOI: 10.1103/PhysRevD.45.1512.

[213] Daniel de Florian and Massimiliano Grazzini. "Next-to-next-to-leading logarithmic corrections at small transverse momentum in hadronic collisions". In: *Phys. Rev. Lett.* 85 (2000), pp. 4678–4681. DOI: 10.1103/PhysRevLett.85.4678. arXiv: hep-ph/0008152 [hep-ph].

[214] Daniel de Florian and Massimiliano Grazzini. "The Structure of large logarithmic corrections at small transverse momentum in hadronic collisions". In: *Nucl. Phys.* B616 (2001), pp. 247–285. DOI: 10.1016/S0550-3213(01)00460-6. arXiv: hep-ph/0108273 [hep-ph].